University of
Waterloo Research Institute

Continuation Study on Hydrogeochemical Processes in Abandoned Uranium Tailings from the Elliot Lake District

FINAL REPORT

Period
May 1, 1982 to March 31, 1983

REQ. NO. 2-9030

CONTRACT REPORT NO. OSU82-00144

UNIVERSITY OF WATERLOO
WATERLOO RESEARCH INSTITUTE

Project No. 204-02

CONTINUATION STUDY ON HYDROGEOCHEMICAL PROCESSES IN ABANDONED URANIUM TAILINGS FROM THE ELLIOT LAKE DISTRICT

Final Report
for the
Period
May 1, 1982 to March 31, 1983

Principal Investigators:
J.A. Cherry, R.W. Gillham and E.J. Reardon

Research Assistants:
N.M. Dubrovsky and R.V. Nicholson

Department of Earth Sciences
University of Waterloo
Waterloo, Ontario
N2L 3G1

Submitted to:
Departmemt of Energy, Mines and Resourses
CANMET Mineral Sciences Laboratories
555 Booth St.
Ottawa, Ontario
K1A 0G1

245pp

APR 5 1984
MICROMEDIA

CONTENTS

Chapter page

1. INTRODUCTION 1

2. THE KINETICS OF PYRITE OXIDATION IN DILUTE ALKALINE SOLUTION . . 4

- ABSTRACT FOR CHAPTER 2 5
- INTRODUCTION 7
  - The Problem 7
  - Pyrite Oxidation Kinetics 11
  - Experimental Rationale 13
  - Objective and Scope 17
- EXPERIMENTAL 18
  - Materials 18
  - Methods and Results 22
    - Pyrite Cleaning Experiment 22
    - Pyrite and Silica Sand Preparation Procedure 26
    - Preliminary Experiment (PYROX1) 28
    - Surface Area Experiment (PYROX2) 30
    - Oxygen Concentration Experiment (PYROX3) 34
    - Temperature Dependence Experiment (PYROX4) 39
    - Pyrite Type Experiment (PYROX 5) 41
- DISCUSSION 43
- IMPLICATIONS FOR ACID GENERATION IN TAILINGS IMPOUNDMENTS . . 51
- SUMMARY AND CONCLUSIONS 56
- RECOMMENDATIONS FOR FURTHER RESEARCH 61
- LIST OF TABLES 65
- LIST OF FIGURES 66
- TABLES IN CHAPTER 2 68
- FIGURES IN CHAPTER 2 80

3. DOWNWARD MIGRATION OF REACTION PRODUCTS 121

- ABSTRACT FOR CHAPTER 3 122
- INTRODUCTION 124
  - Objectives and Scope 126
- CHARACTERIZATION OF TAILING SOLIDS 128
- METHODS 134
  - Chart - Recorded Alkalinity Titrations 134
  - Batch Tests 135
  - Column Experiments 137
  - Sorption of H^+ 141
  - Analytical Methods 142
- RESULTS 143
  - Chart-Recorded Titrations 143

Batch Tests 144
Column Experiments 147
Sorption of H^+ 149
DISCUSSION 150
Chart-Recorded Alkalinity titrations 150
Batch Tests 153
Column Experiments 160
Sorption of H^+ 167
SUMMARY OF CONCLUSIONS 168
LIST OF FIGURES 177
TABLES IN CHAPTER 3 180
FIGURES IN CHAPTER 3 200

REFERENCES 213

Appendix page

A. LISTING OF THE PYROX1 DATA AND RESULTS 217

B. LISTING OF THE PYROX2 DATA AND RESULTS 222

C. LISTING OF THE PYROX3 DATA AND RESULTS 224

D. LISTING OF THE PYROX4 DATA AND RESULTS 231

E. LISTING OF THE PYROX5 DATA AND RESULTS 233

F. XRD TRACES OF TAILINGS MINERALS 238

G. ADDITIONAL EFFLUENT ANALYSES FOR THE COLUMN TESTS 243

Chapter 1

INTRODUCTION

Uranium mining in the Elliot Lake district has resulted in the production of about 300 million tonnes of pyritic, radioactive tailings since operation began in 1957. Tailings from the mills have been discharged into topographic depressions forming impoundments. During milling operations, the active tailings impoundments are characterized by high water-table levels and pore water that is neutral to alkaline and that contains very low concentrations of toxic metals and of most radionuclides. Upon completion of milling operations, however, the original tailings water gradually drains, and is partially replaced by recharge water. The water table declines, exposing the surface to the weathering processes of the atmosphere. Although lime treatment of tailings was performed prior to discharge, the inactive tailings pore-water becomes progressively acidic with time. The concentrations of many metals and some radionuclides, whose solubilities are enhanced by low pH conditions, also increase to unacceptable levels in the tailings pore water. Although the contaminated acidic water is observed throughout much of the inactive tailings mass the production of acid, iron and much of the sulphate occurs almost exclusively in the uppermost one to two metres of these deposits. The near surface zone is characterized by pore-water pH values between 3.5 and 1.5. The acid is produced when the finely ground pyrite within the tailings oxidizes as a result of exposure to atmospheric oxygen (WRI Report 910-03, 1982).

As the rain and snow-melt infiltrate the tailings mass, displacing the pore water below, the acidic water in the shallow subsurface, migrates downward at a rate that is approximately equal to the annual rate of precipitation. During this downward migration, chemical interaction with some mineral phases within the tailings results in a rise in pH. After passage of many volumes of low pH water, however, the tailings become depleted of acid consuming minerals. Eventually, under the existing conditions the entire tailings mass will become acidic with very little change in the low-pH water passing through it. Even when partial neutralization occurs, the pore water retains a high acidity level that is represented by such species as dissolved ferrous iron that would precipitate on exposure to air and result in drastically lower pH values in the seepage or surface water.

Acidic contaminated pore water has been found to occur at a number of tailings impoundments in the Elliot Lake Region. Reports have shown that these conditions exist at the Nordic Main (Blair et al., 1980), the Lancor tailings (Cherry et al., 1982), Stanrock and Williams Lake (Feenstra et al., 1981) tailings areas. In addition to the pore waters within the impoundments, migration of contaminated acidic water has been observed beyond the impoundment perimeter within a sandy aquifer underlying the Nordic tailings (Morin, et al., 1982). If unattended, continual subsurface acid generation and subsequent leaching of radionuclides and metals may contaminate surface water in the region of the impoundments.

This report describes the results the first year of an investigation that was conducted during the period of May, 1982 to March, 1983. The project that was originally proposed over a two year period was funded for one year by the Department of Energy Mines and Resources. The objectives of the investigation were to: (1) determine the kinetic behavior of pyrite oxidation and subsequent acid production by means of laboratory investigations (2) evaluate by means of laboratory experiments the effects of mineral-water interaction resulting in neutralization of low pH pore water in the existing acidic tailings. The results of the investigations performed to meet these objectives are given in Chapter 2 and 3, respectively, of this report.

Chapter 2

THE KINETICS OF PYRITE OXIDATION IN DILUTE ALKALINE SOLUTION

ABSTRACT FOR CHAPTER 2

A laboratory investigation was conducted to study the role of important physiochemical variables on the rate of pyrite oxidation in weak alkaline solution. The results were used to develop an empirical rate equation. The variables that were studied include 1) pyrite surface area, 2) oxygen concentration, and 3) temperature. In addition, six pyrite-types from different geographic locations were tested to determine whether or not differences exist in the oxidation rates.

Column-type experiments were used in which the pore-water solution was maintained at negative pressure. Dilute $NaHCO_3$ solution was passed continuously through beds of pyrite-silica sand mixtures and in most experiments, the desired gas composition was passed continuously through the samples. Careful washing and sieving procedures were used to insure that a uniform surface area (grain size) was maintained for each grain-size fraction used.

A preliminary experiment conducted to determine the magnitude of oxidation rates expected under the experimental conditions showed that the reaction rates were high enough to monitor on a daily basis. The rate-dependence on surface area was then examined utilizing five different grain-size fractions. Although surface area was not measured, the specific surface-areas estimated from particle diameter and assuming spherical geometry revealed a linear relationship with oxidation rate. The results of the experiment to study the effects of oxygen concentration (from 0.01 to 20.0%) suggested that the rate is a function of this variable to the power of 0.2. The results of analyses of the gas in the head space of the solution reservoirs, however, indicated

that contamination had occurred in the low O_2 concentration solutions. A repeat of this experiment is in progress. The rate of oxidation is also a function of temperature. With data from three temperatures (3^{o}, 15^{o} and $25^{o}C$), the activation energy was found to be 80 kJ mol^{-1} (19 kcal mol^{-1}) representing about a tripling of the oxidation rate with a $10^{o}C$ rise in the temperature. The oxidation rates for six pyrite samples, including the Elliot Lake pyrite concentrate, were examined. The results of this final experiment indicated that no observable differences occurred in the oxidation rates among the pyrite types. The results of these experiments were then used to formulate a rate equation for solutions in which the pH was about 7.5 to 8.0.

The rate equation is expressed as the products of the oxygen concentration, the surface area and the rate constant. At $25^{o}C$ the values of the rate constant was found to be about 0.01 when the units for the rate are in mg-SO_4 d^{-1} g^{-1}. Calculations were then made to determine the rate of oxidation expected under field conditions and finally to derive the potential H^+ concentration or pH of the pore water within the tailings. By assuming that atmospheric oxygen penetrates the tailings to a depth of 0.2 m, then the potential H^+ concentration of the pore-water is about 0.14 mol L^{-1}. Without acid-base reactions or complex-ion formation, the equivalent pH is about 0.9 units. Although simplifying assumptions have been used in the estimate of the eventual pore-water pH below the active-pyrite-oxidation zone, these calculations show that oxygen availability is the critical variable that must be reduced substantially in order to maintain neutral conditions in the tailings pore-water.

INTRODUCTION

The Problem

Low pH conditions in the uranium tailings pore water results in elevated concentrations of toxic metals as well as some radionuclides such as ^{210}Pb, U and Th. The concentrations of most metals and some of the radionuclides are usually limited by the formation of sparingly-soluble minerals under neutral pH conditions. At low pH, however, many of these minerals are highly soluble so that the metals and radionuclides are released to the surrounding pore water. Water from rain-fall and snow-melt infiltrates the tailings surface resulting in the downward displacement of the acidic contaminated pore water through the tailings and into the groundwater system below. Although some neutralization occurs initially within the tailings, the acid-consuming minerals are depleted after contact with many pore volumes of acidic water. As the acid-consuming material is depleted, the low-pH pore-water containing elevated concentrations of metals and radionuclides migrates downward through the tailings. Because of the association of high levels of toxic metals and some radionuclides with low-pH pore water, any strategy aimed at limiting the extent of contamination should focus on the reduction of acid production in the uranium tailings. It is therefore necessary to understand the processes that control acid generation in the tailings.

The acid resulting in low-pH pore-water is generated in the shallow subsurface zone of tailings as a result of pyrite oxidation by atmospheric oxygen. At inactive tailings sites, the oxidation reaction occurs rapidly due to the availability of oxygen in the air that migrates into the tailings pore-spaces that are only partially filled with water. At low pH, the reaction is further catalysed by the growth of iron and sulphur oxidizing bacteria. These bacteria, however, do not affect the oxidation rate at pH values above 4. In order to reduce the rate of pyrite oxidation, it is then necessary to maintain near-neutral pH conditions. It is also known that the oxidation reaction cannot proceed faster than the rate of oxygen transfer to the pyrite. Hence, the rate of reaction can also be limited by the availability of oxygen.

Although the rate limiting effects of neutral pH and low oxygen flux are qualitatively understood, no research has been conducted to quantitatively describe these effects. Because it is desirable to sufficiently reduce the rate of oxidation so that neutral pore-water conditions are maintained, it is first necessary to be able to predict the rate of acid generation under conditions that are less than favorable for this reaction. The purpose of this investigation, therefore, was to study the effects of the important variables on the rate of pyrite oxidation at near-neutral to alkaline pH values. The results of this study will then be used to predict the rate of oxidation and subsequent acid generation in the uranium tailings.

The long term objective of the study of pyrite oxidation is to design a disposal system that would effectively reduce the rate of acid generation and maintain neutral pH conditions in the uranium tailings-mass. The placement of an engineered cover-layer on the inactive tailings has been proposed as one remedial option. The cover-layer would be designed to minimize the rate of pyrite oxidation and subsequent acid generation in the underlying tailings.

Because oxygen is the main driving force for the oxidation reaction, one function of the cover would be to minimize the flux of oxygen into the tailings. Oxygen enters the coarser surface of the tailings rapidly because the gas diffuses readily through the open pore spaces. Diffusion of oxygen through water is four orders of magnitude less than that through air. The cover would therefore be designed to retain a maximum amount of water in the pore spaces as a barrier to oxygen diffusion. This could be accomplished with very fine grained material. Such material is available in the Elliot Lake area in the form of homogenized (thickened) depyritized tailings. Moisture retention properties of this and other available materials would need to be examined. Maintenance of neutral to alkaline pH conditions would be necessary to avoid growth of iron-oxidizing bacteria and to consume any additional acid that is generated as a result of the small amount of oxygen entering the pyritic tailings. For this purpose, the cover material would contain a fair percentage of crushed limestone. The calcite that comprises the limestone would dissolve in the infiltrating water thereby raising the pH to a value between 7 and 8 and imparting a component of dissolved alkalinity to the pore water that would be transported downward into the pyritic tailings. The concentration of alkalinity (HCO_3^- and CO_3^{2-}) would depend on the partial pressure of carbon dioxide (PCO_2) in the cover-layer. Without vegetation and an associated root zone, the PCO_2 would be close to that of the atmosphere and the concentration of dissolved alkalinity would be low. As the root-zone develops, the PCO_2 in the cover would increase with a corresponding increase of dissolved alkalinity. In any case, the amount of calcite dissolved in the pore water can be easily predicted from thermodynamic principles. The presence of this dissolved alkalinity, however, does not guarantee that the pore water within the tailings will remain neutral. The pore-water pH is also a function of the oxygen flux, the rate of water movement and the rate of pyrite oxidation.

The concept of limiting the rate of pyrite oxidation and hence the rate of acid generation is straight forward. The question of whether it is practical to do this with a cover-layer system, however, remains unanswered. There is a need to evaluate the effectiveness of the covered-tailings-system in terms of maintaining neutral pH of the pore water down to the water table. Although field experiments could be performed to study this process, the need to examine a large number of variables, suggests that the cost of such experiments would be prohibitively high. However, it is possible to test the effects of a cover-layer through model simulations.

The processes that affect the pore-water pH are generally understood. The flux of oxygen and water into the tailings and the acid-base reactions are important processes that can be mathematically simulated. The rate of pyrite oxidation is a key factor that also affects the resulting pore-water pH. Pyrite oxidation, however, is kinetically controlled and the relationship must be empirically derived. The rate law describing the dependence of oxidation rates on physiochemical variables is needed to successfully predict the amount of acid and other oxidation products released over a given period of time. The rate law in the form of a mathematical model or equation can then be incorporated into an overall model that would quantitatively describe the processes controlling pore water chemistry in the tailings as it is affected by a protective cover layer. However, at this time very little is known about the kinetic controls on pyrite oxidation under conditions that are anticipated in a covered-tailings-system. In order to derive the rate law, the kinetic parameters must be experimentally determined. The purpose of this study is to derive the rate law for pyrite oxidation in a solution whose pH corresponds to that of calcite equilibrium in subsurface pore-water.

Pyrite Oxidation Kinetics

The oxidation of pyrite is a complex process that can involve a number of reactants and products under various conditions. When the reacting solution is alkaline, however, complete oxidation of pyrite is likely and the overall resulting reaction is straight forward:

$$FeS_2(s) + 15/4O_2 + 7/2H_2O \Rightarrow Fe(OH)_3(s) + 2SO_4^{2-} + 4H^+ \quad (1)$$

In alkaline solution containing carbonate or bicarbonate, the hydrogen ion is immediately neutralized in reactions such as;

$$CO_3^{2-} + H^+ \Rightarrow HCO_3^- \quad (2)$$

$$HCO_3^- + H^+ \Rightarrow H_2CO_3^0 \quad (3)$$

When sufficient carbonate is present to maintain near neutral pH conditions, the overall oxidation reaction can be represented by the following;

$$\begin{aligned} &FeS_2(s) + 15/4O_2 + 7/4H_2O + 4CO_3^{2-} \Rightarrow \\ &\qquad Fe(OH)_3(s) + 2SO_4^{2-} + 4HCO_3^- \end{aligned} \quad (4)$$

In this case, acid generation is balanced with acid consumption and the pH remains near neutral. The major net products of oxidation are soluble sulphate and ferric hydroxide precipitate.

In a complex heterogeneous reaction such as the oxidation of pyrite shown in (4), many elementary reactions are probable. In the overall reaction, one electron is transferred to oxidize iron while 14 electrons are exchanged in the oxidation of the sulphur component of pyrite. Because only one or two electrons are transferred per elementary reaction, the complete oxidation must be composed of a number of intermediate steps. Rate-limiting reactions can occur in one or more of these elementary reactions.

For any elementary reaction, the rate is a function of the concentrations of reactants and/or products. In the case of a reversible reaction such as;

$$aA + bB \Longleftrightarrow cC + dD \qquad (5)$$

the rate equation for the forward reaction is

$$R_f = k_+ (A)^v (B)^w \qquad (6)$$

and the corresponding rate of the reverse reaction is

$$R_r = k_- (C)^x (D)^y \qquad (7)$$

in which the brackets denote activities of the components, the exponents represent the order of the reaction with respect to that component and k+ and k are the forward and reverse rate constants respectively. Irreversible reactions can be described as having only a forward rate. When all elementary reactions and their rates are known, the rate equation for the overall process can be derived. Although one objective of reaction-rate studies is to determine the sequence of elementary reactions during a specific process, it is often not practical to do so. In complex reactions with many elementary steps, it may be possible only to determine the rate-dependence of obvious participating variables. It is desirable to derive the rate equation in the form of (6) in which the concentration terms would represent variables such as the concentration of oxygen or specific surface area of pyrite. Whether a particular variable occurs in the final rate equation depends on the nature of the elementary reactions and the rate-limiting steps.

The reaction rate and its dependence on system variables can only be derived experimentally. Although there are a number of approaches, the initial-rate method is commonly applied to slow-reacting processes. This method involves the determination of the early-time reaction-rates resulting from changes in one variable while all other variables are held constant. The rate-dependence on each variable is then studied individually and the results can be synthesized to form the overall rate equation. The reaction rate is also known to be a function of temperature. This variable can also be investigated separately to determine the specific relationship.

Experimental Rationale

The deterioration of environmental quality by acid mine drainage related to mining activities has led to much research into the processes surrounding the oxidation of pyrite and other sulphides. Recent reviews suggest that the study of pyrite oxidation can be separated into two fields, those dealing with the inorganic or non-biologic pathways (Lowson, 1982) and others dealing specifically with microbically-catalyzed processes (Lumdgren and Silver, 1980). Many investigations on oxidation rates have been conducted, of which almost all are confined to conditions that are favourable to rapid oxidation rates. However, even though a great many results have been obtained, there is poor agreement as to the specific controls or the rate dependence on the major variables.

Variables such as the concentration of oxygen, pyrite surface area, pH, the concentration of dissolved ferric iron and temperature as well as the presence of some bacteria have been observed to affect the rate of pyrite oxidation (van Breemen, 1972; Nodstrom, 1982; Lowson, 1982). Although ferric iron can be an important oxidant at low pH, its importance diminishes in neutral to alkaline solutions where it is rather insoluble. The Thiobacillus bacteria that catalyse pyrite oxidation, specifically T. Ferrooxidans do not thrive above pH values of about 3. Other members of the Thiobacillus genus that oxidize sulphur compounds do not catalyse pyrite oxidation at pH values above 4 even though many sulphur oxidizing species thrive in neutral to alkaline solutions (Arkestyn, 1980). Because alkaline conditions would be maintained initially when reclamation of pyritic tailings is performed, the effects of ferric iron and bacterial mediation were not considered in this study. In addition, although the solution pH affects the rate of oxidation (Smith et al, 1968), dissolution of limestone into the pore water would limit the pH to a narrow range of about 7 to 8. The major factors of concern to the rate of oxidation then are restricted to surface area, oxygen concentration and temperature. Even though the number of variables has been reduced to three, there are many practical considerations in the study of pyrite oxidation kinetics if meaningful results are to be obtained.

The study of kinetics involving solid mineral phases is complicated by a number of factors. Because the reaction is likely to be surface controlled, it is critical that the actual surface area be well characterized. The surface area should be within well-defined limits and the actual grain-size distribution of the crushed material should be uniform. It is known that after crushing, ultra-fine material adheres to the coarser-grained particles. Because little is known about cleaning such material, a method must be developed for this purpose. Careful cleaning and sieving methods can reduce the uncertainties of surface area availability. The surface area (grain size) of the particles can also change during autogenic grinding if the pyrite is shaken. In the study of surface area as a kinetic variable, this effect is undesirable. To minimize this effect, the pyrite sample should be undisturbed during the course of the experiment. For this reason, packed columns or beds of pyritic sand through which water is passed were chosen in place of the shake flask designs that are commonly used in reaction kinetic studies.

The oxidation rate of pyrite can also be affected by electrochemical interaction when other sulphide-minerals or impurities within the pyrite are present. In order to determine the rate law for pyrite oxidation, it is therefore necessary to study the reaction rate of pure specimens. After obtaining rate data from pure specimens, a composite sample of sulphide-minerals obtained from Elliot Lake tailings could then be studied to determine whether differences in the oxidation-rates exist.

In the study of reaction kinetics, it is critical that the supply of reactants is sufficient so as not to limit rate of reaction. During the oxidation of pyrite, the concentration of oxygen at the pyrite surface must be equivalent to that in the specified gas-phase. This can be accomplished by maintaining a well oxygenated and mixed solution in contact with the pyrite. This is not practical, however, for water in partially-saturated pyritic sand. Because oxygen transport to the pyrite surface is retarded by slow diffusion through the water phase, the oxygen supply can be maintained by minimizing the thickness of the water in contact with the pyrite. Porous granular pyrite that is held under suction (negative pressure) and remains only partially-water-saturated contains water whose film thicknesses are on the order of microns to millimetres. If the specified gas phase is present in the gas filled pore-spaces, then oxygen transport will be rate-limiting only at extremely high oxidation rates. Because only moderate to low oxidation rates are expected in these studies, oxygen transport in the partially-saturated sand should not be rate limiting.

Finally, it is critical to maintain an accurate mass balance of the reactant or product that is used to monitor the progress of the reaction. In these experiments, SO_4^{2-} will be analysed to determine the extent of pyrite oxidation. Sulphate was chosen in place of iron because iron is lost from solution when it oxidizes and precipitates readily near neutral pH. In solutions containing high sulphate and moderate calcium concentrations, it is also possible to precipitate SO_4^{2-} in the form of gypsum. Therefore, in these experiments, $NaHCO_3$ was used in place of calcite ($CaCO_3$) to simulate dilute alkaline pore water and prevent possible gypsum precipitation.

Objective and Scope

The purpose of this research was to determine, experimentally, the rate expression for pyrite oxidation in dilute-alkaline-solution. The range of variables and the experimental conditions were chosen to reflect conditions occurring in pyritic tailings through which carbonate-buffered alkaline water passes. Crushed and sized granular pyrite was oxidized in continuous-flow leaching columns. Pyrite grains were dispersed in a similarly-sized silica sand and the resulting pyritic sand was only partially water-saturated. Both fluid and gas phase compositions were controlled.

Four potential kinetic variables, that had been identified previously, were investigated. The rate dependence on oxygen concentration in the gas phase was examined for the range of 0.01 to 20.0 % O_2. Pyrite surface area was the second variable whose range of values correspond to particle diameters of 54 to 215 microns. The oxidation-rate dependence on temperature was determined by measuring rates at 3, 15 and 25°C. Finally, the rates of oxidation were determined using samples of pyrite obtained from different geographic locations.

EXPERIMENTAL

Materials

Pyrite was obtained from Wards Scientific Co. as aggregates of euhedral crystals or relatively pure massive specimens. Varieties from 1) Huanzala, Peru; 2) Magma Mine, Arizona; 3) Rico, Colorado; and 4) Lake Balkhash, Siberia, were used in the experiments. In addition, a granular pyrite concentrate, obtained by floatation from fresh Rio Algom uranium tailings, was used in one experiment. Ottawa sand was used for experiments that involved pyritic-sand mixtures.

The leaching solutions used in all experiments consisted of double-deionized water containing 5 mmol L^{-1} of $NaHCO_3$, the compressed gas mixtures used to control oxygen concentrations were specially prepared and analysed. All gas mixtures contained 0.5% CO_2 by volume with various specified levels of oxygen and a balance of nitrogen. The gas phase was bubbled through the influent solution reservoirs in order to equilibrate the water with the concentrations of O_2 as well as to buffer the pH at the specified partial pressure of CO_2.

During the course of this investigation, four types of reaction vessels were used. The choice of apparatus was based on relative cost and difficulty to construct as well as the level of control needed for each experiment. The required experimental control in most experiments included 1) continuous solution flow; 2) maintenance of unsaturated conditions (pore spaces only partially filled with water); and 3) continuous gas flow through the porous material. The first apparatus mentioned below was used in a preliminary experiment and no attempt was made to control the gas composition or flow conditions.

The first device is an ASTM 125 ml buchner funnel with a fritted glass (porous) plate. These funnels were adapted to permit continuous solution flow under negative water pressures by attaching a 1.5 m length of plastic tubing to the funnel spout and a drip-chamber for solution delivery at the top of the funnel (see Fig. 1).

This apparatus was used in a preliminary experiment that was designed to quickly determine the magnitude of the oxidation rates. The grain-size, solution pH and moisture content of the pyritic sand as well as the solution flow rates corresponded to those that would be used in later experiments. No attempt was made to regulate the gas flow or composition.

The second device is termed a "moisture-suction cup" and is basically a modification of the ASTM funnel system. This device was designed to reduce resident-water volume in the effluent end and allow gas flow through the unsaturated porous material. The moisture-suction cups were constructed from 8 cm lengths of 57 mm ID Plexiglas(R) cylinders with a base plate containing an Acropore(R) filter membrane and two stainless steel tubes (2 mm ID) through the bottom of the plate. A two metre length of plastic tubing was attached to the centre steel tube to enable pressure head adjustment to the appropriate level. The other steel tube was used for back flushing to withdraw gas bubbles that accumulate below the membrane. Gas flow is provided through a coiled stainless steel tube that is placed in the sandy material when the cup is filled. The gas exits through the porous surface into the atmosphere. A schematic representation of this device is shown in Fig. 2.

This apparatus was used in experiments in which the gas phase composition was close to that of the atmosphere. This experimental design was chosen because it was relatively uncomplicated and contamination by atmospheric oxygen was not a problem. Oxygen was continuously passed through the pyritic sand and negative water pressure was maintained through the porous membrane.

A specially designed "unsaturated column" is the third device used in the pyrite oxidation experiments. The column consists of two 10.5 cm lengths of cylindrical Plexiglas(R) with end plates containing Acropore(R) filter membranes. The cylindrical sleeves are constructed such that the inner one is uniformly perforated with small diameter holes to allow gas flow into the annular space that exists between the sleeve walls. The outer cylinder contains a stainless-steel-tube port for gas effluent. The end plates each contain a solution-flow port and a flushing port. The Acropore(R) membranes are supported by stainless-steel screens. A 9 cm length of perforated Plexiglas(R) tube (0.5 cm OD) projects through the centre of the bottom plate into the column interior. The gas phase was passed through this tube into the surrounding porous material in the functioning column. Four tensiometer ports were installed through the sides of the column. A tensiometer consists of a 5 cm length of Plexiglas(R) tubing fitted with water column and flushing ports at one end and an Acropore(R) membrane at the other. A view of the unsaturated column in cross-section can be seen in Fig. 3.

The unsaturated-column design is rather complex for a number of reasons. First, the internal gas phase must be completely isolated from the atmosphere. This is especially important when testing the effect of very low oxygen concentrations on the rate of pyrite oxidation. Second, if good hydraulic control were maintained in the unsaturated pyritic sand, then the effect of moisture content on oxygen transport (availability) could be tested later using these devices. And third, in such a large volume of sandy material, it is advantageous to monitor the pressure head (with tensiometers) and thereby have a better estimate of the moisture content. Although these devices are complex and costly to build, they afford good hydraulic control and can be utilized in other experiments related to pyrite oxidation under various conditions of moisture content, gas composition and solution pH.

The fourth apparatus was constructed from a 10 cm^3 plastic syringe containing a bottom layer of glass wool overlain by a coarse paper filter and a rubber O-ring. Solution and air-entry were provided through ports at the top of the syringe. Solution flow rates were drop-controlled while gas flow was induced by positive pressure. Both solution and gas phases exited through a tube at the bottom of the syringe where the solution phase was collected (see Fig. 4).

This device was used in experiments for which very little hydraulic control was needed. The experiments were designed to determine if differences in rates existed between sample types. The positive gas pressure and continuous gas flow insured that oxygen was available for reaction. The gas flow need not be restricted because inexpensive compressed air was used in place of the special compressed gas-mixtures that were utilized in the other experiments. Silica sand was not needed to add bulk to the sample because a porous membrane was not used. This design was the least complex but was the most suitable for dealing with many replicates when strict experimental control was not needed.

Methods and Results

This investigation is comprised of a number of related experiments including a pyrite cleaning study and a preliminary study to determine the magnitude of oxidation rates expected under the experimental conditions. Experiments were conducted to examine the effects of pyrite surface area, oxygen concentration and temperature, the results of which can be used to derive a rate equation. An additional experiment was designed to study the rates of oxidation of pyrite specimens from different geographic locations. A summary of the experiments and their corresponding conditions is given in Table 1.

Pyrite Cleaning Experiment

Mineral dissolution experiments are complicated by many factors. Among these are surface-controlled reactions including active-complex formation, surface coatings derived from reaction products and adsorption reactions. Although these processes must be described when applicable, determination of the controlling processes can only be made under well-defined experimental conditions. One common interpretational problem in surface-controlled reactions is the uncertainty associated with the available specific surface area. It has been found by other researchers that the rate of feldspar dissolution reactions appears to be parabolic with time when extremely fine-grained particles are not first removed from the feldspar surface before the dissolution experiment (Holdren and Berner, 1979). Analogous behaviour is quite probable with pyrite oxidation reactions. In this case, the ultra fine particles produced during crushing and sieving adhere to larger grains and oxidize rapidly. The larger grains oxidize at a slower rate determined by their specific surface area. The combined effect of these different rates could result in misinterpretation of the data. These effects are especially important when testing rate-dependence on surface area. However, variation of rates due to non-uniform grain or surface area would also lead to poor estimates of the effects of other variables on the oxidation rate. Because little is known about maintaining specific surface area and procedures for cleaning pyrite, a qualitative study of cleaning methods was performed.

There are two purposes for proper cleaning of pyrite grains. The first is to insure that grain size varies within a small range only and second to reduce the quantity of reaction products on the mineral surface. The presence of reaction products may pose problems in the interpretation of reaction-rate data. Two experiments were performed. In the first, the method of ultrasonic treatment was evaluated and in the second, washing procedures were evaluated.

During preliminary wash trials, ultrasonic treatment was used to dislodge fine particles adhering to larger grains. It was observed, however, that further ultrasonic treatment resulted in more suspended fines even when the treatments were repeated up to 10 or as many as 15 times. Although it is generally accepted that ultrasonic treatment is non-destructive for most materials, these results suggested that fines were not only being removed from coarser-grained surfaces but were also being produced during treatment. A simple experiment was performed to test this hypothesis.

A 15 g sample of crushed and sieved pyrite (-170+230 mesh) was washed repeatedly with water. The suspended fines were decanted and the washing was repeated until the supernatant was clear and colorless. The pyrite was then rinsed twice with acetone and dried. Six ml of water were then added to each of five 2g subsamples. These samples were then subjected to ultrasonic treatment of varying times. After allowing the fines to settle, the water was decanted and 5 ml of acetone was added before evaporating to dryness. After two weeks of storage, the samples were leached with two 5 ml aliquots of water and the filtrate was analysed for sulphate. A summary of this experiment is shown in Table 2.

The increasing sulphate values with treatment time indicates that a greater degree of oxidation has occurred in these samples. Because the degree of oxidation of pyrite for any time period is related to the surface area, these data suggest that surface area increases with treatment time, probably as a result of production of fine particles. These results suggest that ultrasonic cleaning should not be used for prolonged periods or repeated during pyrite washing. A short treatment may not be harmful, however, if repeated washing is subsequently performed.

In the second experiment, three methods of pyrite treatment were evaluated. The first involved treatment of the pyrite with H_2O_2 (0.5%) in HCl (pH= 1). The second treatment was made with H_2O_2 (0.5%) in NaOH (pH= 12). The third treatment involved water washing only with no pre-oxidation. Samples were rinsed with water after all treatments and some were given a final rinse with acetone. Each sample consisted of 2g of -170+230 mesh Colorado pyrite. After treatment, the samples were decanted and dried in a vacuum dessicator and stored there for 2 weeks. After removing the samples from the desiccator, 5 ml of deionized water was thoroughly mixed with each sample. The water was then decanted and filtered whereupon another 5 ml of water was added to the pyrite sample and decanted. The ten ml sample of water was retained and later analysed for soluble sulphate. Because fine particles oxidize rapidly, those samples containing more fines would produce more sulphate during processing and storage. The concentration of sulphate was used as an indicator of the amount of fine particles remaining on the grains. All numbers are averages of two or more replicates.

The H_2O_2-HCl treatment was used to test the hypothesis that pre-oxidation by H_2O_2 would remove the fine particles and the low pH conditions would maintain iron in solution so that little or no protective coating in the form of ferric hydroxide solids would form. Treatment with H_2O_2-NaOH was used to determine whether more vigorous oxidation is necessary to dissolve the strongly adhering fines. The water wash was used as a control.

A summary of sample treatment and resulting sulphate concentrations is given in Table 3. The sulphate concentrations for the water leach are generally similar. The exceptions occur for the acetone rinsed samples after 30 minutes (W2b) and 2 hours (W2d) of H_2O_2-NaOH treatment. Although these appear to give the best results, there are other points to consider. First, the reacting solutions from the NaOH treatment immediately displayed a rust brown colour during treatment indicating that iron oxidation and precipitation had probably occured. The two samples (W2 band W2d) cited above also developed and retained a brown tarnished appearance. This is indicative of surface oxide coating, which is undesirable. Second, if the pyrite is allowed to oxidize rapidly, etching or pitting of the pyrite surface may occur and rapid increase in surface area can result. Observation under the electron microscope of pyrite grains treated in a manner similar to the H_2O_2-NaOH (2 hour) treatment showed that pitting and etching does indeed occur. If the results for these two samples are judged as undesirable even though lower levels of oxidation are observed, then, only the data from the remaining samples should be considered here. It seems preferable not to preoxidize the pyrite therefore and simple water washing was selected as the preferred treatment. The acid rinse was used to remove excess iron on the pyrite surface and the final acetone rinse removes excess sulphur and quickens the drying process.

Pyrite and Silica Sand Preparation Procedure

The pyrite specimens were obtained as large (0.5kg) masses. After breaking the larger pieces with a hammer, the pyrite was mechanically crushed between ceramic plates to a diameter of about 2 to 10 mm. Initially this material was then pulverized with a mortar and pestal until sufficient fines were present to collect the desired sieved size-fractions. A benchtop ceramic ball mill was later used in place of the mortar and pestal to pulverize the pyrite in preparation for sieving. About 80g portions of the pulverized pyrite were sieved on each run.

Sieving was performed on a Rototap shaker with six screen pans (60,80,120,170,230 and 325 mesh) for 15 minutes per run.

The washing procedure was performed on each size fraction. Up to about 100g of sieved pyrite was placed in a beaker. Double the weight of deionized water was added to each sample. The contents of each beaker was mixed thoroughly with a rubber-tipped stirring rod and after allowing the main size fraction to settle, the supernatant was discarded. This procedure was repeated until the supernatant solution was clear and colorless. The beaker was then immersed in an ultrasonic cleaner for 45 seconds. Washing was then repeated until the supernatant appeared clear and colorless. After allowing the water to drain, reagent grade acetone was added to the pyrite. The contents were mixed and the overlying liquid was discarded. This procedure was repeated until the acetone was clear and colorless. After decanting the final acetone rinse, the beaker was placed in a dessicator and a vacuum was applied. When the pyrite was dry, each sample was resieved through the appropriate mesh-interval. In this way the fine-grained pyrite that was present in the initial unwashed fraction were removed.

The resieved sample was then rewashed with water to remove the small amount of fines produced during sieving. After decanting the last water rinse, a similar volume of 6N HCl was added to the pyrite. The contents of the beaker were thoroughly mixed and allowed to stand for about 10 minutes. Further water washing was performed to remove the HCl and a final two washes with acetone were made. The sample was then placed in a dessicator and stored there under vacuum. The pyrite sample designated for the oxidation experiments were treated only a few days before use.

The sized silica sand was prepared using Ottawa sand that consisted of well rounded quartz with most grains larger than 60 mesh. The sand was pulverized in a ceramic ball mill in preparation for sieving. The sieving procedure was similar to that for pyrite. The selected size-fractions were washed by passing deionized water through a 1.5m length of acrylic cylinder (5cm ID) containing about 1kg of sand. The water flow-rate was adjusted so that the fines would pass through the top overflow port while the main size fraction remained suspended in the column. When the overflow water was clear, the washed sample was removed. This sand was then added to 8N HNO_3 and after mixing was allowed to sit for 2 to 3 days. After decanting the acid, water washing was repeated until the pH of the overflow water approached a value of 6. These sand samples were then air dried and retained for later use.

Preliminary Experiment (PYROX1)

The purpose of the preliminary study was to determine the magnitude of reaction rates expected under experimental conditions. It was expected that the oxidation rates would be low in slightly alkaline solution. In addition, the grain-size diameter that was practical to use in these studies is high compared to the grain sizes used in most pyrite oxidation studies as well as to grain sizes observed for milled tailings. Large grain-size values correspond to small specific surface-area values. Therefore, it was not known whether the oxidation rates would be high enough to produce detectable sulphate concentrations when solution flow was continuous.

Four samples of pyritic sand containing 10g of pyrite and 90g of silica sand (-120+170 mesh or 108 micron diameter) were prepared by gently rolling the mixture in a glass beaker until visibly homogeneous. The pyrite in units 1 and 4 were washed and rinsed using the standard procedure outlined above. Unit 2, however, contained pyrite that had been preoxidized with the H_2O_2-NaOH treatment whereas unit 3 was oxidized with H_2O_2-HCl treatment. These samples were placed in porous-plate buchner funnels. The sand was slowly wetted with the bicarbonate solution through the effluent tube by gravity feed. When water was visible on the surface, the end of the effluent tubing was placed at a distance of 90 cm below the sand layer and the pore water was allowed to drain into collection flasks. The solution delivery systems were then set in position above the funnels and a coarse-grade filter circle was placed on the surface of the sand. The surface filter allowed more uniform application of the solution that was added drop wise in the center. The solution flow rate was adjusted to 1 to 2 drops per minute or about 100 ml per day. A schematic diagram of the experimental system can be seen in Fig. 5.

The solution effluent was collected at one-to-three day intervals. The solution was weighed and a subsample was collected and retained for sulphate analysis. The total mass of sulphate leaching from the pyritic sand was calculated from the product of water mass and sulphate concentration.

The rates of oxidation observed over the first 30 days of the experiment were on the order of 1 mg-SO_4 d^{-1} for each 10g of pyrite. This corresponds to 0.1 mg-SO_4 $d^{-1}g^{-1}$ (pyrite) or 2 x 10^{-5} mmol-FeS^2

$h^{-1}g^{-1}$. The rate was large enough to produce sulphate concentrations that were measurable when solution flow was as high as 1000 ml per day. The total mass of sulphate eluted from each of the funnels over time is shown in Fig. 6. The average oxidation rates represented by the slopes of these curves tend to increase over the first 80 days of the experiment. In the early stage of the experimental run, two trends are evident. Units 1 and 4 exhibit a gentle rise in slope at about 40 days while the slopes of units 2 and 3 increase more markedly. Although display of the data in this form indicates the average rates of oxidation, (represented by the slope) the resulting daily rate values can also be inspected.

A plot of daily rate versus time is shown in Fig. 7 (a to d). Although a fair degree of scatter is evident in these data, the rates are generally in the range of 1 to 3 mg-SO_4d^{-1} or 0.1 to 0.3 mg-SO_4 $d^{-1}g^{-1}$. The rates also trend upward with time as indicated by the regression lines in these plots. The oxidation rates observed in this experiment indicate that sulphate concentrations would be measurable for other experiments with similar solution flow rates, even if the pyrite oxidizes at considerably lower rates.

Surface Area Experiment (PYROX2)

The purpose of this experiment was to examine the functional relationship between the pyrite surface area and the rate of oxidation. Five grain size fractions (-60+80, -80+120, -120+170, -170+230 and -230+325 mesh) of the Colorado pyrite were used. The leaching solution contained 5 mmol L^{-1} $NaHCO_3$. The gas phase contained 20% O_2, 0.5% CO_2

and a balance of N_2. The modified moisture suction cups were used in this experiment. A summary of the designated experimental conditions is given in Table 4.

A 20g sample of pyrite from each of the five grain-size fractions was weighed to the nearest mg. Each pyrite fraction was added to 180 g of similar-sized silica sand, after which the samples were rolled gently in a glass beaker until the mixture appeared homogeneous.

The base plates of the moisture-suction cups were flushed with the $NaHCO_3$ solution to wet the membranes and remove air from the effluent tubing. After placing a 5 mm layer of pyritic sand over the membrane, the perforated coil of stainless steel tubing was positioned in the cup. The remaining sand was then added. The sides of the cup were tapped gently to induce the sand to settle. The cups were then slowly filled with solution through the bottom tubing by gravity feed. When water was visible on the surface, filling was terminated and the end of the effluent tubing was placed at the appropriate elevation. The water was allowed to drain to equilibrium and the effluent was collected in preweighed flasks. A coarse filter circle was placed on the sand surface. The tip of the effluent tubing was placed at an elevation that would maintain a volumetric water content of about 20%. The elevations were based on moisture-drainage tests performed on samples of silica sand from each of the five grain-size fractions.

A rubber stopper was fitted onto the top of each cup. A plastic pipette tip for solution delivery was introduced through a central hole in the stopper. An offset oversized hole allowed the tip of the stainless steel tubing to stand above the rubber stopper. The pipette tip was then connected to the solution-reservoir manifold-system and the solution was allowed to drip onto the filter surface. The drop rate was adjusted to about 3 drops per minute (about 200 ml/day). The steel tubing was connected to the compressed-gas manifold and gas flow of about 100 ml per minute was initiated. Gas escaped through the porous surface of the sand and exited through the hole in the rubber stopper. Because gas was delivered through a manifold, it was not possible to control the flow rate to each cup. The same gas was also constantly bubbled through the solution reservoir to maintain oxygen saturation and to buffer the pH at the selected partial pressure of carbon dioxide (PCO_2).

The moisture-suction cups were placed within an insulated cabinet equipped with a seven-watt fan to circulate the air. The cabinet also contained the flask of water through which the gas, being delivered to the pyritic sand, was bubbled. The temperature within the cabinet was maintained at 25 ± 1°C. A schematic diagram of the experimental system can be seen in Fig. 8.

The effluent from the moisture-suction cups was collected and weighed. Subsamples of these solutions were retained and later analysed for sulphate. The pH of the influent and effluent solutions were monitored periodically.

The total sulphate results of the first 67 days of the grain-size (surface-area) experiment can be seen in Fig. 9. This plot shows the total accumulated sulphate leached from each grain-size fraction with time. Although there are considerable changes in the slope of each curve over this period, the average slope is consistently greater for smaller grain-size units. Inspection of the daily rates of pyrite oxidation indicate that a large degree of scatter is present in the data (Fig. 10, a to e). Smoothing the trend of these data points by taking the average of each three consecutive points (moving average indicated by the solid curve) over the first 24 days' data shows similar trends for each experimental unit. In each case, there is a peak value at about 14 days with generally decreasing values after this time. With the exception of the unit with the finest grain size (PYROX 2-5) the rates of the finer grain fractions are consistently greater at a given specified time.

The observed trends of oxidation rates is consistent over the five experimental units. Although a trend in these data is evident, it is reasonable to use the average oxidation rate of each unit for comparison with the other units. The average rates over this period are consistently greater for units with smaller grain-size values. This trend suggests that a relationship exists between the rate of oxidation and the surface area as determined by the particle grain-size. Because the diameters of the pyrite grains are limited to relatively large values by the ability to physically separate them with different mesh screens, actual surface area measurements could not be made. With conventional gas absorption equipment suited to measure solid surface areas (BET method) the actual grain size must be considerably smaller than the smallest fraction used in this experiment (-230+325 mesh or 54 microns nominal diameter). It is therefore necessary to derive an estimate of surface areas as related to the particle diameter or mesh size of the sieve screens.

It is possible to estimate the surface area of particles or more importantly, the specific surface area (surface area per unit weight) if a simplified geometric shape is assumed. Although pyrite belongs to the cubic crystalographic system, and a cube might appear to be a reasonable shape, pyrite fractures concoidally, producing more spherical surface features. Although quick grinding would probably produce highly angular particles, the surface of each particle would more closely approach the shape of a sphere than that of a cube. If each grain size is assumed to be composed of spheres of equal diameter, then the specific surface area (A_s) becomes a function of the diameter (d) as seen in the following equation;

$$A_s = 6/pd \qquad (8)$$

Because the particle density (p) is constant, the specific surface area is inversely proportional to the particle diameter. Therefore, 1/d can be used as an estimate of the specific surface area. A summary of particle grain sizes, 1/d values and average oxidation rates is given in Table 5. A plot of 1/d versus oxidation rate can be seen in Fig. 11. If the rate from the finest grain-size unit (PYROX2-5) is ignored, the other four consecutive points exhibit a linear trend with a correlation coefficient (r) of 0.993. This linear response of oxidation rate to 1/d indicates that the rate is first order with respect to specific surface area.

Oxygen Concentration Experiment (PYROX3)

The purpose of this experiment was to determine the effect of different oxygen contents of the gas phase on oxidation rates. Five values of oxygen concentration (0.01, 0.10, 1.0, 5.0 and 20.0 % by volume) were used. The solution contained 5 mmol L^{-1} $NaHCO_3$ and the non-oxygen components of all gas phases consisted of 0.5% CO_2 and a balance of N_2. Gas flow and moisture content were controlled by use of the unsaturated columns that were maintained at $25^oC \pm 1^oC$. A summary of the designated experimental conditions is given in Table 6.

Five 40g samples of pyrite (-120+70 mesh, Peru) were weighed to the nearest mg. Each alliquot of pyrite was added to 750 g of silica sand the same grain size range and the material was gently rolled in a glass beaker until the mixture appeared homogeneous. The Acropore$^{(R)}$ membranes were moistened to facilitate stretching during the column packing procedure. The lower end plate was then secured to the column. A 10 g portion of silica silt (-230+325 mesh) was evenly sifted over the bottom membrane. After 200g of pyritic sand was placed into the column the base was tapped repeatedly for about one minute, to induce settling. The addition of sand and the tapping procedure were repeated until the column was filled. An additional 10 g portion of silt was distributed over the top of the pyritic sand. The top end plate was then tightened into position.

After packing the column, the end plates were flushed with bicarbonate solution and the integrity of the membranes was tested. If the membranes were found to be intact, the tubing was clamped off to avoid further wetting of the pyritic sand. The columns were placed in an insulated cabinet and the solution and gas lines were installed. All solution lines remained clamped at this time. Flushing of each column with the appropriate O_2 concentration was initiated at a flow rate of about 100 ml per minute. The same gas phases were bubbled through the corresponding solution reservoirs. Each gas mixture travelling to the columns was bubbled through a column of water, positioned inside the cabinet, in order to humidify the gas and facilitate temperature equilibration before entering the pyritic sand. All gas exit ports were positioned 1 to 2 cm below water surface to avoid atmospheric contamination and to facilitate observation of gas flow.

After 24 hours, gas flow-rates through the columns were adjusted to 40 ml per minute and forced bubbling through the solution reservoirs was terminated. The sand was slowly wetted from the top by opening the influent lines and applying a positive pressure to the solution reservoir. When water drops were observed in the gas exit holes at the base of the inner sleeve, the effluent line was opened and the solution was allowed to drain into a collection flask. The positive pressure was removed from the reservoir whereupon the unsaturated system progressed toward steady-state conditions. The pressure heads of the top and bottom of the column corresponding to the solution reservoir and effluent tip respectively were adjusted to -90 cm of water. Solution reservoirs were maintained at equilibrium with the appropriate gas phase by connection to a gas chamber that was filled with the selected gas. The pressure in each chamber remained at near atmospheric levels and was replenished by continuous gas flow. The Marriot syphon therefore receives only the oxygen concentration of the gas mixture that flows through the corresponding unsaturated column. A schematic representation of the experimental system can be seen in Fig. 12.

During operation, the pressure head at both end plates was maintained at -90 cm. The pressure head existing within the pyritic sand in each column was monitored at least once during operation. The tensiometer results showed that the pressure head remained at -90 cm within the columns. Unfortunately tensiometer lines become obstructed with gas bubbles. Because constant attention was needed to maintain the tensiometer systems, they were used for a period of only a few days. The negative pressure resulted in degassing of CO_2 and probably O_2 as well in the influent line and the end plate spaces. In order to avoid flow blockage from bubble accumulation, it was necessary to flush the top end plate each day and the bottom end plate each second or third day. The top end plate was flushed by withdrawing the influent solution with a syringe through the flushing port. This volume of influent solution was then drawn up through the effluent tubing from a flask by withdrawing from the flushing port on the bottom end plate. All flushing solutions were retained in the appropriate collection flasks. The effluent was weighed daily and a subsample was collected for later analysis of sulphate.

The results of total sulphate leached from each of the five unsaturated columns are plotted against time in Fig. 13. Because of technical difficulties with the columns, each was started on different dates. Units 4 and 5 were initiated about 5 weeks after the first three units. Over the first 25 days, each unit showed consistent trends in that the greater slopes corresponded to higher concentrations of oxygen flowing through those units. Changes in slope are apparent for all curves over time. The daily oxidation rate values are plotted versus time in Fig. 14 (a to e). This plot illustrates the large degree of scatter of data from most units. Less variation in rate values over time is observed for the units corresponding to 0.01 and 0.1% O_2 (PYROX3-1 and PYROX3-2). It was also observed that while rate values of the 1.0% O_2 unit (PYROX 3-3) increased with time, those rates corresponding to the 5.0 and 20.% O_2 concentrations tended to decrease with time.

There is no obvious reason for the observed trend of decreasing rates over such a short time period. The trend of increasing oxidation rates with time, however, suggest that contamination of the column gas with atmospheric oxygen had occured. Because some contamination is probable, the oxidation rates corresponding to early times would likely be more representative of the rates at the designated oxygen concentrations. For this reason, the rates corresponding to averages over the first 20 days were considered representative values. A summary of the rates and oxygen concentrations are given in Table 7. A log-log plot of oxygen concentration versus oxidation rate is used to determine the apparent order of the reaction with respect to oxygen (Fig. 15). This plot is linear with a slope corresponding to the order of the equation, the result of which suggests that the rate is a function of oxygen concentration to a low fractional power. This relationship is represented approximately by;

$$\log(\text{Rate}) = \log(k) + 0.2\log(O_2) \tag{9}$$

in which (O_2) represents the concentration of oxygen and (k) is a composite rate constant.

During operation of the columns, samples of influent and effluent gas were collected and analysed for O_2 and CO_2 concentrations. The influent gas samples were collected through rubber septums located at a T-junction about 30cm before the column. The effluent gas samples were taken through a similar port located about 60cm from the column and 40cm before the bubbling outlet. Gas samples were also taken from septums attached directly to each gas tank regulator outlet. A summary of the O_2 concentrations is given in Table. 8.

Although the PYROX3-2 unit was originally exposed to 0.10% O_2 gas after 38 days, the gas phase composition was switched to the 0.01% O_2 phase. This change was made to observe the effect on the oxidation rate. At the time of this first sampling, both PYROX3-1 and PYROX3-2 were receiving the 0.01% O_2 gas. The results indicate that virtually no changes in O_2 concentration occur between the gas regulator outlet and the bubbling outlet. It appears that neither pyrite oxidation was sufficient to deplete O_2 in the column or diffusion of atmospheric oxygen through the plastic tubing was sufficiently large to elevate the concentration of O_2 in the gas flow systems.

Temperature Dependence Experiment (PYROX4)

It is known that the rate of reaction increases with temperature. The degree of increase, however is dependent on the activation energy (Ea) for a particular reaction. The temperature-rate relationship may be described by the Arrhenius equation;

$$k = A \exp(-Ea/RT) \tag{10}$$

in which k is the rate constant, A is the Arrhenius factor, Ea is the activation energy, R is the universal gas constant and T is the absolute temperature. Taking the log of each side of (10) gives;

$$\log(k) = \log(A) - (Ea/2.303RT) \tag{11}$$

A plot of log k (or log rate) versus 1/T yields a line with slope of -Ea/2.303R from which Ea is derived. Therefore, in addition to the rate-dependence on major chemical variables, the change in rate can also be determined as a function of temperature.

The purpose of this experiment was to determine the activation energy of the pyrite oxidation reaction. Reaction rates at two temperatures ($3^{o}C$ and $15^{o}C$) were monitored. Gas mixtures containing 20% O_2, 0.5% CO_2 and a balance of N_2 were utilized. The leaching solution contained 5 mmol L^{-1} $NaHCO_3$. Gas and solution control was achieved with moisture-suction cups.

Two 10 g aliquots of pyrite (-120+170 mesh Peru) were weighed to the nearest mg. Each of these was mixed with 90g of similar-sized silica sand by rotating gently in a glass beaker. Two moisture-suction cups were prepared and run in a manner similar to those in the Surface Area experiment. One unit was placed in a temperature controlled room that was maintained at $3^{o} \pm .5^{o}C$. The second unit was placed in a temperature-controlled cabinet where the temperature remained at $15^{o}C \pm 1^{o}C$. Gas delivery to each cup was controlled individually at about 10 ml per minute. Solution flow was approximately 2 drops per minute. The effluent was collected and weighed daily after which subsamples were retained and later analysed for sulphate.

The total sulphate leached from the pyritic-sand samples over time at both 3^{0} and $15^{0}C$ are shown in Fig. 16. The curve with the larger slope represents data from the higher temperature unit. The data are plotted as daily rate versus time in Figure 17. Although the data from the $15^{0}C$ unit (PYROX 4-2) exhibits slightly more variation, the rate values during the period of 4 to 28 days are consistent within a small range. Data representing the oxidation rate at $25^{0}C$ was obtained from the -120+170 mesh grain-size fraction of the surface area experiment (PYROX2-3). As was mentioned in the results of that experiment, some disruption in the rates was apparent during the first 40 days of the run. An average rate value from 40 to 67 days was used for the activation energy calculations. A summary of the temperature-rate data can be seen in Table 9.

In accordance with equation (9) above, the log-rate data was plotted versus 1/T in Figure 18. The three points fall on a line in which the slope is directly related to the activation energy. The value of Ea derived from these data is 80 kJ mol^{-1} or 19 kcal mol^{-1}. With a known value of the activation energy, the rate-constant governing the overall pyrite oxidation rate can be adjusted to the appropriate temperature.

Pyrite Type Experiment (PYROX 5)

The purpose of this experiment was to determine whether or not differences in oxidation rates existed among pyrite samples obtained from various geographic locations. It was also important to know whether significant differences in oxidation rates existed between pure pyrite specimens and the pyrite concentrate obtained from Elliot Lake uranium tailings. The pyrite types include; 1) pyrite concentrate (fresh Rio Algom tailings - Elliot Lake); 2) Peru (a); 3) Peru (b); 4) Arizona; 5) Colorado; and, 6) Siberia. The Peru (a) and (b) samples were obtained from the same location but (a) was pulverized by hand with mortar and pestal and (b) was pulverized in a bench-sized ceramic ball mill. Leaching was performed in the syringe apparatus utilizing a 5 mmol L^{-1} $NaHCO_3$ solution and a gas phase comprised of compressed air. The experiment was maintained at an ambient room temperature of 23°C ± 2°C.

Two 10 g samples of each pyrite type (-170+230 mesh) were weighed to the nearest mg. Each of the 12 pyrite samples was placed in a syringe apparatus over which an additional filter circle was placed. Solution and gas were delivered to each syringe through outlets from a manifold designated for each phase. The solution flow was individually controlled to rates on the order of 3 drops per minute. The total gas flow was adjusted to about 1200 ml per minute which corresponded to a gas pressure above the pyrite equivalent to about 80 to 120 cm of water. The gas pressure resulted in continuous gas flow through the pyrite and maintenance of unsaturated conditions. The effluent from each unit was collected and weighed daily. Samples of effluent were retained and later analysed for sulphate.

The results of total sulphate leached versus time for each of the pyrite samples can be seen in Fig. 19. The data for each sample are linear and the slopes are quite similar between the samples of each pair as well as among the pyrite types. The narrow band of data points indicates that very little differences occur among the slopes corresponding to the different pyrite types. The data representing daily rate values versus time are given in Fig. 20 (a to f). It is observed that almost all data points fall within the range of 2.5 to 4.5 mg-SO_4 d^{-1} or 0.25 to 0.45 mg-$SO_4 d^{-1} g^{-1}$. Although the PCO_2 of the gas phase (atmospheric) was considerably less than that used in previous experiments and hence the pH of the influent solution would be higher, the resulting oxidation rates are quite similar to that determined from the same grain-size fraction in the surface area experiment (PYROX2-2). This suggests that the experiments utilizing the moisture suction cup and the syringe-leaching apparatus produce consistent results. These results demonstrate that the types of pyrite tested in this study, oxidized at the same rates when subjected to similar conditions. Because of the wide range of pyrite types used, it is suggested that all varieties of pyrite in the absence of surface coatings and under similar environmental conditions, oxidize at approximately the same rate.

DISCUSSION

The results of the preliminary experiment (PYROX 1) were significant in that they indicated that pyrite oxidation does not cease nor does it become insignificant at neutral to alkaline pH values. This experiment was performed with fairly coarse-grained pyrite with an estimated surface area of about 150 cm^2 g^{-1}. In contrast, the surface area of pyrite in the uranium tailings is likely to be on the order of 1200 cm^2 g^{-1} or greater. Because a greater surface area results in higher reaction rates, the rates observed in this preliminary experiment are likely to be in the low range of rates observed in the tailings under similar conditions. Although oxidation rates given by Goldhaber (1983) for crushed pyrite in alkaline and neutral solutions, the grain size was reported as less than 43 micron diameter and hence surface area cannot be estimated for comparison to the present study.

The surface-area experiment showed that the oxidation rate is related to the total specific surface area of pyrite. The relationship, although not definitively linked to actual surface-area measurements, has been found in terms of the grain size related to the mesh size on the sieves that were used to segregate the crushed material into size-fractions. Although the results of some other studies suggest that the rate is a function of $1/d^2$ or of surface area to some other integer order, a number of studies have presented findings suggesting that the rate is proportional to the specific surface area or 1/d (Lowson, 1982; Nordstrom, 1982). The results of the present study confirm the simple first-order or linear relationship.

Although it could be argued that the assumption of spherical particles shapes is probably in error, the choice of a different geometry does not alter the proportionality between surface area and 1/d. It can be shown for instance that the specific surface area is also proportional to 1/d for a cube for which d is the edge length. Similarly, specific surface area is inversely proportional to the edge-lengths of plate-shaped or other othogonally-shaped particles. The only difference in the relationship given in equation (8) is that the proportionality constant differs for each geometric form. This suggests that although the linear relationship between oxidation rate and specific surface area is correct, the actual values of specific surface area probably cannot be accurately determined from d. As seen in Fig. 11, the line passing through the data does not pass through the origin. It is expected that if 1/d gave a true estimate of the specific surface area, the line would regress to the origin. This would occur because a limit of zero for 1/d represents a zero-value for specific surface area as well. However, determination of the grain-size distribution could be used for the purposes of predicting oxidation rates for other granular pyrite samples with the present information.

The oxidation-rate dependence on oxygen concentration is critical if prediction of the rate under field conditions is to be made. If diffusion, is the principal transport mechanism for oxygen, the flux of oxygen into the pyritic media will be highly dependent on the rate of uptake of O_2 by pyrite oxidation (Shumate et al, 1971). This factor affects not how fast acid is produced in the shallow subsurface but also the depth to which active oxidation occurs. The results of field studies suggest that oxygen concentration profiles with depth are a function of the physiochemical properties of the pyritic deposits (WRI Rept. 910-03, 1982; Erickson, et al., 1982).

A number of relationships between oxidation rate and concentration of oxygen have been reported in the literature (van Breemen, 1972; Nordstrom, 1982). Many studies conclude that the rate is proportional to the partial pressure of oxygen. Fractional orders of reaction have also been suggested with values of 0.8, 2/3 and 1/2 (Lowson, 1982). In addition, complex adsorption-desorption models have been used to describe the rate mechanism (Shumate et al, 1971).

The results of the present study suggest a low fractional order for this reaction. Although this result may indicate that the reaction is controlled by a complex non-linear adsorption mechanism, there is evidence to suggest that the observed rates are not representative of the assigned concentrations of oxygen. Some inconsistencies involving the results and experimental control can be discerned. For instance, the rate observed for the unit receiving the 20% O_2 gas (PYROX3-5) is about one-fifth that of the unit containing the same size-fraction in the surface area experiment (PYROX2-3). Although consideration was initially given to the differences in pyrite type between the two experiments, the results of the final experiment (PYROX5) indicated that little or no differences exist between rates of oxidation observed for the samples obtained from various geographic locations. The low-order response to O_2 concentration also suggested that perhaps oxygen supply was not maintained at the desired levels. Further insight into the potential problems was obtained when additional gas samples were obtained.

A new suite of gas samples was obtained not only from influent and effluent lines but also from the gas head-space in the solution reservoirs and within the columns of pyritic sand. The gas head-space was sampled through the rubber stoppers and the resulting O_2 concentrations represent the values that are at equilibrium with the solution phase. Five samples were also obtained from three selected columns by inserting a fine stainless steel tube through the tensiometer membranes. Although this sampling method was likely prone to contamination, it does give some indication of actual O_2 levels at points within the columns. The results are listed in Table 10.

The analyses show that although influent and effluent concentrations of O_2 exhibit levels that were designated to each, the oxygen concentrations in the head-space of the solution reservoirs do not represent the corresponding input values. While the 20% O_2 reservoir contains only about 15% oxygen, the four other flasks exhibit values that are higher than expected. The 0.01 and 0.10% O_2 reservoirs contain 100 and 10 times the designated concentrations respectively. A reason for the lower-than-expected value in the 20% O_2 flask is not yet known. A trend of greater contamination with lower O_2 content in other units suggests, however, that diffusion of atmospheric O_2 has occurred into each reservoir. It is likely that this occurred in the gas delivery line between the gas reservoir flask and the solution reservoir (see Fig. 12). The gas flow in this line is controlled by the flow of solution out of the flask. This low flow rate would provide ample time for O_2 diffusion through the plastic tubing. Because gas flow rates to the columns were high, the contamination due to diffusion in those lines was not significant. The high gas flow rates through the column masked the contamination from the more oxygenated solutions that passed through the column at much slower rates. Oxygen concentrations within the columns reflected the expected values for the 20% and the 1.0% O_2 units indicating that gas penetration and flow are probably uniform throughout the pyritic sand in these columns. The high value obtained from the 0.01 % O_2 unit suggests that contamination has occurred either through column operation or during sampling.

The contamination of the influent solutions with atmospheric oxygen has yielded oxidation rates that are the result of reaction with a specified level of O_2 in the gas combined with a different level of O_2 dissolved in the water. This process suggests that the observed rates of the low O_2 units are higher than would be expected without contamination. The results of this experiment are therefore likely to be in error and the run will be repeated.

A modified version of the moisture-suction cup was used in the experiment designed to repeat the study of rate-dependence on oxygen concentration. The apparatus and system are similar to the ones used in the grain-size (PYROX 2) experiment (Fig. 8) except that the top of the cup is closed and contains a controlled outlet tube for the gas effluent. The system was also modified so that the designated gas phase was passed continuously through each corresponding solution reservoir. The choice of the suction-cup device was made for two reasons. First, it was found that the setup time for the unsaturated columns is relatively long. And second, a large quantity of pyrite and silica sand would be needed to reestablish these columns. This procedure would have been very time-consuming in itself. At the time of writing this report, the experiment was in progress for about one month. The results of the SO_4^{2-} analyses are expected shortly and findings will be given in an addendum to the final report.

The determination of rate dependence on temperature is less complicated by extraneous factors such as in experimental control. The observed rates in these experiments are consistent with time and a linear response between log (rate) and 1/T was obtained. Results from the literature include a range of values for the activation energy (Ea) from 39 to 88 kJ mol^{-1} that were determined over a variety of experimental conditions (Lowson, 1982). The value of 80 kJ mol^{-1} derived from the experimental data in this study is within the range of reported values. This relationship represents an approximate tripling of the oxidation rate with a 10°C rise in temperature. The relatively high value of Ea also suggests that the reaction is controlled by atom- or molecular-transfer rather than by diffusion as would be implied by an Ea value of about 10 kJ mol^{-1} or less.

A number of features deserve further consideration at this point. First, a large degree of scatter in the rate results from the preliminary experiment (PYROX1) is observed (Fig. 7). In addition to the scatter, however, the rates exhibit an increasing trend with time. Second, the rate values observed in the surface area experiment show peak values at about 14 days with an apparent leveling out at lower values at later times (Fig. 10, a to e). And third, although the rate experiments were performed with $NaHCO_3$ solution having a limited range of pH values, it is likely that pH variation may have had an effect on the rate of oxidation.

With regard to high degree of scatter, it should be noted that the preliminary experiment was designed only to determine the magnitude of oxidation rates and therefore few experimental controls were implemented. Nevertheless, some pertinent information may be obtained from these variations. Three factors may contribute to the observed inconsistencies in oxidation rates; 1) O_2 gas supply was not controlled; 2) constant temperature was not maintained and; 3) the solution flow rates were quite variable. Because gas was not passed through the pyritic sand samples, it is possible that the oxidation rates were affected to some extent by limited oxygen transport (diffusion) to the total available quantity of pyrite. If the oxygen supply to the pyrite was transport controlled, then the additional flux of O_2 dissolved in solution may have been important in contributing to the oxidation rates. It is therefore likely that the oxidation rates are linked to the solution flow-rate. Some indication of this trend is suggested by the oxidation rate versus flow rate plots (Fig. 21, a to d). The regression lines are shown in these plots and although the values of the slopes are variable, they are consistently positive.

The trends observed for the oxidation rates corresponding to the surface area experiment cannot be readily explained. These, however, could be linked to disruptions and alterations of the gas delivery, at early times. Initially, the gas phase consisted of 20% O_2, 1.0% CO_2 and a balance of N_2 gas. However, the solution phase was not subjected to gas flow until the ninth day of the run. Further problems with the gas phase were encountered when the gas tanks were depleted (after 25 days) before the replacement tanks had arrived. The new cylinder containing 20% O_2, 0.5% CO_2 and a balance of N_2 were connected after 34 days into the run, whereupon more stable oxidation rates apparently developed (Fig. 10, a to e). More recent data obtained from the PYROX2-3 unit has shown rates that are consistently in the range of 0.1 to 0.2 mg-SO_4 $d^{-1}g^{-1}$ over a period of 65 to 150 days. Regardless of the cause of these trends, a similar behavior over the five units is observed, and the cause would appear to be due to an experimental design factor. Because of the consistency trend between units however, it seems reasonable to make comparisons between the average rates for each unit or the rates corresponding to a specific period of time. The resulting linear trend of oxidation rate with inverse grain size appears to support this argument.

The unknown effects of pH on the oxidation rate would limit the use of the rate model if large changes in pH were to occur. One study has indicated that the rate increases by a factor of about 1.4 for one unit increase in pH in the range of 6 to 8 (Smith et al, 1968). In a system in which the solution pH is controlled by calcite dissolution and hence by the partial pressure of CO_2 gas, the variation of pH would be limited to a small range.

IMPLICATIONS FOR ACID GENERATION IN TAILINGS IMPOUNDMENTS

It should be valuable at this stage to estimate the rate of pyrite oxidation expected to occur in the tailings with a protective cover system. At this time only simple approximations can be made but they may illustrate the magnitude of acid production expected when oxygen is not rate-limiting and the pore water pH remains in the neutral to alkaline range. If at this point the rate equation is assumed to be first order with respect to oxygen, some calculations of expected oxidation rates can be made. This assumption can be superceded by the actual relationship when further data are available. If it is also assumed that the pH is initially held constant in the 7.5 to 8.0 range, then the rate equation can be expressed as;

$$R = \frac{-d(FeS_2)}{dt} = \frac{1.6d(SO_4)}{dt} = k(O_2)(A_s) \qquad (12)$$

where k,(O_2) and (A_s) represent the rate constant, PO_2 and specific surface area respectively. The left-hand quotient expresses the weight of pyrite oxidized per unit time and the right-hand quotient represents the weight of sulphate produced per unit time. With the available data and the assumptions noted above, the value of k is found to be 0.010 at 25°C. The units for rate and surface area are $mg\text{-}SO_4 d^{-1} g^{-1}$ and $cm^2\ g^{-1}$ respectively. The (O_2) term is in atmospheres if the partial pressure is used.

An estimate of surface area is needed to utilize the rate equation. It is known that more than 50% by weight of the tailings is less than about 70 microns in diameter (-200 mesh). Although a large range of pyrite grain-size is possible, it is likely that the sub-micron particles have been consumed during oxidation in the mill circuit. The large amount of dissolved iron in the acid leach solution suggests that some pyrite has dissolved and/or oxidized there. The nominal size of pyrite grains is therefore likely to be between 1 and 70 microns. A representative value of 20 microns for the average particle diameter was chosen for the purpose of these calculations. The surface area can then be computed from this particle diameter if a spherical geometry is assumed.

Another factor that is needed to predict the oxidation rate is the temperature in the active-oxidation zone of the tailings. Temperature estimates are complicated by seasonal fluctuations and the heat that is produced during the oxidation reaction. However it is likely that the mean annual temperature of shallow subsurface is only a few degrees higher than the mean annual air temperature. For the purpose of this calculation the average temperature is taken as 10^oC. Using the estimate of surface area in eq. 12 and correcting for temperature, the rate equation reduces to;

$$R = k'(O_2) \tag{13}$$

where the value of k' is 1.8. at 10^oC.. When the maximum O_2 concentration of 0.2 atm is assumed, the overall rate of pyrite oxidation is about 0.4 $mg\text{-}SO_4 d^{-1} g^{-1}$ or about $9x10^{-5}$ $mmol\text{-}FeS_2\ h^{-1}\ g^{-1}$. As discussed above, the rate will vary within the tailings according to the level of oxygen present at any particular depth and the temperature, which will be seasonably variable. The oxygen concentration, however, is linked to both diffusion into the tailings and the rate of consumption by pyrite oxidation.

To place the value of the predicted maximum rate in perspective, a list of oxidation rates was compiled from the data in a number of reported investigations (Table 11). These values in many instances have been estimated from data that was not intended to determine the effects of different variables on oxidation rates. In addition, the experimental conditions or means of estimating the oxidation rates from the data given by the various authors differ significantly. It can be seen that one of the highest reported rates corresponds to a low pH environment with active bacteria. Other high values, however, are observed for soil samples at pH=4 and crushed pyrite at pH=9. The lowest reported value was obtained by estimating the H^+ ion balance in pyritic tailings that were generating acidic pore water. Because of the effects of mineral dissolution and other buffering reactions, this estimate is probably too low. The value of the maximum rate estimated from results of the present study occurs at the low end of the range of values in Table 11. This suggests that under the conditions of low temperature, moderate specific surface area and carbonate-buffered pH, pyrite oxidation is somewhat diminished. Although the previous estimate of grain size and subsequently, surface area could be in error so as to underestimate the rate, the relatively low rate-value reported here, offers encouraging evidence in terms of reducing oxidation rates for tailings close-out. However, better insight into the possible outcome of pore water pH may be obtained if further calculations are made.

With the oxidation rate given above and a simplified estimate of the depth of oxygen penetration, an estimate can be made of the rate of acid generated per unit area of tailings. From field evidence, it is known that oxygen depletion occurs in the tailings at depths ranging from 0.2 to about 1.0 metres. For the purpose of these calculations it will be assumed that atmospheric oxygen penetrates the tailings to a depth of 0.2 metres. The quantity of pyrite available for oxidation is known to be about 5% by weight of the tailings. The bulk density of the tailings is about 1700 kg m^{-3} which yields a pyrite content of 85 kg m^{-3} or 17 kg m^{-2} in the top 0.2 m of tailings. Calculating the oxidation rate in terms of pyrite and then converting this stoichiometrically to H^+ yields a rate of 6.1 mmol-H^+ m^{-2} h^{-1} or 54 mol-H^+ m^{-2} each year. Although this shows how much H^+ is produced, it would be illustrative if the H^+ concentration in the pore water were known.

The major events that create water infiltration into the tailings occur twice each year, once in the spring, as snow-melt, and again in the autumn as rain-fall. Because of high evaporation rates in the summer and sub-freezing conditions in the winter, infiltration during these seasons is generally insignificant. Water in the shallow subsurface, above the water table, moves downward, in effect, only when water infiltrates from above. The pore water profile rapidly regains its equilibrium condition after each infiltration event. In this manner, the movement of pore water can be envisioned as a slug moving downward twice each year. If it is assumed that the moisture content is about 20% and the infiltration for each event is about 0.2 m of rain, then each slug will occur within a 1.0 m zone in the depth profile of the tailings. If it is assumed that the acid produced in the 0.2 m zone of active oxidation is diluted into the 200 litres over the 1.0 m interval in each of the two seasons, then the concentration of H^+ is found to be 0.135 mol-H^+ L^{-1}. The equivalent pH of this pore water, assuming that complexing or other reactions are insignificant, would be about 0.9.

Although some simplifying assumptions have been made in the preceding calculations, most are within reasonable limits that have either been observed or are expected within the tailings. The very low computed pH of the pore water suggests that with atmospheric oxygen, the chemical rate of oxidation is high enough to produce acidic conditions in the tailings pore-water. This implies that it is necessary to restrict the availability of oxygen, which is the only other controllable parameter, if neutral pH conditions are to be maintained. it can be shown that with a 100 fold decrease in either oxygen concentration or depth of oxygen penetration, the computed pore water pH remains low at about 2.9. It is concluded then that the oxygen flux into the pyritic tailings must be reduced considerably if the rate of acid generation is to be controlled to a tolerable level. Therefore, material that is used in a cover-layer to be deposited on the pyritic tailings should be studied to determine its properties in terms of a barrier to oxygen diffusion.

SUMMARY AND CONCLUSIONS

A laboratory investigation was conducted to study the role of important physiochemical variables on the rate of pyrite oxidation in weak alkaline solution, the results of which were used to develop an empirical rate equation. The variables that had been identified from previous experiments and a survey of the literature include 1) pyrite surface area, 2) oxygen concentration and 3) temperature. In addition, the rates of oxidation corresponding to pyrite samples from different geographic locations, including Elliot Lake, were examined to determine if differences in rates exist. Because surface areas of crushed and sieved minerals are quite variable and difficult to characterize, a study of cleaning and treatment techniques was also performed. A solution of 5 mmol L^{-1} $NaHCO_3$, that contains an alkalinity comparable to that of water in equilibrium with limestone ($CaCO_3$), was used in all the oxidation experiments.

The cleaning experiment consisted of washing treatments with water, H_2O_2 in HCl and H_2O_2 in NaOH. In addition, the effect of prolonged ultrasonic treatment of crushed and sieved pyrite grains was studied. The results of this study showed that repeated water washing to remove the visible suspended fines and a short ultrasonic treatment yielded results that were as good as the chemical treatments. While treament with H_2O_2 in NaOH resulted in the least residual sulphate on the pyrite grains, observations indicate that ferric hydroxide formed on the pyrite surfaces. The presence of surface coatings on samples used in kinetic studies is undesirable. It was also found that ultrasonic treatment beyond one minute significantly increases the surface area of the pyrite probably as a result of autogenic grinding. All experiments in this investigation were performed with crushed and sieved (1/2 phi intervals) pyrite that had undergone a standard chosen washing procedure. This procedure included repeated washing in water until no suspended fines were observed. The granular pyrite was then rinsed in HCl and then in acetone to remove iron oxide coatings and residual sulphur respectively. The samples were then resieved through the appropriate mesh intervals to insure that the grain size distribution remained relatively uniform.

A preliminary oxidation experiment was conducted to determine the magnitude of the reaction rates expected in dilute alkaline solution for pyrite samples with moderate to low specific surface areas. Four units were run with modified ASTM porous plate funnels used as reaction vessels. The $NaHCO_3$ solution was passed continuously in a slow drop-wise fashion through mixtures of specific quantities of granular pyrite and silica sand. The mass of sulphate eluting from the funnel was monitored daily. The results of this experiment indicated that pyrite oxidation under the experimental conditions was significant and could readily be measured on a daily basis even if the rates had been many times less.

A second experiment was conducted to determine the rate-dependence on pyrite surface area. Five units were run, each containing a different size fraction from coarse (60 mesh) to fine (325 mesh) that represented a convenient range of specific surface area. Pyritic-sand mixtures were placed in specially constructed moisture-suction devices in which the pore water remained under negative pressure. The $NaHCO_3$ solution as well as an oxygen-gas-mixture were passed continuously through the sand. The effluent was collected daily and the mass of SO_4^{2-} eluted from each unit was monitored. Although it was not possible to measure the specific surface area of each pyrite grain-size fraction, an estimate of surface area was computed after assuming spherical particle geometry and a nominal particle diameter related to the mesh screen size was assumed for each fraction. The relationship between oxidation rate and estimated surface area was linear, indicating that the rate is first-order with respect to this variable.

The third experiment was performed to evaluate the relationship between oxygen concentration and the rate of oxidation. Five units were run in unsaturated columns in which the gas phase passing through each was maintained at a specified level between 0.01 and 20.0% O_2. Each unit contained equal weights of the same size-fraction of pyrite in a silica sand mixture. The solution flow rates and the moisture content within the sand mixture were adjusted to appropriate levels by controlling the pressure at the influent and effluent ports. The results of the sulphate mass balance showed that the relationship between O_2 concentration and oxidation rate is nonlinear. By plotting the data on log-log axes, the order of the reaction was found to be about 0.2 with respect to oxygen. This implies that large decreases in the oxygen concentration result in much smaller decreases in the oxidation rate. Analysis of the gas phase in the reservoir head-space above the influent solution, however, indicated that contamination of the low O_2-concentration units from atmospheric oxygen had occurred. These findings suggest that the order of 0.2 should actually be higher and that further experiments are needed to clarify this experimental error. A repeat experiment is presently in progress and the results will be reported in an addendum to this final report.

The fourth experiment in this investigation was conducted to determine the activation energy associated with the pyrite oxidation reaction, the result of which was used to adjust the constant in the rate equation to correspond to the desired temperature. Two units were run in the moisture-suction devices at temperatures of 3° and 15°C respectively. Both units contained the same size-fraction of pyritic sand and other conditions in the systems were similar to the surface area experiment. Arrheniums behavior indicates that the relationship between log (Rate) and 1/T (absolute temperature) is linear and the activation energy is derived from the slope. The results of the two unit-runs noted above, combined with a third data point at 25°C taken from the surface area experiment, were found to follow Arrhenius behavior. The activation energy for the reaction is about 80 kJ mol^{-1} (19 kcal mol^{-1}) that results in about a tripling of the oxidation rate for every 10°C rise in temperature.

The final experiment was conducted to determine whether or not differences in the oxidation rate were apparent among pyrite samples from different geographic locations and, in addition, whether the pyrite concentrate derived from Elliot Lake tailings behaved differently from pure pyrite. Six units were run in duplicate, each containing a 10 g aliquot from the six pyrite types. A 10 cm^3 syringe column was used as the oxidation apparatus, through which gas flow was maintained by positive pressure and solution was added in a slow drop-wise manner. The effluent was collected daily and the reaction rate was computed from the sulphate mass balance. No observable difference in rates occurred during the first twenty days, for which the data was analysed. These results suggest that all pyrite specimens oxidize at equal rates and in addition, the pyrite concentrate from Elliot Lake tailings behaves like pure pyrite.

The results of the preceding experiments were then used to formulate a rate equation for the pyrite-oxidation reaction. Because the oxygen-concentration experiment was likely subject to experimental error, it is assumed, until other data are available, that the rate is proportional to this variable. The overall rate of oxidation can then be computed from the products of the oxygen concentration, the specific surface area and the rate constant. The value of this rate constant was found to be 0.01 at 25^0 when the rate is in the units mg-SO_4 d^{-1} g^{-1}. The rate of oxidation was then computed for a tailings impoundment by assuming reasonable values for specific surface area and temperature. At levels of oxygen present in the atmosphere, the rate of oxidation under the estimated conditions within the tailings was found to be 0.4 mg-SO_4 d^{-1} g^{-1} or 9×10^{-5} mmol-FeS_2 h^{-1} g^{-1}. If it is assumed that atmopspheric oxygen penetrates to a depth of about 0.2 m in the tailings, the pore water can attain a concentration of H^+ on the order of 0.135 mol L^{-1} or an equivalent pH of about 0.9 units. Although many simplifying assumptions have been made in these calculations, the low computed pH suggests that the chemical rate of oxidation and subsequent acid generation, in the presence of atmospheric oxygen, is sufficient to produce acidic pore water in the tailings. This implies that the flux of oxygen into the tailings must be reduced substantially if neutral-pH conditions are to be maintained in the pyritic uranium-tailings after abandonment. If a covered-layer system is used for close-out of these tailings, the cover should be designed to minimize the flux of oxygen into the underlying tailings.

RECOMMENDATIONS FOR FURTHER RESEARCH

This report is based on an investigation that was originally proposed to be conducted over two years. The results presented above were the results of the first year of study. In addition to the experiment needed to repeat the study of rate-dependence on oxygen concentration, there are other laboratory investigations needed to gain a better understanding of the pyrite oxidation process.

Although the solution pH was fixed for all experiments at a value that reflects limestone ($CaCO_3$) dissolution, some change in pH can occur if the pyrite oxidation rate is sufficient. From previous calculations, it was shown that sufficient acid could be generated in the tailings pore-water to consume the available dissolved carbonate if high concentrations of oxygen are present. Although it is the purpose of a cover-layer to maintain neutral conditions in the pore-water by minimizing the rate of pyrite oxidation, it is probable that titration of the dissolved carbonate by the generated acid would result in some change in pH. Because the oxidation rate is dependent on the solution pH, the relationship should be examined in the laboratory. It would be necessary to study the effect of pH only in the range of about 5 to 8. Below a pH of 5, the carbonate buffer is completely depleted and it is likely that acidophilic bacteria would soon add to the oxidation mechanism and hence would alter the nature of the reaction kinetics. Therefore, there is little purpose to extending the range of the rate equation below a pH of 5. Experiments could be conducted to determine the rate-dependence on pH in the range of values noted above. These experiments would be similar to those for the surface area experiment but would involve $NaHCO_3$ solutions with different pH values that would be controlled by the appropriate concentrations of CO_2 in the gas mixture.

The rate-equation that was derived from the results of this investigation can be applied to predict acid-generation rates at relatively early times. There are, however, some uncertainties in extending the use of the rate equation over long periods of time. There are two opposing factors that can affect the reaction rate. One effect is that of increasing surface area with time. During oxidation, the mineral surface is often corroded to the point that pitting occurs and micro-troughs are formed. This process tends to increase the available surface area and therefore increases the oxidation rate. It would be advantageous to examine the effects of increased surface area with the progress of oxidation. The opposing effect is that of surface armoring by ferric hydroxide precipitation. In neutral to alkaline solution, the ferric iron produced during oxidation readily precipitates. If some or all of this precipitation occurs on the pyrite surface, the reaction rate can be limited by the diffusion of oxygen through the precipitate layer. The effect of a precipitate buildup on the pyrite would be to decrease the generation of acid. This effect could be studied with long-term experiments such as those in progress. However, some observations of iron precipitate behavior in the experiments presented above suggest that different results may be obtained for experiments in which the pore-water solution remains static for prolonged periods before flushing. The contrast in results with the experiments in which solution was continuously passed through the pyritic sand may be significant. As noted in a previous section above, it is expected that in the field, pore water would remain static for extended periods in contact with the pyrite in the zone of active oxidation before it is displaced by fresh infiltrating water. It appears that this effect should also be investigated if reliable predictions of oxidation rates over the long term are to be made.

In addition to laboratory experiments, further study is needed to predict the evolution of pore water chemistry in the covered-tailings system. It has become evident during the course of this investigation that a simulation model is needed to predict the evolution of pore-water chemistry, including pH, in a covered-tailings system. The envisioned model would incorporate oxygen transport (diffusion/advection), pyrite oxidation, equilibrium chemical speciation for acid base reactions in solution and pore-water movement to derive the resultant pore-water chemistry below the active pyrite-oxidation-zone. This computer-based model would then be used to study the sensitivity of pH to variations in cover-layer parameters. The results of such a model would indicate the theoretical limits for such parameters as oxygen diffusion and alkalinity concentrations needed to maintain neutral pH conditions in the tailings pore water.

LIST OF TABLES

Table 1: A summary of the pyrite oxidation experiments that were conducted during the 1982-83 contract period.

Table 2: The treatment times and sulphate results obtained in the ultrasonic treatment experiment.

Table 3: A summary of the treatments and results in the pyrite washing experiment.

Table 4: The pyrite mesh sizes, negative pore pressures and a summary of experimental conditions assigned to the units in the surface-area experiment (PYROX2).

Table 5: A summary of particle diameters and oxidation rates for the surface area experiment.

Table 6: A summary of the column packing results and the experimental conditions assigned to the oxygen-concentration experiment (PYROX3).

Table 7: The measured oxygen concentrations and the observed oxidation rates for the oxygen-concentration experiment.

Table 8: A summary of oxygen concentrations of gas samples taken from the influent and effluent lines connected to the unsaturated columns in the oxygen-concentration experiment (taken March 2, 1983).

Table 9: A summary of results for the temperature-dependence experiment.

Table 10: The oxygen concentrations of gas samples representing influent, effluent, reservoir head-space and column gas of the unsaturated columns used in the oxygen-concentration experiment (taken May 5, 1983).

Table 11: A summary of pyrite oxidation rates estimated from data reported in the literature.

LIST OF FIGURES

Fig. 1: A schematic cross-section of the ASTM porous-plate funnel. (1)-Glass wall; (2)-Scintered glass (porous) plate; (3)-Effluent solution space.

Fig. 2: A schematic diagram of the moisture-suction-cup and stainless steel coil. (1)-Cylindrical wall; (2)-Membrane; (3)-Stainless steel screens; (4) Rubber O-ring seal; (5)-Bottom plate; (6)-Effluent port; (7)-Flushing port.

Fig. 3: A schematic diagram of the unsaturated column. (1)-Top end plate; (2)-Influent port; (3) Flushing port; (4)-Tightening bolt; (5)-Stainless steel screens; (6)-Top end-plate membrane; (7)-Perforated center tube; (8)-Perforated inner sleeve; (9)-Tensionmeter; (10)-Outer wall; (11)-Annular air space; (12)-O-ring seal; (13)-Bottom end-plate membrane; (14)-Bottom end-plate; (15)-Flushing port; (16) Effluent port; (17)-Gas exit port.

Fig. 4: A schematic diagram of the syringe-column device.

Fig. 5: A diagramatic representation of the experimental system used for the preliminary study (PYROX1).

Fig. 6: A plot of accumulated sulphate leached from each pyritic sample versus time for the preliminary experiment (PYROX1).

Fig. 7: A plot of the rate of sulphate leached (per day) versus time for each unit in the preliminary experiment (PYROX1). (a) PYROX1-1; (b) PYROX1-2; (c) PYROX1-3; (d) PYROX1-4.

Fig. 8: A diagramatic representation of the experimental system used for the surface area study (PYROX2).

Fig. 9: A plot of accumulated sulphate leached from each pyritic sample versus time for the surface area experiment (PYROX2).

Fig. 10: The rate of sulphate leached (per day) is plotted against time for each unit in the surface-area experiment (PYROX2). (a) -230+325 mesh; (b) -170+230 mesh; (c) -120+170 mesh; (d) -80+120 mesh; (e) -60+80 mesh.

Fig. 11: The oxidation rate (rate of sulphate leached) is plotted against the inverse of the particle diameter that is an estimate of surface area.

Fig. 12: A diagramatic representation of the experimental system used for the oxygen-concentration study (PYROX3).

Fig. 13: A plot of accumulated sulphate leached from the pyritic sand in each column versus time for the oxygen-concentration experiment (PYROX3).

Fig. 14: The rate of sulphate leached (per day) is plotted against time for each unit in the oxygen-concentration experiment (PYROX3). (a) 0.01% O_2; (b) 0.10% O_2; (c) 1.0% O_2; (d) 5.0% O_2; (e) 20.% O_2.

Fig. 15: The oxidation rate (rate of sulphate leached) is plotted against the percent oxygen concentration on log-log axes.

Fig. 16: A plot of accumulated sulphate leached from the two pyritic samples versus time for the temperature-dependence experiment (PYROX4).

Fig. 17: The rate of sulphate leached (per day) is plotted against time for the two units in the temperature-dependence experiment (PYROX4).

Fig. 18: The log of oxidation rate is plotted against the inverse of absolute temperature for the temperature-dependence experiment (PYROX4). The data point representing 25°C corresponds to the PYROX2-3 unit.

Fig. 19: A plot of accumulated sulphate leached from each granular pyrite sample versus time for the pyrite-type experiment (PYROX5). (a) Elliot Lake - pyrite concentrate; (b) Peru-1; (c) Peru-2; (d) Arizona; (e) Colorado; (f) Siberia.

Fig. 20: The rate of sulphate leached (per day) is plotted against time for each pair of units in the pyrite-type experiment (PYROX5).

Fig. 21: The oxidation rate plotted against effluent weight (per day) for the units corresponding to the preliminary experiment (PYROX1). (a) PYROX1-1; (b) PYROX1-2; (c) PYROX1-3; (d) PYROX1-4.

TABLES IN CHAPTER 2

Table 1: A summary of the pyrite oxidation experiments that were conducted during the 1982-83 contract period.

Experimental Designation	No. of Units	Variable Investigated	Range of Values	Experimental Apparatus
PYROX1	4	Preliminary-Magnitude of Oxidation Rates	---	Moisture-Drainage Cups (ASTM)
PYROX2	5	Grain size (Surface Area)	215 to 54 micron particle diameter	Moisture-Suction Devices
PYROX3	5	Oxygen Concentration	0.01 to 20.0%	Unsaturated Columns
PYROX4	3	Temperature	4^0, 15^0 and 25^0C	Moisture-Suction Devices
PYROX5	12	Pyrite Variety	6 types	Column-Syringe Devices

Table 2: The treatment times and sulphate results obtained in the ultrasonic treatment experiment.

Experimental Unit	Treatment Time (min)	SO_4^{2-} (mg/L)
UST1	0	16
UST2	1	26
UST3	2	39
UST4	5	48
UST5	15	82

Table 3: A summary of treatments and results in the pyrite washing experiment.

Experimental Unit	Treatment*	Rinse	SO_4^{2-} (mg/L)
W1a	1-5 min	Acetone	27.0
W1b	1-30 min	Acetone	26.8
W1c	1-2h	Water	30.0
W1d	1-2h	Acetone	28.6
W2a	2-5 min	Acetone	25.2
W2b	2-30 min	Acetone	18.2
W2c	2-2h	Water	20.0
W2d	2-2h	Acetone	14.7
W3a	3	Acetone	32.6
W3b	3	Water	27.2

*1 = H_2O_2 + HCl - reaction time
2 = H_2O_2 + NaOH - reaction time
3 = H_2O wash only

Table 4: The pyrite mesh sizes, negative pore pressures and a summary of experimental conditions assigned to the units in the surface-area experiment (PYROX2).

Experimental Unit	Grain Size (Mesh)	Head (cm water)
PYROX2-1	-120 + 325	-195
PYROX2-2	-170 + 230	-160
PYROX2-3	-120 + 170	- 95
PYROX2-4	-80 + 120	- 60
PYROX2-5	-60 + 80	- 45

Approximate Moisture Content : 0.2
Influent Solution: 5 mmol/L $NaHCO_3$
Gas Phase: 20% O_2, 1.0% CO_2, balance N_2
Temperature: 25°C
Start Date: December 1, 1982 (1600 hrs)

Table 5: A summary of particle diameters and oxidation rates for the surface area experiment.

Unit	Particle Diameter (d) (microns)	1/d $(\times 10^3)$	Oxidation Rate (mg-SO_4 $d^{-1}g^{-1}$)
PYROX2-1	54	18.5	0.48
PYROX2-2	76	13.1	0.41
PYROX2-3	108	9.3	0.32
PYROX2-4	153	6.5	0.25
PYROX2-5	215	4.7	0.19

Slope = 0.52
r = 0.999

Table 6: A summary of the column packing results and the experimental conditions assigned to the oxygen-concentratin experiment (PYROX3).

Experimental Unit	Sand Wt (g)	Sand Ht (cm)	Bulk Dens. (g/cm^3)	Oxygen Content (%)
PYROX3-1	891.9	10.5	1.56	0.01
PYROX3-2	878.9	10.3	1.57	0.10
PYROX3-3	905.7	10.5	1.59	1.0
PYROX3-4	888.6	10.5	1.56	5.0
PYROX3-5	908.8	10.7	1.56	20.

Influent Solution: 5mmol/L $NaHCO_3$
Gas Phase Balance: 0.5 % CO_2, bal. N_2
Grain Size: -120+170 mesh
Weight of Pyrite: 40.0 g
Gas Flow Rates: 1800 ml/h
Temperature: 25°C

Table 7: The measured oxygen concentrations and the observed oxidation rates for the oxygen-concentration experiment.

Experimental Unit	Oxygen Conc. (%)	Rate* ($mg\text{-}SO_4 d^{-1} g^{-1}$)
PYROX3-1	0.02	0.016
PYROX3-2	0.10	0.022
PYROX3-3	1.0	0.050
PYROX3-4	5.0	0.053
PYROX3-5	20.	0.066

*The average rate from the first twenty days' data was chosen as the representative value.

Table 8: A summary of oxygen concentrations of gas samples taken from the influent and effluent lines connected to the unsaturated columns in the oxygen-concentration experiment (taken March 2, 83).

Unit	Labelled $O_2\%$	Analysed $O_2\%$	Influent $O_2\%$	Effluent $O_2\%$
PYROX3-1	0.01	0.02	0.02	0.01
PYROX3-2	0.01	0.02	0.02	0.02
PYROX3-3	1.0	1.1	1.0	0.71
PYROX3-4	5.0	5.0	5.0	4.9
PYROX3-5	20.0	20.4	20.5	20.0

Table 9: A summary of results for the temperature-dependence experiment.

Unit	Rate ($mg-SO_4$ $d^{-1}g^{-1}$)	Temp. (^oC)	Log Rate	$1/T x 10^3$ (K^{-1})
PYROX4-1	0.018	3	-1.74	3.62
PYROX4-2	0.071	15	-1.15	3.47
PYROX2-3	0.22	25	-0.65	3.36

Y(int) = 13.4
Slope = -4177
r = -0.999

Table 10: The oxygen concentrations of gas samples representing influent, effluent, reservoir head-space and column gas of the unsaturated columns used in the oxygen-concentration experiment (taken May 5, 83).

Unit	Influent $O_2\%$	Effluent $O_2\%$	Reservoir Head Space $O_2\%$	Column* Samples $O_2\%$
PYROX3-1	0.02	0.04	0.98	Top = 1.6
PYROX3-2	0.11	0.10	0.95	
PYROX3-3	1.1	1.1	1.55	Top = 0.98 Bot = 2.3
PYROX3-4	5.1	5.3	5.4	
PYROX3-5	19.7	20.3	14.6	Top = 20.3 Bot = 18.9

*Top and Bot refer to the sample location from the upper and lower tensiometer ports respectively.

Table 11: A summary of pyrite oxidation rates estimated from data reported in the literature

Oxidation Rate ($mmol\text{-}FeS_2 h^{-1} g^{-1}$)	Experimental Conditions	pH	Source*
5×10^{-4}	-Soil Samples Calcite Buffered	7-8 (?)	(1)
3×10^{-2}	-Soil Samples Sterile/Innoculated	4	(1)
5×10^{-4}	-Unknown rough calculation sterile	1	(2)
2×10^{-2}	-Bacteria	(Low)	(2)
1×10^{-2}	-Crushed Pyrite $<$44 microns at 30°C	9	(3)
1×10^{-3}	-Crushed Pyrite $<$44 microns at 30°C	6.5	(3)
2×10^{-3}	-Crushed Pyrite $<$90 microns	2	(4)
3×10^{-4}	-Crushed Pyrite $<$90 microns	8	(4)
2×10^{-6}	-Sulphur Ball Pyrite 100% O_2 Atm.	8	(5)
2×10^{-6}	-Pyritic Tailings based on H^+ mass balance Acidic/Bacteria probable	(Low)	(6)

* (1) = Arkestyn (1980)
(2) = Van Breemen (1972)
(3) = Goldhaber (1983)
(4) = LeRoux (1980)
(5) = Shumate et al. (1971)
(6) = Snodgrass et al. (1982)

FIGURES IN CHAPTER 2

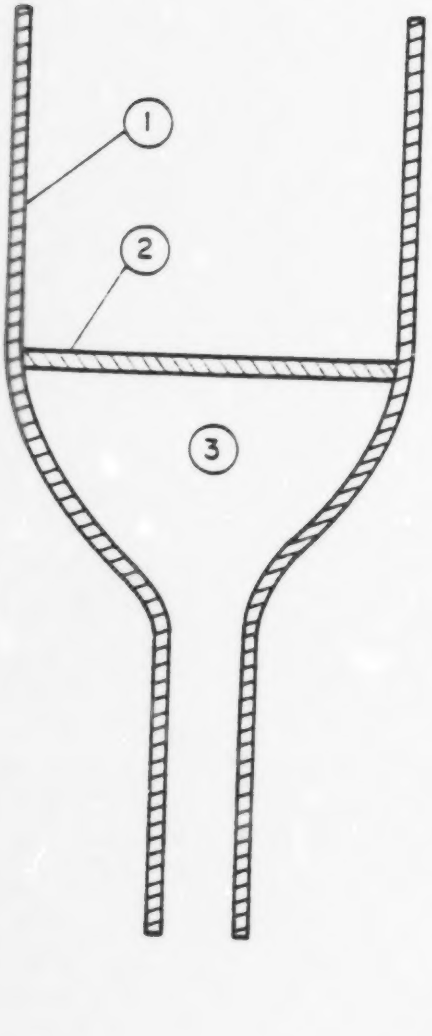

Fig. 1: A schematic cross-section of the ASTM porous-plate funnel. (1)-Glass wall; (2)-Scintered glass (porous) plate; (3)-Effluent solution space.

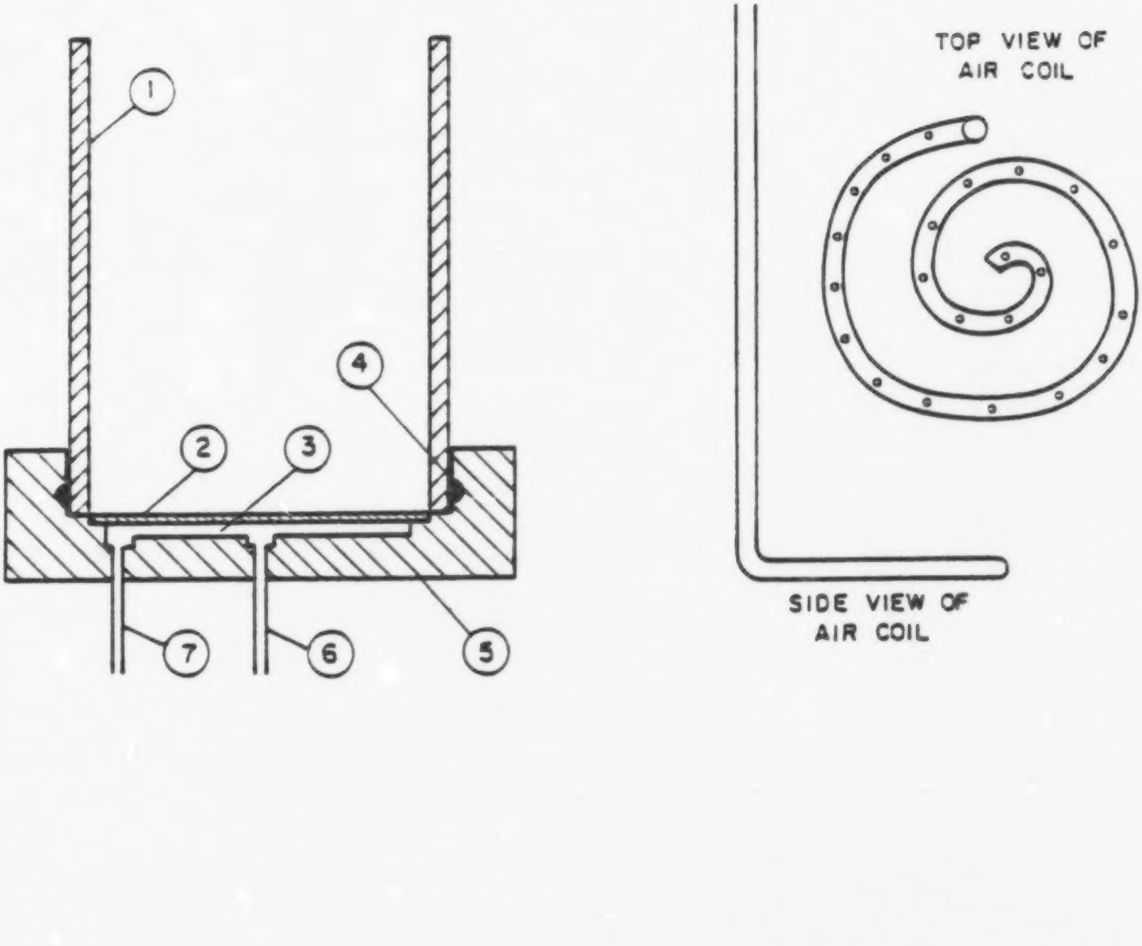
1
2
3
4
5
6
7
TOP VIEW OF AIR COIL
SIDE VIEW OF AIR COIL

Fig. 2: A schematic diagram of the moisture-suction-cup and stainless steel coil. (1)-cylindrical wall; (2)-Membrane; (3)-Stainless steel screens; (4) Rubber O-ring seal; (5)-Bottom plate; (6)-Effluent port; (7)-Flushing port.

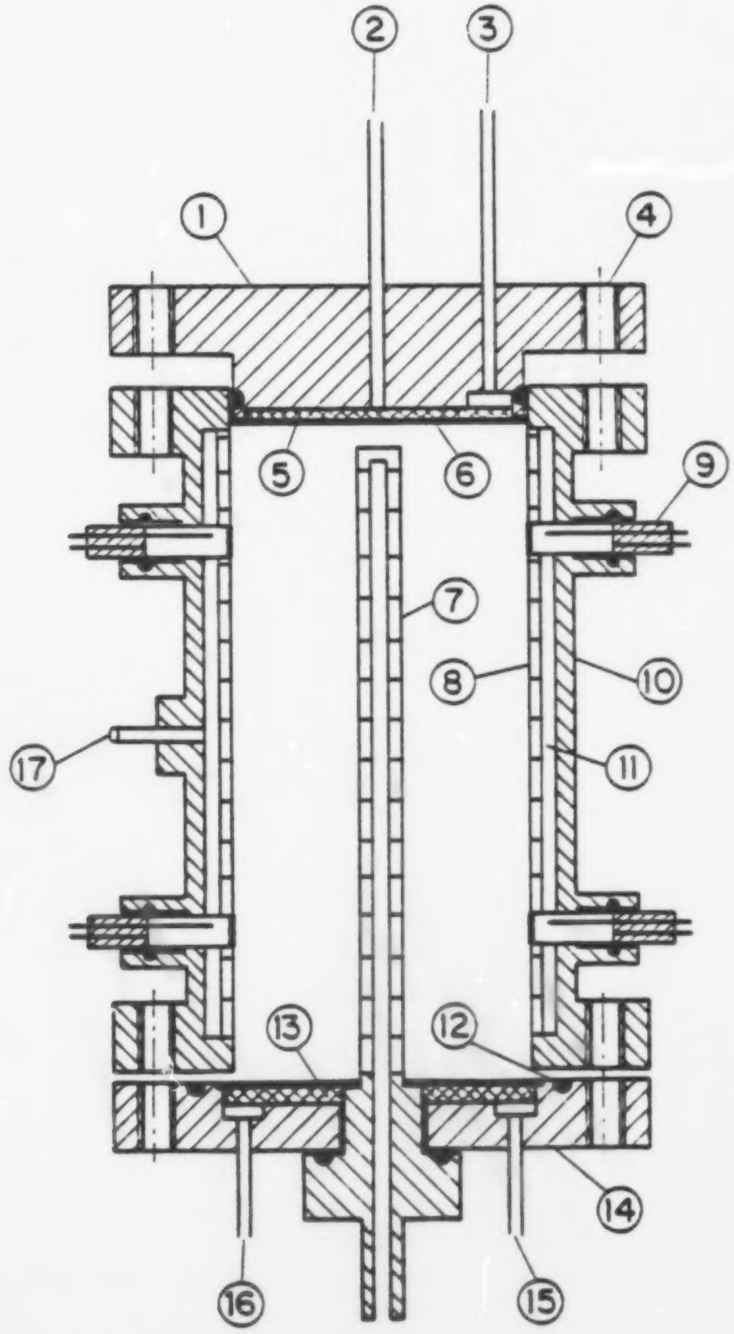

Fig. 3: A schematic diagram of the unsaturated column. (1)-Top end plate; (2)-Influent port; (3) Flushing port; (4)-Tightening bolt; (5)-Stainless steel screens; (6)-Top end-plate membrane; (7)-Perforated center tube; (8)-Perforated inner sleeve; (9)-Tensionmeter; (10)-Outer wall; (11)-Annular air space; (12)-O-ring seal; (13)-Bottom end-plate membrane; (14)-Bottom end-plate; (15)-Flushing port; (16) Effluent port; (17)-Gas

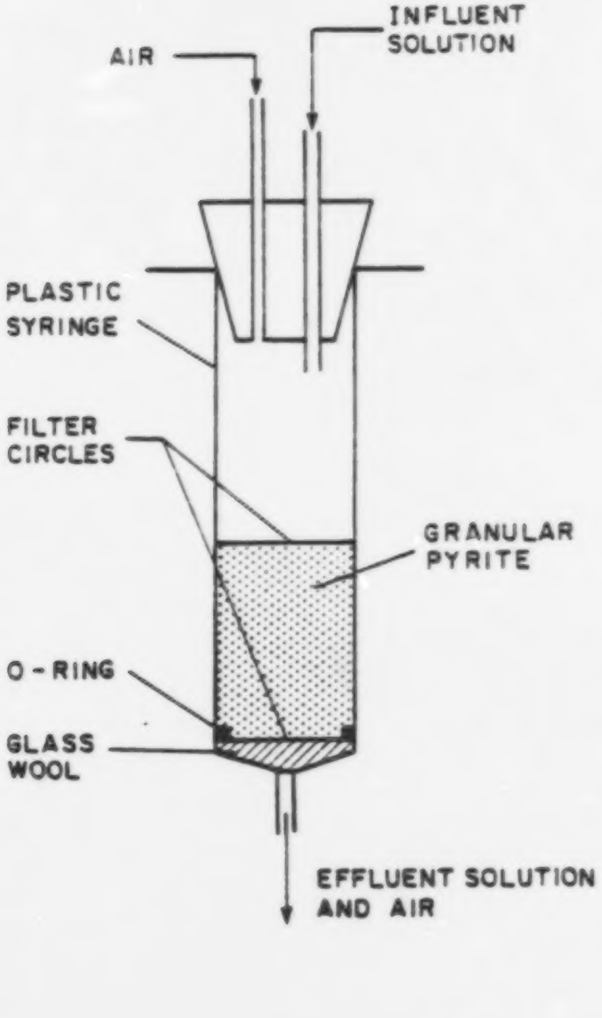
INFLUENT SOLUTION
AIR
PLASTIC SYRINGE
FILTER CIRCLES
GRANULAR PYRITE
O-RING
GLASS WOOL
EFFLUENT SOLUTION AND AIR

Fig. 4: A schematic diagram of the syringe-column device.

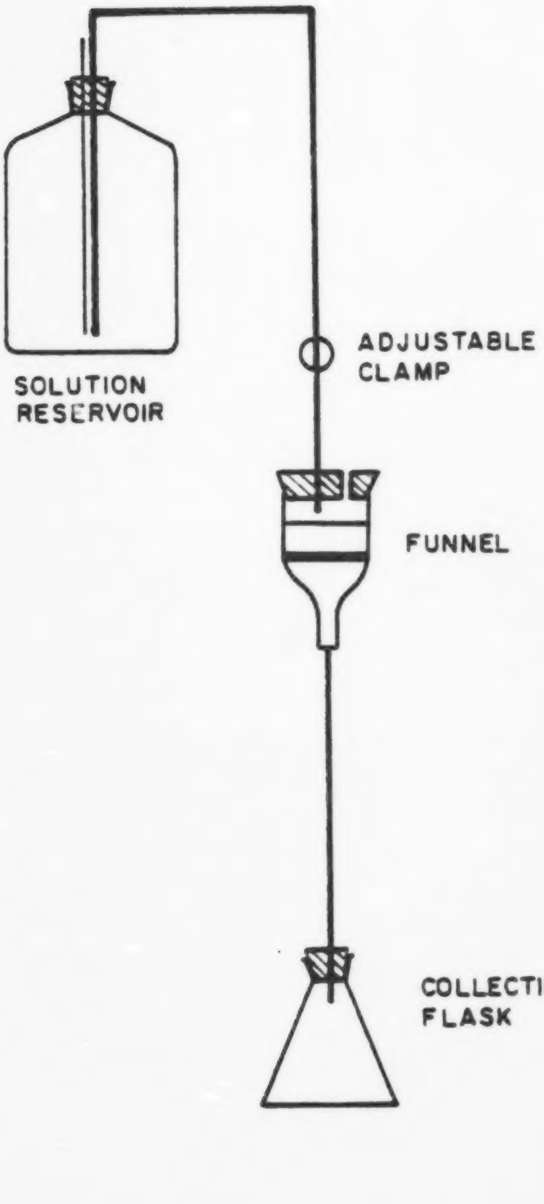
ADJUSTABLE CLAMP
SOLUTION RESERVOIR
FUNNEL
COLLECTION FLASK

Fig. 5: A diagramatic representation of the experimental system used for the preliminary study (PYROX1).

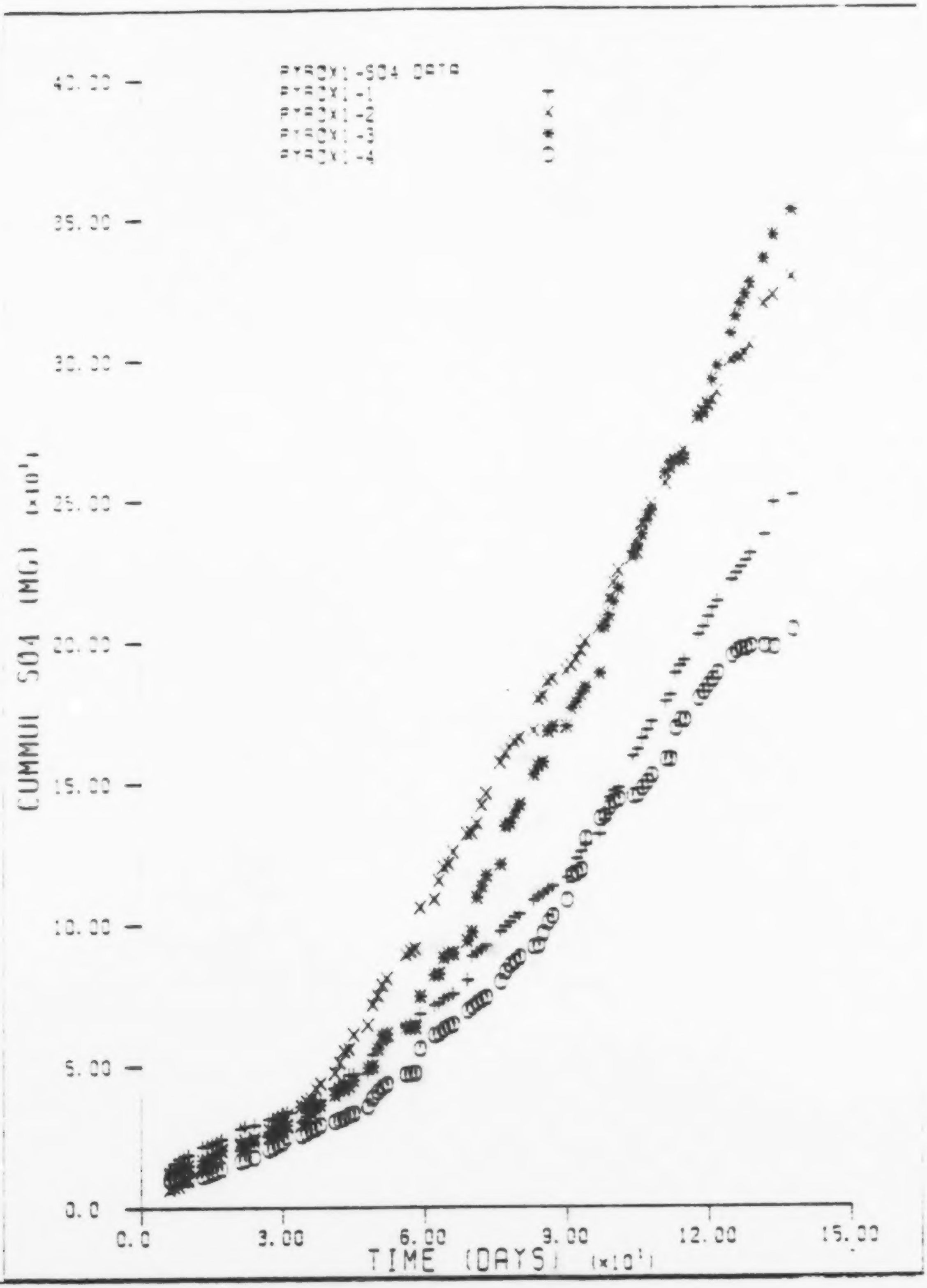

Fig. 6: A plot of accumulated sulphate leached from each pyritic sample versus time for the preliminary experiment (PYROX1).

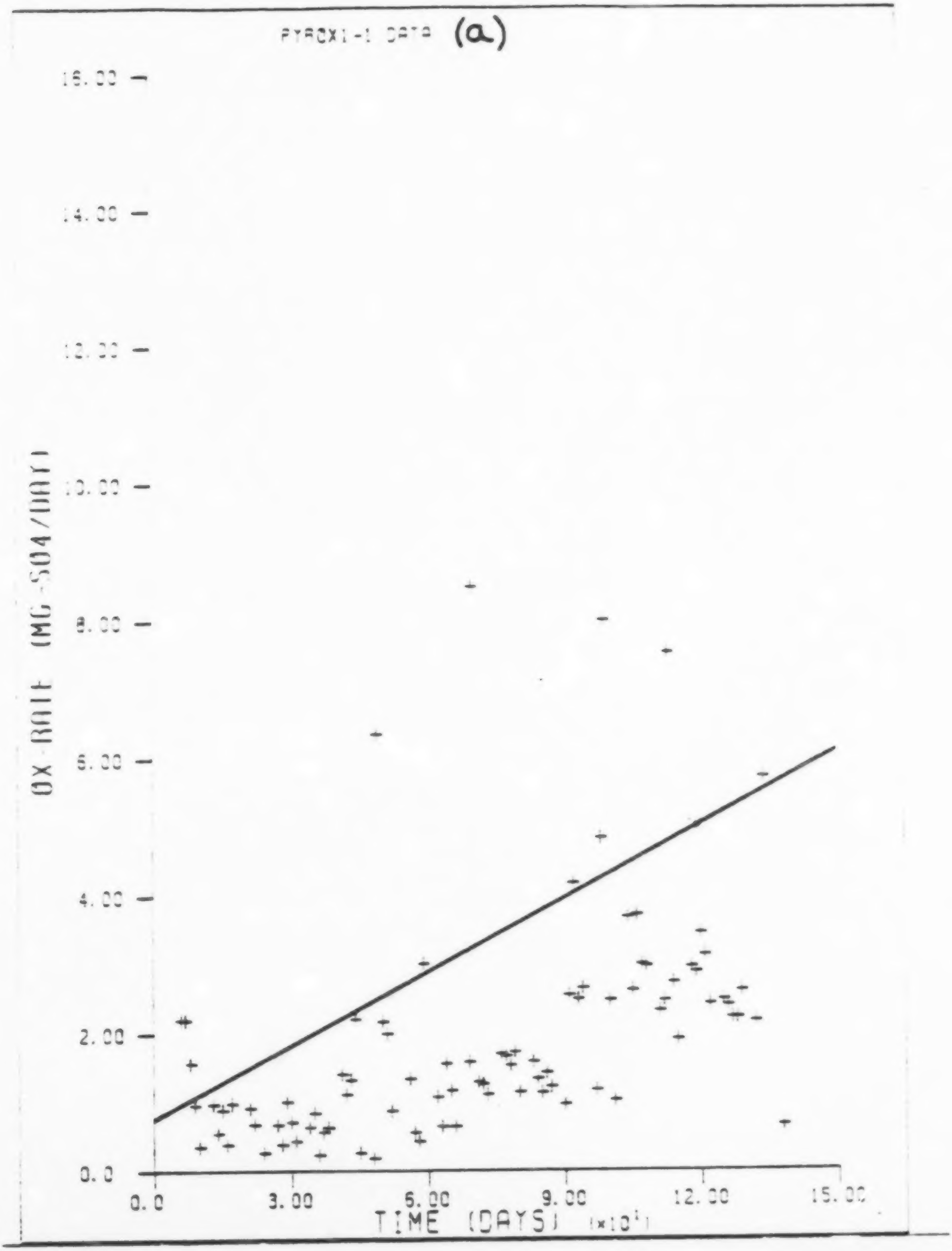

Fig. 7: A plot of the rate of sulphate leached (per day) versus time for each unit in the preliminary experiment (PYROX1). (a) PYROX1-1; (b) PYROX1-2; (c) PYROX1-3; (d) PYROX1-4.

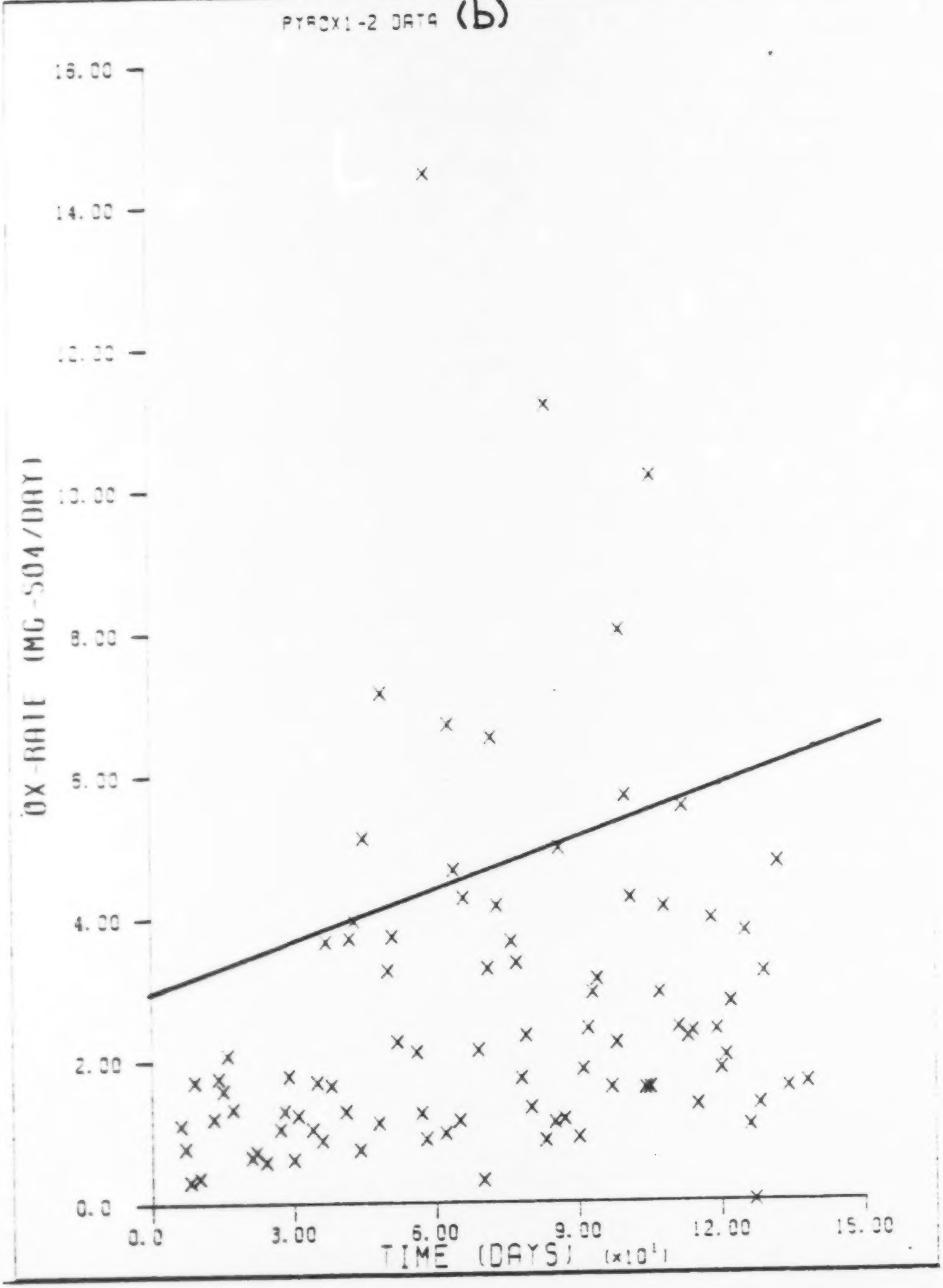
PYROX1-2 DATA (b)
OX-RATE (MG-SO4/DAY)
16.00
14.00
12.00
10.00
8.00
6.00
4.00
2.00
0.0
0.0
3.00
6.00
9.00
12.00
15.00
TIME (DAYS) (x10¹)

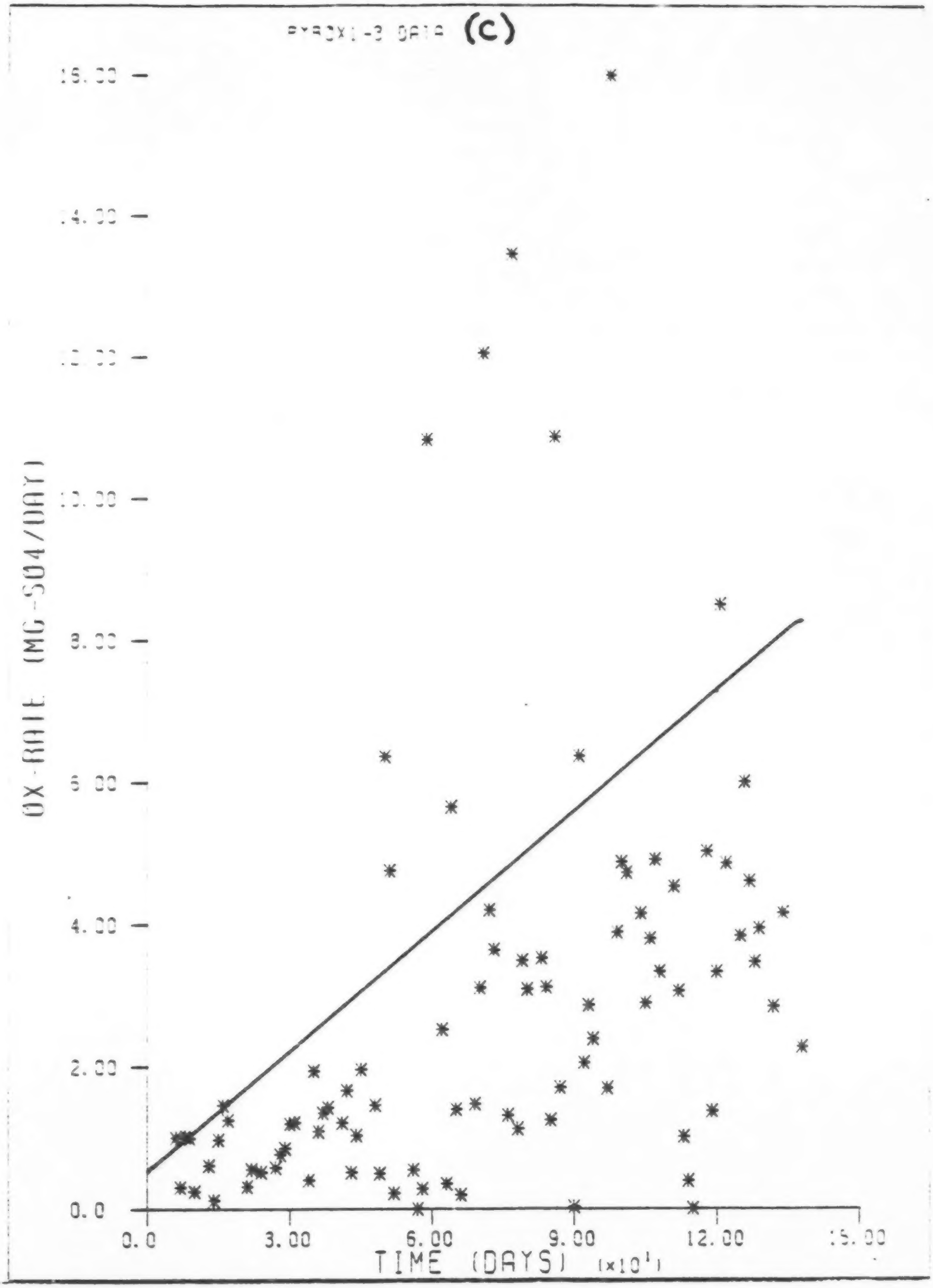
PYROXI-3 DATA (c)
OX-RATE (MG-SO4/DAY)
16.00
14.00
12.00
10.00
8.00
6.00
4.00
2.00
0.0
0.0
3.00
6.00
9.00
12.00
15.00
TIME (DAYS) (x10¹)

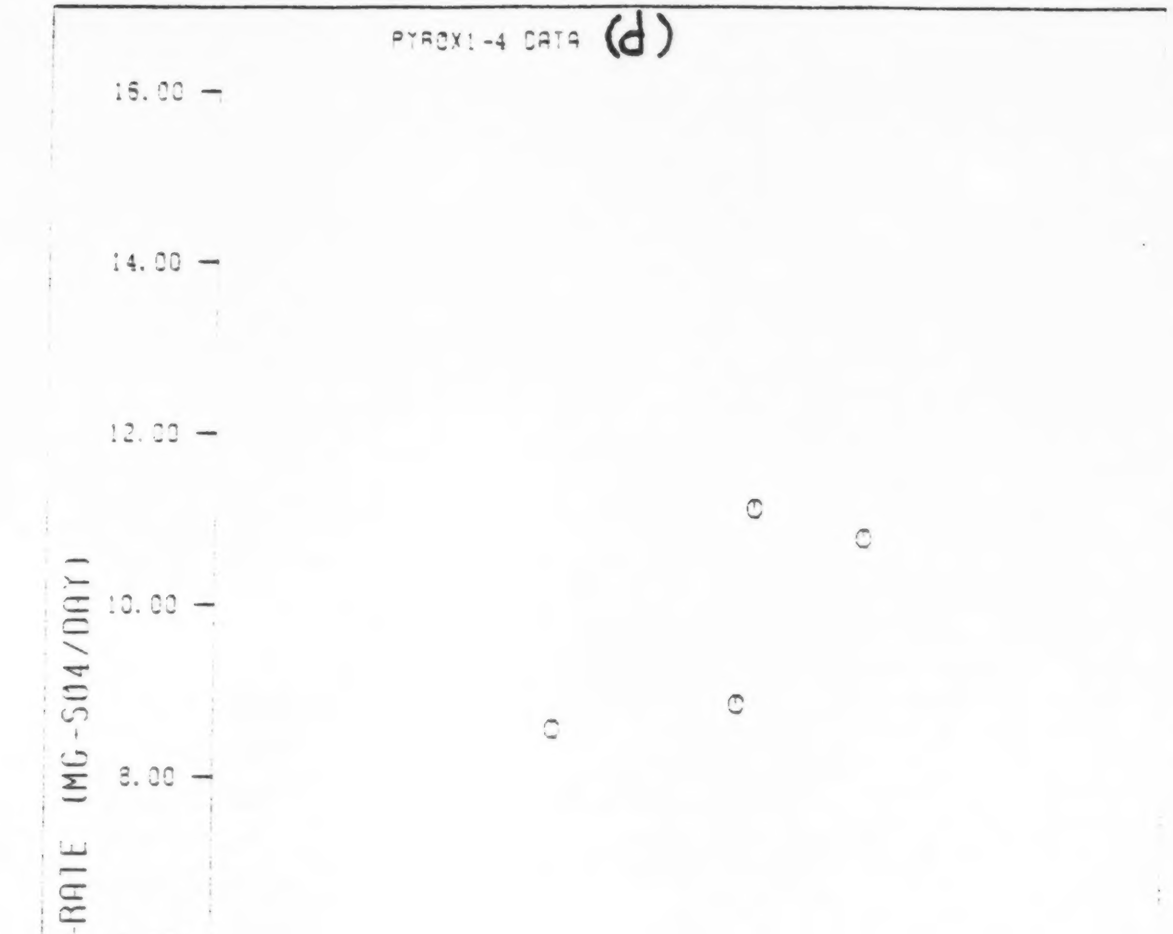
PYROX1-4 DATA
(d)
OX-RATE (MG-SO4/DAY)
16.00
14.00
12.00
10.00
8.00
6.00
4.00
2.00
0.0
0.0
3.00
6.00
9.00
12.00
15.00
TIME (DAYS) (x10¹)

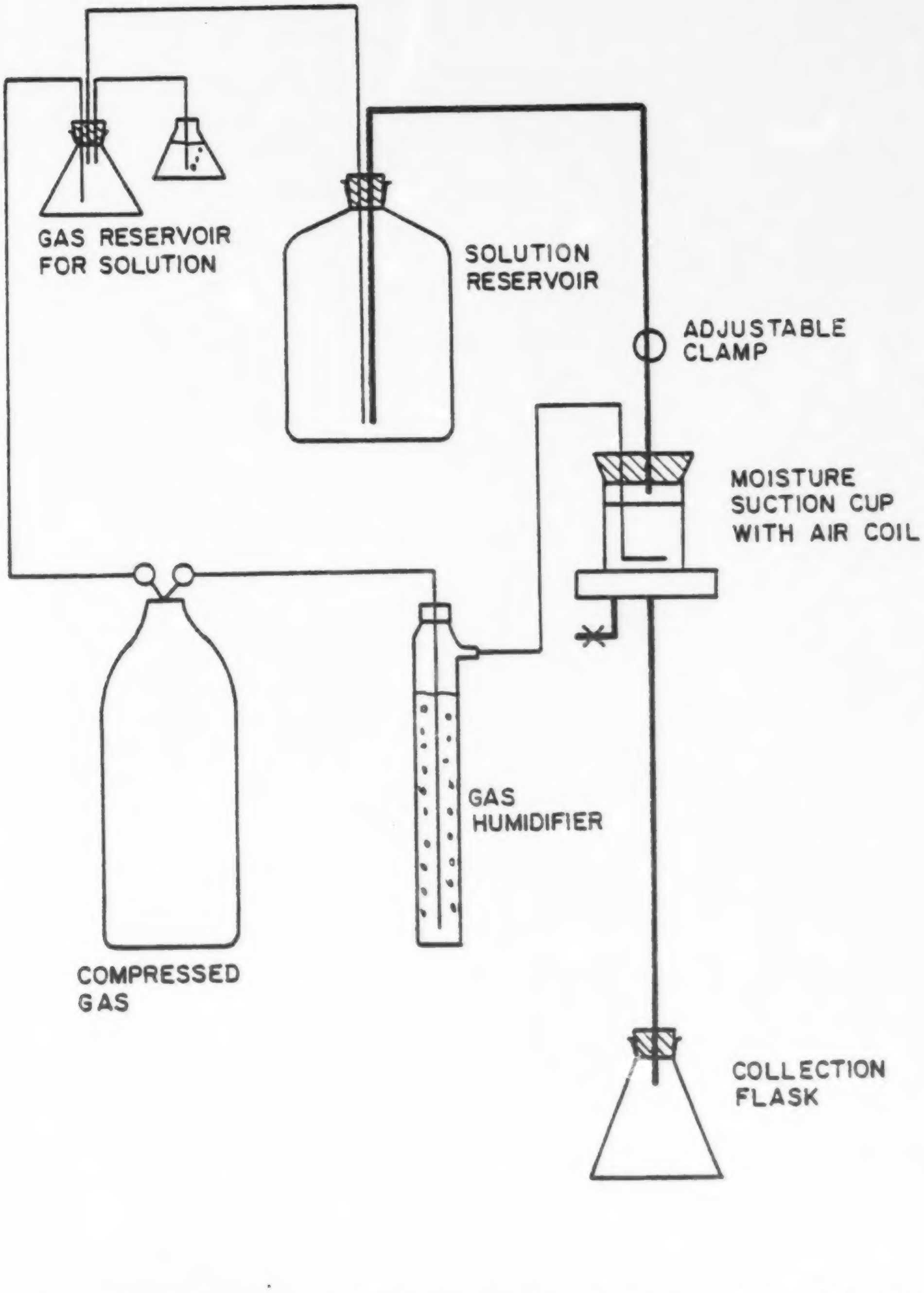
GAS RESERVOIR FOR SOLUTION
SOLUTION RESERVOIR
ADJUSTABLE CLAMP
MOISTURE SUCTION CUP WITH AIR COIL
GAS HUMIDIFIER
COMPRESSED GAS
COLLECTION FLASK

Fig. 8: A diagramatic representation of the experimental system used for the surface area study (PYROX2).

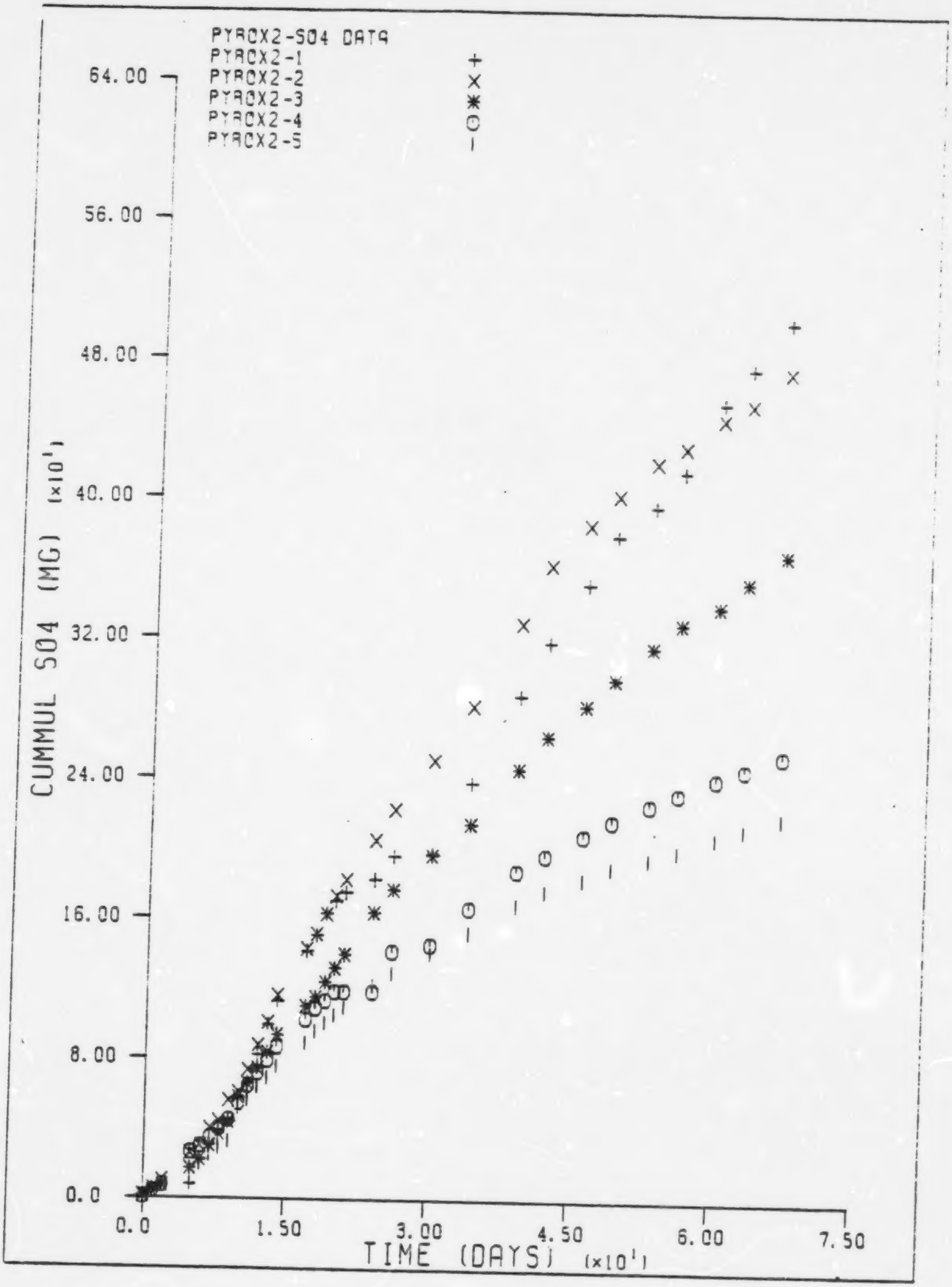

Fig. 9: A plot of accumulated sulphate leached from each pyritic sample versus time for the surface area experiment (PYROX2).

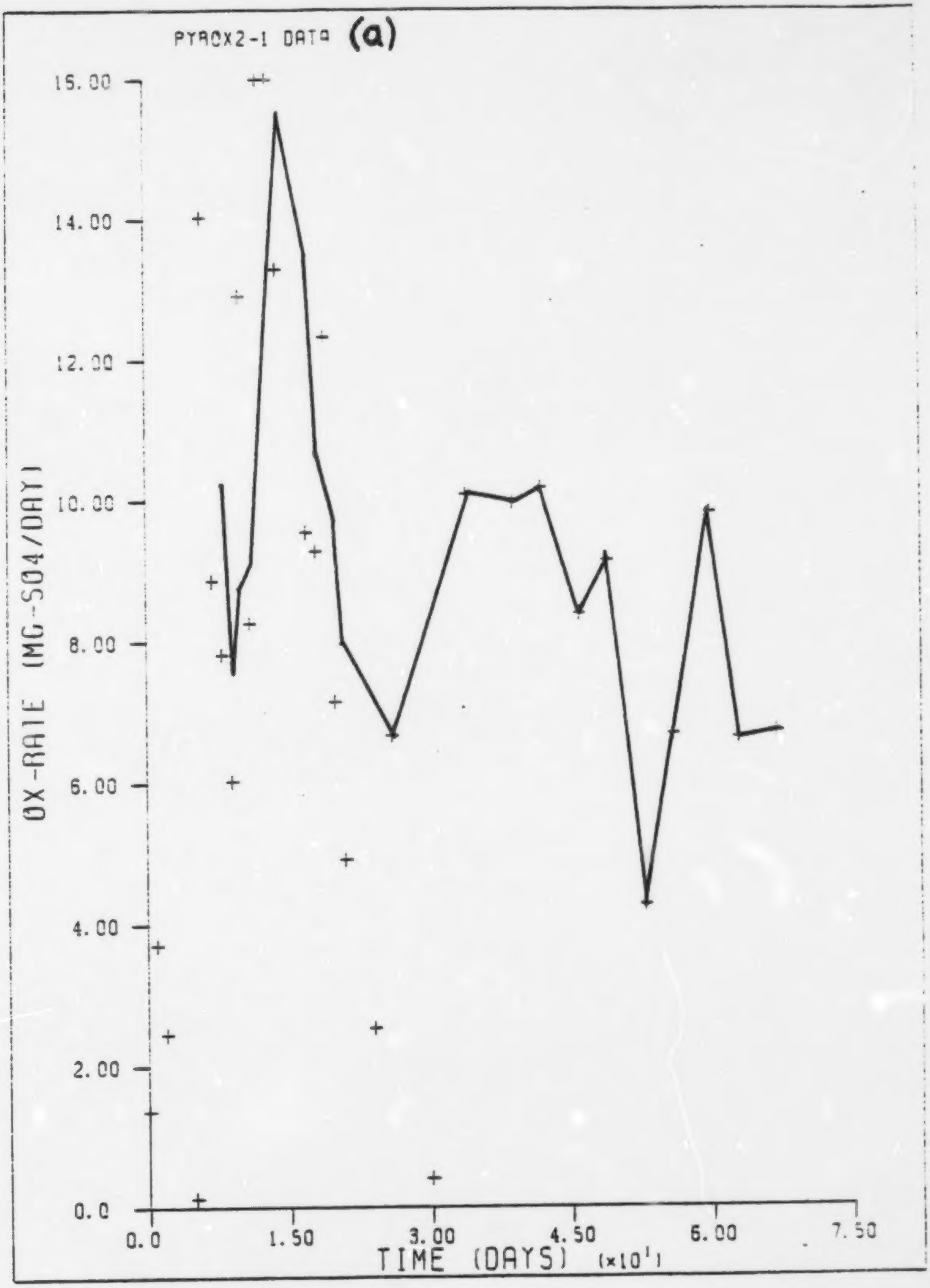

Fig. 10: The rate of sulphate leached (per day) is plotted against time for each unit in the surface-area experiment (PYROX2). (a) -230+325 mesh; (b) -170+230 mesh; (c) -120+170 mesh; (d) -80+120 mesh; (e) -60+80 mesh.

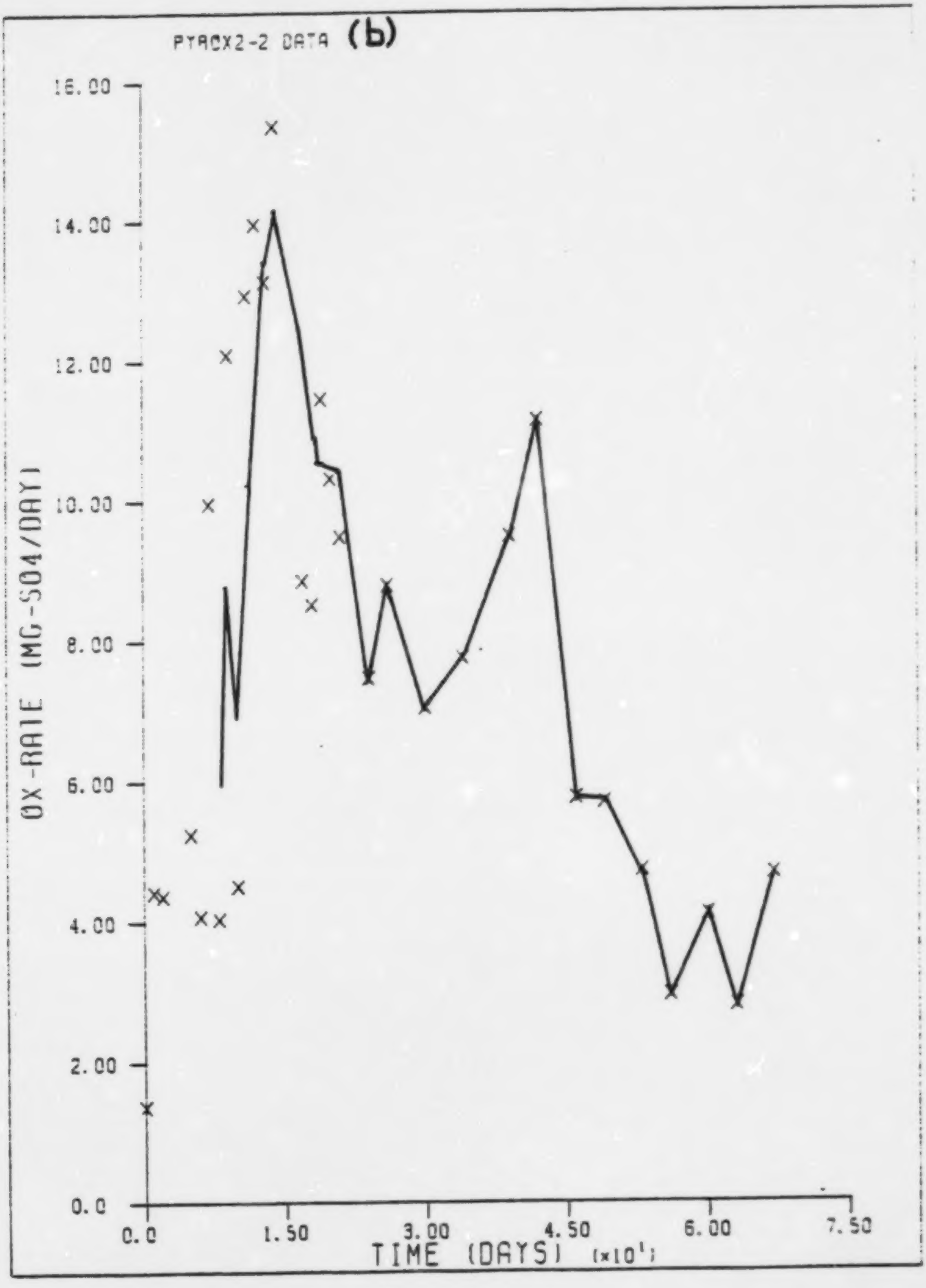
PYROX2-2 DATA
(b)
16.00
14.00
12.00
10.00
8.00
6.00
4.00
2.00
0.0
OX-RATE (MG-SO4/DAY)
0.0
1.50
3.00
4.50
6.00
7.50
TIME (DAYS) (×10¹)

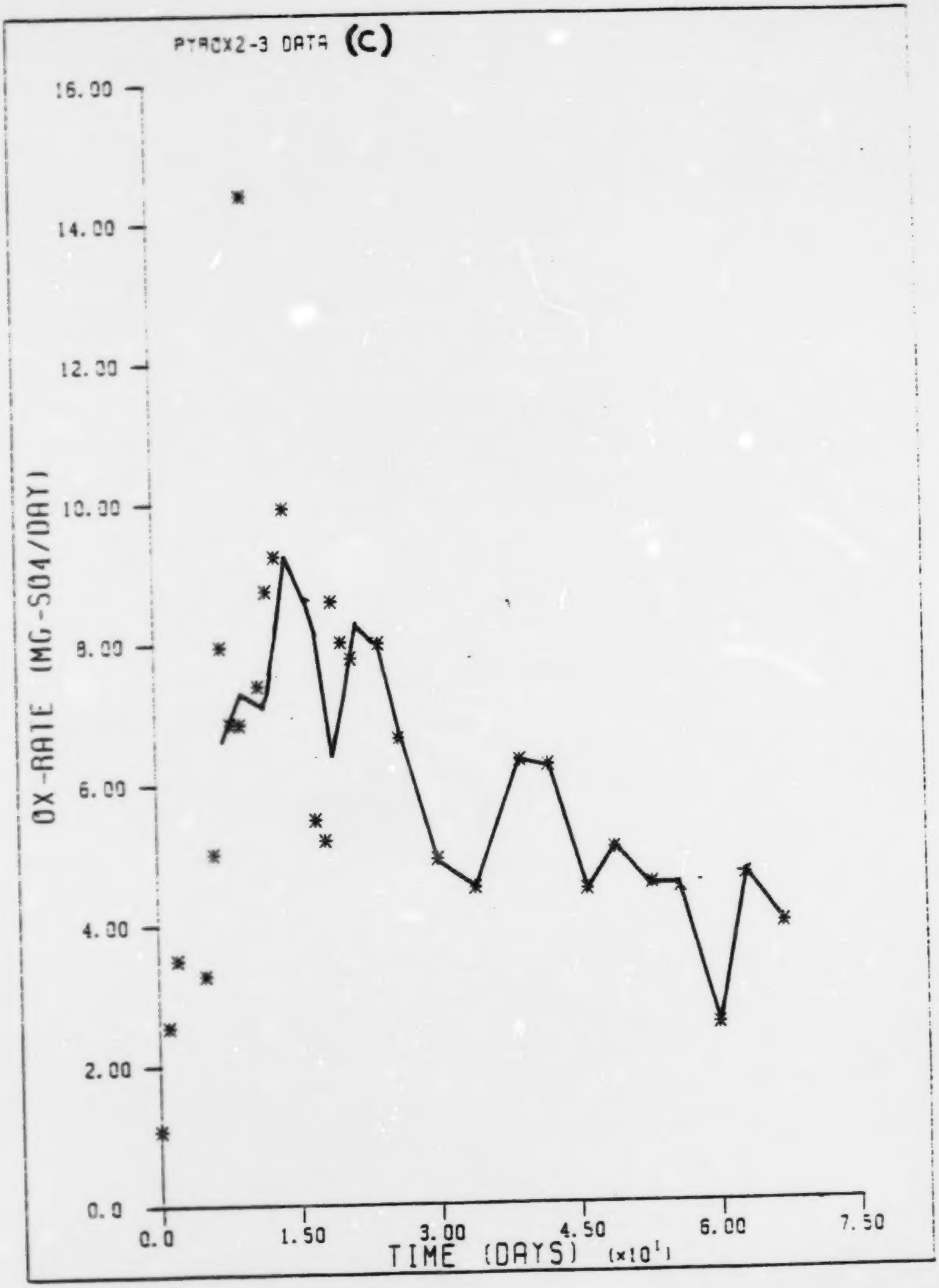
PYROX2-3 DATA (C)
OX-RATE (MG-SO4/DAY)
16.00
14.00
12.00
10.00
8.00
6.00
4.00
2.00
0.0
0.0
1.50
3.00
4.50
6.00
7.50
TIME (DAYS) (x10¹)

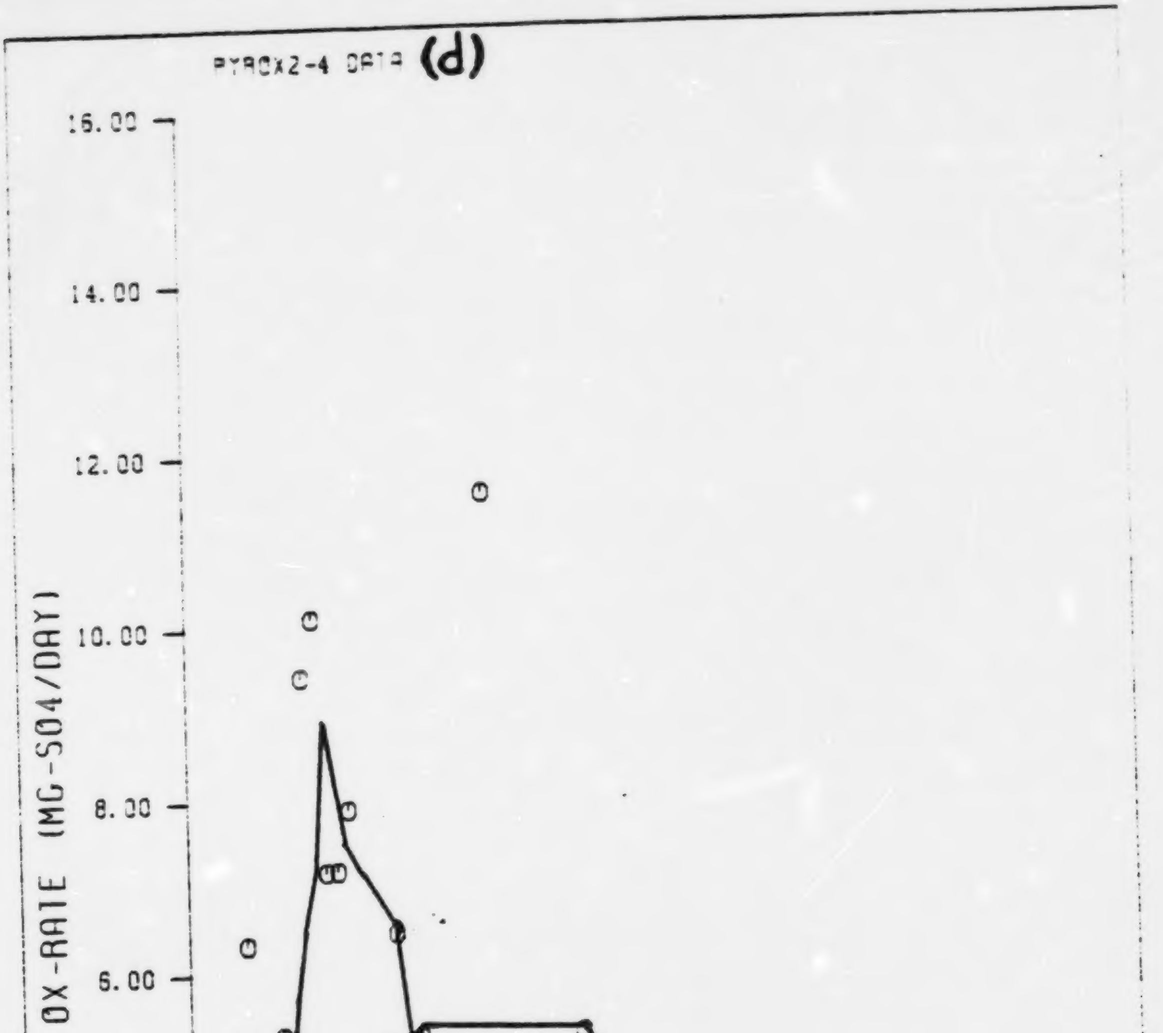
PYROX2-4 DATA (d)
OX-RATE (MG-SO4/DAY)
16.00
14.00
12.00
10.00
8.00
6.00
4.00
2.00
0.0
0.0
1.50
3.00
4.50
6.00
7.50
TIME (DAYS) (x10¹)

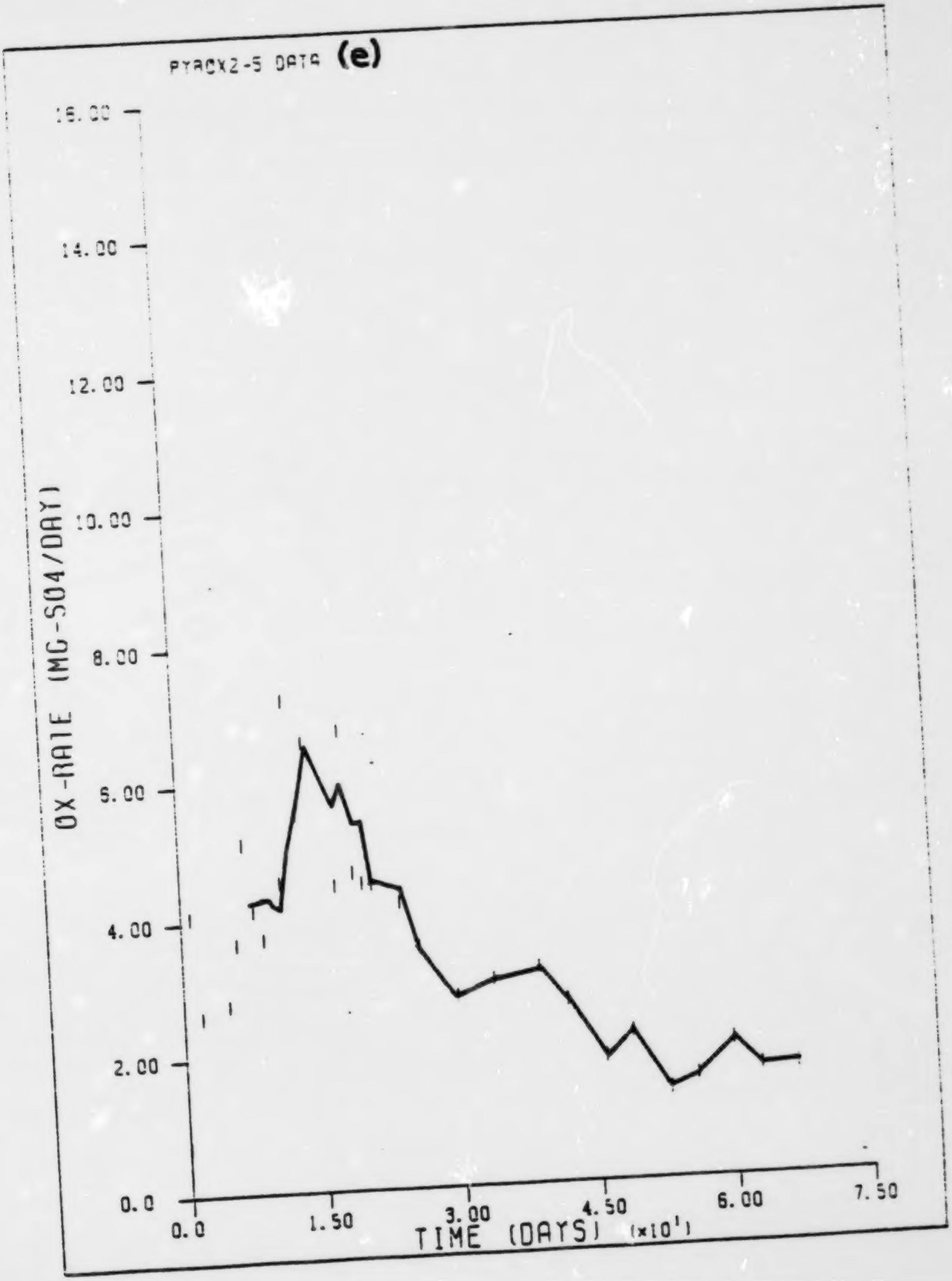
PYRCX2-5 DATA
(e)
OX-RATE (MG-SO4/DAY)
16.00
14.00
12.00
10.00
8.00
6.00
4.00
2.00
0.0
0.0
1.50
3.00
4.50
6.00
7.50
TIME (DAYS) (×10¹)

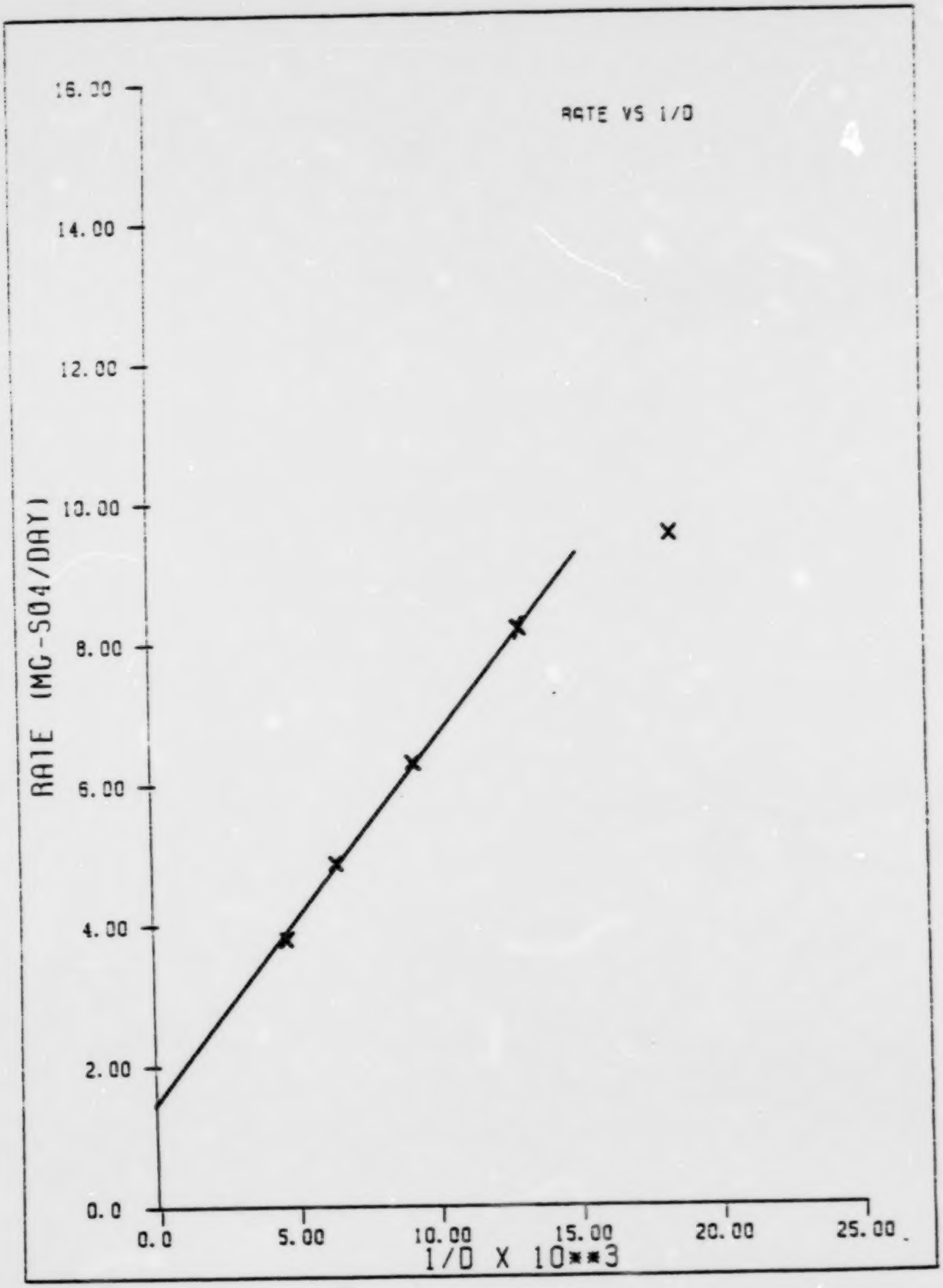

Fig. 11: The oxidation rate (rate of sulphate leached) is plotted against the inverse of the particle diameter that is an estimate of surface area.

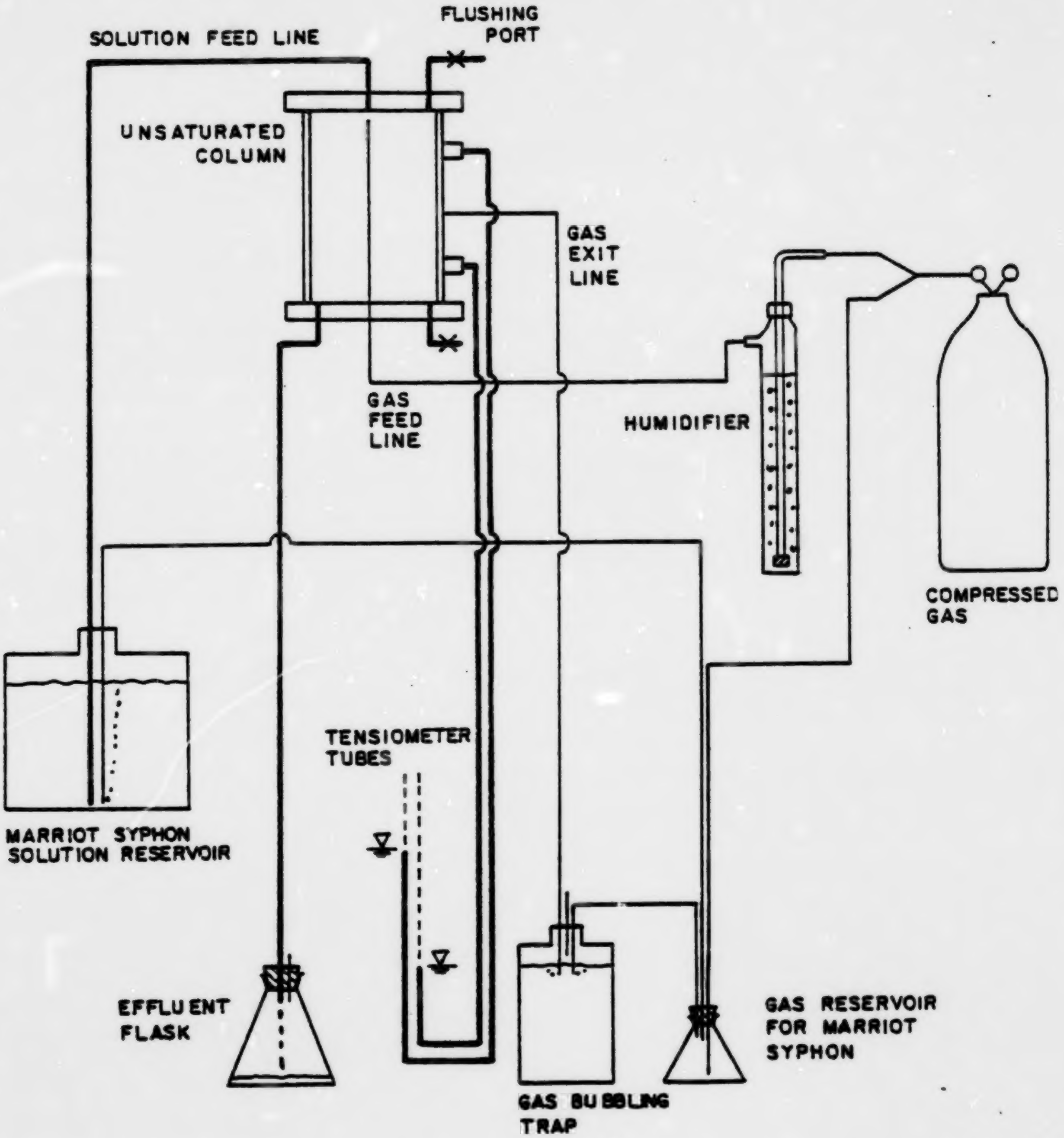
SOLUTION FEED LINE
FLUSHING PORT
UNSATURATED COLUMN
GAS EXIT LINE
GAS FEED LINE
HUMIDIFIER
COMPRESSED GAS
MARRIOT SYPHON SOLUTION RESERVOIR
TENSIOMETER TUBES
EFFLUENT FLASK
GAS BUBBLING TRAP
GAS RESERVOIR FOR MARRIOT SYPHON

Fig. 12: A diagramatic representation of the experimental system used for the oxygen-concentration study (PYROX3).

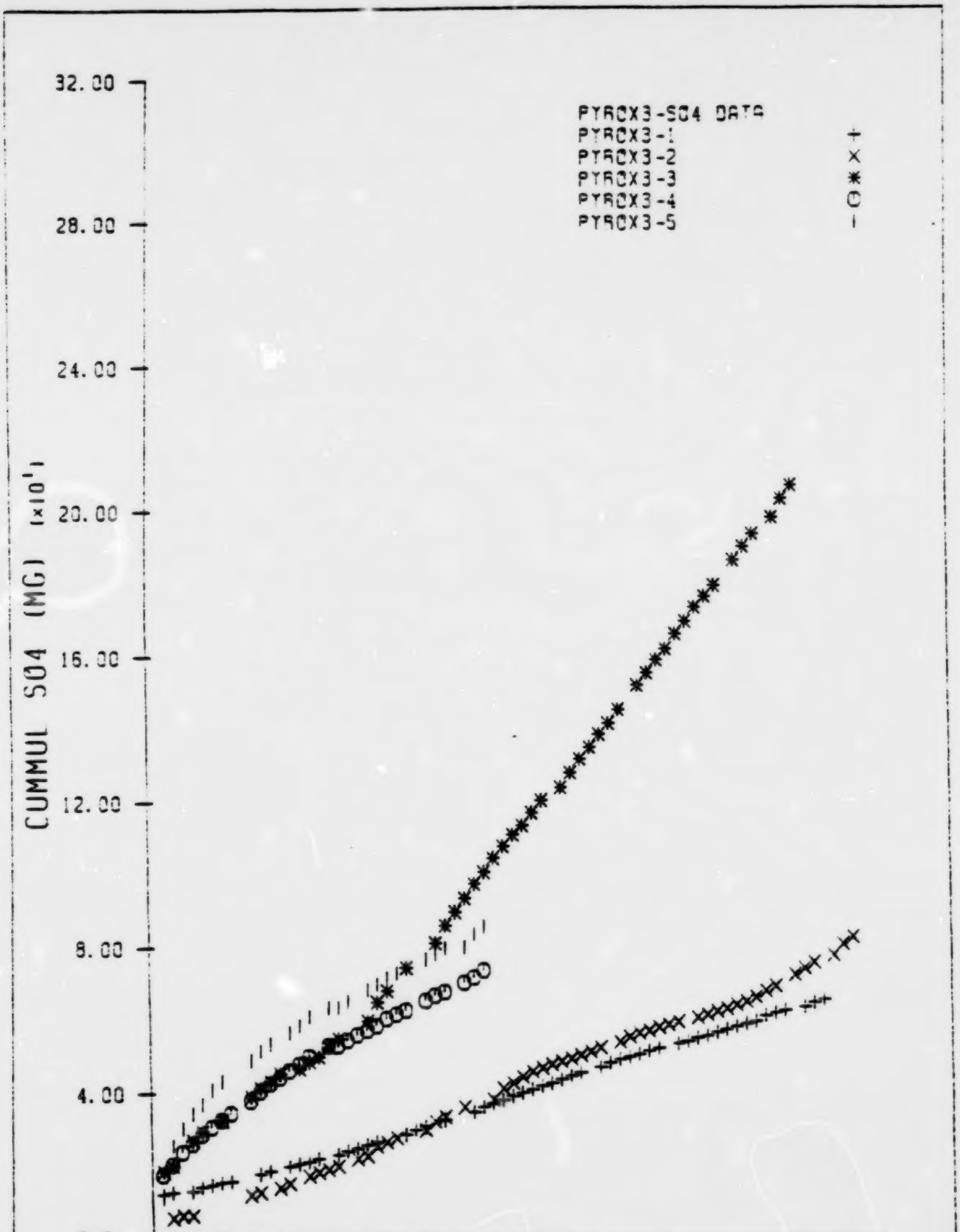

Fig. 13: A plot of accumulated sulphate leached from the pyritic sand in each column versus time for the oxygen-concentration experiment (PYROX3).

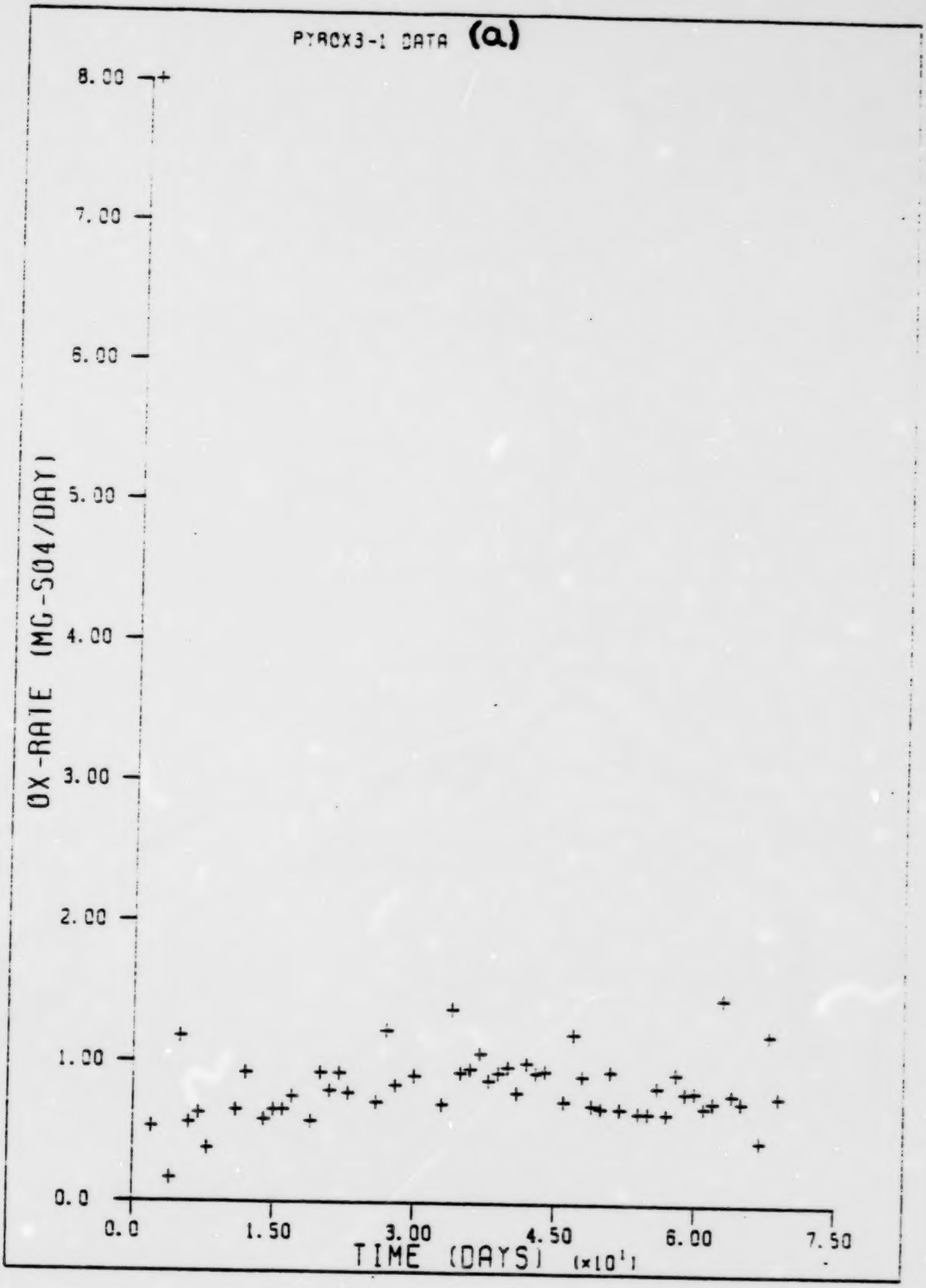

Fig. 14: The rate of sulphate leached (per day) is plotted against time for each unit in the oxygen-concentration experiment (PYROX3). (a) 0.01% O_2; (b) 0.10% O_2; (c) 1.0% O_2; (d) 5.0% O_2; (e) 20.% O_2.

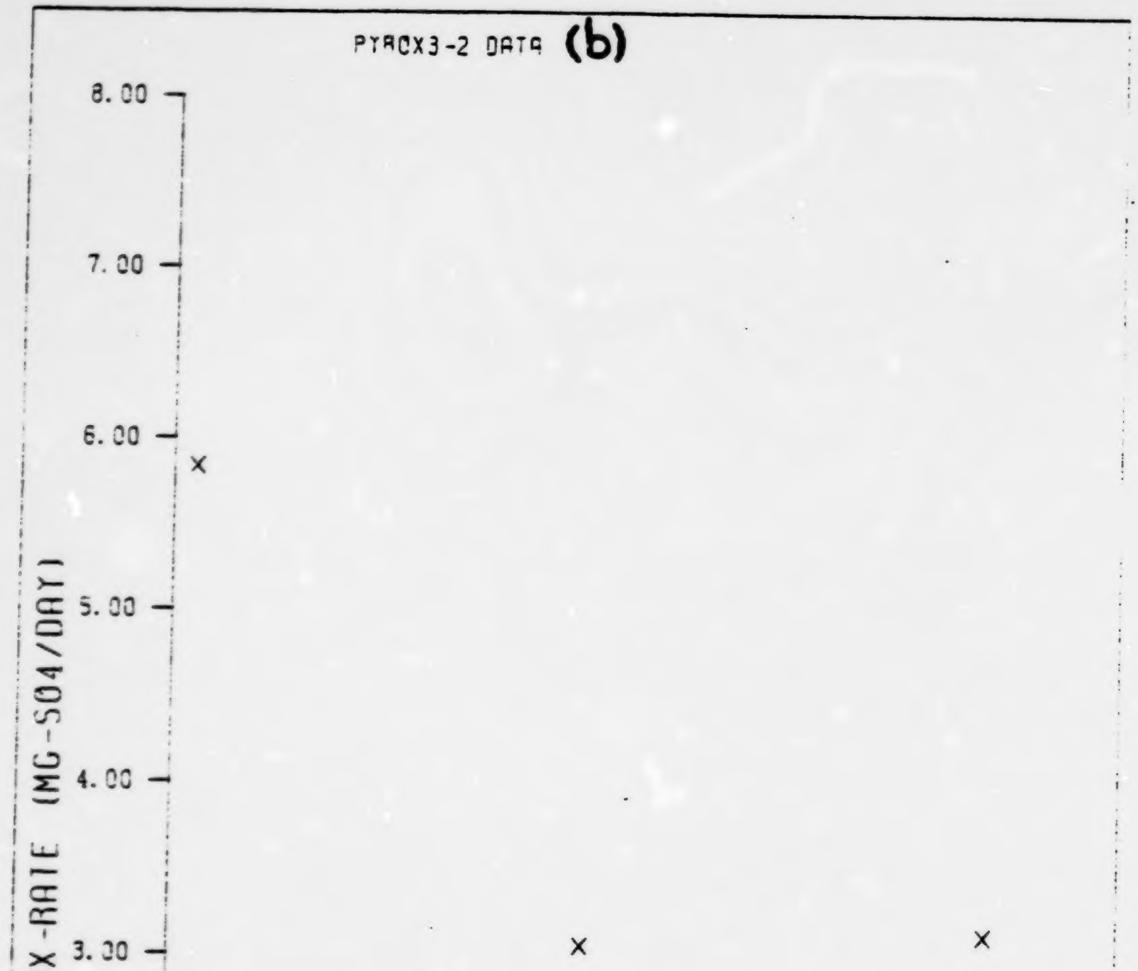
PYROX3-2 DATA (b)
8.00
7.00
6.00
5.00
4.00
3.00
2.00
1.00
0.0
OX-RATE (MG-SO4/DAY)
0.0
1.50
3.00
4.50
6.00
7.50
TIME (DAYS) (×10¹)

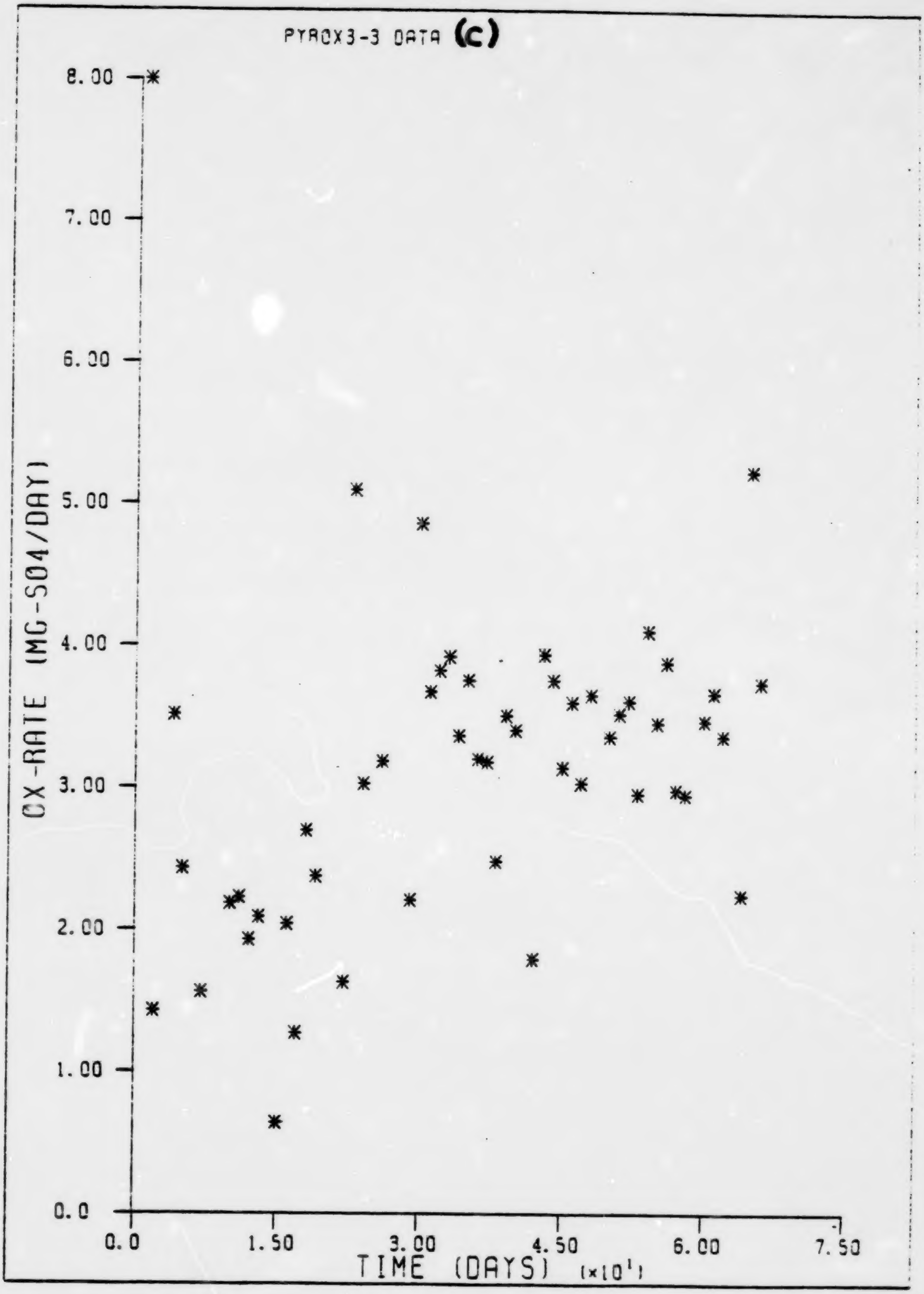
PYROX3-3 DATA (c)
OX-RATE (MG-SO4/DAY)
8.00
7.00
6.00
5.00
4.00
3.00
2.00
1.00
0.0
0.0
1.50
3.00
4.50
6.00
7.50
TIME (DAYS) (×10¹)

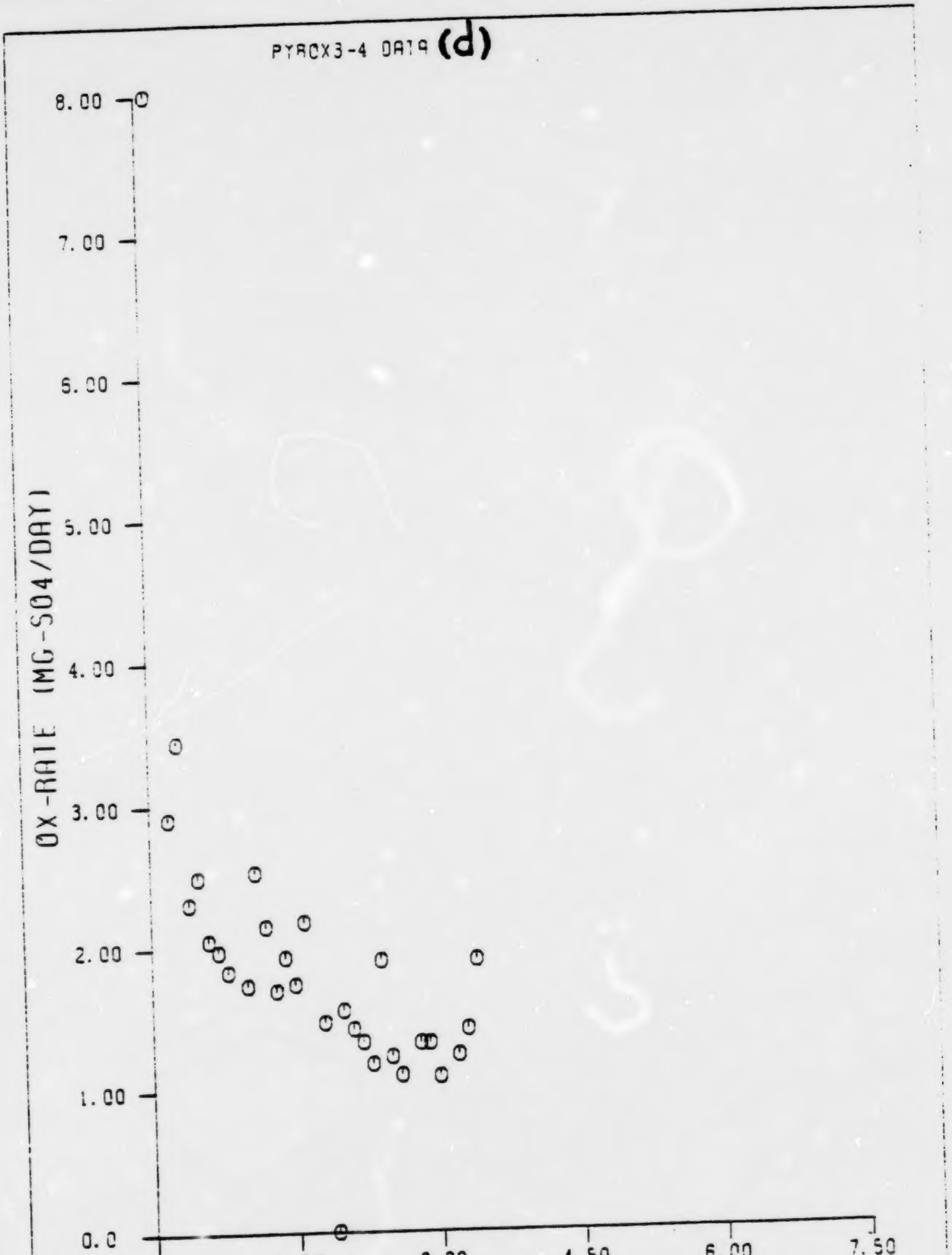
PYROX3-4 DATA (d)
8.00
7.00
6.00
5.00
4.00
3.00
2.00
1.00
0.0
OX-RATE (MG-SO4/DAY)
0.0
1.50
3.00
4.50
6.00
7.50
TIME (DAYS) (x10¹)

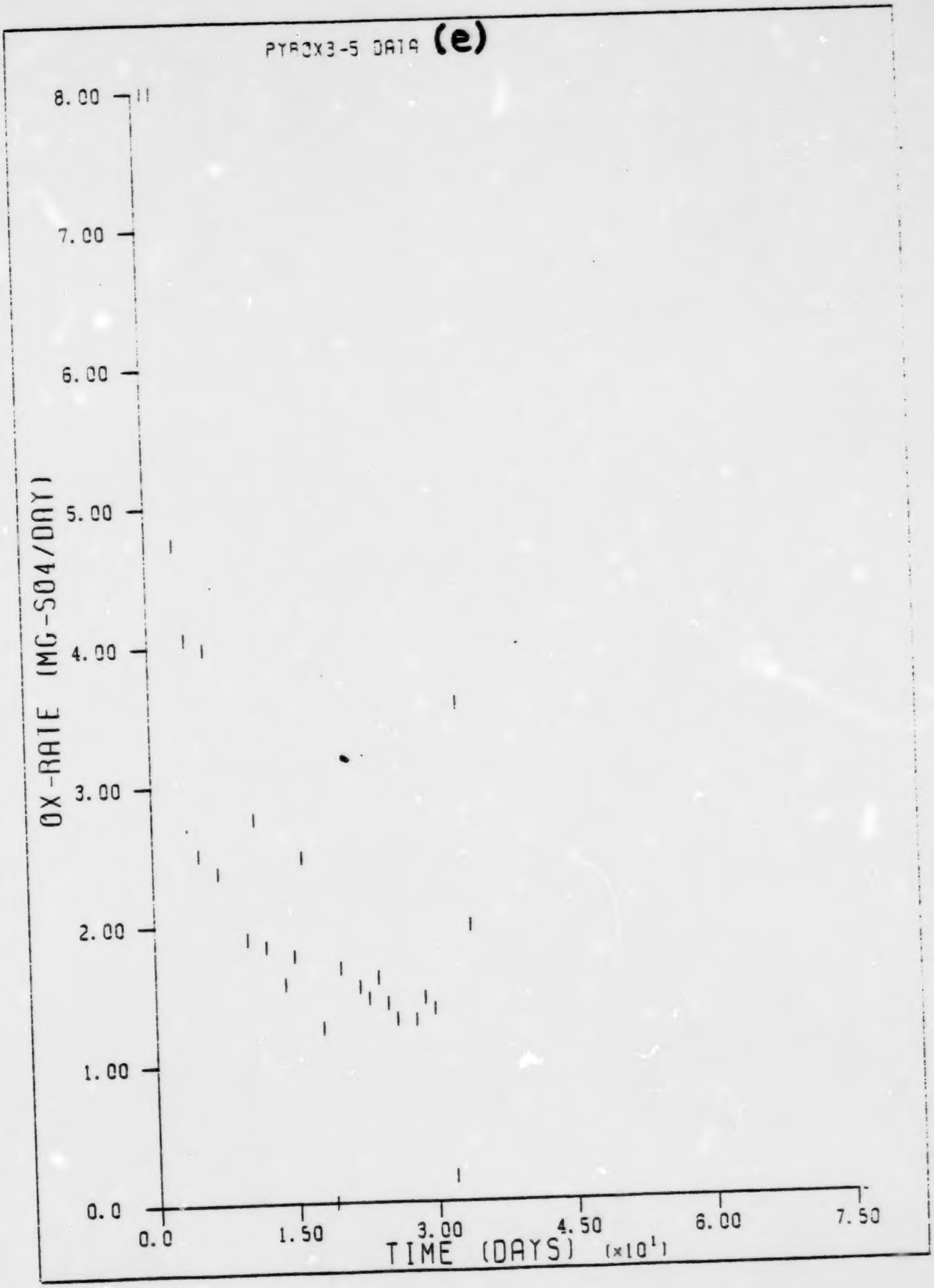
PYROX3-5 DATA
(e)
OX-RATE (MG-SO4/DAY)
8.00
7.00
6.00
5.00
4.00
3.00
2.00
1.00
0.0
0.0
1.50
3.00
4.50
6.00
7.50
TIME (DAYS) (x10^1)

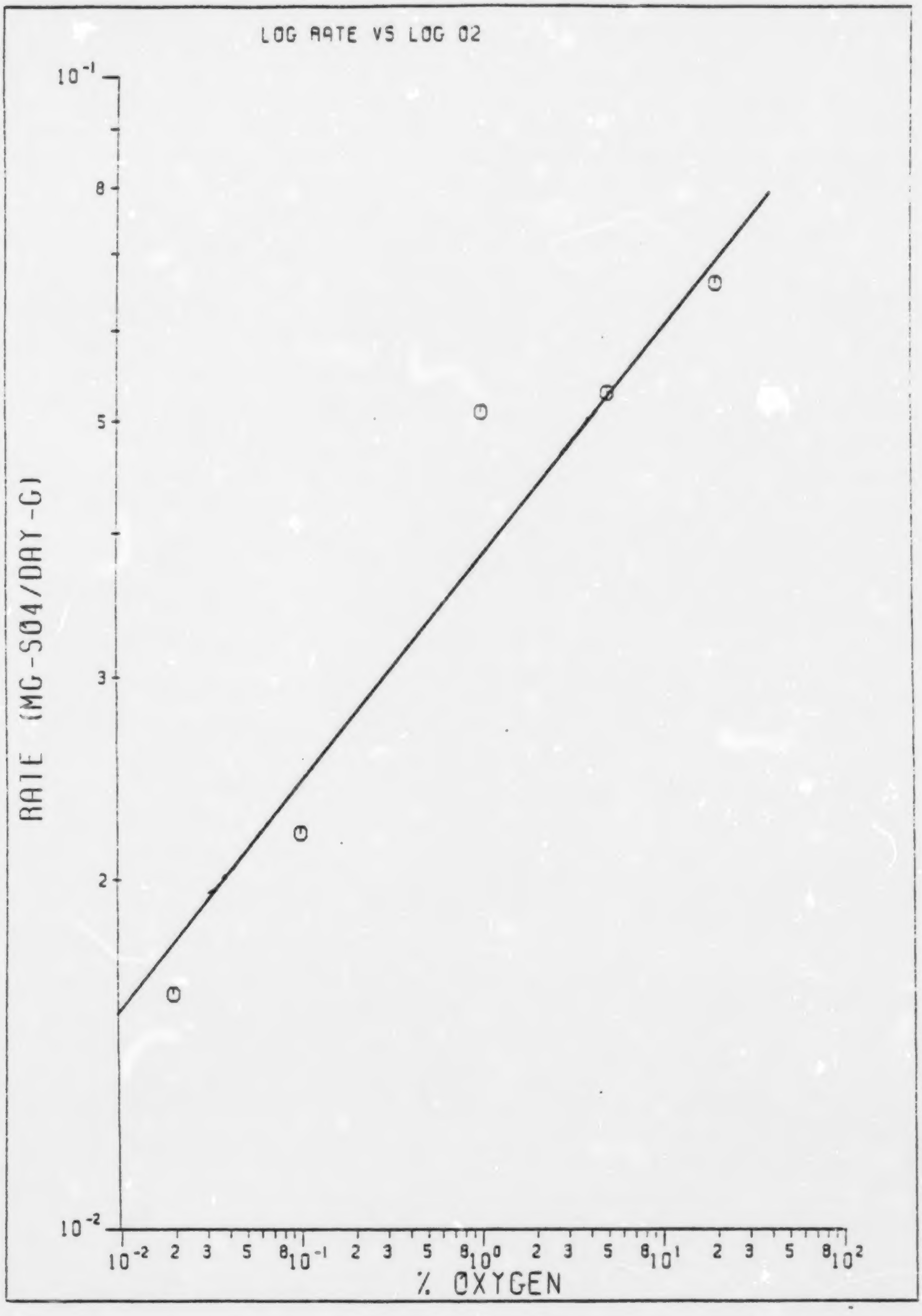

Fig. 15: The oxidation rate (rate of sulphate leached) is plotted against the percent oxygen concentration on log-log axes.

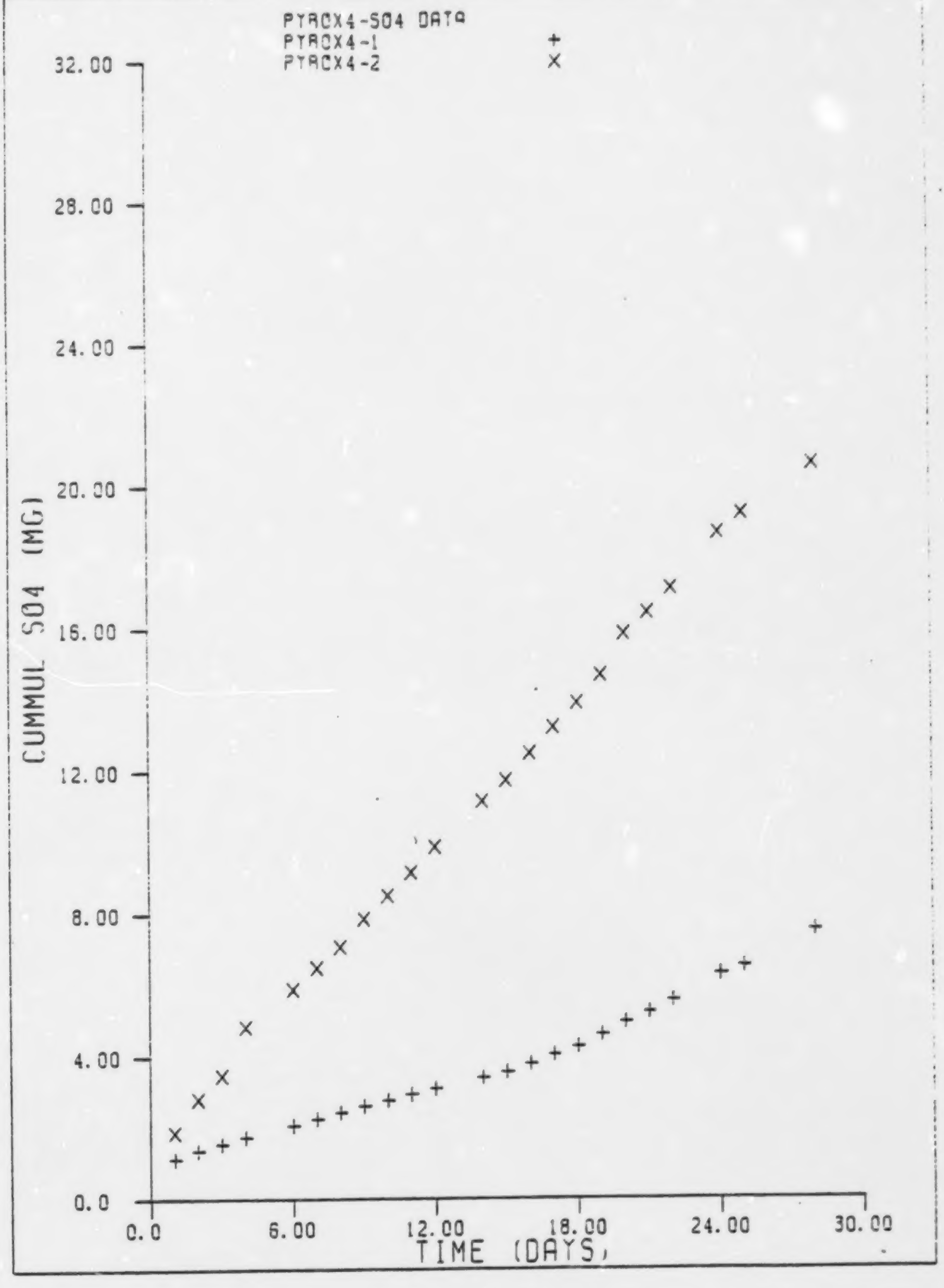

Fig. 16: A plot of accumulated sulphate leached from the two pyritic samples versus time for the temperature-dependence experiment (PYROX4).

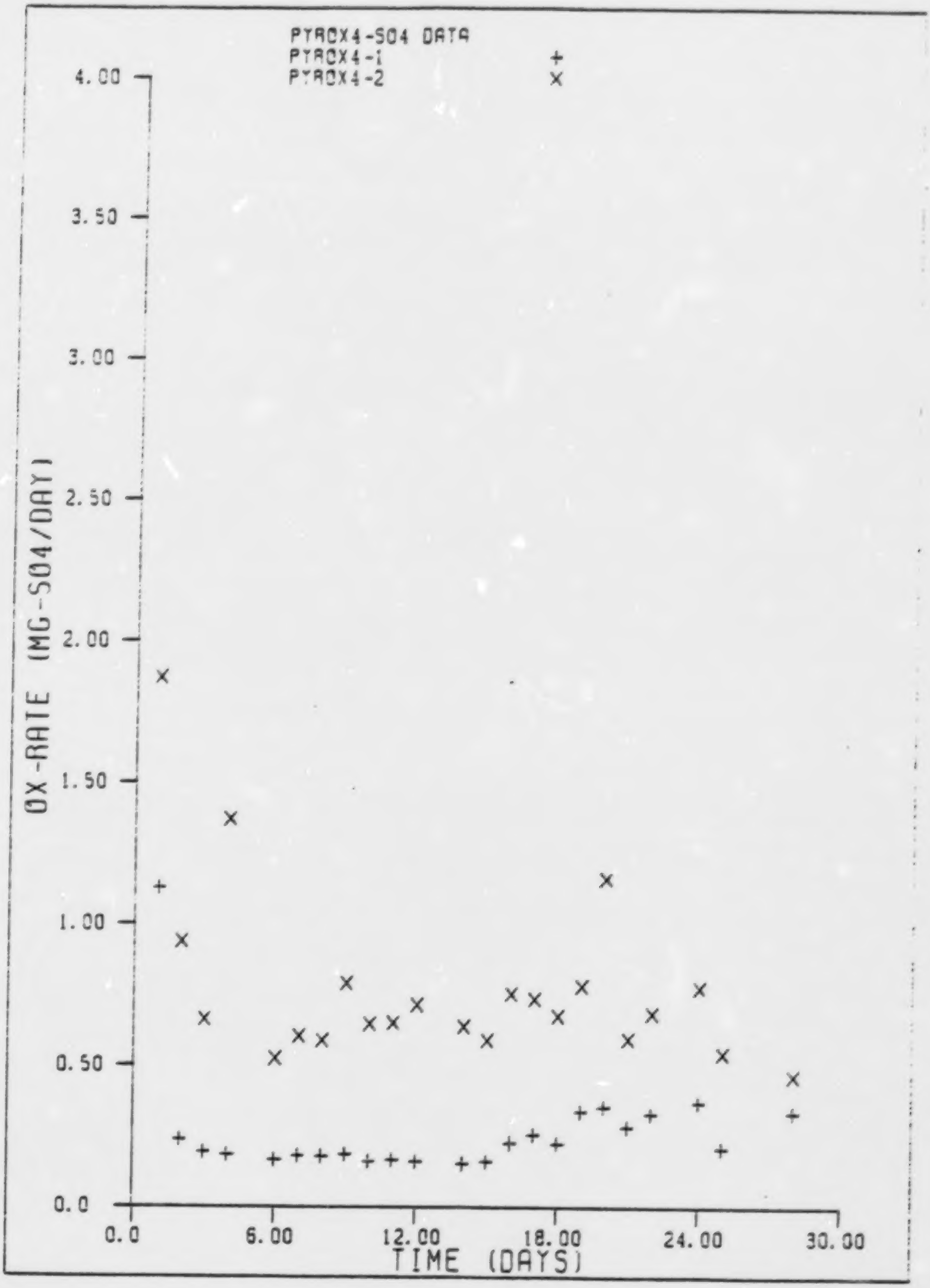

Fig. 17: The rate of sulphate leached (per day) is plotted against time for the two units in the temperature-dependence experiment (PYROX4).

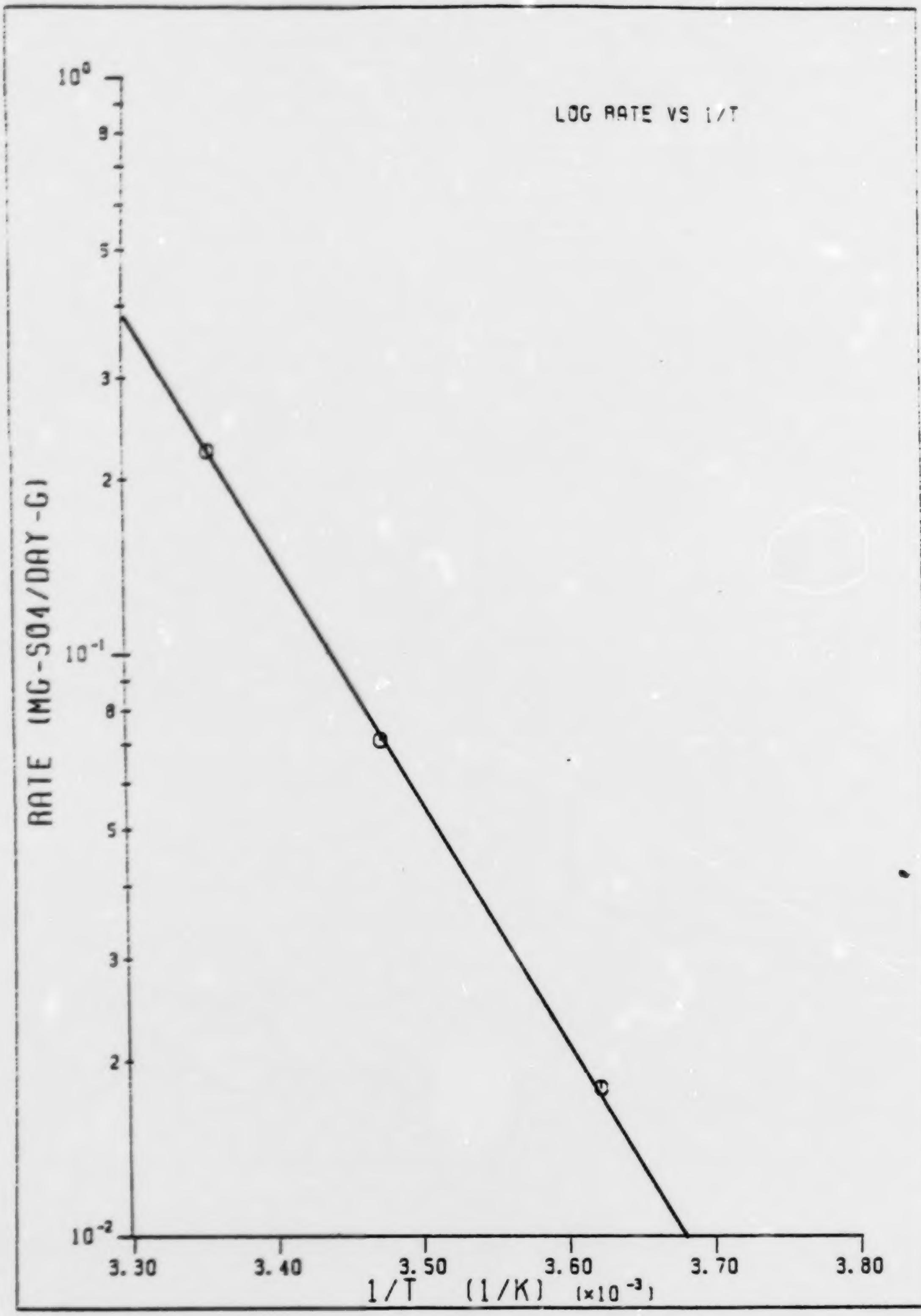

Fig. 18: The log of oxidation rate is plotted against the inverse of absolute temperature for the temperature-dependence experiment (PYROX4). The data point representing 25°C corresponds to the PYROX2-3 unit.

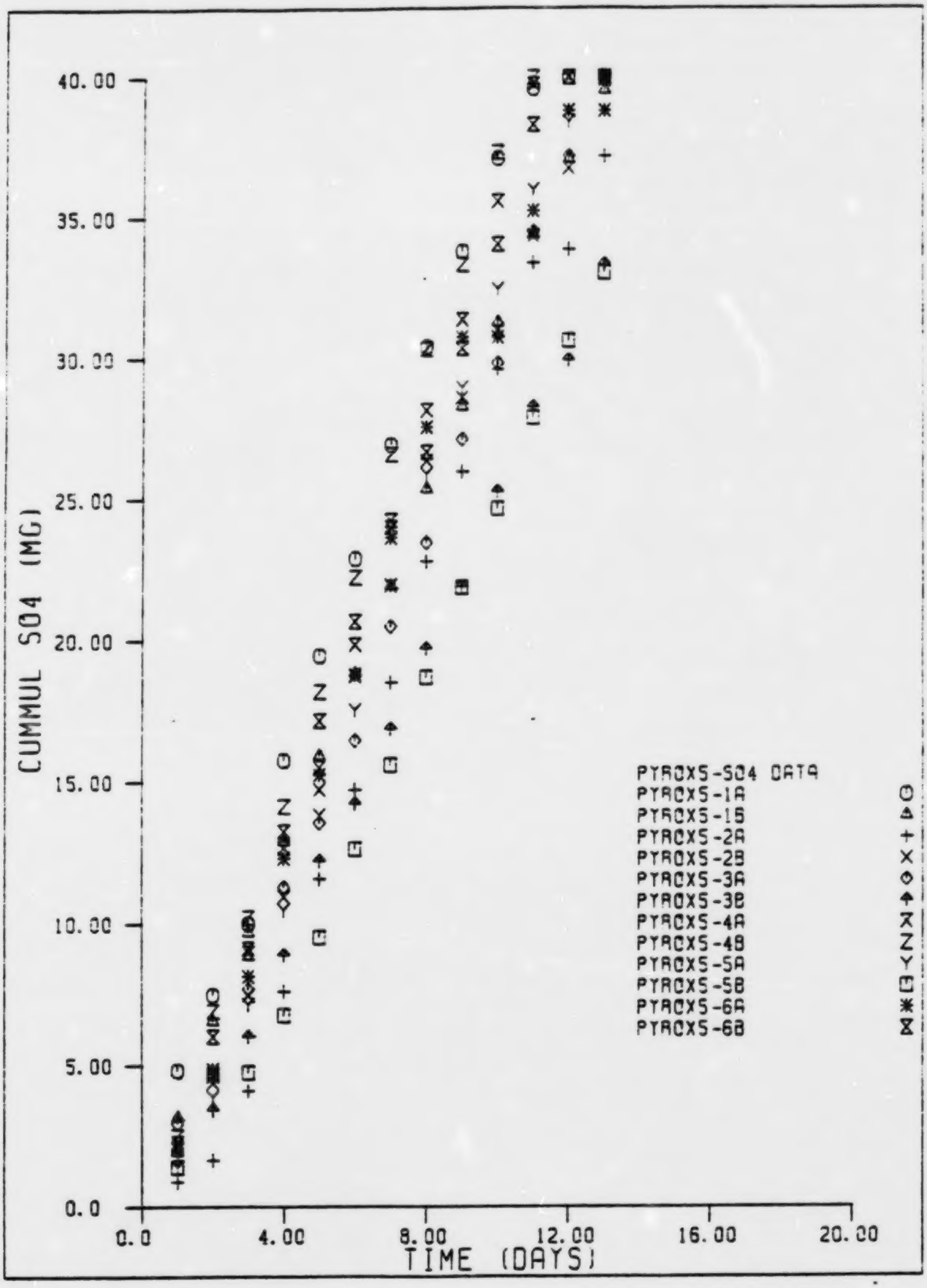

Fig. 19: A plot of accumulated sulphate leached from each granular pyrite sample versus time for the pyrite-type experiment (PYROXS).

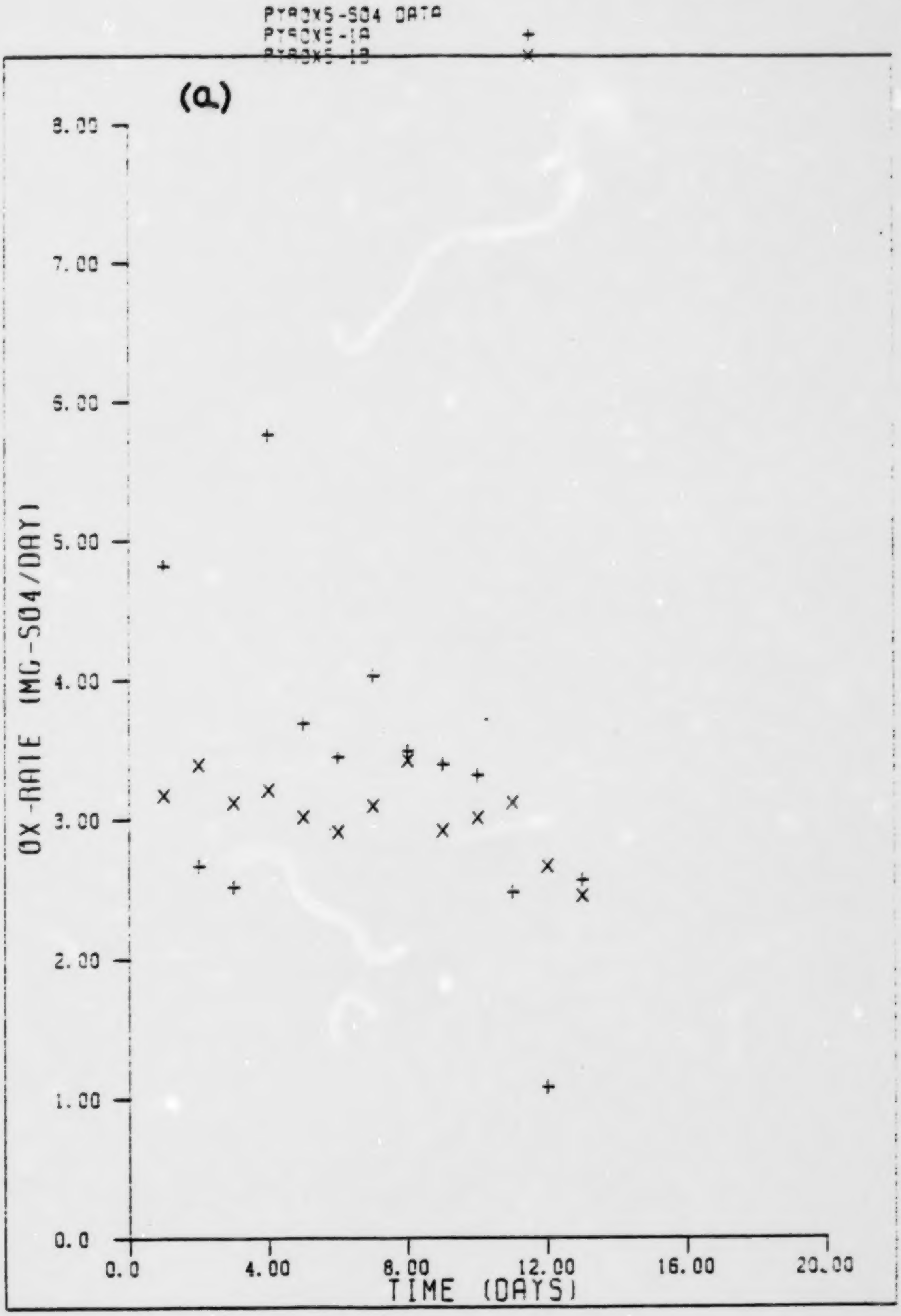

Fig. 20: The rate of sulphate leached (per day) is plotted against time for each pair of units in the pyrite-type experiment (PYROX5).

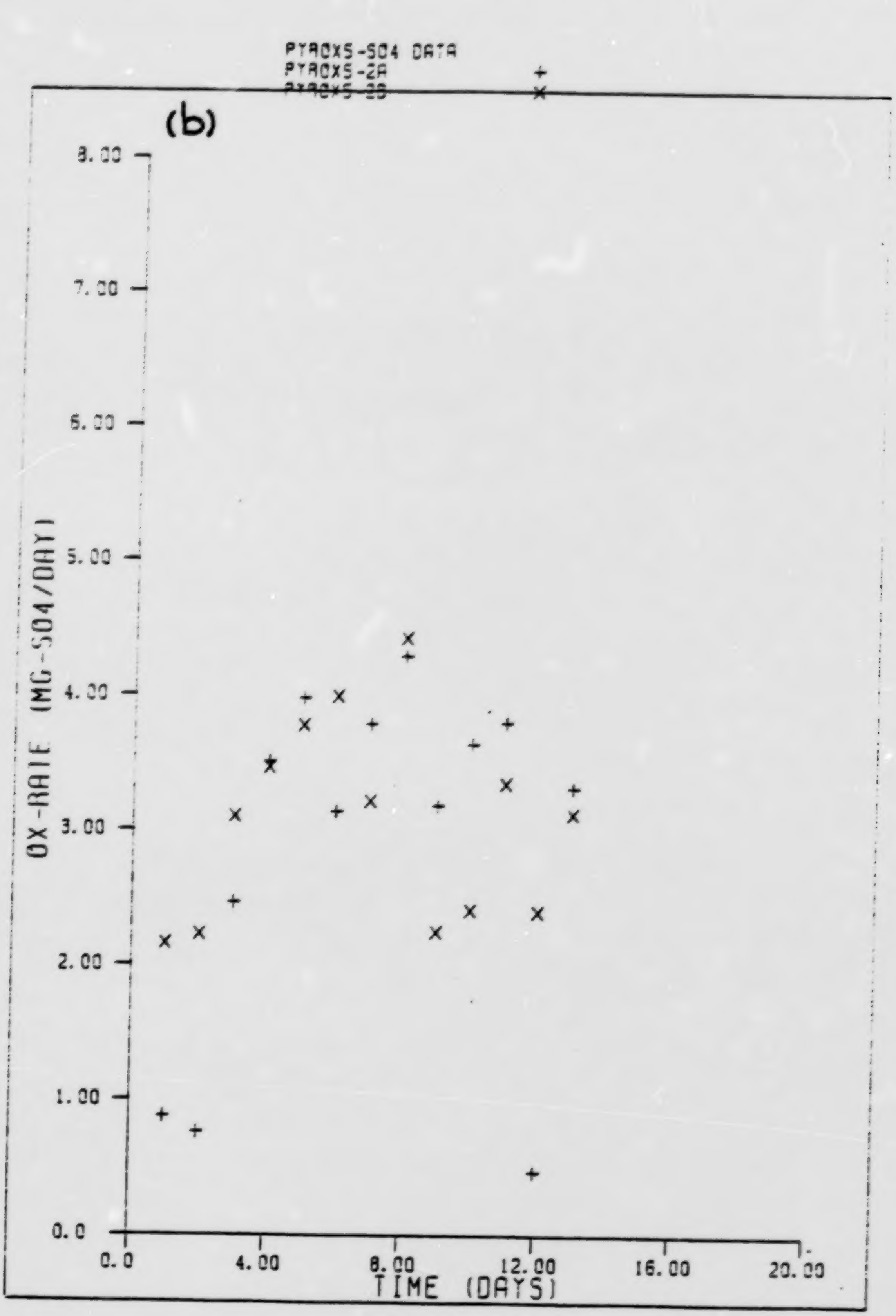
PYROXS-SO4 DATA
PYROXS-2A +
PYROXS-2B ×
(b)
8.00
7.00
6.00
5.00
4.00
3.00
2.00
1.00
0.0
OX-RATE (MG-SO4/DAY)
0.0
4.00
8.00
12.00
16.00
20.00
TIME (DAYS)

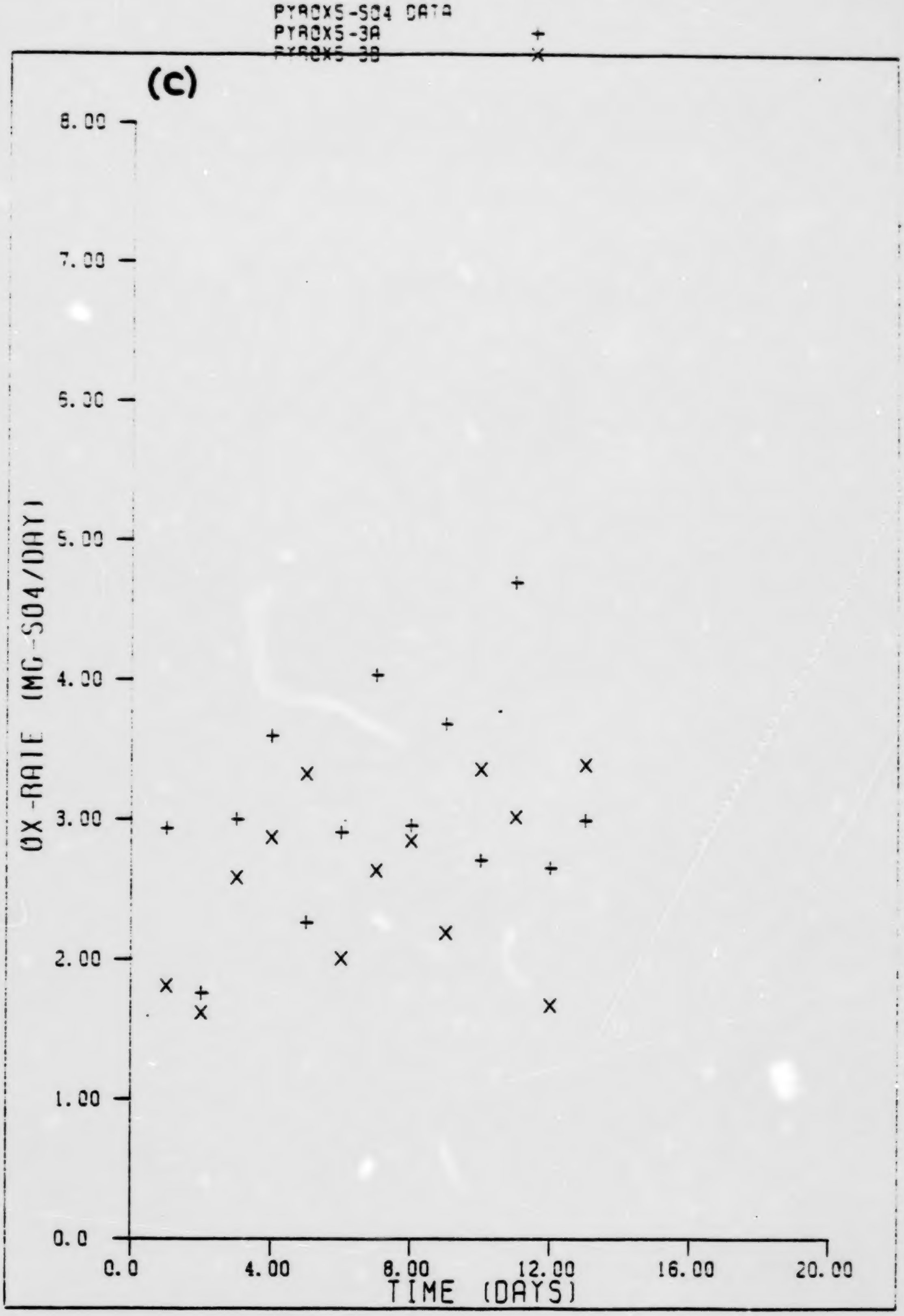
PYROX5-SO4 DATA
PYROX5-3A +
PYROX5-3B ×
(c)
OX-RATE (MG-SO4/DAY)
8.00
7.00
6.00
5.00
4.00
3.00
2.00
1.00
0.0
0.0
4.00
8.00
12.00
16.00
20.00
TIME (DAYS)

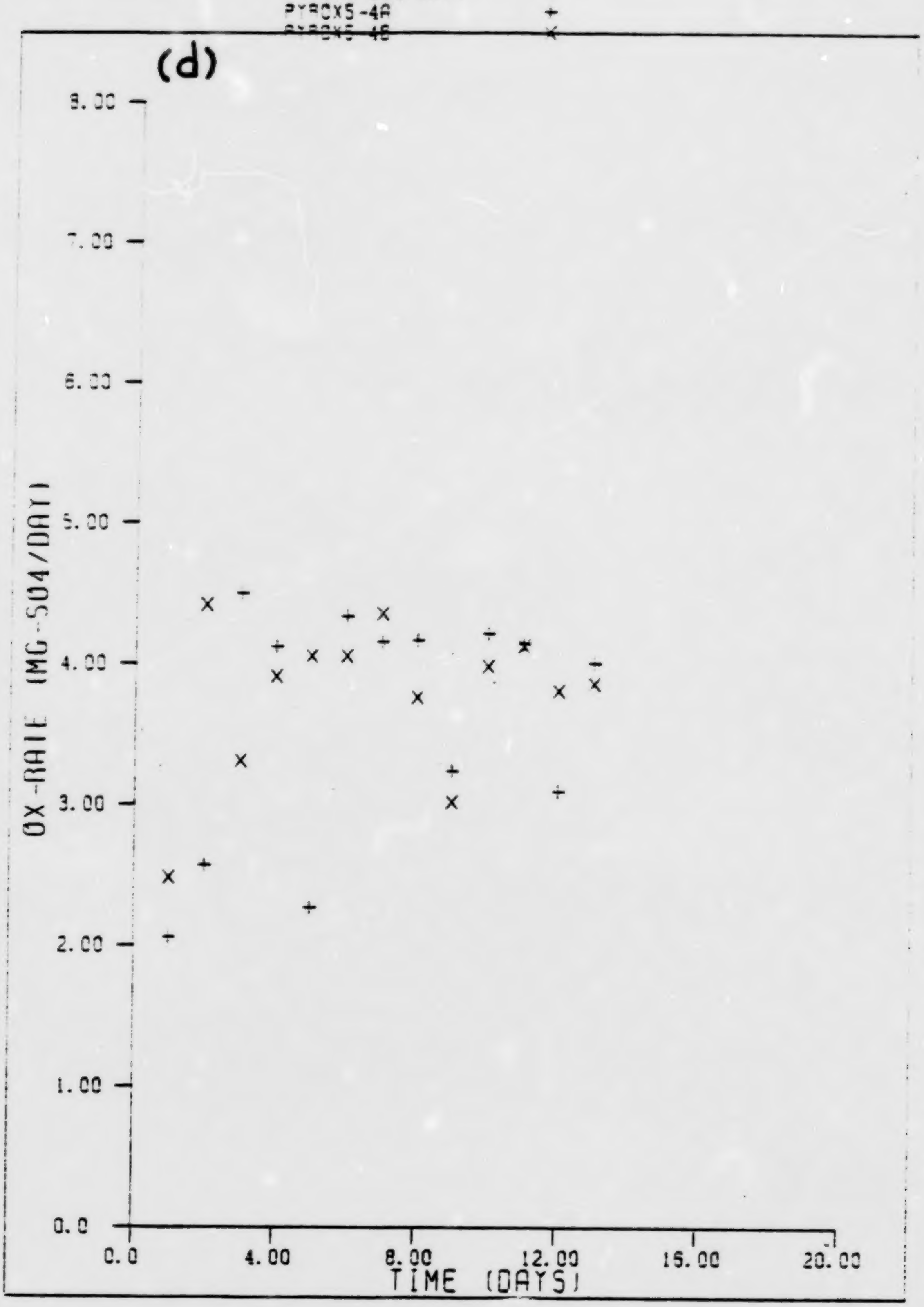
PYROX5-SO4 DATA
PYROX5-4A +
PYROX5-4B ×
(d)
8.00
7.00
6.00
5.00
4.00
3.00
2.00
1.00
0.0
OX-RATE (MG-SO4/DAY)
0.0
4.00
8.00
12.00
16.00
20.00
TIME (DAYS)

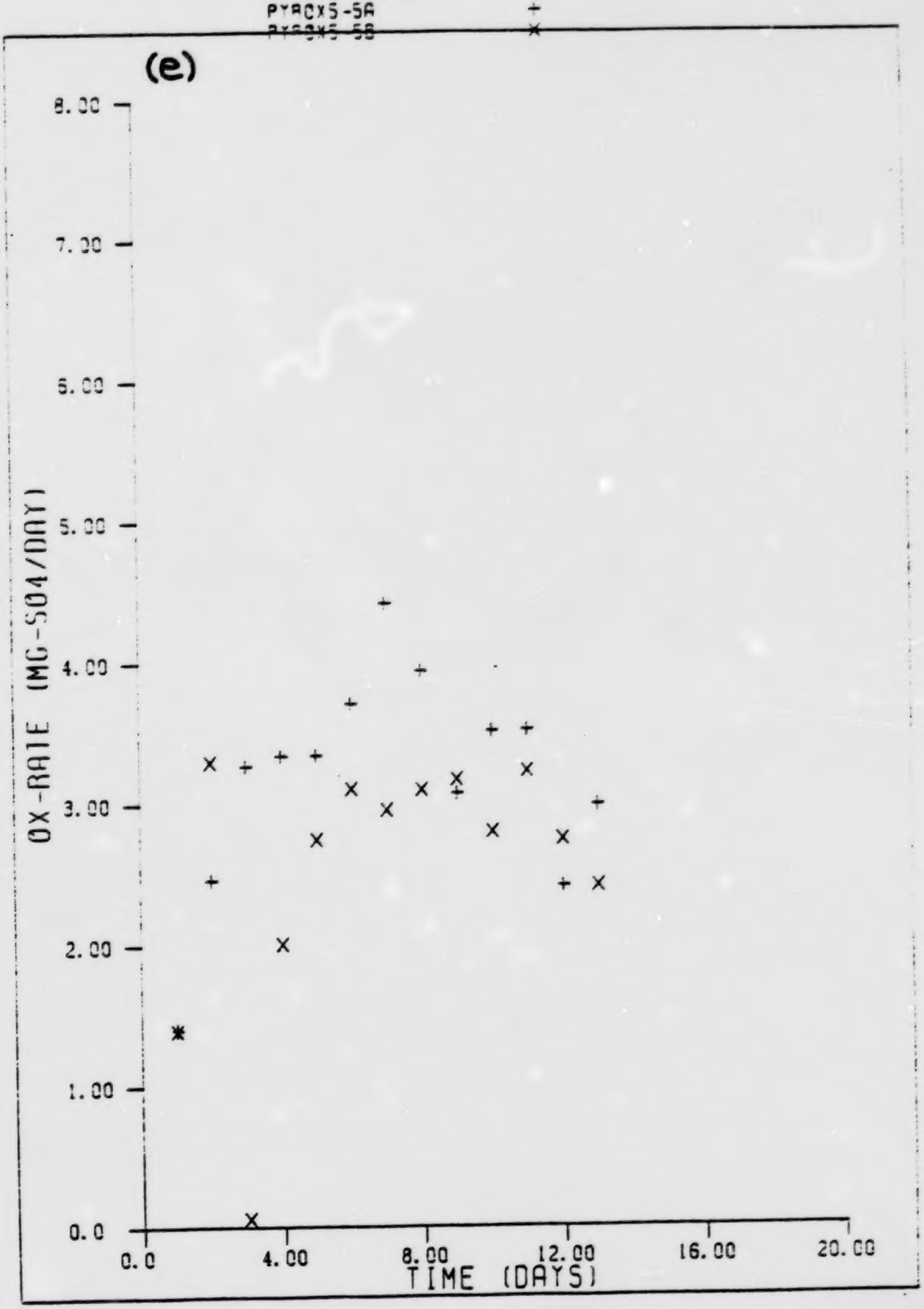
PYROXS-SO4 DATA
PYROXS-5A +
PYROXS-5B ×
(e)
OX-RATE (MG-SO4/DAY)
8.00
7.00
6.00
5.00
4.00
3.00
2.00
1.00
0.0
0.0
4.00
8.00
12.00
16.00
20.00
TIME (DAYS)

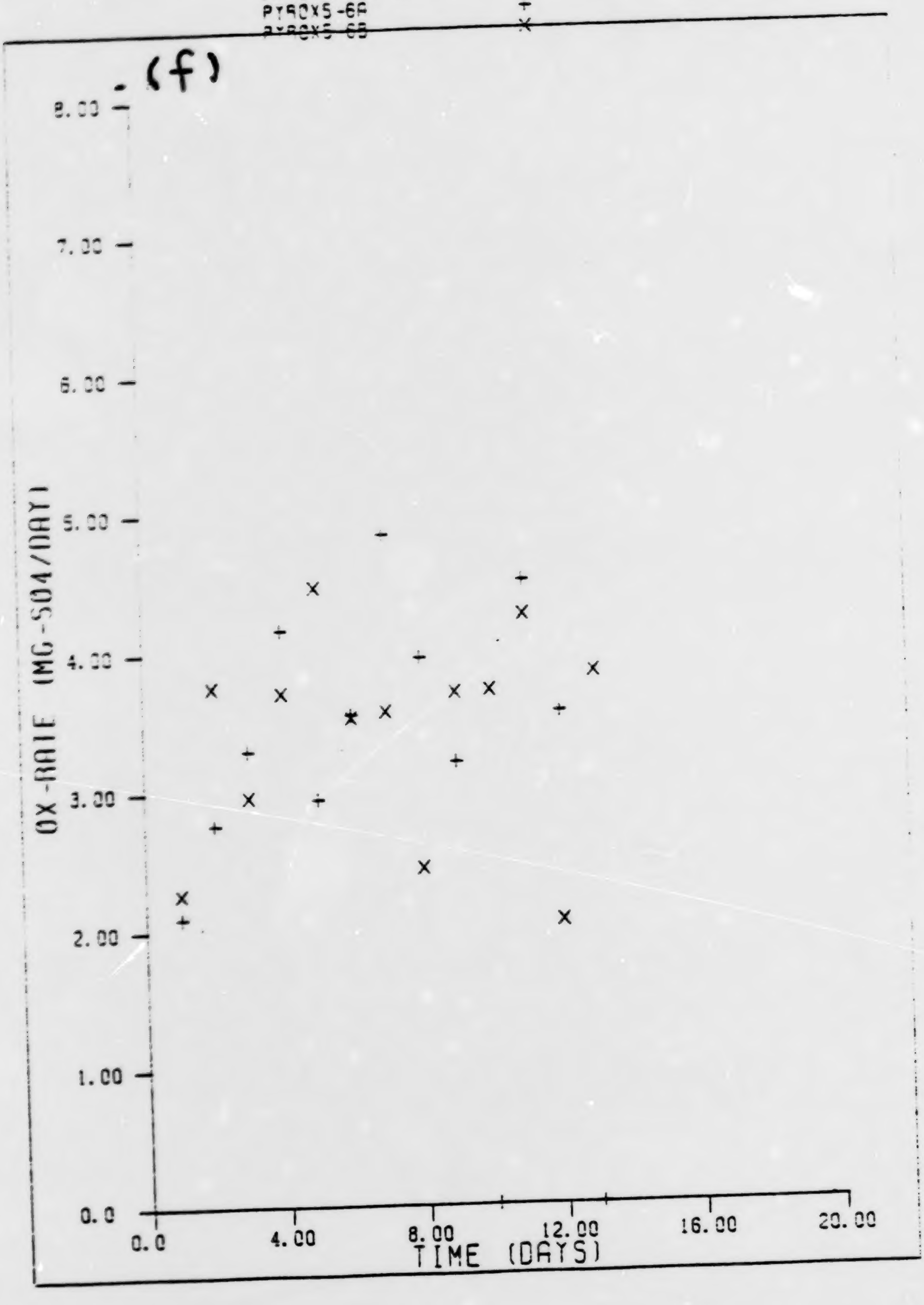
PYROXS-SO4 DATA
PYROXS-6A +
PYROXS-6B ×
(f)
OX-RATE (MG-SO4/DAY)
8.00
7.00
6.00
5.00
4.00
3.00
2.00
1.00
0.0
0.0
4.00
8.00
12.00
16.00
20.00
TIME (DAYS)

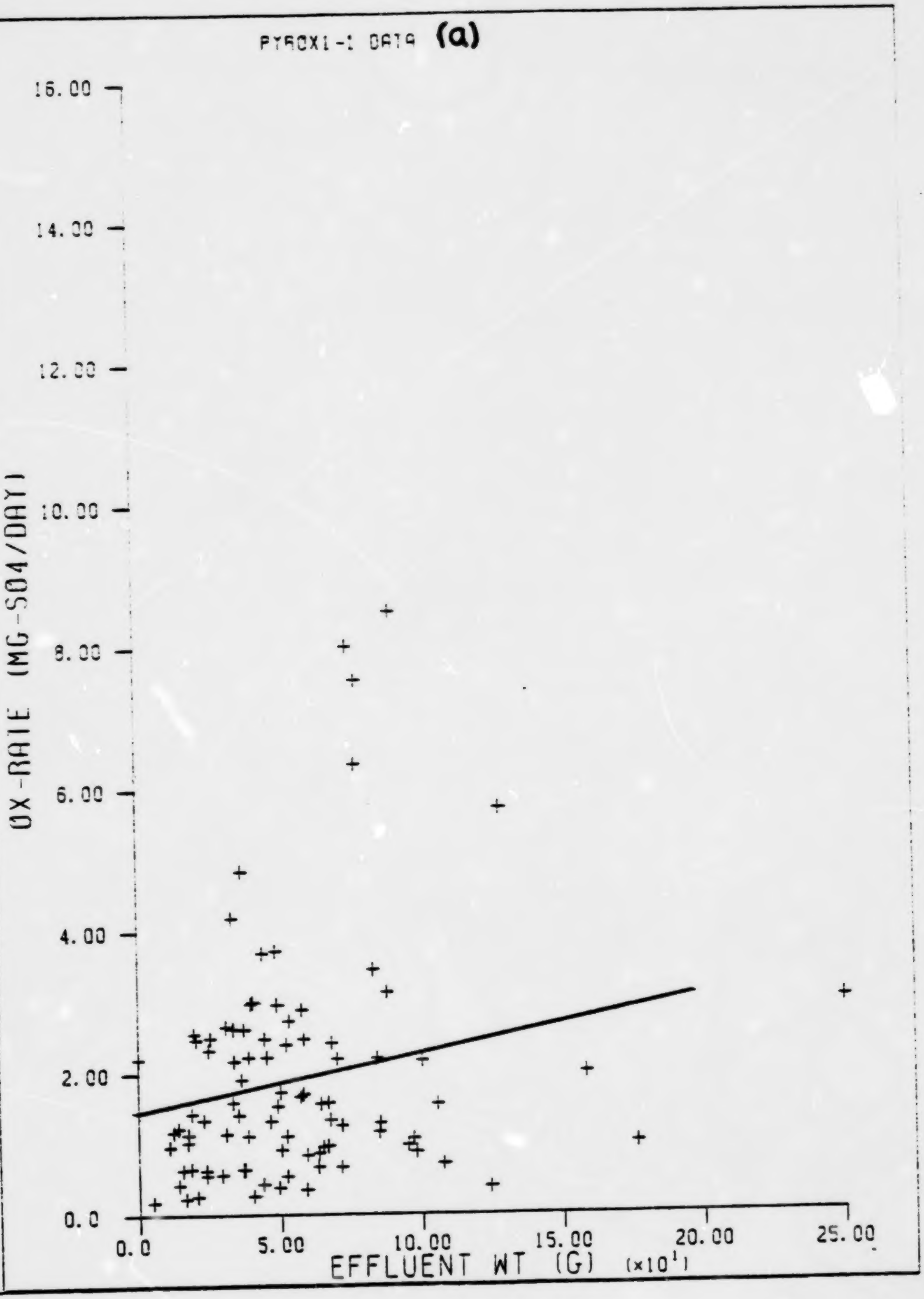

Fig. 21: The oxidation rate plotted against effluent weight (per day) for the units corresponding to the preliminary experiment (PYROX1). (a) PYROX1-1; (b) PYROX1-2; (c) PYROX1-3; (d) PYROX1-4.

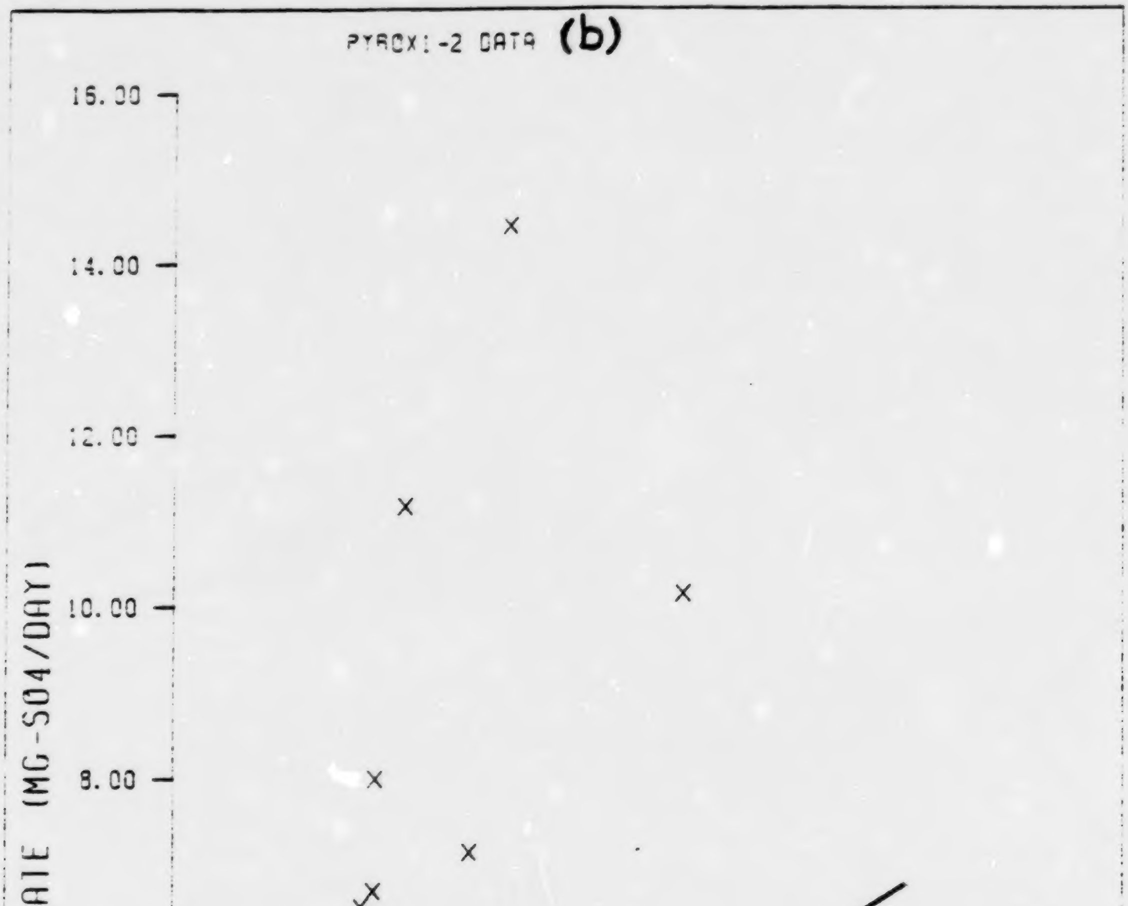
PYROXI-2 DATA (b)
OX-RATE (MG-SO4/DAY)
16.00
14.00
12.00
10.00
8.00
6.00
4.00
2.00
0.0
0.0
5.00
10.00
15.00
20.00
25.00
EFFLUENT WT (G) (×10^1)

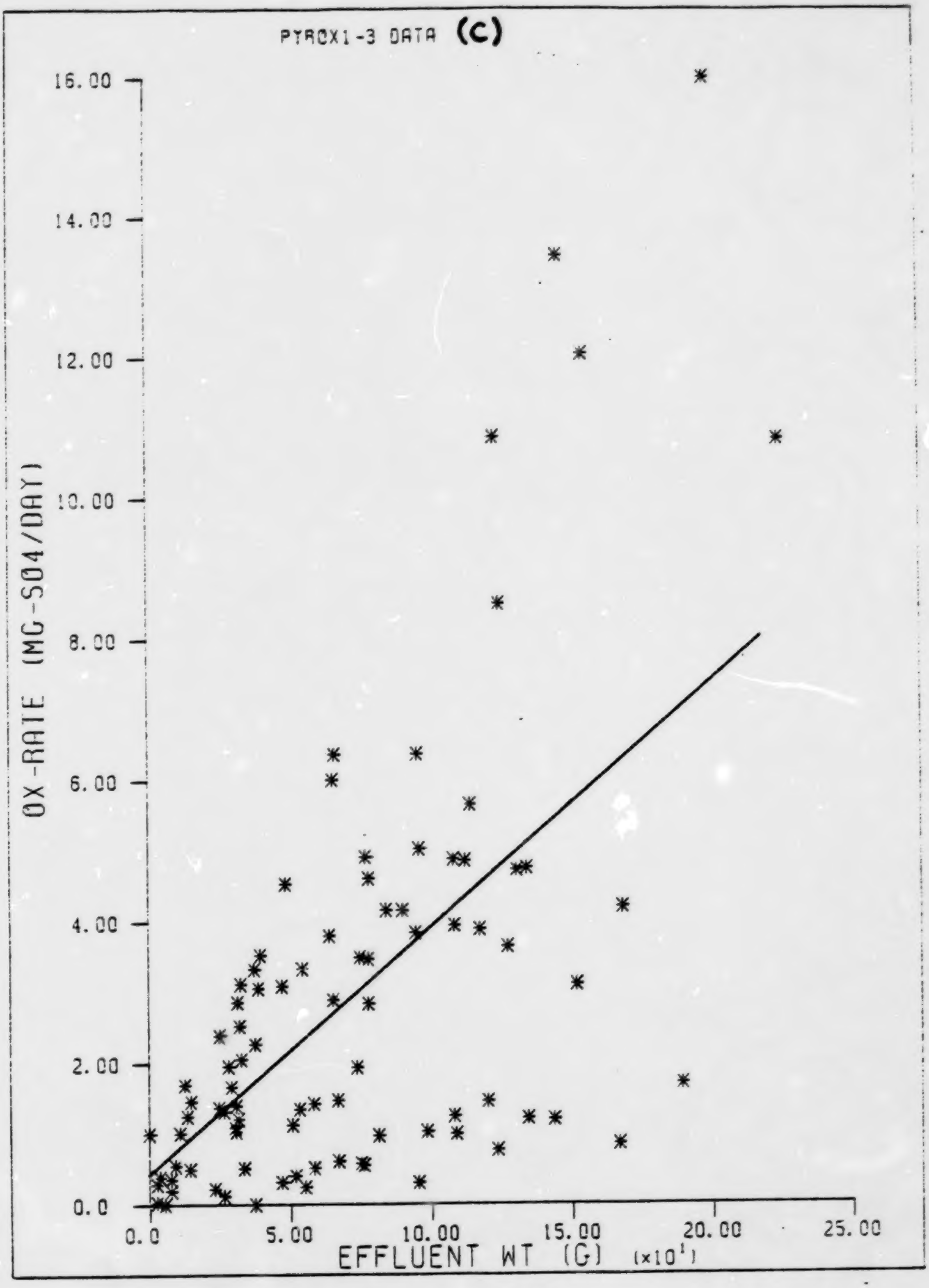
PYROX1-3 DATA (C)
16.00
14.00
12.00
10.00
8.00
6.00
4.00
2.00
0.0
OX-RATE (MG-SO4/DAY)
0.0
5.00
10.00
15.00
20.00
25.00
EFFLUENT WT (G) (x10¹)

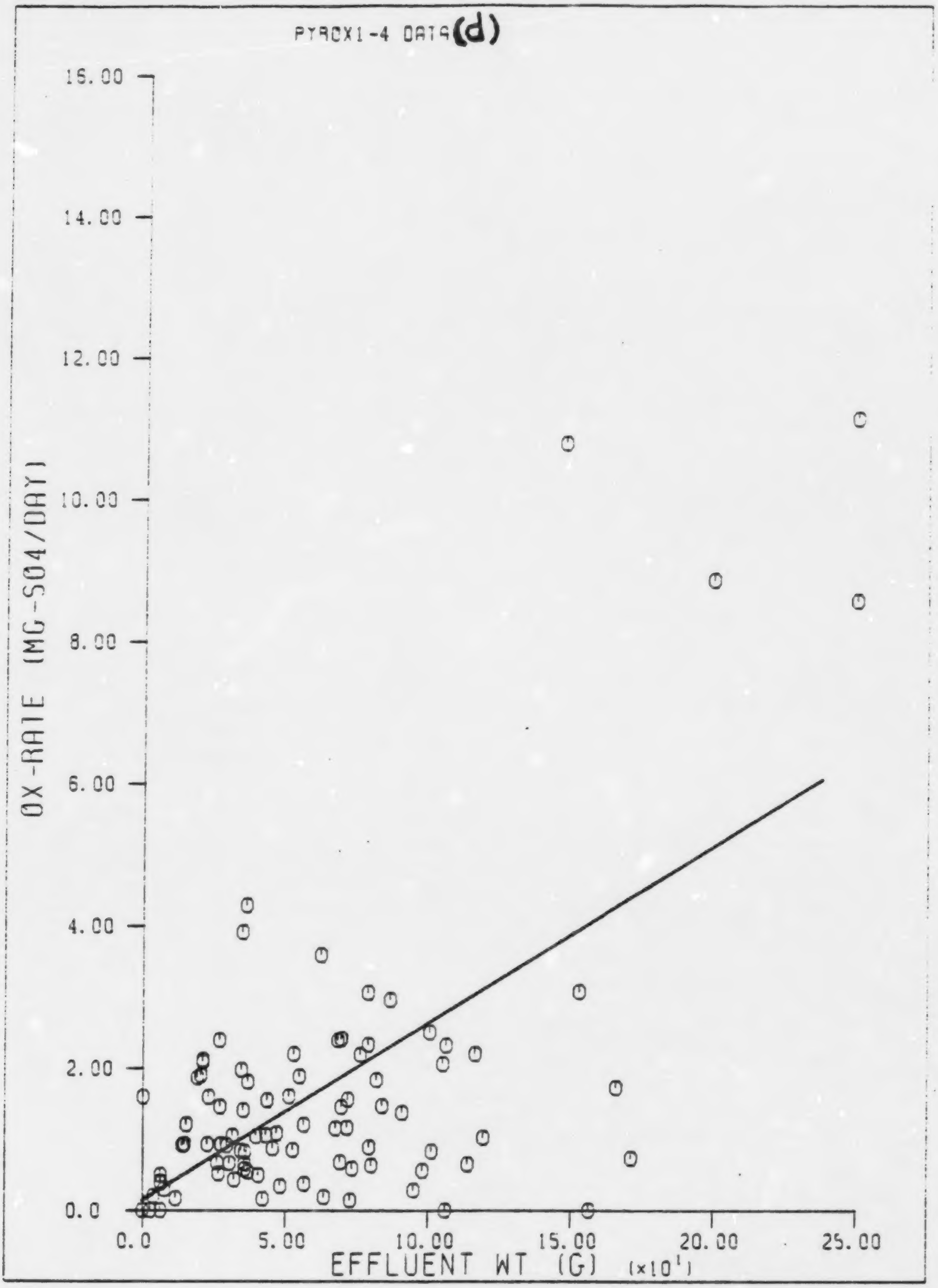

PYROX1-4 DATA (d)
0X-RATE (MG-SO4/DAY)
16.00
14.00
12.00
10.00
8.00
6.00
4.00
2.00
0.0
0.0
5.00
10.00
15.00
20.00
25.00
EFFLUENT WT (G) (x10^1)

Chapter 3

DOWNWARD MIGRATION OF REACTION PRODUCTS

ABSTRACT FOR CHAPTER 3

Samples of fresh Quirke tailings were studied in the laboratory with the objective of describing the pH neutralization behavior of Elliot Lake tailings. Attention was focussed on dissolved Al and Fe because of the tendency of those ions to influence pH through hydrolysis and precipitation as hydroxides. Attempts were made to deduce the identity of solid phases reacting with solution to alter pH.

Laboratory experiments included both batch and column experiments so that the tailings geochemistry could be studied under static and dynamic conditions. Results of batch experiments showed that long-term pH neutralization occurred over a period of 550 hours. Release of Na, K, Mg and Ca suggests that the observed increases in pH are the product of alumino silicate dissolution. Experimental results and calculated saturation indices indicate the precipitation of Al and Fe hydroxysulfates occurred in most batch tests, thus prohibiting calculation of dissolution rates.

Records of effluent pH versus time for two column experiments show that the pH dropped in a series of short plateaus to a pH of approximately 4. Effluent with a pH of 7.6 from a column containing whole tailings was found to be supersaturated with respect to calcite. The effluent from both a column containing whole tailings and one containing tailings leached of its sulfate mineral content remained at a pH of approximately 4 for over 30 pore volumes, before dropping rapidly toward the influent pH of 2. Equilibrium calculations show that the effluents are slightly supersaturated with respect to gibbsite, and it is likely that the long pH=4 plateau is a result of pH neutralization by

the dissolution of $Al(OH)_3$. Simulation of geochemical solid-solution reactions in tailings with the ADNEUT mixing cell computer model predicted a sequence of equilibrium mineral assemblages that explain many of the features in the observed data.

INTRODUCTION

Moffet and Tellier (1978) published the first report on the chemistry of groundwater in an inactive Elliot Lake uranium tailings impoundment, the Nordic West Arm tailings area. They found that some of the groundwater in this impoundment had developed a low pH and had become extremely ferrous-iron rich due to the oxidation of pyrite in the tailings. These acid waters were also found to contain high concentrations on some heavy metals and radionuclides. Since the publication of this study, the investigation of the acidification of tailings groundwaters by pyrite oxidation has been actively pursued, in particular by researchers from the Department of Earth Sciences at the University of Waterloo in coorperation with the Elliot Lake laboratory of CANMET and Rio Algom Limited. As a result of this work it has been found that in addition to the Nordic West Arm, groundwater acidification has occurred in the Nordic Main (Blair et al, 1980; Cherry et al, 1980), Lacnor (Cherry et al, 1980), Stanrock (Feenstra et al, 1981) and Williams Lake (Feenstra et al, 1981) tailings areas.

Tailings groundwater that has become acidic due to pyrite oxidation characteristically has a low pH, high concentrations of Fe and SO_4 released from the pyrite and high concentrations of some heavy metals and radionuclides. The pH of tailings groundwater is a particularly important parameter because the solubilities of many metal-containing solid phases are pH dependant. The adsorption of metal ions onto charged surfaces is often pH dependant as well. These relationships form a direct link between the potential for transport of metals and radionuclides in groundwater in the tailings and the pH of these solutions.

Data from the Nordic Main tailings area show that during the downward migration of low pH groundwaters H+ ions are consumed, primarily by reactions with solid phases, resulting in increased pH (Cherry et al, 1980). This causes the front of low-pH water to advance downward at a slower rate than that of the groundwater itself. Evaluation of the field data collected during the last two years indicates that since deposition of tailings has ceased, the low pH front has travelled downward with a component of vertical velocity between approximately 30 to 75% of the vertical groundwater velocity (Dubrovsky et al, in preparation). If the migration of low pH water continues at this rate, the groundwaters in the Nordic Main tailings will be completely acidic within several decades. When this occurs, all of the water that is seeping into the Quaternary deposits and bedrock below the tailings will be acidic and contain high concentrations of metals and radionuclides.

Small areas where acidic water occupies the entire tailings thickness have already been found in the Nordic West Arm, Nordic Main, and Lacnor tailings areas (Cherry et al, 1980). In one of these areas a plume of groundwater with a pH as low as 4.3 has been found in the aquifer adjacent to the Nordic Main tailings area (Blair et al, 1980;Morin et al, 1982).

The migration of low pH groundwaters from tailings impoundments in the Elliot Lake area constitutes a threat to the environment due to the high capacity for transporting heavy metals and radionuclides in solution. If the pH of groundwater effluent can be maintained at a high level, the amount of metal and radionuclides transported will be greatly reduced and the negative impact on the environment lessened. The field work referred to above has shown that large quantities of low-pH groundwater already exist in several tailings impoundments in the Elliot Lake area. This quantity will continue to grow until either effective measures for the abatement of acid production are found, or the acid producing capacity of the tailings is depleted. Even when effective abatement measures are implemented, the mass of low-pH groundwater already present in the tailings will continue to migrate. Depending on the pH buffer capacity of the tailings solids, discharge of low-pH groundwater from the tailings could result. At present there is a lack of detailed information on reactions between tailings solids and groundwaters that affect the rate of transport of low pH conditions.

Objectives and Scope

The goal of this research is to conduct laboratory experiments in order to characterize the acid neutralization behavoir of the Elliot Lake tailings. Specific objectives of the study are the identification of (1) solid phases that are active in pH buffering, (2) the magnitude of buffering produced by different mechanisms, and (3) kinetics of dissolution of the reacting solid phases. Particular attention will be paid to reactions involving dissolved Al and Fe because of the tendency of these ions to hydrolyze and precipitate as hydroxides, thus affecting pH. In addition, observations of high concentrations of Al and Si in groundwater in Elliot Lake tailings (Dubrovsky et al, in prep.) have led to the hypothesis that pH neutralization occurs due to the dissolution of aluminosilicate minerals under low pH conditions in the tailings.

The increased solubility of aluminosilicate minerals has been demonstrated by Helgeson (1971). In order to achieve these goals the physical properties and mineralogy of the tailings must be characterized first. This entails the determination of various physical properties of the tailings as well as the tailings mineralogy.

Tailings produced by the Rio Algom Quirke Mill were selected for use in this study rather than samples of old tailings from an inactive area. This source was chosen because the Quirke tailings have not been subject to any post-depositional weathering processes which affect their acid-neutralization behavior and are therefore in their initial state. In view of the similarity between the ore extraction processes at the Quirke and Nordic mills, tailings from the Quirke mill should be similar to the Nordic main tailings prior to the initiation of weathering. Collection of tailings from the effluent line of the Rio Algom Quirke Mill also allowed a large homogeneous source to be used for all experiments.

After characterization batch and column experiments were carried out on the tailings. In both cases the main objective was to identify the solid phases that buffer the pH under low pH conditions by studying the chemistry of waters in contact with the solids.

The objective of the batch tests was to determine the pH neutralization processes that operate in the tailings under low-pH conditions in a static solid-solution system. The approach involved the determination of changes in solution composition and pH brought about by the dissolution of solid phases. Column experiments were used to study the pH buffering reactions under dynamic conditions in order to more closely simulate conditions in a tailings pile. By studying pH neutralization under dynamic conditions the effects of kinetics on the neutralization could be better appraised. Finally, a test was run to investigate the component of pH neutralization due to sorption of H+ ions onto tailings solids.

In experimental work on mineral dissolution and in particular dissolution kinetics, the interpretation of results is made much more difficult if precipitation occurs, thereby removing dissolved constituents from solution at an unknown rate. The likelihood of precipitation of sulfate minerals while working with the tailings was anticipated because of the high concentrations of Ca and SO_4^{2-} that result from dissolution of gypsum in the tailings. In order to reduce the likelihood of precipitation most experiments were performed on tailings from which the soluble sulfate minerals were removed by leaching. Duplicate experiments performed on whole tailings could then be compared to investigate whether the sulfate removal affected the pH-neutralization behaviour of the tailings.

CHARACTERIZATION OF TAILING SOLIDS

Before geochemical interpretation of the behavior of acid in the tailings can be developed in detail, a characterization of the tailings solids is required to assist in the identification of solid phases that react to produce the observed changes in solution chemistry. This task is difficult because the bulk of the tailings mass is quartz which has no major influence, but the important reactive phases occur in low quantities. An additional complication is that solids precipitated during tailings neutralization are usually amorphous and therefore cannot be identified by x-ray methods. Due to these problems and the preliminary nature of this work, complete quantification of the tailings mineralogy was not performed. Rather, the approach taken was to use standard techniques to establish the presence of reactive minerals, measure the abundance of these phases where possible, and use representative tailings values from the literature otherwise.

Grain-size analyses were done on the tailings using wet and dry sieve methods. The raw data is presented in Table 1 and the average results of both methods were plotted on an cumulative % graph (Figure 1). It was anticipated that wet sieving would reduce the tendency of the tailings fines to aggregate and thus increase the amount of fines relative to the dry sieving. However, the results show no significant difference between the data from the two methods. During the mill cycle the uranium ore is ground until 50% pass a 75 mesh. Data from the sieve analysis shows that the sample of Quirke tailings collected is significantly coarser, with only about 25% of the sample finer than 75 . The relatively coarse grain size of the sample has geochemical implications that will be discussed later.

Sieved samples of the tailings were examined under a binocular microscope. Similar appearing grains were selected for XRD analysis in an effort to identify aluminosilicate minerals (XRD traces are appended). The XRD trace of a ground sample of pink coloured grains from the ½35 mesh size fraction showed quartz to be the most abundant mineral in this subsample. However, peaks at approximately 25.7, 27.5 and 30.8 2 are interpreted as indicating the presence of orthoclase or albite feldspar. It is suspected that albite is present in the pink coloured grains as well, in view of observation of red albitization of matrix and in some cases quartzite related to some dikes in the ore zones (Pienaar, 1963; Derry, 1962). While Roscoe (1969) describes the Matinenda Formation ore zone as containing potash feldspar clasts, Pienaar (1963) reports that "feldspar pebbles are common in the small - pebble conglomerates but are essentially absent in the ore conglomerates". It is estimated that feldspars constitute less than 5% of the tailings.

Samples of pale green, micaceous-appearing grains were hand-picked from the >35 mesh fraction for XRD analysis. The XRD trace shows that in addition to abundant quartz, the sample contains approximately 10% muscovite mica. The XRD trace of the <325 mesh fraction shows an even greater amount of muscovite mica. Sericite has been reported to be the most common interstitial mineral in the ore-bearding conglomerates (Pieneer, 1963).

Jongejan (1973), in a mineralogical study of several mine tailings including samples from Elliot Lake, found that Elliot Lake tailings have approximately 19.2% orthoclase plus sericite. The above data and literature on the mineralogy at the uraniferous conglomerates suggests that sericite is far more abundant than orthoclase, and a reasonable estimate would be 10-15% sericite and 5% or less orthoclase.

Determination of the carbonate mineral content of the tailings was done by acidifying small samples of tailings solids and measuring the quantity of CO_2 gas evolved (Barker and Chatten, 1982). Duplicate analysis gave values of 0.127 and 0.129 weight percent $CaCO_3$, for an average of 0.128 wt. % $CaCO_3$. This value is greater than the 0.048 wt. % $CaCO_3$ measured by R. Nicholson (unpublished data) on a different sample from the Quirke Mill. Results of analyses of the carbonate mineral contents of tailings from three sites in the Nordic Main tailings area showed a maximum of 0.056 wt. % $CaCO_3$ (Dubrovsky et al, in prep.). Samples of Quirke tailings that were stored moist lost a large portion of their carbonate content likely due to precipitation of $Fe(OH)_3$; analyses of the whole tailings used in the batch and column experiments had 0.080 wt.% $CaCO_3$, and the leached tailings used in these experiments contained 0.004 wt. % $CaCO_3$. Although all of the weight-percentages indicated above are small,they do in fact represent a considerable capacity for consumption of H^+. Low pH neutralization by carbonate minerals will be considered in more detail later in this report.

It has been observed by other researchers that the carbonate mineral content of tailings is usually higher in the finer-grained fractions (R. Nicholson, unpublished data; S. Feenstra et al, 1982). Carbonate analysis were performed on separate sieved grain-size fractions of Quirke tailings in order to evaluate this possibility. A graph of the results of the carbonate content versus grain size (Figure 1) shows that the carbonate content of the tailings increases rapidly with decreasing grain size. Approximately 52% of the carbonate mineral content of the sample is in the silt-size or finer fraction (<45) which constitutes only about 25% by weight of the total tailings.

Analysis of the soluble sulfate content of the tailings was performed by repeatedly leaching 25 g samples of tailings with deionized water until the specific conductance was less than 40 micromhos. Results of triplicate analysis gave values of 1.9, 2.3, and 3.2 weight % gypsum ($CaSO_4 2H_2O$). The value from the first analysis must be discarded due to the excessive amount of pyrite oxidation and iron hydroxide precipitation that occurred during the leaching. By accelerating the leaching we were able to achieve a rapid rise in specific conductance of the leachate before products of pyrite oxidation ($Fe(OH)_3$ precipitates) were observed. The average value of 2.75 weight % gypsum is within the range of values observed by other researchers (Jongejan, 1973; Smyth, 1981). However, this figure is lower than the 7 weight (%) gypsum found by Kaimen (1977) and calculated from mass-balance considerations by Blair (1981). The lower value for the tailings used in this study is due to the coarse-grained nature of these tailings, as it has been noted that gypsum is concentrated in the fine-grained tailings

Chemical analyses of solutions in the neutralization segment of the Quirke mill cycle were studied in an effort to deduce the amount of Fe and Al hydroxides added to the tailings solids prior to discharge of the tailings to the impoundments. This was done by taking the concentrations of Fe and Al found in the largest sources of dissolved solids for the tailings effluent and assuming all Fe and Al was precipitated as hydroxides. The flow rate was then used to calculate the weight % solids that these hydroxides constitute. The calculations show that tailings solids discharged are approximately 0.32 weight % $Fe(OH)_3$ and 0.46 weight % $Al(OH)_3$ (Table 2). This analysis does not take into account the possible precipitation of Fe and Al as hydroxysulfate minerals during neutralization, and it does not consider the input of additional Fe and Al solids already present in the IX, CCD, and cycloned solutions.

In order to investigate the nature of the Fe and Al precipitates formed during neutralization of mill solutions before discharge to the tailing, samples of the IX barren solution and CCD underflow were neutralized in the laboratory. This was done by the slow addition of lime to 0.5 L of IX or CCD solution until a pH of approximately 9 was achieved. The sample was bubbled with air during the lime addition. The resulting precipitate was then filtered and a subsample was washed with deionized water to remove the gypsum. The XRD analysis of precipitates from both the IX and CCD solutions showed that the solids were essentially amorphous, and no peaks indicative of crystalline Fe or Al hydroxides or hydroxysulfates of Fe or Al were identified.

The work on characterization has shown that the tailings contain small but significant amounts of carbonate minerals that are concentrated in the finer grain-size fractions. The tailings also contain an estimated 10 to 15% sericite, which is also concentrated in the fine grained fraction. Dissolution of sericite is a strong pH-buffering reaction, however, the reaction is very slow and may not be quantitatively significant in flow regime found in the tailings. Concentration of the carbonate minerals and sericite in the finer-grained fraction of the tailings due to grain size segregation during tailings deposition will have an important effect on the distribution of buffer capacity in tailings impoundments and the above results have implications regarding the comparison of laboratory tests on homogeneous tailings samples and data gathered in the field.

METHODS

Chart - Recorded Alkalinity Titrations

Chart - recorded alkalinity titrations were performed on two types of tailings solids: whole tailings and tailings which were leached with deionized water to remove the soluble sulfate minerals (primarily gypsum). Preparation of the sulfate-leached tailings also removed approximately 66% of the carbonate-mineral content of the whole tailings. Four titrations were performed; two on Quirke tailings collected in 1980 and two on Quirke tailings collected in 1982.

The titrations on the 1980 samples were performed on 50 gram samples of tailings suspended in 50 ml of deionized water by stirring from above and 0.1 N H_2SO_4 was used as a titrant. Titrations on the 1982 samples were 25 g samples suspended in 100 ml of deionized water were carried out using 0.1 N HCl as the titrant. The pH of the solution was monitored by a combination pH electrode placed in the solution, and the pH meter was attached to a chart recorded to provide a continuous record of solution pH. The container was covered with parafilm (TM) with ports for the stirrer, pH electrode, and burret.

The solids were titrated by addition of 0.5 or 1.0 ml aliquots of acid. The addition of an aliquot of acid produces a rapid pH decrease followed by a slow rise as pH neutralizing reactions proceed. When the chart record of pH showed that upward pH drift had stabilized (less than 0.02 pH units/hr), the next aliquot of acid was added.

Batch Tests

Batch tests for pH neutralization were performed on both whole and sulfate leached samples of tailings. Composition of solutions used were calculated on the basis of preliminary small-volume batch tests that were run to determine the quantity of acid required to produce an initial solution pH in the range of 1.5 to 3.0. The results showed that 30 ml of 0.1 N HCl were sufficient to reduce the pH of 100 ml of solution in contact with 25 g of tailings to approximately 2 (Table 3). A mass balance on the mH+ in the acid added (3 millimoles H+) and the H+ concentration in the final solution (estimated by the pH as 0.82 millimoles H+) indicates that about 0.087 mmole H+/g tailings were consumed by neutralization reactions. Assuming a specific gravity of 2.75 g/cm3, a batch test porosity of 0.5, and using a conservative figure of 0.1 mmole H+/g tailings, it is calculated that a minimum H+ concentration of 0.275 mH+/L is required to produce a pH of approximately 2 in the pore water.

Two solutions were prepared for the batch tests, one containing 0.135 m/L sulfuric acid and one containing 0.135 m/L sulfuric acid plus 0.05 m/L ferrous iron. The solution compositions were calculated to provide 0.275 m/L H_T^+, where H_T^+ is calculated as the sum of the mH^+ and $mHSO_4^-$ in solution. Actual input solutions compositions were 0.135 m/L SO_4^{2-} for the iron-free solution, while the high-iron solution contained 0.056m/L Fe and 0.188 m/L SO_4^{2-}.

Two kg of tailings were used in each batch test. Using a specific gravity of 2.75 g/cm^3 calculated by assuming a tailings composition of 90% quartz, 5% pyrite, and 5% gypsum, and a porosity of 0.5, it is calculated that the pore volume of the batch will be 0.73 litres. Collection of 15 samples of approximately 20 ml each will result in 350 ml of solution being removed during a batch test. Difficulty in the removal of this large a volume from the tailings pore volume was anticipated due to the high field capacity of the tailings. Therefore, it was decided that a volume of water in excess of the tailings porosity would be injected into each reaction container to produce a reservoir of standing water on the tailings, thus insuring that adequate solution volume would be available for sampling during the duration of the test.

A schematic of the nalgene reaction vessels used in the batch tests is shown in Figure 2. The vessel is designed so that the solution is injected from the bottom to reduce the possibility of entrapping gas in the pore space. Sampling ports consist of septums attached to a porous polyethylene screen (Vyon) which excludes tailings fines and prevents clogging of the needle during sampling. The top of the container is fitted with vents to permit flushing of the headspace with N_2 gas, and a septum for sampling of the water ponded on the tailings surface.

The tailings were placed in the reaction vessels in 4 lifts, and each layer was lightly tamped. This resulted in a total tailings thickness of 12.5 to 13.5 m. After the containers were full, the pore space of the solids was flushed with CO_2 gas through the bottom solution inlet for 9 hours to fill the pore space with a soluble gas and reduce the entrapment of air.

The solution was introduced to the tailings via the bottom inlet, and the tailings were allowed to wet slowly from the bottom under a slight positive head. When the bottom quarter of the tailings was saturated a weak suction was applied to the outlet at the top of the reaction vessel and the solution injection rate was increased slightly. Injection continued until there was approximately 2.5 cm of solution ponded on top of the tailings, and the filled reaction vessels were weighed to determine the total amount of solution introduced. Total time required to inject the desired quantity of solution was 3.5 to 4.0 hours.

The batch tests were sampled by withdrawing 15 to 18 ml of solution using a 50 ml syringe inserted through the sampling port. The first three samples were filtered during collection through a 0.45μfilter. However, these samples appeared slightly cloudy after filtering, and all subsequent samples were filtered through a 0.1μfilter. Immediately upon collection pH and Eh measurements were made on 1 ml aliquots. The sample was then split, and 10 ml were acidified with HCl for cation analysis, while the remaining sample was reserved for anion analysis. At times greater than 50 hours the pH of a 1 ml sample of the water ponded on the tailings was measured as well. After each sampling the head space of the reaction vessel was flushed with N_2 gas, and the entire vessel was stored in a N_2 atmosphere until the next sampling.

Column Experiments

Column experiments were run on two types of tailings solids, whole tailings and tailings leached of their soluble sulfate and carbonate mineral contents. The latter tailings were prepared by first removing the highly soluble sulfate minerals by leaching with deionized water until the specific conductance of the leachate is less than approximately 40 micromhos . The carbonate-mineral content of the tailings was then removed by leaching 210 g of tailings with 120 ml 0.1 N HCl. After the acid leach, the tailings were rinsed with deionized water until the pH of the effluent was 5.9, and then air dried.

In selecting a flow rate for the column experiments it is necessary to compromise the conflicting goals of achieving a long residence time for solid/solution reactions to occur in, and the need for high enough flow rates to produce low pH effluent within the time available for completion of the experiment. Because the results from the chart-recorded alkalinity titrations indicated that after the addition of an aliquot of acid the pH drift stabilized within 4 to 8 hours, 8 hours was selected as the residence time for 1 pore volume. This flow rate allowed the elution of about 90 pore volumes in a 1 month period.

An HCl solution with a pH of 2 was used as an input solution for both column experiments. The apparatus for the column experiments is shown in Figure 3. A reservoir of 8 L of low pH water was used for both columns. The input solution was bubbled with N_2 gas prior to and during the experiment in order to minimize the amount of oxygen entering the system and thereby reduce the potential for pyrite oxidation in the columns.

Column dimensions of 4 cm in length and 5.08 cm in diameter were chosen, giving a column volume of 81 cm. The columns were packed in 12 lifts, and each layer was vibrated and tamped before the addition of the next layer. A total of 152.3 g of whole tailings were packed into column 1, and 167.4 g of leached tailings were packed into column 2. Using the above weights and assuming a specific gravity of 2.75 g/cm3 for the tailings, porosities of 0.32 and 0.25 were calculated for columns 1 and 2, respectively. These porosities are no doubt slightly low because the calculation does not consider the volume contributed by the shallow wells in the end plates to the total volume of the column. Three layers for fine-mesh nylon screen were placed in both ends of the column to contain the fine-grained tailings. The columns were flushed with CO_2 gas for 1.5 hours prior to the introduction of solution in order to reduce the likelihood of occurrence of entrapped gas in the matrix while wetting-up the columns.

The columns were mounted vertically and the flow of solution was upward during the experiment. This arrangement minimizes entrapment of gas during the wetting-up of the columns and also reduces loss of fines from the matrix.

Prior to the introduction of the pH=2 solution, both columns were flushed with deionized water. After the injection of the pH=2 HCl solution, the Cl concentration of the column effluent was monitored constantly with a Cl^- selective electrode so that a breakthrough curve for this non-reactive tracer could be plotted. The breakthrough curve of a packed column can be used to calculate the pore volume and porosity of a sample. During this period the flow rate of the columns was adjusted so that one pore volume was eluted in 3 to 4 hours. A flow rate of 0.109 ml/min +/-0.001 (standard deviation) was achieved during the breakthrough curve of column 1, and a flow rate of 0.111 ml/min +/- 0.001 was measured for the duration of the breakthrough curve for column 2. Assuming a porosity of 0.4 (see the following calculations of column pore volumes) this discharge represents a linear groundwater velocity of $2.3*10^{-6}$m/s.

The breakthrough curves measured for column 1 and 2 are shown in Figure 4. The location of the dimensionless concentration C/C_0 of 0.5 marks the elution of one pore volume, and the data gives a pore volume of 32.2 cm^3 (ml H_2O) for column 1 and 30 cm^3 for column 2. Due to the use of small diameter tygon tubing for the effluent lines, it is estimated that the volume of the end cap and effluent line is less than 1 ml and need not be corrected for. Both breakthrough curves are slightly asymetrical and effluent C/C_0 of 1.0 was never observed. Asymetry observed in the breakthrough curves by other researchers has been attributed to aggregation of the porous medium . In this case the fact that the curves flatten at C/C_0 value less than 1.0 suggests that the lower-than-expected readings are caused by drift of the Cl electrode. Similarity between the two breakthrough curves reflects the homogeneity of the two tailings samples and the similarity of the packing.

Using the pore volumes calculated from the Cl breakthrough data the flow rates were then adjusted to produce a residence time of 8 hours per pore volume. In order to elute one pore volume in 8 hours a flow rate of 0.067 ml/min was required for column 1 and a flow rate of 0.063 ml/min for column 2. Total effluent from each of the columns was collected during an 8 hour period. This sample was then split: 10 ml were acidified with HCl for cation analysis, and the remaining volume reserved for anion analysis. Because iron oxidation occurred in the sample during the 8 hour collection period, a separate sample was collected at the end of each collection period for the analysis of iron speciation in the effluent. This was done by collecting approximately 1 ml of effluent directly into a 1 ml aliquot of acid, thereby eliminating oxidation during collection. Although desirable, a continuous record of effluent pH can not be taken because an in-line pH electrode will contaminate the effluent with potassium from the electrodefilling solution. Rather, the pH of the column effluents was measured at the end of each 8 hour collection period. The measurements were made by attaching a pH flow-through cell with a volume of 0.5 to 1.0 ml to the effluent line. Platinum electrode measurements of the Eh of the effluents were made periodically, also using flow-through cells.

Sorption of H^+

A new method for measuring pH buffering due to sorption of H^+ onto solids was tested on fresh Quirke tailings. The method, developed recently at the University of Waterloo (Locama, 1983, unpublished MSc. thesis), measures the rapid loss of H^+ from solution and pH change due to sorption by measuring the decrease in SO_4^{2-} concentration in solution that occurs in order to maintain solution charge balance.

The procedure consists of saturating the surface exchange sites of the solids with cesium by reacting the sample with a 0.02N CsCl solution in a plastic bag until equilibration. The purpose of this treatment is to displace any sorbed cations and sulfate with Cs and Cl ions. After equilibration residual CsCl solution is flushed from the sample by packing the sample into a column and flushing with distilled water until Cs and Cl levels in the effluent declined to the background level. The CsCl saturated sample is then air dried.

The tailings sample was then split into four subsamples of approximately 15.7g each and acidified with 150 ml of acid. Each subsample was acidified with a different strength of sulfuric acid: strengths of 0.207, 0.613, 1.02 and 1.42 meq/L were used. These input solutions had pH's of 3.65, 3.20, 2.99, and 2.87, respectively. The input solution was pipetted into a 'zip-lock' bag containing the tailings sample, and solution and sample were mixed by kneading the bag for 15 seconds. The solid and solution were then allowed to react for 2 minutes, after which a 7 ml sample of pore water was removed. The pore water was subsequently sampled after 15 minutes, 60 minutes, 3 hours, 20 hours and 5 days of reaction time, while the bag was kneaded periodically.

Each porewater sample was filtered through a 0.45 filter paper after removal. The pH of the sample was then measured and the acidity determined by titration using a Metrohm Potentiograph Model E536 and a KOH titrant. The remaining sample was analysed for sulfate using a Dionex AutoIon System 12 ion chromatograph. In addition the samples removed at 2 minutes were analyzed for cesium by atomic absorption.

Analytical Methods

Acidified samples were analysed for cations using atomic adsorption. Anion analysis of water samples was done using a Dionex Auto Ion System 12 ion chromatograph. Alkalinity and acidity titrations were done using a Metrohn Potentiograph Model ES36. Ferrous iron was measured by the bathophenanthroline method (Lee and Stumm, 1960). The WATEQ2 equilibrium computer model (Ball et al, 1979) was used to calculate aqueous speciation and saturation indices.

RESULTS

Chart-Recorded Titrations

The alkalinity titration curves for whole and sulfate-leached samples of Quirke tailings collected in 1981 are shown in Figure 5. The data for the whole tailings show the presence of buffer reactions at pH values of 7.6 and 4.2 as indicated by the abrupt changes in the slopes of the graphs at these values. Data for the leached sample show no evidence of buffer at a high pH and only a very slight inflection in the titration curve at pH 4.2. Below pH=3.5 both titration curves have similar slopes.

Data from the acidity titrations performed on samples of the solution collected after the alkalinity titrations were complete are presented in Figure 6. The shape of the curves are very similar, and indicate a strong source of acidity at a pH of 4.5. In addition the data for the leached sample show a small inflection at pH=6.

The alkalinity titration curves for a sample of the tailings collected from the Quirke tailings area in 1982 and used throughout the rest of this study are shown in Figure 7. The titration curve for the sample of whole tailings shows a significant buffer capacity at pH 7 to 8, while the data for the leached sample shows only a slight amount of buffering in this pH range. Below pH=7 the titration curves for the two samples are very similar, with changes on slope at approximately pH=4.2 and pH=3.6.

Analyses of samples of solutions from the alkalinity titrations of both whole and leached tailing collected in 1982 are presented in Table 4. The solution chemistry of the solutions resulting from the titrations are very similar. The data show that moderate amounts of Al, Fe, Mg, Ca, and K were solubilized during the titrations.

Batch Tests

Data on pH of the batch test solutions plotted against time (Figure 8) show that the pH rises rapidly at early times in each of the experiments. With the exception of batch C, the pH trends for each batch show a great deal of scatter at times less than 50 hours. At greater times the rate of pH change decreases smoothly in batches A and B. The pH of pore water from batch A was 2.60 after 50 hours and increased to 3.73 after 530 hours. Pore water from batch B had a pH of 2.60 after 48 hours and increased to 3.58 after 528 hours. In batches C and D the increase in pH with time is almost linear after 50 hours. Pore water pH in batch C increases from 1.72 at 50 hours to 2.47 after 527 hours; pore water pH in batch D increases from 2.03 to 2.65 over approximately the same interval.

The results of platinum electrode measurements made on pore waters are presented in Table 5 as both Eh and pe, and are plotted on a pe/pH diagrams for the iron system (Figures 9A and B). Calculated values for pe range from 7.97 to 11.9, and in all four batches there is an inverse relationship between pe and pH. This trend is well defined, except for the data at times less than 50 hours for batch D which show scatter. Eh values measured in batch B are consistently about 20 mV lower than these for batch A at corresponding pH values. Similarly, the Eh values measured in batch D are about 20 mV higher than those for batch C at corresponding pH values. There is little overlap between measured Eh values on batches A and B with these measured on batches C and D.

The results of chemical analysis on water samples from the batch tests are shown in Table 5 A through D. Concentrations of Na, K, Ca, and Mg for batch A are plotted versus time in Figure 10a. The data show that Na concentrations increase for a period and then vary erratically. Potassium concentration is variable with a peak concentration of 83.2 mg/L at 98 hours and a low of 65.2 at 26 hours. Concentration of Ca is relatively constant at slightly 600 mg/L for the first 50 hours after which it steadily decreases. Mg concentrations increase from 342 mg/L to 540 during the experiment, and show little change after 190 hours. Concentrations of Fe, Al, and SO4 for batch A were plotted versus time (Figure 10B). Fe concentrations increase to a peak of 1210 mg/L at 147 hours then decrease to 760 mg/L. A large proportion of the iron is ferric at early times, but the proportion decrease during the experiment at only 8% of the total iron is ferric at 528 hours (Table 6A). Al concentrations decrease sharply during the experiment from 1135 mg/L to 260 mg/L. Concentration of SO_4^{2-} decrease steadily from almost 12,000 mg/L to 5,670 mg/L.

The trends in the concentration of Na, K, Ca, and Mg with time in batch B are very similar to these observed in batch A (Figure 11A). The data for Fe and SO_4^{2-} concentrations reflect the high $FeSO_4$ content of the input solution, but also show the same trends as batch A with steadily decreasing Fe concentrations and a large loss of SO_4^{2-} from solution (Figure 11B). Initially 35% of the total iron is ferric; this figure then ranges from 23 to 29% until 147 hours, after which it declines to 16%. Al concentrations decrease from an initial high of 1310 mg/L to 260 mg/L.

Concentrations of Na, K, Ca and Mg for batch C are plotted versus time in Fig. 12A. Na concentrations increase erratically from 1.20 mg/L to 3.80 mg/L at 528 hours, with an anomalously high value of 6.50 at 385 hours. Concentrations of K increase slightly from 25.0 to 29.5 mg/L during the first 73 hours, then decrease slightly to the last reading of 24.0 mg/L. Ca concentrations increase sharply during the first 97 hours of the experiment from an initial value of 2.81 mg/L to 416 mg/L, after which they are fairly constant. Mg concentrations increase from 198 mg/L to 423 mg/L at 193 hours, and vary little after this time. Graphs of Fe, Al, and SO_4 concentrations versus time (Fig. 12B) show that Fe concentrations vary only slightly during the experiment, although the proportion of ferric iron decreases. Concentration of SO_4^{2-} in the pore water decreases episodically during the experiment from a high of 14100 mq/L to 9180 mg/L. Al concentrations show little variation during the first 73 hours, then show a slowly decreasing trend with the exception of the last sample.

Data for the concentrations of Na, K, Ca, and Mg in batch D are presented in Fig. 13A. The Na concentration shows the same trend as in batch C, including the high value at 385 hours. Concentration of K decreases steadily from 27.8 mg/L to 4.45 mg/L during the experiment. Ca concentrations were similar throughout the experiment, with the exception of the first analysis. Mg concentrations show a substantial increase from 259 to 502 mg/L during the first 193 hours, then vary only slightly. The graphs of Fe and SO_4 concentrations versus time show no trends for these constituents (fig 13B). Al concentrations are only slightly variable ranging from a high of 1250 mg/L at 26 hours to a low of 881 mg/L at 97 hours before increasing again to 1080 mg/L at 528 hours.

Column Experiments

The pH values measured on the effluents from the column experiments on leached and whole tailings are plotted versus cumulative volume and number of pore volumes (pv) in Figure 14. The data show that the effluent from column 1, the whole tailings, had a pH of 7.6 for the first 8 to 11 pore volumes. The data from 11 to 29 pore volumes show the pH to decline from 7.6 to 4.5 in a series of steps, with short pH plateaus in between. These plateau pH values of 6.5, 6.25 and 5.75 were maintained for approximately 5, 3, and 2 pore volumes respectively. The effluent pH then dropped rapidly to a pH of 4.6 at 28 pore volumes, after which the pH gradually declines to 4.1. After a pH of 4.1 was reached there is a further flatting of the pH decline and pH is almost constant at 4.0±0.1 until 64 pore volumes were eluted. The pH readings then decrease steeply but regularly toward the input value of 2.0.

The pH data for column 2, the leached tailings,show that effluent pH dropped from an initial value of 6.5 to 5.8 during the 2.5 pore volumes eluted in the measurement of the breakthrough curve. After 2 additional pore volumes a pH of 4.6 was observed, and by 5.7 pore volumes an effluent pH of 4.1 was measured. The effluent pH was then nearly constant for 37 pore volumes, declining 0.35 pH units during the period. After 43 pore volumes the pH decreased rapidly toward the input pH of 2.0, reaching a pH of 2.1 after an additional 18 pore volumes.

In addition to pH, Eh measurements were made on the column effluents periodically. Drift during the 30 minutes to 1 hour measurement period was rarely greater than 30 mV and often less than 10 mV. The results of these measurements are given in Tables 6 and 7.

Several samples of the effluent from both columns were submitted for analysis of their aqueous chemistry, the locations of which are shown in Figure 14. Results of analyses received to date are presented in tables 6 and 7. Concentrations of Na in column 1 effluent are slightly over 0.4 mg/L in samples 16, 20, 24 and 34, and then decrease to 0.20 in sample 72. The concentrations of K decreases from a high of 4.29 mg/L to 1.72 mg/L in successive samples. Ca, Mg, and SO_4^{2-} all show similar trends with high and relatively constant concentrations in samples 16 through 34, and sharply decreasing concentrations in the following samples. Fe_{TOTAL} is low in sample 16, but samples 20 through 72 show values consistently between 83.6 mg/L and 108 mg/L. Measured Fe^{2+} concentrations are erratic, varying from 45 mg/L to 130 mg/L. The concentration of Al is below detection in samples 16, 20, and 24, then increases to 74.8 mg/L in sample 45 and remains close to 80 mg/L in samples 54, 65, and 72.

Results of chemical analyses on column 2 effluent are presented in table 7. Concentration of Na was found to be low in all samples with no discernable trend. Concentration of K is relatively high in sample 5 and varies from 1.65 to 2.2 mg/L in all other samples. The concentrations of Ca are higher than K but varies similarly. Mg concentrations show a steadily decreasing trend from 13.4 mg/L to 0.50 mg/L in sample 5 and 16 respectively. SO_4^{2-} concentrations increase from

0.92 mg/L in sample 5 to 23.6 mg/L in sample 52, then decrease slightly. Fe_{TOTAL} concentrations are fairly uniform in sample 5 through 52, ranging from 128 to 141, however only 50 mg/L were found in sample 63. Reported Fe^{2+} concentrations were similar to but slightly higher than Fe_{TOTAL} The concentration of Al was 20.7 mg/L in sample 5, varies from 39.6 to 58.9 mg/L in samples 16 through 52, and drops to 9.0 mg/L in sample 63.

Sorption of H^+

The results from the experiment to determine pH buffering due to H^+ sorption are given in table 8 (only the results for the run using 0.207 meq/L H_2SO_4 are shown). The data show that after addition of the sulfuric acid to the sample the pH of the solution rises rapidly from the initial value of 3.65 to 5.06 after 2 minutes. The pH increase slows down with additional time, and a pH of 6.30 was measured at 7200 minutes. The pH increase is paralleled by a large decrease in acidity at early times. No solution acidity was measured after 180 minutes. The concentration of SO_4^{2-} in solution increased in the first 2 minutes to 0.219 meg/L, decreased slightly during the next 180 minutes, only to increase again at later times in the experiment.

The same data presented above has been recalculated to show the change in the solution chemistry with time (table 8). The data again show the large changes in pH and acidity at early times. Also presented in the table are analysis of Al and Cs concentrations in solution. The amount of Al released to solution during the experiment was below detection. The one analysis of Cs concentration shows that a small amount of Cs was released to the solution in the first 2 minutes of the experiment.

DISCUSSION

Chart-Recorded Alkalinity titrations

The titration curve of the chart-recorded alkalinity titrations performed on the sample of whole Quirke tailings collected in 1980 shows pronounced pH buffering at pH values of approximately 7.6 and 4.2 (Fig. 5). The buffering that occurs at pH = 7.6 is attributed to the dissolution of carbonate minerals, although the observed pH is lower than the equilibrium pH values calculated for pure calcite under open-system conditions which is close to 8.2 (Fig. 7). A pH of 7.6 is maintained for the addition of 0.6 meq of H^+, which compares well with the 0.48 meq of neutralization that would occur due to the dissolution of the 0.048 wt % carbonate mineral in the sample. The buffer that occurs at pH = 4.2 is attributed to the dissolution of aluminum hydroxide minerals, because the location of the buffer is close to the equilibrium pH calculated for the dissolution of amorphous $Al(OH)_3$ (Fig. 7).

The titration curve for the sample of 1980 Quirke tailings that were leached of their gypsum content shows a lack of buffering in the high-pH range, which suggests that the carbonate content of this tailings sample was lost during the gypsum leaching. In addition, the pH buffering at 4.2 observed for the whole tailings is not observed in the titration curve of the leached tailings, suggesting the absence of aluminum hydroxide.

Acidity titrations were performed on 100 ml of solution that resulted from the alkalinity titrations to further investigate the soluble components that contributed to the tailings buffer capacity. The resulting titration curves show a large componenent of acidity at pH = 4.5 for solutions from both the whole and leached tailings (Fig. 6). This acidity is interpreted as the hydrolysis of Al as described by the equation:

$$Al^{3+} + 2H_2O = Al(OH)_2^+ \quad pK = 9.3 \tag{1}$$

At equilibrium the equation can be written:

$$\frac{Al(OH)_2^+}{Al^{3+}} = \frac{10^{-9,3}}{H^{+\,2}} \tag{2}$$

The above equation shows that this buffer will be strongest at pH = 4.65, close to the location of the buffer inflection seen in Fig. 2.

The acidity titrations verify that Al was solubilized during the alkalinity titrations but does not address the source of the Al. In view of the apparent absence of an aluminum hydroxide buffer in the alkalinity titration of the leached tailings, it is possible that the aluminum present in solution was derived from the dissolution of primary aluminosilicate minerals in the tailings.

The alkalinity titration curve for a sample of whole tailings collected in 1982, the material used in all subsequent experiments in this report, is somewhat similar to the curves discussed above (Fig. 7). The data between pH = 7.7 and 8.2 follow a trend described by equilibrium with calcite ($CaCO_3$) under open-system conditions. Using the analyzed carbonate-mineral content of 0.128 wt %, it is calculated that calcite dissolution can account for 0.64 meq of neutralization. The titration curve departs from a calcite-equilibrated pH slightly before a total of 0.64 meq of acid was added.

The alkalinity titration curve for the 1982 sample of tailings differs from its 1980 counterpart in that there is no evidence for equilibrium with aluminum hydroxide, although there is a change in slope in the titration curve at a pH of approximately 4.3. In the course of the titration a total of 4.4 meq of H^+ was added to the sample. After accounting for the observed change in pH, it is found that 4.1 meq H^+ were lost due to pH neutralization reactions. 0.64 meq of the neutralization can be attributed to calcite dissolution. Analysis of the solution resulting from the titration (table 4) shows that 1.8 meq of Al was solubilized during the titration, although the source of the Al cannot be specified. However, the addition of Al by either $Al(OH)_3$ dissolution or the congruent dissolution of muscovite mica would produce an approximate charge equivalent amount of H^+ consumption. Formation of HSO_4^- from gypsum dissolved during the titration would produce an estimated 0.5 meq of H^+ consumption, leaving 1.2 meq H^+ unaccounted for. This quantity represents 4.8 meq/100g, which is close to the average cation exchange capacity of 2.9 meq/100g determined for old Elliot Lake tailings (S. Feenstra, unpublished report). There is little doubt that some component of the remaining neutralization capacity is due to dissolution of other aluminosilicates, and the possible effects of pyrite oxidation during the course of the experiment have not been evaluated.

A breakdown of likely pH neutralization components for the titration of a sample of leached 1982 tailings produces a similar remainder of 4.4 meq/100 g (Fig. 7 and table 4). The alkalinity titration curve of the leached sample is important because it closely parallels the titration curve for the leached sample at pH less than 6.5 in spite of the fact that 66% of the carbonate mineral content and all gypsum has been leached from it. This indicates that these minerals can be leached from a tailings sample in order to more easily study the remaining pH-buffering reactions without affecting the reactions one wishes to study.

Batch Tests

Analytical results on porewater samples from batch test A show that when a sulfuric acid solution is added to a sample of whole tailings solids there is a rapid increase in pH, from 0.86 to 2.27 in the first 15.5 hours. This rise is caused by the dissolution of minerals in the tailings (Fig. 8). At these pH values the entire 0.083 wt % carbonate mineral content of the tailings will be immediately dissolved causing the consumption of 0.043 moles H^+. Gypsum dissolution will also occur rapidly, and gypsum is calculated to be slightly supersaturated in all of the samples taken from batch A (table 9).

It is evident from the increasing concentrations of Na, K and Mg with time that continued mineral dissolution takes place during the first 150 hours of the experiment. In view of the slow release of these cations, the reaction is likely to be the dissolution of an alminosilicate. 379 mg/L of Mg were solubilized during the first 15.5

hours of the experiment and an additional 206 mg/L entered solution during the following 514 hours. It is likely that much of the Mg was released by dissolution of carbonate minerals, but additional sources include the aluminosilicate chlorite, and to a lesser extent, muscovite mica, where Mg substitutes for Al in the octahedral layers. The Na and K are probably released by the weathering of interlayer cations from muscovite. In the first 100 hours during which Na increases by 57%, the ratio of Na:K ranes from 0.069 to 0.085, averaging 0.074. Although common source for Na and K is suggested by the constancy of the Na:K ratio, it is likely that Na is being released by albite dissolution as well. After 100 hours the concentration of K in solution declines and the ratio increases.

The primary source of the Al in solution is the dissolution of aluminum hydroxide, and the Al concentration observed in sample 2 represents 40% of the predicted $Al(OH)_3$ content of the tailings (table 2). It was hoped that at the low pH values produced there would be no precipitation of secondary aluminum-containing solid phases, and therefore increases in Al concentration could be used to examine the rate of muscovite dissolution. The data show that this was not the case, and rather it was found that Al concentrations in batch A porewaters decrease throughout the experiment.

The most tenable cause of loss of Al from solution is precipitation of an Al-containing solid phase. Saturation indices (SI) for selected Al-containing solid phases show that amorphous $Al(OH)_3$ is undersaturated for the duration of the experiment (table 9), which indicates that gibbsite, the crystalline $Al(OH)_3$ solid phase, is undersaturated as well.

Likely candidates for aluminum solid phases being precipitated are allophane and aluminum hydroxysulfate minerals. Allophane is an amorphous aluminosilicate mineral of variable composition with the formula $Al(OH)_{3\,(1-X)}\ SiO_{2\,X}$. where X is a function of pH. Results of allophane saturation indices calculated for the batch tests range from -0.45 to 0.61, indicating near saturation in most cases. These saturation indices suggest that precipitation of allophane may account for loss of aluminum from solution.

However, the existence of an aluminosilicate with pH dependent composition as proposed by Paces (1975) is still controversial. In evaluating possible causes of incongruent dissolution during a kinetic study of mica dissolution, Lin and Clemency (1981) noted that their data fit Paces theoretical expression for allophane equilibrium but reported that "we do not except the existence of this hypothetical aluminosilicate in this experiment". The fact that the allophane SI's show undersaturation while aluminum concentrations continue to decrease indicates that precipitation of this mineral is not responsible for all of the removal of Al from solution.

It has been proposed that in groundwaters with high SO_4^{2-} concentrations, the concentration of Al in solution may be limited by the precipitation of aluminum hydroxysulfate minerals (Nordstrom, 1982; van Breemen, 1973; van Breemen, 1976). In batch A it was observed that SO_4^{2-} concentrations decrease with time, and in the first 150 hours of the run 17 mmol of Al and 22 mmol of SO_4^{2-} were lost from solution. This data suggests the precipitation of an $Al\text{-}SO_4^{2-}$ solid phase. Although loss of SO_4^{2-} may also be occurring due to the precipitation of Ca and

Fe-SO_4^{2-} phases, Ca concentrations are fairly constant and Fe concentrations increase during the first 150 hours of the batch test indicating that loss of large amounts of these cations is unlikely.

The saturation indices given in table 9 indicate that jurbanite ($AlSO_4OH \cdot 5H_2O$), with SIs of 0.58 to 1.56 indicating slight supersaturation, is the aluminum hydroxysulfate mineral most likely to have precipitated from solution. Basaluminite ($Al_4SO_4(OH)_{10}.5H_2O$) is undersaturated in all cases, and alunite, although supersaturated most of the time, is kinetically inhibited from precipitating (Nordstrom, 1982). The average molar ratio of loss of Al to loss of SO_4^{2-} in successive samples was calculated to be approximately 1:2, although it varies from 1:4 to one instance of net SO_4^{2-} gain. None of the above aluminum hydroxysulfates have an Al:SO_4 ratio of 1:2, and the fact that the ratio does not correctly reflect the stoichiometry of one of these phases is probably due to input of Al and SO_4^{2-} from other sources.

During the first 150 hours of batch test A 1320 mg/L of Fe were solubilized mostly from the dissolution of amorphous $Fe(OH)_3$. This is indicated by the relatively high values of the pIAP (Langmuir and Whittemore, 1971) (table 9). Additional sources of Fe are the oxidation of pyrite by Fe^{3+} released by $Fe(OH)_3$ dissolution, and weathering of minor amounts of mafic minerals in the tailings. After 150 hours the concentration of Fe decreases steadily, as does the concentration of Al and SO_4^{2-} (Fig. 10B). Shortly before this time, the concentration of K reaches a peak and then also declines.

The simultaneous decrease in K, Fe, and SO_4^{2-} suggests the precipitation of K-jarosite. High degrees of jarosite supersaturation in acid mine waters have been observed by other researchers (Nordstrom et al., 1979; Miller, 1979; Peterson and Krupka, 1981). Reported K-jarosite pKs vary from 94.6 (van Breemen, 1976) to 98.8 (Ball et al., 1970) and uncertainty in the equilibrium constant may contribute to the apparent supersaturation.

A pe-pH plot of data for batch test A shows that measured values plot close to the boundary indicating equilibrium between the solution and K-jarosite (Fig. 9A). This figure is drawn for constant Fe and SO_4^{2-} concentrations, and due to the variation of these concentrations between samples and the uncertainty in the equilibrium constant, the actual position of the boundary is not well defined. However, it is considered significant that the trend parallels the jarosite line, and we conclude that there is a strong probability that jarosite precipitation is removing Fe from solution at times greater than 150 hours in batch test A.

The results for batch B are very similar to those for batch A and show little effect from the 0.05 mol/L of $FeSO_4$ in the input solution. The additional SO_4^{2-} provided a better buffer at pH close to 2, but the shapes of the pH versus time curves for the two tests are alike and within 0.25 pH units at most times (Fig. 8). The patterns of release of Na, K and Mg to solution are the same in batch A and B and it is believed that the geochemical processes are the same as described above for batch A. Loss of large amounts of Al and SO_4^{2-} are also observed in batch B, and again calculated SIs indicate that jurbanite ($AlSO_4OH{\bullet}5H_2O$) is most likely the solid phase being precipitated (table 10).

The major difference between the batch A and B results is that only a small increase in Fe is seen during the first 25 hours of the batch B results, and the Fe concentration decreases throughout the rest of the experiment. The total amount of Fe in solution in batch B at early times is roughly equivalent to the amount input, and apparently little dissolution of amorphous $Fe(OH)_3$ occurred. Calculated SIs for amorphous $Fe(OH)_3$ and the jarosite are in the same range as those observed for batch A (table 10) and the trend of pe-pH data for batch B parallels that of batch A (Fig. 9).

The tailings used for batch experiments C and D differ from those in tests A and B in that all of the gypsum and most of the carbonate minerals were leached from the former prior to the experiment. Due to the removal of the carbonate buffer component the pHs measured on porewaters from batches C and D were lower throughout the experiment than those measured on A and B by 0.75 to 1.5 pH units (Fig. 8). The pH versus time curves for batches C and D flatten rapidly, however pH is a log scale and the actual rate of change of H^+ concentration for batches C and D is greater than that for batches A and B at times greater than 50 hours.

The pattern of release of Na and Mg in batch C is similar to that for batches A and B, however the increase and subsequent decrease of K concentrations is not as marked in batch C. A notable difference is the variation in Ca concentration: due to the removal of the samples gypsum prior to the test, batch C porewaters are initially undersaturated with respect to gypsum (table 11). The Ca in the porewaters increased until saturation was reached after about 97 hours, after which Ca concentration is about constant.

Trends of decreasing concentrations of Al, Fe and SO_4^{2-} with time are seen in the batch C data. The concentration of Al is relatively constant for 73 hours after which it slowly declines. Saturation indices for the batch C data show that jurbanite ($AlSO_4OH \cdot 5H_2O$) is undersaturated at times less than 73 hours, essentially at saturation from 73 to 147 hours, and supersaturated at later times (table 11). The fact that Al concentrations do not begin to decrease until saturation with respect to jurbanite is reached suggests that the precipitation this mineral is removing Al from solution.

Although Fe concentrations in batch C decrease with time as observed in the other batch tests, the decline is more irregular and quantitatively smaller. SI values for several Fe-solid phases suggest that the precipitation of Na-jarosite is the cause of the Fe loss (table 11). This hypothesis is supported by the lower concentrations of Na in batch C porewaters than in samples from batch A and B.

The release of Na and Mg in batch test D is similar to that observed in other batch tests, although there is considerably more scatter in the Na data. As in batch C, the batch D porewaters are initially undersaturated with respect to gypsum, but achieving saturating more rapidly (table 12). Batch D results differ from other tests in that K concentrations decrease throughout the experiment. It is highly unlikely that K is not being released from muscovite dissolution at least at early times, and it appears that precipitation of a K-containing solid phase occurs almost from the outset of batch test D. While saturation indices for jurbanite and the jarosite minerals show supersaturation there is little indication of major losses of Al, Fe or SO_4^{2-} from solution, and the precipitation of a particular solid phase is not implicated.

Column Experiments

The objective of the column experiments was to examine the pH buffering of tailings under dynamic conditions in order to simulate conditions more like a tailings impoundment. It was hoped that data on the release of cations due to dissolution of solid phases involved in pH- buffering reactions could be used to identify the phases involved. This task is easier if equilibrium with respect to a solid phase occurs, but much more difficult if equilibrium is not achieved. The identification of particular solid phases is especially difficult due to the large number of potentially reactive solid phases present.

The pH versus time records of experiments on the whole (column 1) and leached (column 2) tailings show distinct plateaus that suggest temporary equilibrium or steady-state conditions (Fig. 14). While it is likely that reaction rates of most of the carbonate, sulfate, and hydroxide minerals are rapid enough to achieve equilibrium in the 8 hours of residence time in the column, the dissolution rates of aluminosilicates are usually slow and disequilibrium will respect to these minerals is expected.

In order to investigate the equilibrium chemistry of the column effluents, the laboratory analyses of solution chemistry were evaluated using the WATEQ2 equilibrium computer model (Ball et al, 1978). Calcite saturation indices were calculated for samples for which alkalinity data was available. The SI's range from 0.57 to 0.92, indicating that both the effluent that preceded acid injection (samples 1-1, 1-3, and 1-4) and samples from the first 7 pore volumes of acid input effluted are supersaturated with respect to calcite (Appendix G, Table G.1). The aluminum concentrations for all of these samples were below detection, and calculations using the only iron analysis (sample 10) indicate supersaturation with respect to amorphous iron hydroxide.

There are three ways in which calcite supersaturation can be produced: 1) addition of Ca^{2+} to solution; 2) addition of CO_3^{2-} to solution; or 3) any pH-increasing process. The first possibility may occur if solution equilibrium with respect to calcite is reached prior to saturation with respect to gypsum, in which case subsequent gypsum dissolution would cause calcite to become supersaturated. The case is an additional source of CO_3^{2-} is not likely to occur in the tailings sample.

Calcite supersaturation has been observed to occur due to pH-increasing processes. In particular, degassing of CO_2 during sampling can result in an increase in pH and apparent calcite supersaturation. However, the use of an in-line flow through cell for pH measurements will minimize degassing. The cause of calcite supersaturation in the column 1 effluent remains unknown at this time.

The saturation indices calculated for the effluent from column 1 show that at pH=6.18 or greater the effluent is slightly supersaturated with respect to gibbsile (crystalline $Al(OH)_3$), and all other Al-contain solids are undersaturated (table 13A). This suggests the dissolution of an aluminum hydroxide with a solubility product slightly greater than gibbite but lower than amorphous $Al(OH)_3$. The high pH of the effluent indicates that the pH is controlled by reactions other than $Al(OH)_3$ dissolution.

Column 1 samples 34 through 54 are also close to equilibrium with gibbsite, and the pH is approaching the equilibrium pH calculated for amorphous $Al(OH)_3$ (Fig. 7). Several aluminum hydroxysulfate minerals become slightly supersaturated in this pH range and precipitation of minor amounts of Al may be occurring.

Data for column 2 (leached tailings) are very similar to that discussed above (Table 13B). All of the column 2 samples from the long pH plateau of about 3.9 show near saturation with respect to gibbsite, however due to the absence of gypsum the concentrations of sulfate in solution are much lower and as a result the only aluminum hydroxysulfate to exceed saturation is alunite. In both column 1 and 2 the pH of the effluent drops steeply at approximately the same time as gibbsite undersaturation occurs.

A plot of the pe- pH data for columns 1 and 2 show that supersaturation with respect to amorphous $Fe(OH)_3$ occurs in the higher - pH samples (Fig.15). An orange precipitate that accumulated in the effluent lines of both columns is assumed to be $Fe(OH)_3$. The supersaturation and precipitation probably occur due to pH neutralization reactions occurring near the effluent end of the column. The increased pH would decrease Fe^{3+} solubility and the colloidal-sized precipitation could then be flushed out of the column. At lower pH values the data for both columns 1 and 2 are near the boundary indicating jarosite equilibrium.

The values of pIAP for $Fe(OH)_3$ amorphous calculated using WATEQ2 confirm that samples 16 through 20 are highly supersaturated with respect to this solid phase, while samples 24 to 34 show a lesser degree of supersaturation. The rest of the samples along the pH 4.2 plateau in column 1 show approximate equilibrium with amorphous $Fe(OH)_3$, as do samples 5 through 45 from column 2. Samples with a pH of less than 3, however, show high pIAP values, indicating that the solutions are dissolving amorphous $Fe(OH)_3$ or in equilibrium with a more crystalline Fe- hydroxide. In the data calculated for both column 1 and 2 K jarosite is the only iron hydroxysulfate mineral above saturation.

It is thought that the Fe in the column effluents is solubilized as Fe^{3+} by the dissolution of $Fe(OH)_3$ under low pH conditions near the influent end of the column. The Fe is then kept in solution through reduction to the 2^+ oxidation state by reaction with pyrite. Analyses of column 2 effluent show that 0.07 to 0.25 mmol/L SO_4^{2-} were released due to pyrite oxidation during the experiment. This amount of oxidation would result in the release of 2 to 7 mg/L of Fe^{2+}. If the pyrite oxidation is due solely to oxidation by Fe^{3+} as shown by the following reaction:

$$14Fe^{3+} + FeS_2 + 8H_2O = 15Fe^{2+} + 2SO_4^{2-} + 16H^+ \qquad (3)$$

then a concentration of 28 to 105 mg/L of Fe^{2+} would be predicted from the amount of SO_4^{2-} found in the effluent. The observed effluent Fe concentrations of 50 to 141 mg/L are in the same range as the predicted values, indicating that the proposed mechanism is a likely source of the Fe.

The only evidence for dissolution of aluminosilicate minerals in the column experiments is the release of K, Na, Mg, and in column 2, Ca. Because of the abundance of muscovite mica, attention is focussed on the possibly release of K from mica interlayers. After an initially high release rate, K concentrations in the column 1 effluent are fairly constant at an average of 1.97 mg/L during the pH = 4.2 plateau (samples 45, 54 and 65). Analyses of samples 16 through 45 from column 2 show a similar average of 1.85 mg/L K.

When the flow rate for the columns is taken into consideration, the above concentrations of K represent a K release rate of $5.0 * 10^{-5}$ mol/L/8 hr. or $5.2 * 10^{-11}$ mol/sec. In a recent paper it has been proposed that after an initial period of rapid release of K from mica interlayers, the dissolution of muscovite mica is controlled by the slow destruction of silica tetrahedral layers (Lin and Clemency, 1981). The rate of silica release, expressed as a linear function of time, was found to average $2.5 * 10^{-17}$ mol/cm^2/sec. for samples of two different muscovites at a pH of 4.6 to 5.1. Although the lack of surface area data for the tailings prohibits direct comparison of K release rates, by assuming the literature value and dividing it into the observed K release rate, a muscovite surface area of $1.2 * 10^4$ cm^2/g is calculated. Considering the grainsize of the tailings and weight percent muscovite, there is a rough order-of-magnitude correspondence between the predicted surface area and what one would expect for the tailings material. This indicates that further work on tailings samples with known surface area may be fruitful.

The fairly constant concentrations of Na, Mg, and in column 2, Ca, suggests that these cations are being released by the slow dissolution of aluminosilicate minerals. The source of the Na is probably dissolution of albite, with a minor contribution from the muscovite mica. No source of Ca and Mg is apparent, although the later may be due to dissolution of small quantities of chlorite in the tailings.

A new geochemical computer model recently developed at the University of Waterloo for simulating reactions of tailings pore water in tailings or aquifers was used to futher test how well equilibrium reactions describe the pH history of the effluent from the whole tailings (column 1). The program, ADNEUT (K. Morin, unpublished PhD thesis), is a geochemical mixing cell model that will execute specified thermodynamically-represented solid-solution reactions. To model the reactions in the whole tailings sample the reactive solid phases specified were calcite, gypsum, amorphous $Al(OH)_3$ with a pK = 32.16, and amorphous $Fe(OH)_3$ with a pK = 37.1. In addition, when the concentration of Fe^{2+} in solution is high, ADNEUT will dissolve calcite incongruently and precipitate siderite ($FeCO_3$). The amounts of Al and Fe hydroxides present in the tailings calculated in Table 2 were used as model input. The measured gypsum content of 2.75 wt. % and a carbonate mineral content of 0.128 wt. % were also specified.

The results of the model calculations using the minimum of 2 reaction cells are shown along with the pH records of columns 1 and 2 (Fig. 16). The pH record for column 2 has been shifted so that the point at which the pH drops sharply after the long pH = 3.9 plateau occurs at the same location as the similar feature in the column 1 data.

Lines A through E represent pH plateaus which would be observed in the effluent if equilibrium were maintained with the assemblage of solid phases listed for each line. The calculations show that the closed-system dissolution of calcite in the presence of gypsum will produce an effluent pH of 6.53 due to the large amounts of calcium released by gypsum dissolution. During the elution of the calcite, some of the calcite is altered to siderite. After all of the calcite is removed, the dissolution of siderite will dominant neutralization reactions producing an effluent pH of 5.59.

When all of the siderite is dissolved equilibrium with amorphous $Al(OH)_3$ will be established. The model predicts an equilibrium pH of 4.46 when gypsum is present but only 4.26 when gypsum is absent. This predicted difference of 0.2 pH units is in agreement with two features of the data: the gradual decrease in the pH of column 1 effluent during gypsum elution, and the 0.2 pH unit difference between the gypsum-free (column 2) and whole tailings (column 1).

After all aluminum hydroxides are removed the model predicts that equilibrium with $Fe(OH)_3$ will produce an effluent pH of 2.87. The data for column 1 show a slight flattening near this pH but there is no evidence of equilibrium with a Fe - hydroxide solid phase with a pK = 37.1 in either column.

In addition to predicting the equilibrium pH values, the model also calculates the total amount of effluent discharged before a solid phase is completely dissolved. The number of pore volumes at which calcite, amorphous $Al(OH)_3$, and gypsum are predicted to be removed from column 1 are shown in Figure 16. Calcite depletion is predicted to occur in approximately 6.5 pore volumes. This volume is reached and exceeded while the effluent pH remains at 7.6, and it is apparent therefore that there are other important pH - buffering characteristics of the tailings at high pH values that have not been defined yet and therefore were not represented in the model runs.

The model predicts that 40 pore volumes of solution will equilibrate with gypsum before this mineral is removed. The prediction corresponds well with the column 1 data, where gypsum undersaturation is reached between samples 34 and 45 (Table 13A). Amorphous $Al(OH)_3$ persists in the column until 56 pore volumes have been eluted, which is similar to the 64 pore volumes observed to be eluted from column 1 prior to undersaturation with respect to this phase and a sharp drop in pH.

The model predictions are in good agreement with the observed effluent pH for column 1 in terms of both pH values and volume of solution required for the removal of solid phases. In addition Fig. 16 shows that the pH neutralization behaviour of the whole and leached tailings was very similar for pH less than 6.5, indicating that the leaching of the sulfate minerals had only minor effects on the low-pH buffer reactions.

Sorption of H^+

Results of the experiments on sorption of H^+ show that although large amounts of H^+ are lost from solution within 2 minutes and there is a los of 0.174 meq/L of acidity, there is no loss of SO_4^{2-} from solution. Rather there is a slight gain of SO_4^{2-}. This indicates that the neutralization is due to mineral dissolution reactions rather than sorption of H^+ onto grain sufaces. The data for cesium shows that only 0.0134 meq/100g were released to solution after 2 minutes of reaction, an indication of the low cation exchange capacity of this material.

The slight gain in SO_4^{2-} shown by the solution after 2 minutes indicates that small quantities of SO_4^{2-} minerals remained in the tailings samples in spite of efforts to leach them, or that SO_4^{2-} was added after leaching by pyrite oxidation. Results from the same tailing solids using stronger H_2SO_4 also showed no loss of SO_4^{2-} from solution. Although interpretation of the results are complicated due to the apparent presence of an unknown SO_4^{2-} source, we conclude that at low pH the tailings solids have essentially no buffer capacity due to the sorption of H^+ .

SUMMARY OF CONCLUSIONS

The goal of describing the pH neutralization behaviour of Elliot Lake tailings was approached through the use of several different laboratory experiments. Because of anticipated complications due to incongruent dissolution and precipitation of secondary sulfate solid phases during aqueous reactions with tailings solids, tailings that were leached of all of their soluble sulfate minerals as well as whole tailings were used in the experiment. This procedure increases the likelihood of identifying solid phases dissolving to neutralize low pH conditions.

Preliminary work using chart-recorded alkalinity titrations on samples collected in 1980 and 1981 showed that the tailings contain a high-pH buffer that apparently is caused by the dissolution of trace amounts of carbonate minerals in the tailings. A prominent inflection at pH=4.2 in the titration curve of the sample of 1980 whole tailings indicates that dissolution of amorphous $Al(OH)_3$ is buffering the pH at this level. This buffer reaction was not observed in other samples. Both an acidity titration on the solution resulting from the alkalinity titration on the 1980 leached tailings, and an analysis on the solution resulting from the alkalinity titration of the 1982 sample of leached tailings show that Al was solubilized during the alkalinity titrations. This data confirms that during the alkalinity titrations Al is released from an additional source of Al, probably an alminosilicate mineral. Finally, the similarity between the titration curves at pH 6.5 for whole and leached 1982 tailings shows that the sulfate minerals can be leached from the tailings without grossly changing the pH-neutralization characteristics of the tailings.

An experiment designed to determine the amount of pH buffering due to sorption of H^+ onto grain surfaces demonstrated that essentailly no buffering can be attributed to this mechanism.

The batch tests were specifically designed to examine the dissolution of pH-neutralizing solid phases under low pH conditions, and thus test the hypothesis that dissolution of aluminosilicate minerals in the tailings are important pH-neutralizing reactions. The four batch tests that were done involved two materials (whole and leached tailings) and 2 solution types (sulfuric acid with high or low Fe concentrations).

The pH neutralization behaviour of the batches of the same material was similar for both low and high Fe input solutions. Large increases in pH occurred in all of the batches. These changes in pH were accompanied by the release of Na, K, Ca, and Mg, which is believed to result from dissolution of aluminosilicate minerals. However, the loss of large amounts of Al, Fe and SO_4^{2-} from solution at later times in all of the experiments with the exception of batch D, indicates that incongruent dissolution is occurring. Calculations of saturation indices suggests that Al, Fe and SO_4^{2-} are being removed from solution through the precipitation of Al and Fe hydroxysulfate minerals. Because of the precipitation reactions, it was not possible to calculate any cation release rates and the use of cation ratios to determine the identity of the dissolving phases was also prohibited.

Column experiments on pH-neutralization by tailings under dynamic conditions were performed on a sample of whole tailings and a sample of tailings leached of carbonate and sulfate minerals. An influent solution of 0.01 N HCl was used to simulate a low-pH source. The resulting records of effluent pH versus time show that the effluent pH was initially high (6.5 to 7.6) and decreased in a series of distinct plateaus. The pH records of the leached and whole tailings were very similar below a pH of 6.5. The occurence of pH plateaus suggests equilibrium with and subsequent removal of a number of solid phases.

Equilibrium calculations show that effluent from column 1 was supersaturated with respect to calcite for the first 7 pore volumes eluted. The cause of the supersaturation is unclear. In addition, equilibrium calculations show that effluent from column 1 was supersaturated with respect to calcite in at least the first 7 pore volumes eluted. Effluent from both columns with a pH greater than 3.8 was near saturation with respect to gibbsite. It is suggested that an amorphous $Al(OH)_3$ phase is dissolving in these solutions. Concentrations of Fe in column effluents were found to be fairly high. It is hypothesized that the Fe is solubilized by the dissolution of amorphous $Fe(OH)_3$ under the low pH conditions near the influent end of the column. The Fe is then kept in solution by reduction to the 2^+ oxidation state by reaction with pyrite.

Dissolution of aluminosilicate minerals in the tailings is indicated by a fairly constant release rate for Na, K, and Mg. Data from the leached tailings also shows that there is a low-solubility source of Ca as well. Application of a dissolution rate for muscovite mica from the literature to the average rate of K release in columns 1 and 2 predicts a mica surface area of $1.2 * 10^4$ cm^2/g. Additional work with tailings materials of known surface area may be fruitful.

Results of the application of a new geochemical mixing cell model to the tailings predict a sequence of equilibrium pHs in the effluent depending on the solid phases present. The pH of the effluent was dominated by the following solid phases in succession: calcite (pH=6.53), siderite (pH=5.59), amorphous $Al(OH)_3$ (4.26), and amorphous $Fe(OH)_3$ (pH=2.87). The presence of gypsum was shown to be less influential. The pH plateaus predicted by the model describe many of the features observed in the effluent from the columns. In addition the model predictions for the number of pore volumes of solution required to elute all of the gypsum and amorphous $Al(OH)_3$ are similar to the observed volumes of flow.

In general the results from the testing show that the Elliot Lake tailings have a considerable buffer capacity imparted to them due to the presence of carbonate minerals and aluminum hydroxides. In addition there is an unknown component of buffering active in the range of pH 6.5 to 7.6. These results indicate that the pH of groundwater exiting the inactive tailings can be expected to be buffered at a pH of approximately 4.2 for an extensive period of time, although the groundwater will retain a high acidity due to dissolved Fe^{2+} and Al. In fact column results suggest that if the amount of acid production in the tailings could be reduced there is the possibility that a neutral pH could be maintained in the groundwater exiting the tailings.

The original proposal for work on acid neutralization and transport of reaction products in tailings called for two years of laboratory work. In view of the large amount of incongruent dissolution that took place in the batch tests, a repetition of a batch-type test in which precipitation of sulfate-containing solid phases is prevented by prior leaching of the tailings sulfate mineral content and use of HCl acid would better indicate the identity of solid phases dissolving during pH neutralization.

Results of the column experiments left some question as to whether the pH plateaus observed were equilibrium reactions or were the result of a temporary kinetic steady-state. Additional work using the same experimental apparatus but using different flow rates would help answer this question. It is also recommended that additional column experiments be undertaken to determine the level of pH and acidity in the groundwater that will issue from the tailings after all of the carbonate and aluminum hydroxide minerals have been depleted and the pH drops below 4.2.

The continued increase in pore water pH with time observed in the batch tests indicate that dissolution of aluminosilicates may be an important mechanism, but only at low pH's and in areas where the groundwater flow rate is low enough to allow this slow reaction to occur.

List of Tables

Table 1: Grain size analysis of Quirke tailings by wet and dry sieve methods. Percentages are based on total weight of sample after sieving. Loss of material in all cases was $\leq$ 1% original weight.

Table 2: The concentrations of Fe, Al, and SO_4 in Quirke mill effluents that are disposed of with the tailings solids are used to calculate the weight percent of the total tailings solids of $Fe(OH)_3$, $Al(OH)_3$, and gypsum ($CaSO_4 \cdot 2H_2O$).

Table 3: Preliminary tests for batch reaction of tailings and low-pH water; titration of 25 grams of gypsum-leached tailings with 0.1 N HCl.

Table 4: Chemical analysis of samples of final solution composition from chart-recorded alkalinity titrations on whole and leached Quirke tailings collected in 1982. All analyses are reported as mg/L.

Table 5A: Chemical analyses of pore water samples from batch A.

Table 5B: Chemical analyses of pore water samples from batch B.

Table 5C: Chemical analyses of pore water samples from batch C.

Table 5D: Chemical analyses of pore water samples from batch D.

Table 6: Chemical analyses of column 1 effluent.

Table 7: Chemical analyses of column 2 effluent.

Table 8: Solution chemistry from the determination of pH buffering by H^+ sorption onto tailings solids. Initial solution pH=3.65 and initial concentration of SO_4 was 0.207 meq/L. Changes in solution chemistry are also tabulated on a per-gram weight of solids basis.

Table 9: Saturation indices of selected Al and Fe containing solid phases calculated for batch A data using the WATEQ2 equilibrium model.

Table 10: Saturation indices of selected Al and Fe- containing solid phases for batch B data calculated using the WATEQ2 equilibrium model.

Table 11: Saturation indices of selected Al and Fe containing solid phases calculated for batch C data using the WATEQ2 equilibrium model.

Table 12: Saturation indices of selected Al and Fe containing solid phases calculated for batch B data using the WATEQ2 equilibrium model.

Table 13A: Saturation indices of selected Al- containing solid phases calculated for column 1 data using the WATEQ2 equilibrium model.

Table 13B: Saturation indices of selected Al- containing solid phases calculated for column 2 data using the WATEQ2 equilibrium model.

Table 14A: Saturation indices of selected Fe- containing solid phases calculated for column 1 data using the WATEQ2 equilibrium model.

Table 14B: Saturation indices and pIAP of selected Fe- containing solid phases calculated for column 2 using WATEQ2 equilibrium model.

LIST OF FIGURES

Fig. 1: Plot of the tailings grain size distribution curve and grainsize versus carbonate content expressed as weight percent $CaCO_3$.

Fig. 2: Schematic of nalgene reaction vessel used in the batch tests. Samples of pore water were collected through the septum using a 50 ml syringe. Use of porous polyethylene screens (Vyon) prevents tailings material from clogging the needle during sample collection. The solution inlet loop is constructed of air approximately 28 cm length of 3/32" ID tygon perforated with a needle. The inlet loop is covered with a sheet of fine nylon screen not shown in the figure.

Fig. 3: Schematic of column experiment. The input solution was bubbled with N_2 gas before injection. A flow-through cell was used to make periodic pH and Eh measurements on the effluent.

Fig. 4: Chloride breakthrough curves for column 1 and 2. The flow rate for both columns was approximately 0.11 ml/min. Concentrations are plotted at as the dimensionless ratio of measured outflow concentration (c) to input concentration (C_0).

Fig. 5: Alkalinity titration curves for 1980 samples of whole and leached Quirke tailings. The titrations were performed on 50 g samples suspended in 100 ml of deionized water with 0.1 N H_2SO_4 as the titrant.

Fig. 6: Acidity titrations of 100 ml of final solution collected from alkalinity titrations on 1980 samples of Quirke tailings 0.1 N NaOH was used as the titrant.

Fig. 7: Alkalinity titration curves for 1982 samples of whole and leached Quirke tailings. The titrations were performed on 25 g samples suspended in 100 ml of deionized water with 0.1 N HCl as the titrant. Also shown are theoretical titration curves calculated for pure $Al(OH)_3$ amorphous and $CaCO_3$ solid phases using equilibrium constants.

Fig. 8: Plot of pH versus time for batch test results.

Fig. 9: Data for batch tests A(+) and B(-) (9A) and C(+) and D(.) (9B) are plotted on pe - pH diagrams for iron species and selected solid phases. The boundaries on the diagram were drawn for the following conditions; Fe $=10^{-4,05}$, K $=10^{-3}$, SO_4^{2-} $=10^{-2}$, pK of $Fe(OH)_3=38$.

Fig. 10A: Concentration of Na, K, Ca, and Mg in batch A pore waters plotted versus time.

Fig. 10B: Concentration of Fe, Al, and SO_4 in batch A pore waters plotted versus time.

Fig. 11A: Concentration of Na, K, Ca, and Mg in batch B pore waters plotted versus time.

Fig. 11B: Concnetration of Fe, Al, and SO_4 in batch B pore water plotted versus time.

Fig. 12A: Concentration of Na, K, Ca, and Mg in batch C pore waters plotted versus time.

Fig. 12B: Concentration of Fe, Al, and SO_4 in batch C pore waters plotted versus time.

Fig. 13A: Concentration of Na, K, Ca, and Mg in batch D pore waters plotted versus time.

Fig. 13B: Concentration of Fe, Al, and SO_4 in batch D pore waters plotted versus time.

Fig. 14: pH of effluent volume for column 1 (14A) and column 2 (14B) plotted versus cumulative vlume and number of pore/volumes. Effluent samples submitted for analyses are indicated on the graph.

Fig. 15: Data for columns 1 and 2 plotted on a pe-pH diagram for iron species and selected solid phases. The boundaries on the diagram are drawn for the following conditions; Fe $=10^{-4,05}$, K $=10^{-3}$, SO_4 $=10^{-2}$, pK of $Fe(OH)_3=38$.

Fig. 16: Data for column 1 and 2 overlain so that the points at which pH drops below approximately 3.9 coincide.The horizontal lines

show equilibrium pH values predicted by the ADNEUT mixing cell model for the following sequence of solid phases: A) calcite-gypsum-$Al(OH)_3$-$Fe(OH)_3$; B) siderite-gypsum-$Al(OH)_3$-$Fe(OH)_3$; C) gypsum-$Al(OH)_3$- $Fe(OH)_3$; D) $Al(OH)_3$-$Fe(OH)_3$; E) $Fe(OH)_3$.

TABLES IN CHAPTER 3

Table 1: Grain size analysis of Quirke tailings by wet and dry sieve methods. Percentages are based on total weight of sample after sieving. Loss of material in all cases was ≤ 1% original weight.

		DRY SIEVE				WET SIEVE			
GRAIN SIZE ANALYSIS WEIGHT OF SAMPLE BEFORE SIEVING (g) :		SAMPLE 1 146.20		SAMPLE 2 143.30		SAMPLE 3 185.00		SAMPLE 4 196.92	
Mesh size		wt. (g)	%	wt. (g)	%	wt. (g)	%	wt. (g)	%
> 35	(>425μ)	20.69	14.20	20.39	14.33	27.61	15.04	30.05	15.42
< 35 >45	(<425, >355μ)	10.12	6.95	9.72	6.83	11.50	6.27	12.77	6.55
< 45 >60	(<355, >250μ)	25.05	17.19	24.20	17.01	34.24	18.66	36.05	18.50
< 60 >80	(<250, >180μ)	20.97	14.39	20.01	14.06	24.80	13.51	25.25	12.95
< 80 >120	(<180, >125μ)	14.30	9.81	14.24	10.01	17.59	9.59	18.70	9.59
< 120 >170	(<125, >90μ)	12.01	8.24	11.63	8.32	14.39	7.84	15.09	7.74
< 170 >230	(<90, >63μ)	9.01	6.18	9.10	6.40	9.69	5.28	11.30	5.80
< 230 >325	(<63, >45μ)	4.58	3.14	4.61	3.24	5.20	2.83	5.70	2.92
< 325	(<45μ)	28.98	19.89	28.18	19.81	38.50	20.98	40.01	20.53
WEIGHT OF SAMPLE AFTER SIEVING (g)		145.71		142.28		183.52		194.92	

Table 2: The concentrations of Fe, Al, and SO_4 in Quirke mill effluents that are disposed of with the tailings solids are used to calculate the weight percent of the total tailings solids of $Fe(OH)_3$, $Al(OH)_3$, and gypsum ($CaSO_4 \cdot 2H_2O$).

Source*	Flow Rate (L/s)	Fe_T (mmole/L)	$Fe(OH)_3$ kg/Day*10^{-3}	Al (mmole/L)	$Al(OH)_3$ kg/Day*10^{-3}	SO_4 (mmole/L)	$CaSO_4 \cdot 2H_2O$ kg/Day*10^{-3}
IX barrens	61	28.2	15.89	55.1	22.65	135.9	123
last CCD underflow	36.2	12.9	4.31	24.1	5.88	58.8	31.7
CYCLONE underflow	11.9	1.6	0.18	2.3	0.18	9.1	1.6
WEIGHT % SOLIDS			0.32		0.46		2.5

*The analysis are from a 1977 sampling of the Quirke mill circuit, A. Vivyurka personal communication. A mill feed rate of 6928 tonnes/day of ore was used in the calculation.

Table 3: Preliminary tests for batch reaction of tailings and low-pH water; titration of 25 grams of gypsum-leached tailings with 0.1 N HCl.

BT 1

mls Acid	pH	Date	Time
0.00	9.10	11/11/82	13:46
4.50	5.52		13:50
	6.10		13:55
5.12	5.50		13:56
	5.95		14:13
5.50	5.50		14:14
	5.73		14:29
5.84	5.42		14:30
	5.80		14:45
6.25	5.30		14:46
	5.68		15:10
6.42	5.48		15:11
	5.65		15:30
7.50	4.50		15:30
	5.50		16:58
13.00	3.30		17:03
13.56	4.25	12/11/82	10:25
15.00	3.35		10:27
	3.80		10:40
15.50	3.45		10:41
	3.78		11:03
16.00	3.45		11:04
	3.70		11:25
16.56	3.45		11:26
	3.65		11:44
17.00	3.40		11:45
	3.60		11:56
18.00	3.10		11:57
	3.50		13:00
18.50	3.30		13:00
	3.50		13:28
20.00	2.95		13:29
30.00	2.20		13:32
	2.32		14:02
38.00	2.06		14:04
	2.18		15:20
40.00	2.10		15:22
	2.48	16/11/82	
	3.00	16/02/83	

BT2

ml Acid	pH	Date	Time
0.00	9.10	16/11/82	15:35
7.25	3.80		15:36
	4.34		15:50
	4.50		15:30
	5.42	17/11/82	9:00
18.00	2.30		9:04
	3.20		16:30
30.00	2.15		16:40
40.00	1.95		18:41
	1.95		23:54
	1.98	18/11/82	9:43
	2.93	16/02/83	

Table 4: Chemical analyses of samples of final solution composition from chart-recorded alkalinity titrations on whole and leached Quirke tailings collected in 1982. All analyses are reported as mg/L.

	Na	K	Ca	Mg	Mn	Fe	Al	pH
November 1982 (whole)	1.73	75.1	87.6	40.7	2.75	99.3	133	2.66
November 1982 (leached)	1.19	42.3	95.7	29.0	2.28	142.6	112.	2.45

Sample #	1	2	3	4	5	6	7	8	9	10	11	12
TIME (hours)	5	15.5	26.5	37.7	49.9	73.8	98.2	148.2	193.9	298.6	386.0	529.5
pH	1.68	2.27	2.69	2.72	2.60	2.81	2.98	3.23	3.42	3.60	3.62	3.73
Eh (mV)	.668	.631	.611	.607	.609	.593	.578	.546	.522	.497	.486	.489
pe	11.30	10.68	10.34	10.27	10.30	10.03	9.78	9.29	8.83	8.41	8.22	8.27
Na		2.66	2.69	3.08	3.19	3.51	4.17	5.74	8.51	6.86	14.12	10.93
K		65.8	65.2	75.1	76.0	76.6	83.2	78.8	74.1	67.5	59.0	73.6
Ca		608	581	606	578	564	552	546	531	522	508	525
Mg		379	431	457	478	484	506	537	561	583	596	585
Fe^{2+}	N.S	416	839	824	881	919	948	1040	1020	919	889	731
FeTOTAL		871	1040	1120	1130	1220	1240	1320	1200	1140	993	793
$\%Fe^{3+}$	N.S	52	20	26	22	25	23	21	15	19	10	8
Al		1260	1240	1170	1040	960	906	799	637	527	408	287
SO_4^{2-}	12600	11900	11600	11100	10700	11000	9910	9750	8750	7670	6700	5670
Si												
F		5.90	5.45									
acidity												
pH*												

Table 5A : Chemical analyses of pore water samples from batch A.

Sample #	1	2	3	4	5	6	7	8	9	10	11	12
TIME (hours)	4.5	13.5	25.3	36.5	48.5	72.7	96.9	146.8	192.4	290.3	385	528
pH	2.67	2.49	2.44	2.53	2.60	2.73	2.83	2.97	3.15	3.40	3.51	3.58
Eh (mV)	613	608	605	595	590	579	571	548	528	495	478	471
pe	10.37	10.29	10.24	10.07	9.98	9.80	9.66	9.27	8.93	8.38	8.09	7.97
Na		2.65	2.56	3.03	3.57	3.40	3.99	6.55	9.31	7.69	8.22	10.43
K		50.6	61.8	70.7	71.9	74.9	73.8	64.7	54.2	41.2	35.6	30.2
Ca		606	580	556	556	538	521	524	526	519	502	506
Mg		370	425	483	480	533	554	585	589	598	602	598
Fe^{2+}		2910	3250	3090	3150	3080	2930	2720	2740	2670	2490	2430
FeTOTAL		4500	4530	4380	4310	4160	3970	3550	3390	3130	3010	2880
$\%Fe^{3+}$		35	28	29	27	26	26	23	19	15	17	16
Al		1450	1310	999	1030	795	706	578	537	472	373	285
SO_4^{2-}	20300	18900	18500	NS	18400	16200	15500	12900	12400	11300	10700	10100
Si												
F		6.67	6.89									
acidity												
pH*												

Table 5B : Chemical analyses of pore water samples for batch B.

Sample #	1	2	3	4	5	6	7	8	9	10	11	12
TIME (hours)	5.5	14.4	26.1	37.4	49.7	73.0	97.3	147.2	192.9	290.7	385.5	527.3
pH	1.47	1.62	1.68	1.67	1.72	1.82	1.85	1.91	2.00	2.13	2.26	2.47
Eh (mV)	704	669	658	653	647	637	629	616	608	591	577	558
pe	11.91	11.32	11.13	11.05	10.95	10.78	10.64	10.42	10.29	10.00	9.76	9.44
NA		1.32	1.54	1.87	1.70	1.92	2.03	3.77	4.04	3.89	7.13	4.18
K		27.4	29.5	30.0	30.6	32.4	31.3	30.9	31.4	31.6	30.5	27.3
Ca		308	312	340	349	376	416	414	430	423	432	446
Mg		217	235	267	295	332	363	399	462	434	442	465
Fe^{2+}		1090	1270	1220	1290	1470	1500	1630	1600	1640	1640	1670
FeTOTAL		2200	2230	2010	2000	2100	2020	2120	1970	1980	1920	1910
%Fe^{2+}		50	43	39	35	30	26	23	19	17	15	12
Al		878	842	841	841	863	818	753	693	663	636	682
SO_4^{2-}	14100	14100	14000	14300	12400	12400	12300	12100	12300	10900	9320	9180
Si												
F		1.69	1.06	2.01	2.01	2.22	2.48	2.43	1.64	2.47	2.47	2.11
acidity												
pH*												

Table 5C : Chemical analyses of pore water samples for batch C.

Sample #	1	2	3	4	5	6	7	8	9	10	11	12
TIME (hours)	4.8	14.0	25.5	36.9	48.8	72.5	96.8	146.6	192.3	290.2	385.5	528
pH	2.43	1.90	2.19	2.05	2.03	2.06	2.11	2.18	2.27	2.41	2.50	2.65
Eh (mV)	618	636	615	621	618	612	606	598	590	578	569	556
pe	10.46	10.76	10.41	10.51	10.46	10.36	10.25	10.12	9.98	9.78	9.63	9.41
Na		1.97	1.87	2.09	1.81	2.08	2.13	3.89	3.32	3.35	10.71	5.50
K		27.8	26.8	26.9	26.4	23.6	20.6	15.1	12.0	6.97	5.76	4.45
Ca		358	487	470	482	477	468	477	503	473	499	499
Mg		259	388	373	411	444	480	501	523	506	502	502
Fe^{2+}		3080	3710	3290	3260	3280	3210	3320	3400	3460	3390	3640
FeTOTAL		5270	4700	4750	4700	4630	4600	4770	4690	4800	4800	4730
$\%Fe^{3+}$		42	21	31	31	29	30	30	28	28	29	23
Al		1020	1250	1190	1100	1010	881	948	982	ns	1100	1080
SO_4^{2-}	15500	15100	12500	17500	18300	18200	16700	16800	16400	17100	16500	16300
Si												
F		1.60	2.39									
acidity												
pH*												

Table 5D : Chemical analyses of pore water samples for batch D.

SAMPLE	16	20	24	34	45	54	65	72
pH	6.82	6.59	6.18	4.47	4.09	4.01	3.85	2.86
Eh(mV)	0.185 ●	0.188 ●	0.168	0.437	0.452	0.473	0.493	0.588
pe	3.16	3.21	2.87	7.46	7.72	8.08	8.42	10.04
Na	0.48	0.48	0.44	0.42	0.34	0.29	0.18	0.20
K	4.29	4.18	3.80	2.81	2.11	1.94	1.85	1.72
Ca	809	750	785	756	541	406	139	18.4
Mg	26.4	22.0	22.6	16.0	5.9	3.1	2.1	1.7
Fe^{2+}		121	130	45	68.8	69.4	104	82.7
Fe_{TOTAL}	30.1	91.9	108	106	84.2	86.9	88.0	83.6
Al	< 0.6	< 0.6	< 0.6	20.4	74.8	82.0	79.8	77.0
SO_4^{2-}	1290	1335	1401	1599	1212	915	--	78.1
Si								
Cl*	444							436
F							< 0.1	< 0.1
Alkalinity								

* Unless otherwise indicated, input Cl = 440 mg/L assumed.

● #16 - Eh is estimated from Eh measurements made ~ 5 pv before it;
#20 - Eh is estimated from Eh measurements made ~ 5 pv after it.

Table 6: Chemical analyses of column 1 effluent.

SAMPLE	5	16	23	36	45	52	63
pH	4.08	3.96	3.88	3.88	3.78	2.58	2.09
Eh(mV)	0.442	0.493	0.490	0.496	0.490	0.627	0.660
pe	7.48	8.34	8.29	8.38	8.29	10.61	11.17
Na @	0.20	0.10	0.15	0.20	0.15	0.15	0.10
K	4.02	1.65	1.71	2.04	2.09	2.20	1.80
Ca	12.0	4.59	3.10	3.23	3.12	2.82	2.28
Mg	13.4	8.80	7.04	5.08	4.84	3.08	0.50
Fe^{2+}	NA	167	179	132	137	123	52
Fe_{TOTAL}	133	141	134	129	131	128	50
Al	20.7	48.4	54.5	58.9	58.3	39.6	9.0
SO_4^{2-}	0.92	6.78	9.92	19.4	22.5	23.6	16.6
Si							
Cl *							
F	< 0.8	<0.1	<0.1	<0.1	<0.1	<0.1	<0.1
Alkalinity							

* - Cl- - 440 mg/L is assumed

@ - Na analyses are preliminary

Table 7: Chemical analyses of column 2 effluent.

Table 9. Saturation indices of selected Al and Fe containing solid phases calculated for batch A data using the WATEQ2 equilibrium model

Sample	pH	$Al(OH)_3$ amorphous	$AlSO_4OH$	$AL_4SO_4(OH)_{10}$	Alunite	Gypsum	pIAP $Fe(OH)_3$	Jarosite Na	Jarosite K	Jarosite H
2	2.27	- 6.81	0.58	- 14.01	- 1.24	0.16	40.43	1.86	6.63	4.44
3	2.69	- 5.56	1.00	- 9.85	- 4.56	0.15	39.40	3.70	8.47	5.86
4	2.72	- 5.47	1.00	- 9.60	1.45	0.16	39.33	3.84	8.60	5.90
5	2.60	- 5.88	0.84	- 10.99	+ 0.58	0.14	39.65	3.25	8.00	5.42
6	2.81	- 5.33	1.01	- 9.16	1.70	0.15	39.27	3.90	8.62	5.82
7	2.98	- 4.80	1.16	- 7.41	2.74	0.12	38.97	4.24	8.92	5.91
8	3.23	- 4.12	1.35	- 5.17	4.04	0.12	38.74	4.36	8.88	5.64
9	3.42	- 3.62	1.45	- 3.59	4.90	0.11	38.61	4.33	8.65	5.25
10	3.60	- 3.12	1.56	- 1.98	5.76	0.08	38.50	3.95	8.32	4.78
11	3.62	- 3.13	1.47	- 2.10	4.96	0.06	38.67	3.63	7.05	4.12
12	3.73	- 2.91	1.44	- 1.46	5.92	0.06	38.37	4.04	8.25	4.52

Table 10. Saturation indices of selected Al and Fe- containing solid phases for batch B data calculated using the WATEQ2 equilibrium model

Sample	pH	$Al(OH)_3$ amorphous	$AlSO_4OH$	$AL_4SO_4(OH)_{10}$	Alunite	Gypsum	$pIAP_{Fe(OH)_3}$	Jarosite Na	Jarosite K	Jarosite H
2	2.49	- 6.24	0.84	-12.05	- 0.07	0.22	39.47	4.31	8.96	6.68
3	2.44	- 6.44	0.74	-12.74	- 0.43	0.12	39.66	3.86	8.61	6.30
4	2.53	- 6.36	0.70	-12.54	- 0.29	0.21	39.60	3.98	8.71	6.26
5	2.60	- 6.13	0.78	-11.79	+ 0.18	0.21	39.47	4.20	8.87	6.34
6	2.73	- 5.82	0.81	-10.84	0.69	0.19	39.27	4.36	9.07	6.39
7	2.83	- 5.58	0.86	-10.04	1.13	0.18	39.12	4.57	9.21	6.43
8	2.97	- 5.17	0.93	- 8.75	1.77	0.15	39.11	4.29	8.66	5.79
9	3.15	- 4.65	1.08	- 7.06	2.69	0.15	38.93	4.45	8.59	5.61
10	3.40	- 3.93	1.28	- 4.68	3.95	0.14	38.76	4.07	8.17	5.06
11	3.51	- 3.70	1.29	- 3.98	4.25	0.12	38.74	3.84	7.85	4.69
12	3.58	- 3.60	1.24	- 3.72	4.27	0.13	38.66	3.95	7.79	4.63

Table 11. Saturation indices of selected Al and Fe containing solid phases calculated for batch C data using the WATEQ2 equilibrium model

Sample	pH	$Al(OH)_3$ amorphous	$AlSO_4OH$	$AL_4SO_4(OH)_{10}$	Alunite	Gypsum	pIAP $Fe(OH)_3$	Jarosite Na	Jarosite K	Jarosite H
2	1.62	- 8.89	- 0.22	-21.06	- 5.96	- 0.14	41.49	0.27	4.96	3.80
3	1.68	- 8.75	- 0.18	-20.62	- 5.65	- 0.13	41.44	0.37	5.02	3.77
4	1.67	- 8.81	- 0.20	-20.79	- 5.73	- 0.08	41.58	0.08	4.66	3.41
5	1.72	- 8.59	- 0.14	-20.10	- 5.35	- 0.10	41.47	0.10	4.73	3.42
6	1.82	- 8.30	- 0.03	-19.12	- 5.04	- 0.05	41.30	0.42	5.02	3.58
7	1.85	- 8.25	- 0.03	-18.97	- 4.64	0.00	41.55	- 0.36	4.21	2.76
8	1.91	- 8.12	0.00	-18.54	- 4.40	0.01	41.35	0.34	4.63	3.13
9	2.00	- 7.93	0.05	-17.92	- 4.02	0.04	41.26	0.46	4.73	3.13
10	2.13	- 7.52	0.17	-16.57	- 3.24	0.02	41.12	0.40	4.69	2.95
11	2.26	- 7.08	0.29	-15.14	- 2.44	0.00	40.95	0.67	4.68	2.82
12	2.47	- 6.42	0.53	-12.91	- 1.14	0.01	40.64	0.72	4.92	2.90

Table 12. Saturation indices of selected Al and Fe containing solid phases calculated for batch B data using the WATEQ2 equilibrium model

Sample	pH	$Al(OH)_3$ amorphous	$AlSO_4OH$	$AL_4SO_4(OH)_{10}$	Alunite	Gypsum	pIAP $Fe(OH)_3$	Jarosite Na	K	H
2	1.90	- 7.99	0.108	-18.04	- 4.12	- 0.10	40.67	2.03	6.55	5.11
3	2.19	- 6.97	0.48	-14.59	- 4.57	- 0.02	40.14	2.59	7.63	5.40
4	2.05	- 7.50	0.32	-16.59	- 3.16	0.08	40.54	2.21	6.69	5.12
5	2.03	- 7.72	0.26	-17.06	- 3.45	0.11	40.66	1.90	6.43	4.89
6	2.06	- 7.68	0.25	-16.98	- 3.46	0.11	40.68	1.85	6.27	4.75
7	2.11	- 7.57	0.24	-16.64	- 3.36	0.10	40.62	1.86	6.21	4.70
8	2.18	- 7.33	0.35	-15.81	- 2.98	0.10	40.52	2.20	6.16	4.72
9	2.27	- 7.03	0.45	-14.82	- 2.48	0.12	40.38	2.26	6.18	4.75
10	2.41	- 6.65	0.59	-13.54	- 1.92	0.11	40.17	2.56	6.24	4.91
11	2.50	- 6.30	0.73	-12.33	- 1.27	0.12	40.03	3.13	6.23	4.89
12	2.65	- 5.86	0.87	-10.89	- 0.52	0.12	39.81	3.07	6.35	4.97

Table 13A : Saturation indices of selected Al-containing solid phases calculated for column 1 data using the WATEQ2 equilibrium model.

Sample	pH	gypsum	Amorphous $Al(OH)_3$ (pK=31.715)	gibbsite (pK=33.9)	$AlSO_4OH$	$Al_4SO_4(OH)_{10}$	Alunite
16	6.82	0.02	-2.06	0.14	-4.32	-4.67	-2.84
20	6.59	0.01	-2.07	0.12	-3.85	-4.24	-2.16
24	6.18	0.04	-2.14	0.05	-3.09	-3.68	-1.16
34	4.47	0.06	-1.47	0.72	1.05	2.46	5.95
45	4.09	-0.16	-1.94	0.25	1.23	1.25	5.35
54	4.01	-0.35	-2.06	0.13	1.17	0.82	4.99
65	3.85	-1.11	-2.33	-0.14	0.83	-0.35	3.86
72	2.86	-2.54	-5.17	-2.97	-0.63	-10.31	-2.90

Table 13B : Saturation indices of selected Al-containing solid phases calculated for column 2 data using the WATEQ2 equilibrium model.

Sample	pH	gypsum	amorphous $Al(OH)_3$ (pK=31.715)	gibbsite (pK=33.9)	$AlSO_4OH$	$Al_4SO_4(OH)_{10}$	Alunite
5	4.08	-4.48	-2.01	0.18	-1.72	-1.92	-0.31
16	3.96	-4.12	-2.02	0.18	-0.68	-0.91	1.23
23	3.88	-4.13	-2.21	-0.02	-0.56	-1.36	1.22
36	3.88	-3.83	-2.18	-0.01	-0.25	-0.98	1.94
45	3.78	-3.78	-2.49	-0.29	-0.29	-1.93	1.48
52	2.58	-3.81	-6.23	-4.03	-1.62	-14.47	-6.10
63	2.09	-4.02	-8.27	-6.08	-2.84	-21.83	-11.15

Table 14A : Saturation indices of selected Fe- containing solid phases calculated for column 1 data using the WATEQ2 equilibrium model

Sample	pH	pIAP	Jarosites		
		$Fe(OH)_3$	Na	K	H
16	6.82	35.51	1.16	5.51	-0.13
20	6.52	35.67	1.43	5.76	0.37
24	6.18	37.18	-1.88	2.45	-2.44
34	4.47	37.74	1.66	5.88	2.78
45	4.09	38.68	-0.36	3.83	1.23
54	4.01	38.52	0.11	4.33	1.84
65	3.85	38.56	-0.52	3.90	1.57
72	2.86	39.88	-2.66	1.68	0.37

Table 14B : Saturation Indices and pIAP of selected Fe - containing solid phases calculated for column 2 data using WATEQ2 equilibrium model.

Sample	pH	pIAP $Fe(OH)_3$	Jarosites Na	 K	 H
5	4.08	38.46	-5.65	-0.95	-3.86
16	3.96	37.95	-2.46	2.16	-0.24
23	3.88	38.26	-2.68	1.78	-0.56
36	3.88	38.20	-1.79	2.63	0.21
45	3.78	38.58	-2.62	1.93	-0.40
52	2.58	39.84	-2.81	1.76	0.61
63	2.09	41.14	-5.70	-1.04	-1.61

FIGURES IN CHAPTER 3

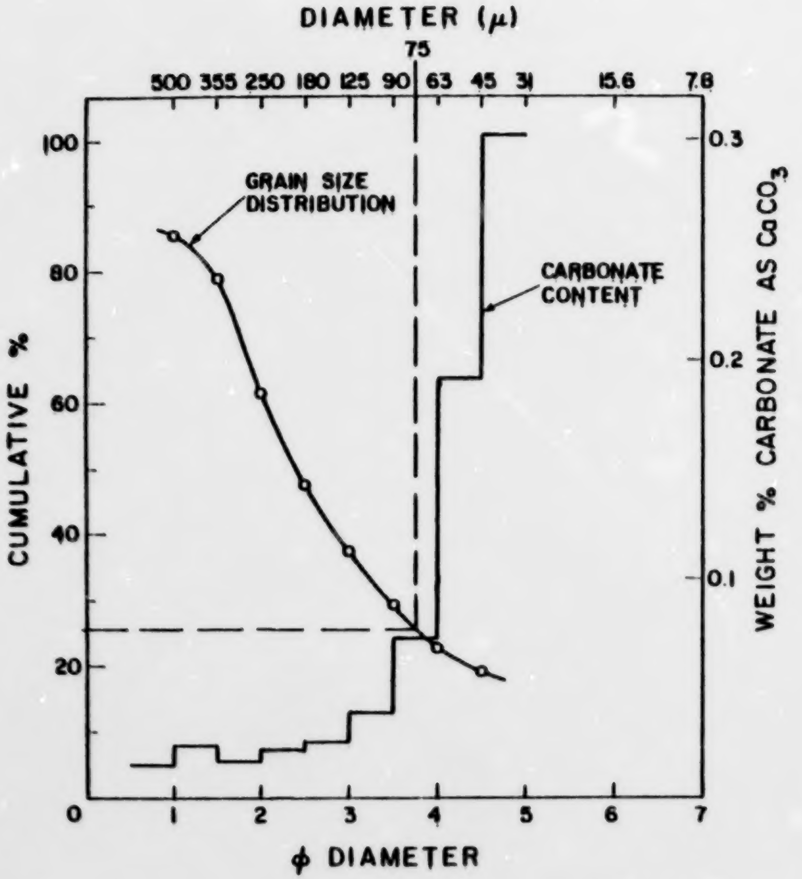

Fig. 1: Plot of the tailings grain size distribution curve and grainsize versus carbonate content expressed as weight percent $CaCO_3$.

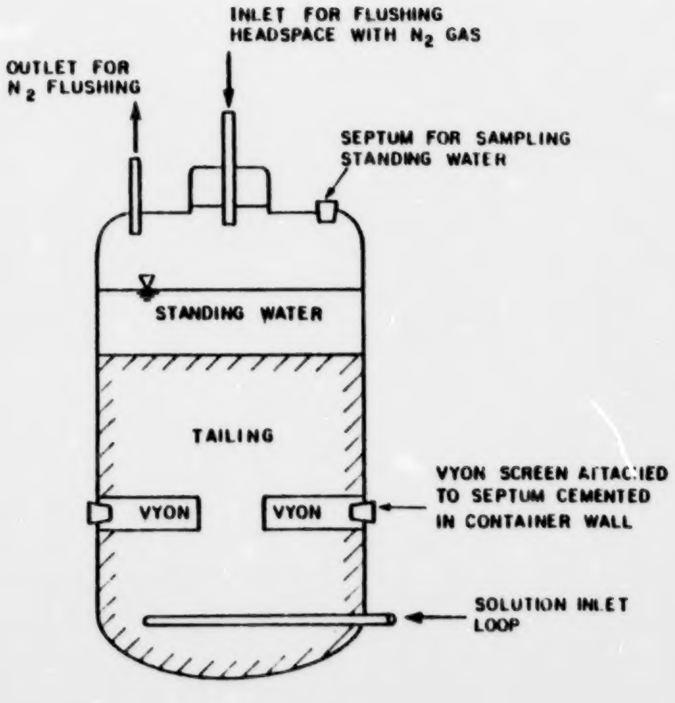
INLET FOR FLUSHING HEADSPACE WITH N_2 GAS
OUTLET FOR N_2 FLUSHING
SEPTUM FOR SAMPLING STANDING WATER
STANDING WATER
TAILING
VYON
VYON
VYON SCREEN ATTACHED TO SEPTUM CEMENTED IN CONTAINER WALL
SOLUTION INLET LOOP

Fig. 2: Schematic of nalgene reaction vessel used in the batch tests. Samples of pore water were collected through the septum using a 50 ml syringe. Use of porous polyethylene screens (Vyon) prevents tailings material from clogging the needle during sample collection. The solution inlet loop is constructed of air approximately 28 cm length of 3/32" ID tygon perforated with a needle. The inlet loop is covered with a sheet of fine nylon screen not shown in the figure.

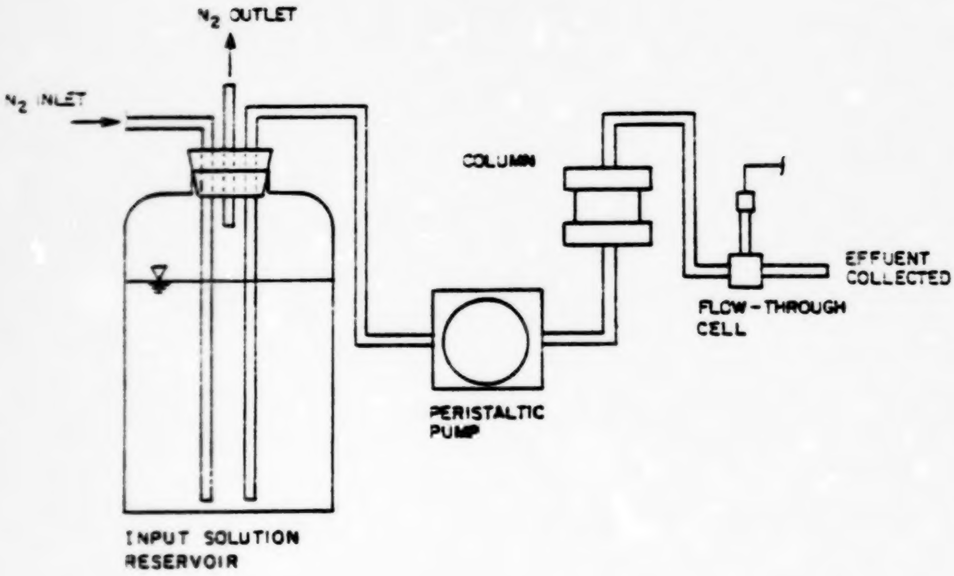

N_2 OUTLET
N_2 INLET
COLUMN
EFFUENT COLLECTED
FLOW-THROUGH CELL
PERISTALTIC PUMP
INPUT SOLUTION RESERVOIR

Fig. 3: Schematic of column experiment. The input solution was bubbled with N_2 gas before injection. A flow-through cell was used to make periodic pH and Eh measurements on the effluent.

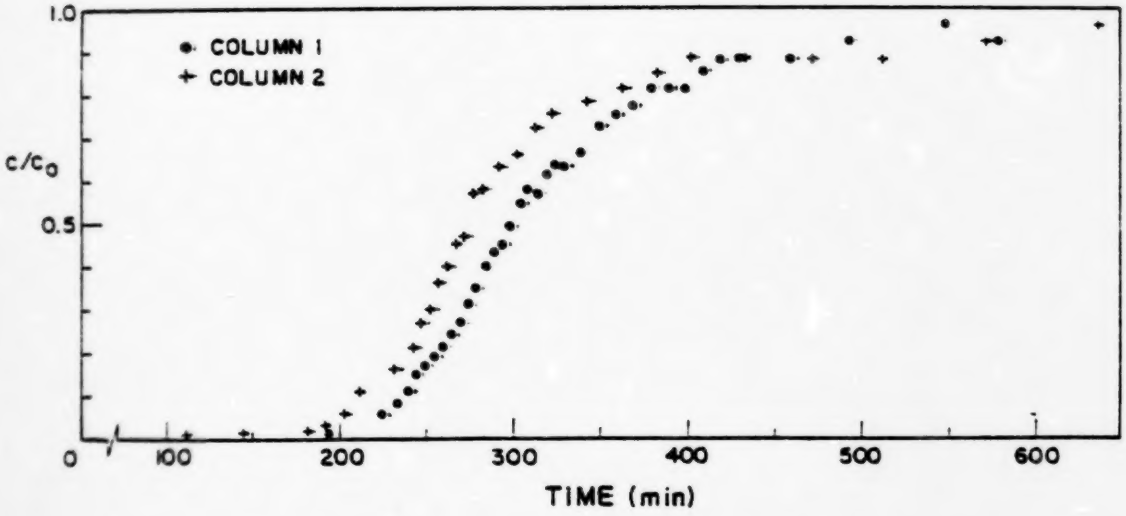

Fig. 4: Chloride breakthrough curves for column 1 and 2. The flow rate for both columns was approximately 0.11 ml/min. Concentrations are plotted at as the dimensionless ratio of measured outflow concentration (c) to input concentration (C_o).

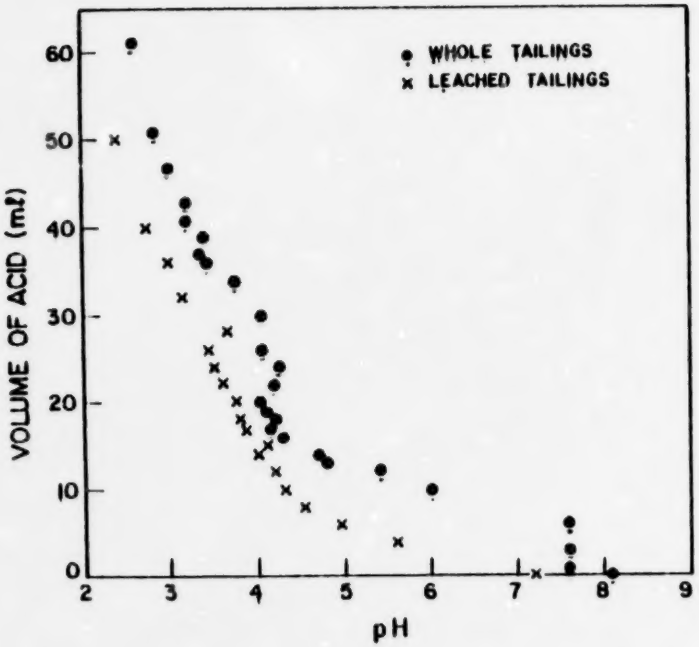

Fig. 5: Alkalinity titration curves for 1980 samples of whole and leached Quirke tailings. The titrations were performed on 50 g samples suspended in 100 ml of deionized water with 0.1 N H_2SO_4 as the titrant.

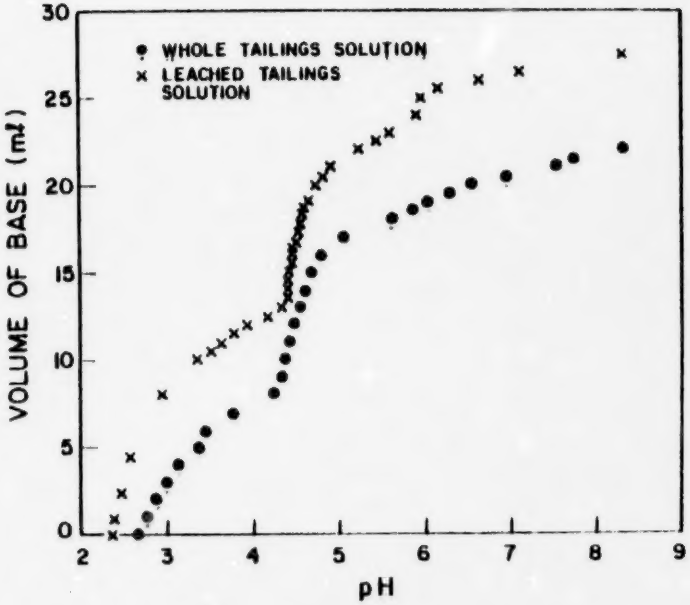

Fig. 6: Acidity titrations of 100 ml of final solution collected from alkalinity titrations on 1980 samples of Quirke tailings 0.1 N NaOH was used as the titrant.

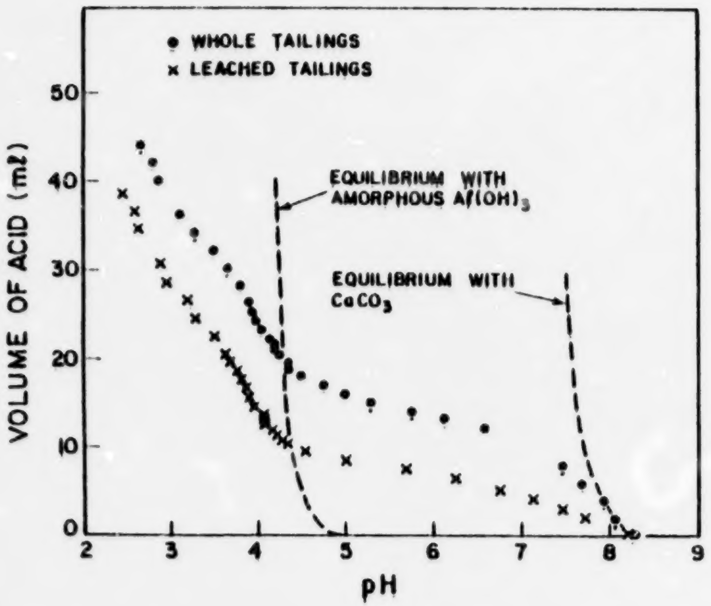

Fig. 7: Alkalinity titration curves for 1982 samples of whole and leached Quirke tailings. The titrations were performed on 25 g samples suspended in 100 ml of deionized water with 0.1 N HCl as the titrant. Also shown are theoretical titration curves calculated for pure $Al(OH)_3$ amorphous and $CaCO_3$ solid phases using equilibrium constants.

Fig. 8

BATCH TEST RESULTS
PLOTS OF PH VS TIME FOR BATCH TESTS ON ELLIOT LAKE TAILINGS

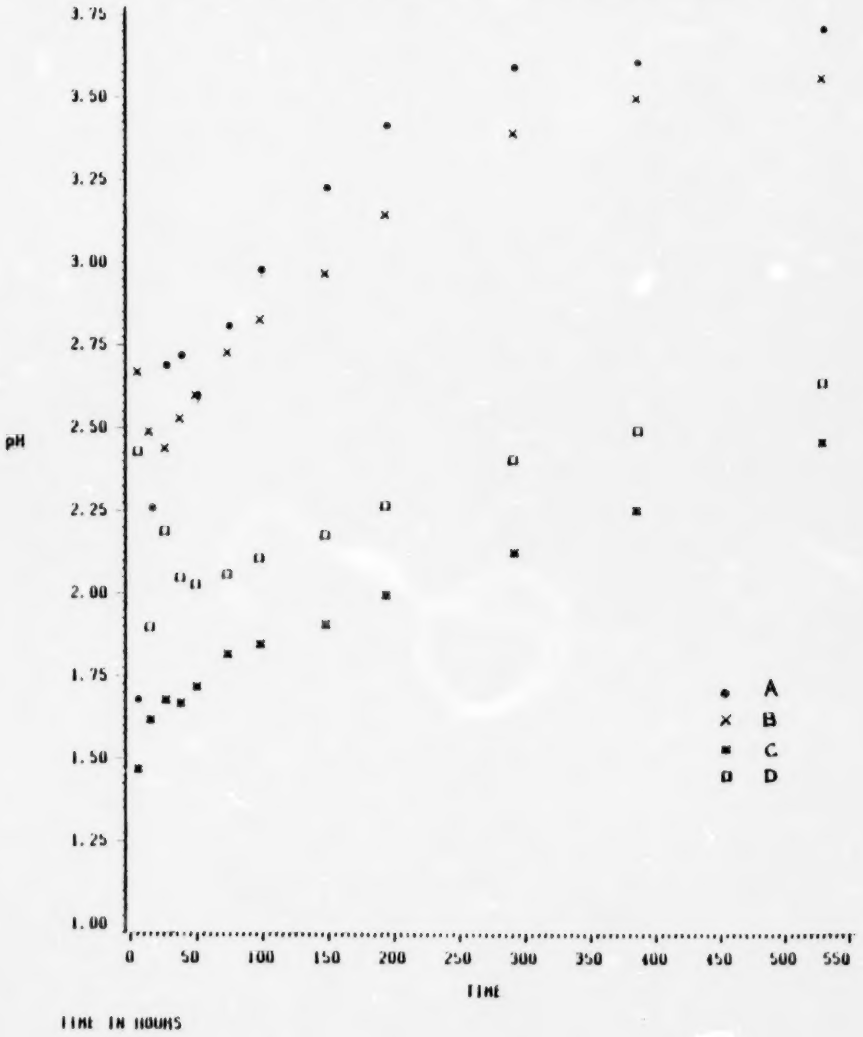

Fig. 9: Data for batch tests A(+) and B(-) (9A) and C(+) and D(.) (9B) are plotted on pe - pH diagrams for iron species and selected solid phases. The boundaries on the diagram were drawn for the following conditions; Fe $=10^{-4,05}$, K $=10^{-3}$, $SO_4^{2-}=10^{-2}$, pK of $Fe(OH)_3=38$.

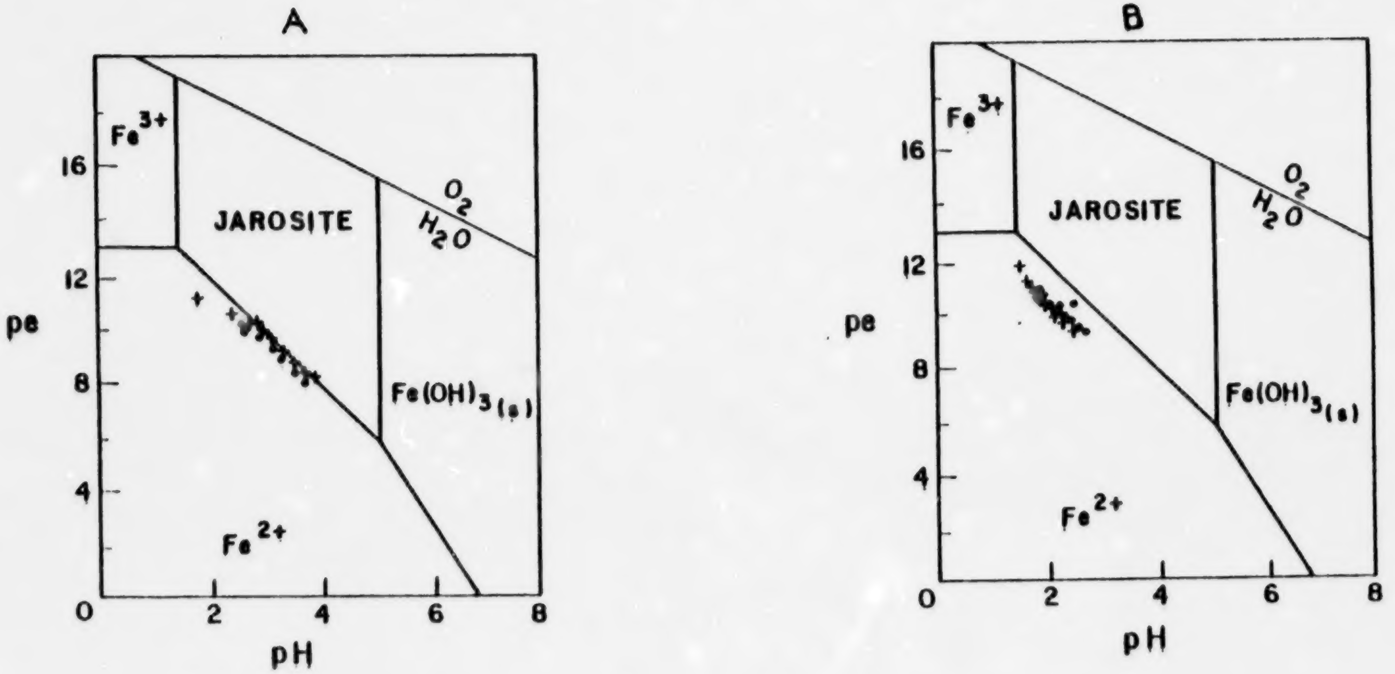

Fig. 10A

BATCH TEST RESULTS
ELLIOT LAKE TAILINGS
PLOT OF NA, K, CA, AND MG VS TIME

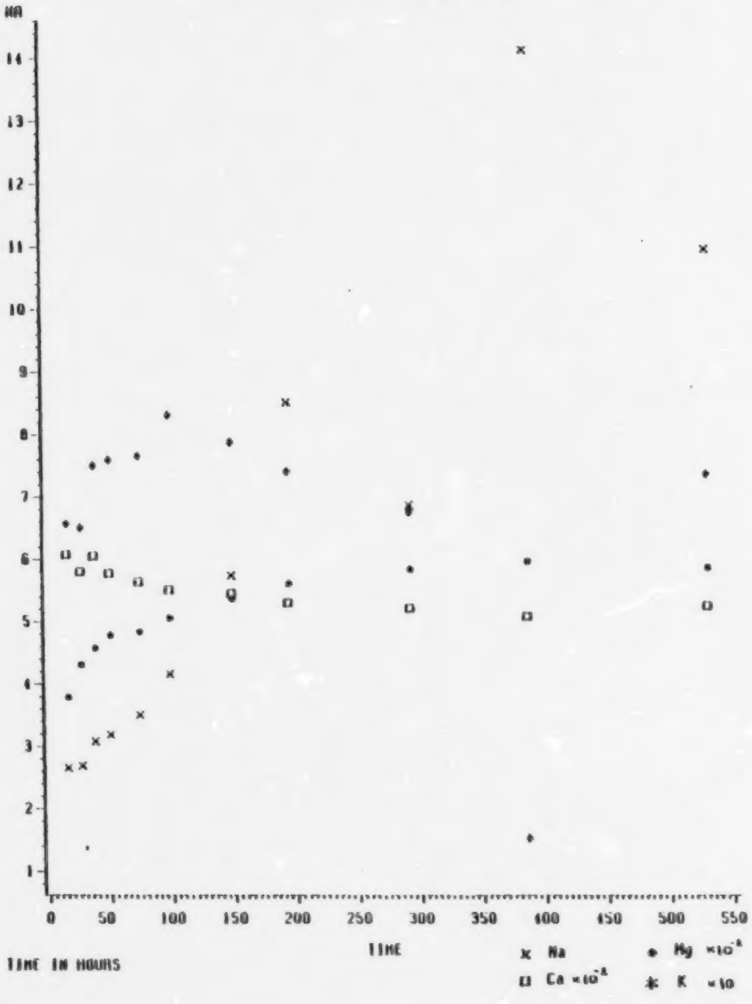

Fig. 10B

BATCH A TEST RESULTS
ELLIOT LAKE TAILINGS
PLOT OF FE, AL, AND SO4 VS TIME

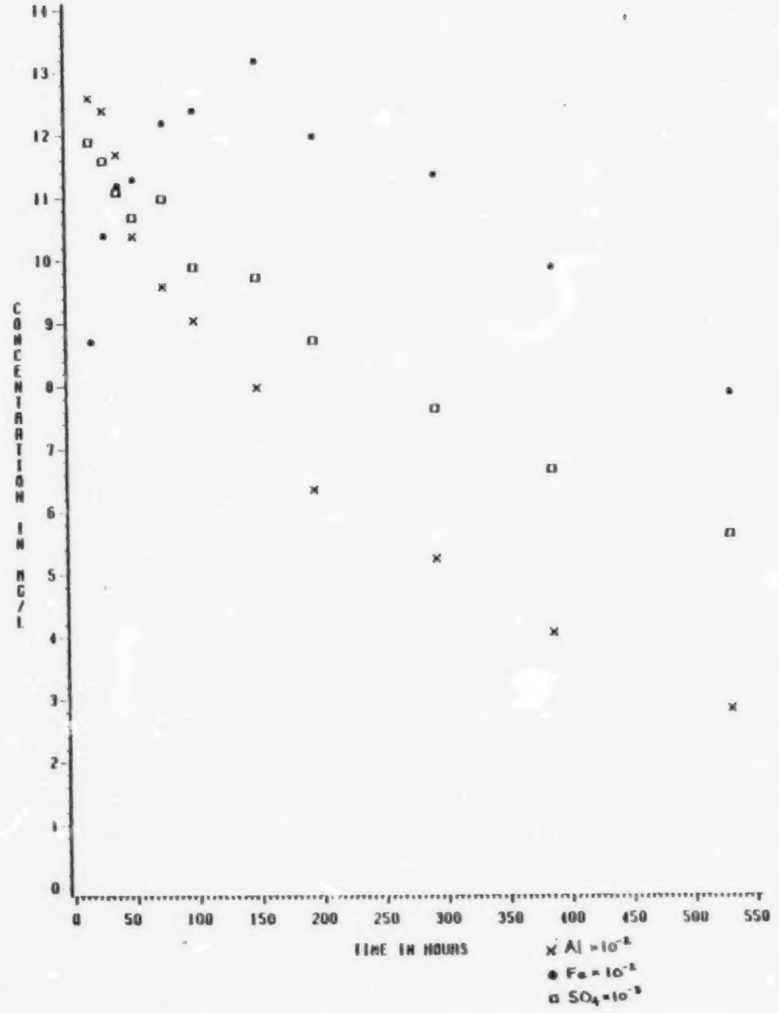

Fig. 11A

BATCH TEST RESULTS
ELLIOT LAKE TAILINGS
PLOT OF NA, K, CA, AND MG VS TIME

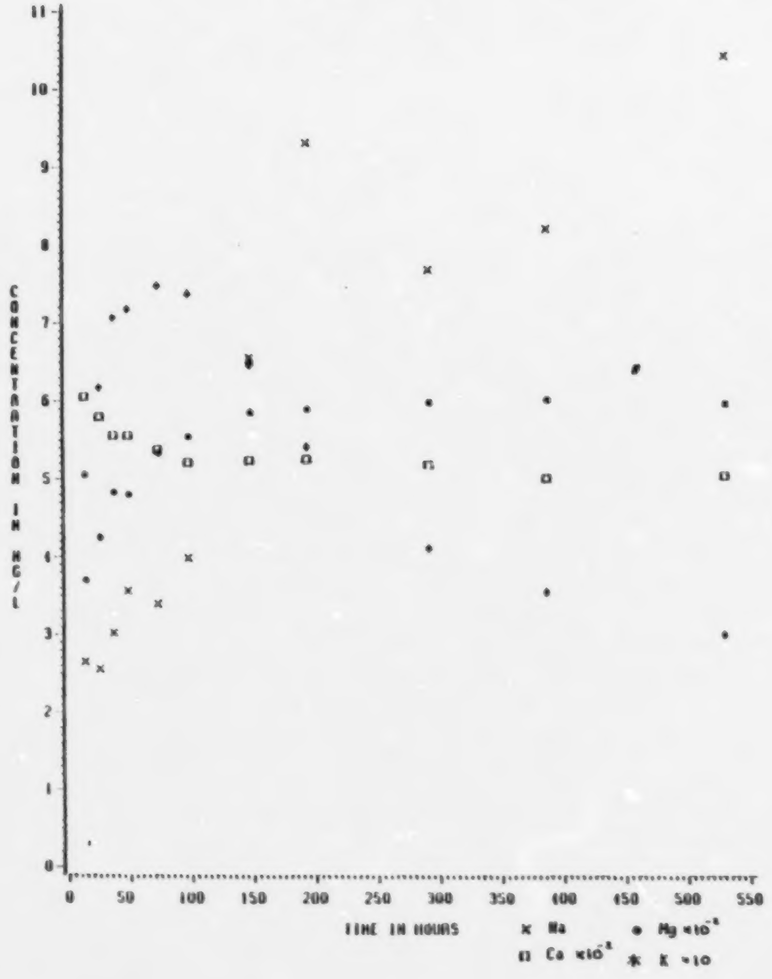

Fig. 11B

BATCH B TEST RESULTS
ELLIOT LAKE TAILINGS
PLOT OF FE, AL, AND SO4 VS TIME

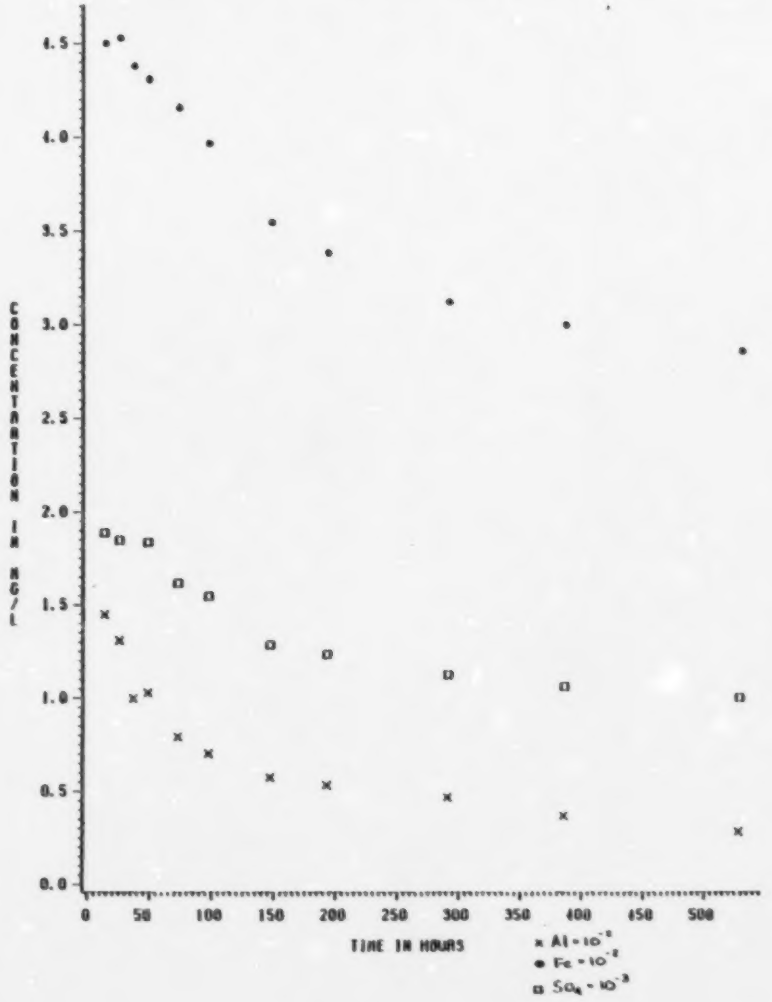

Fig. 12A

BATCH C TEST RESULTS
ELLIOT LAKE TAILINGS
PLOT OF NA, K, CA, AND MG VS TIME

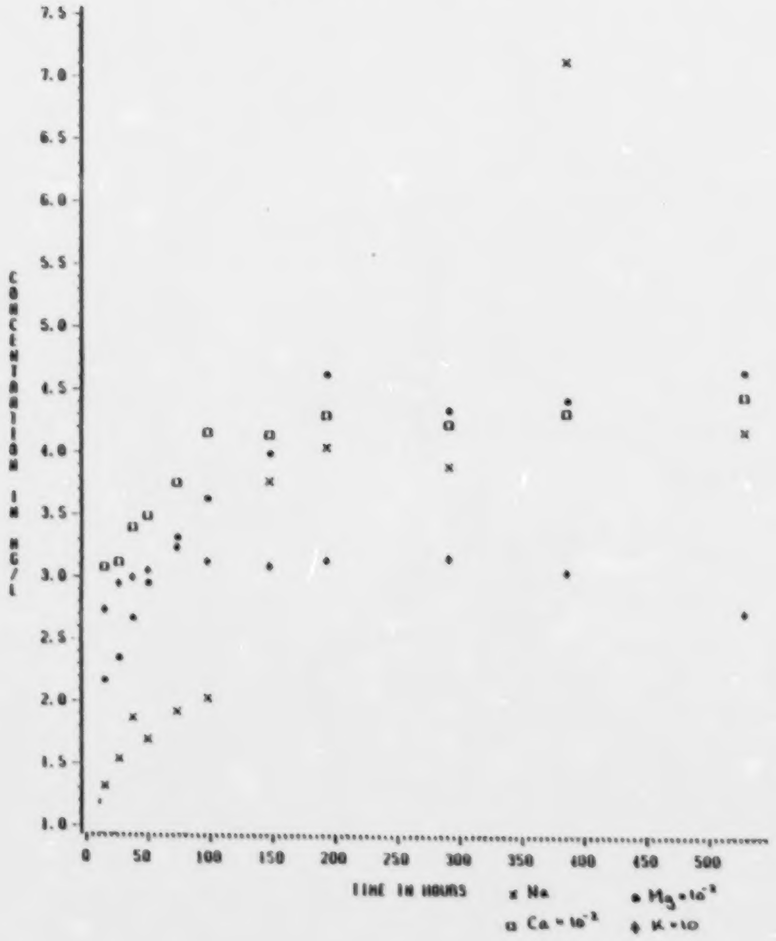

Fig. 12B

BATCH C TEST RESULTS
ELLIOT LAKE TAILINGS
PLOT OF FE, AL, AND SO4 VS TIME

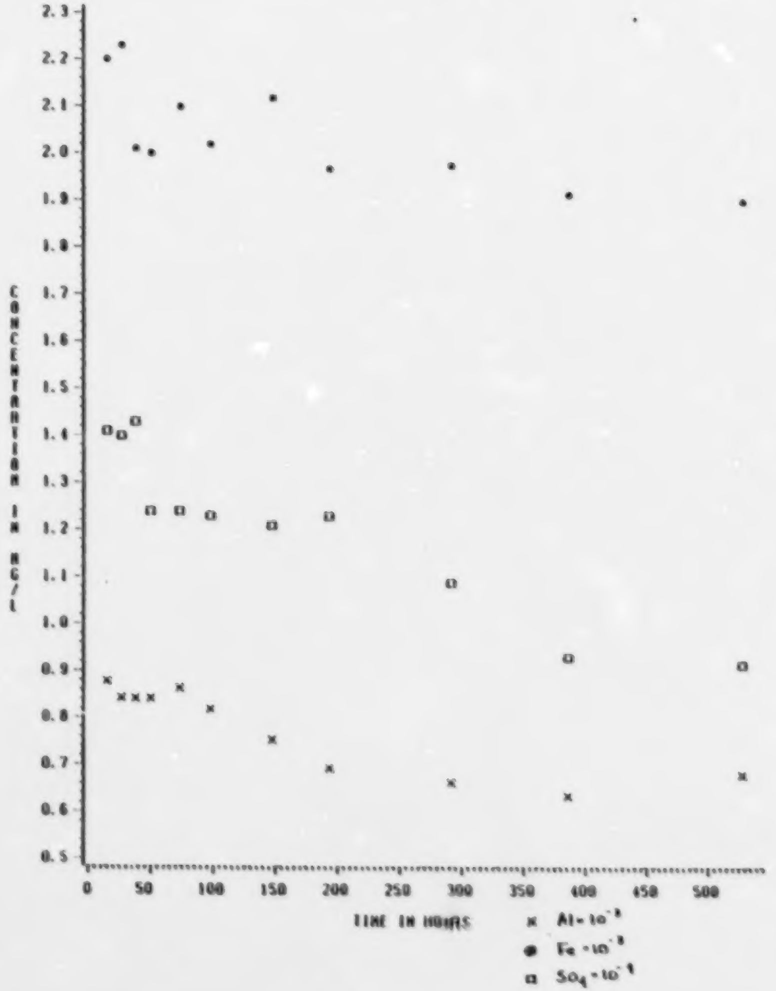

Fig. 13A
BATCH D TEST RESULTS
ELLIOT LAKE TAILINGS
PLOT OF NA, K, CA, AND MG VS TIME

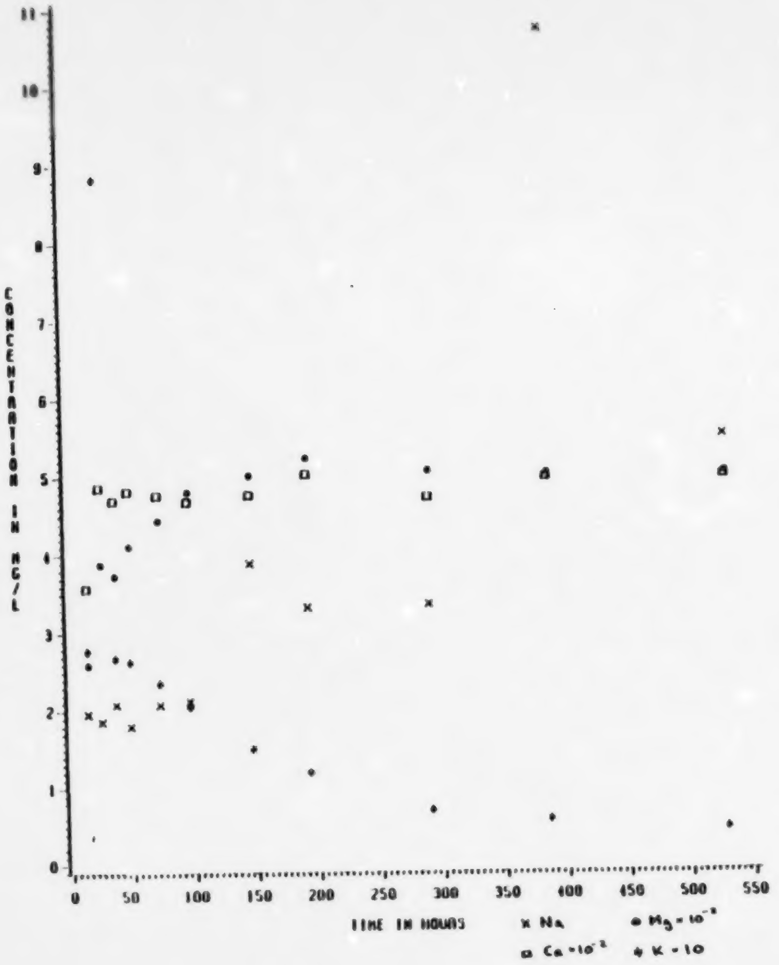

Fig. 13B
BATCH D TEST RESULTS
ELLIOT LAKE TAILINGS
PLOT OF FE, AL, AND SO4 VS TIME

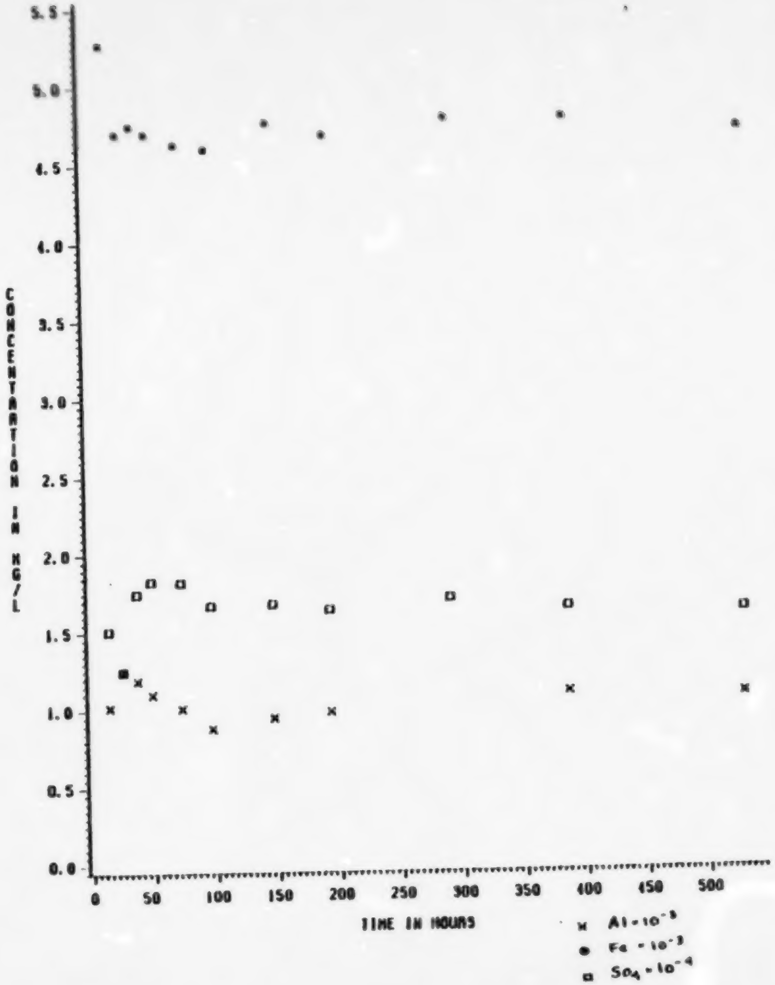

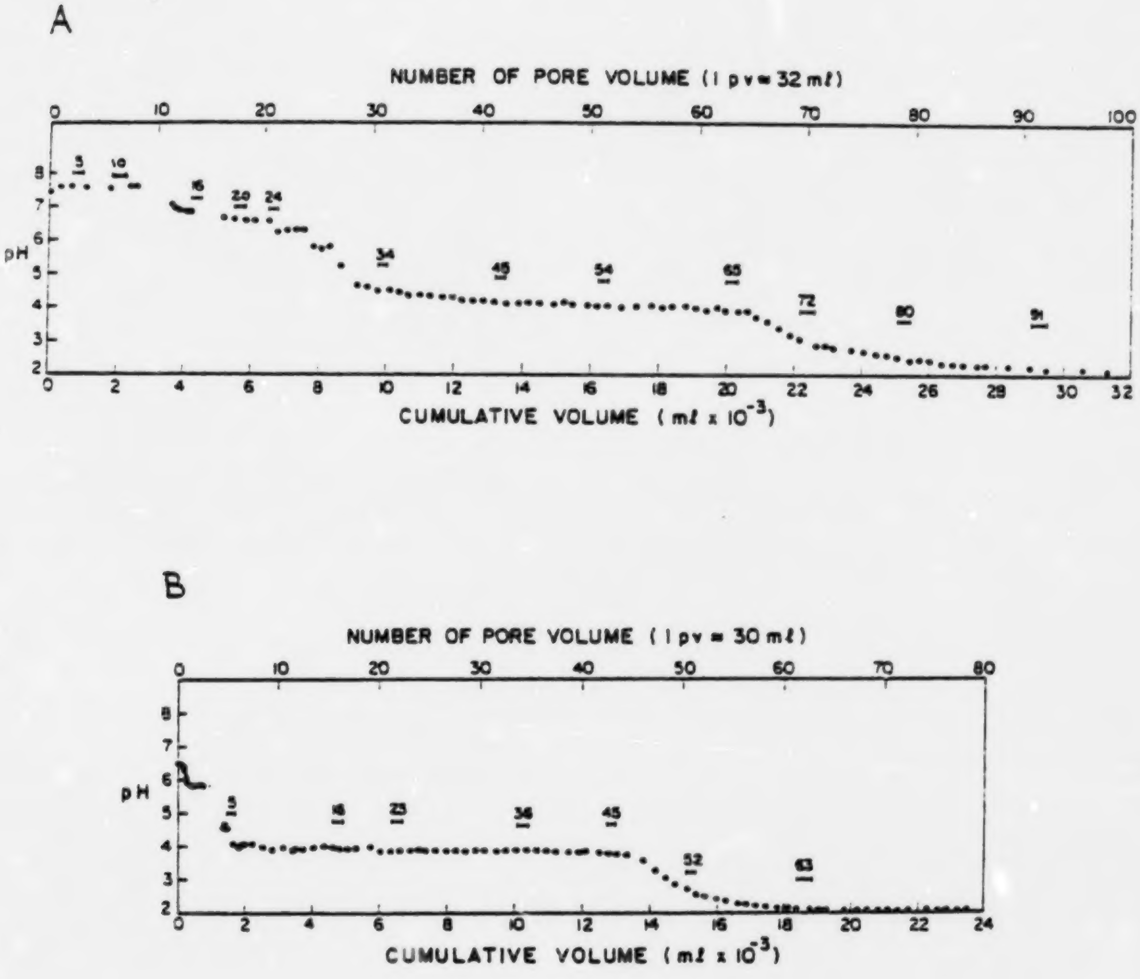

Fig. 14: pH of effluent volume for column 1 (14A) and column 2 (14B) plotted versus cumulative vlume and number of pore/volumes. Effluent samples submitted for analyses are indicated on the graph.

Fig. 15: Data for columns 1 and 2 plotted on a pe-pH diagram for iron species and selected solid phases. The boundaries on the diagram are drawn for the following conditions; $Fe = 10^{-4.05}$, $K = 10^{-3}$, $SO_4 = 10^{-2}$, pK of $Fe(OH)_3$=38.

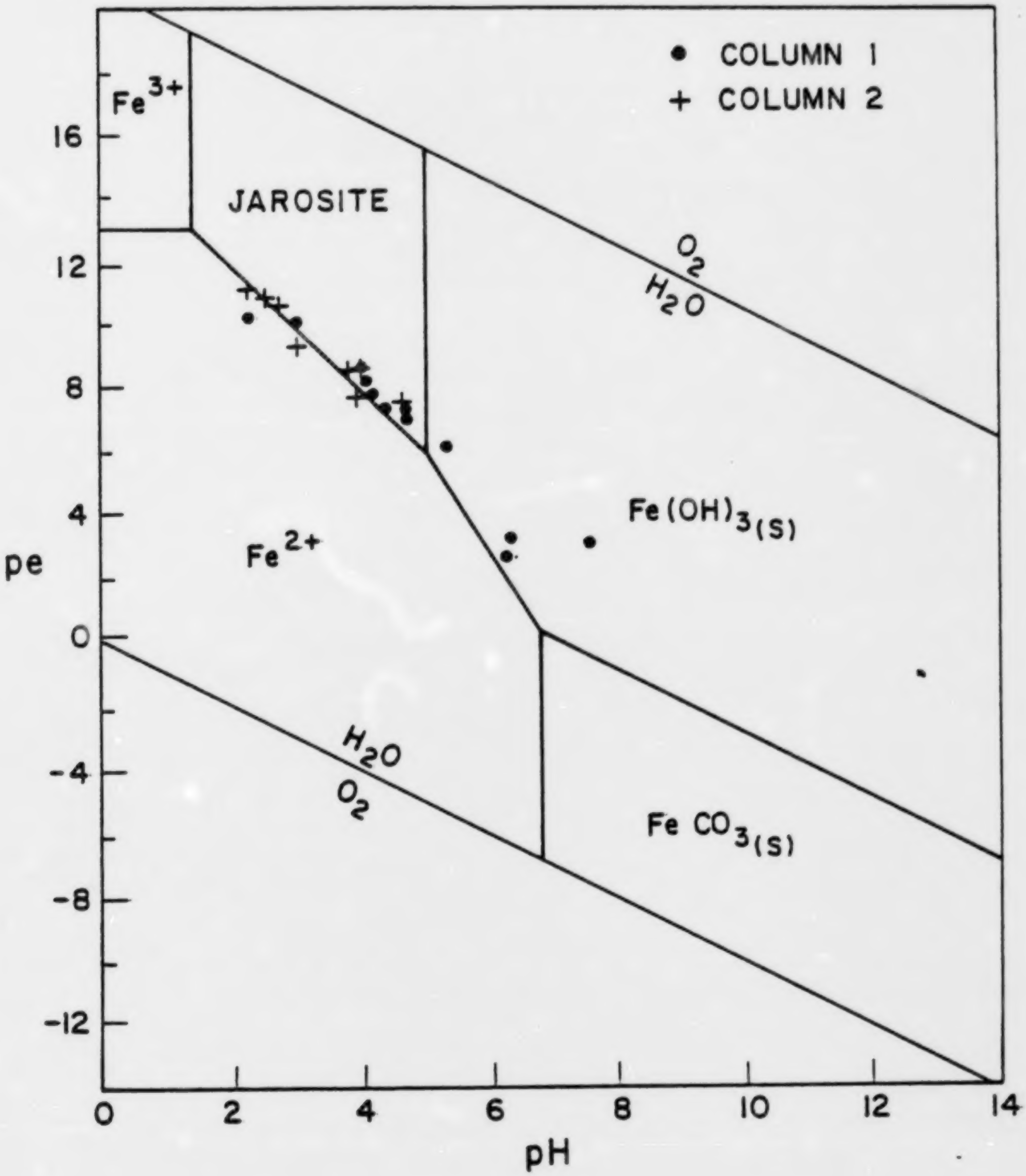

Fig. 16: Data for column 1 and 2 overlain so that the points at which pH drops below approximately 3.9 coincide. The horizontal lines show equilibrium pH values predicted by the ADNEUT mixing cell model for the following sequence of solid phases: A) calcite-gypsum-$Al(OH)_3$-$Fe(OH)_3$; B) siderite-gypsum-$Al(OH)_3$-$Fe(OH)_3$; C) gypsum-$Al(OH)_3$- $Fe(OH)_3$; D) $Al(OH)_3$-$Fe(OH)_3$; E) $Fe(OH)_3$.

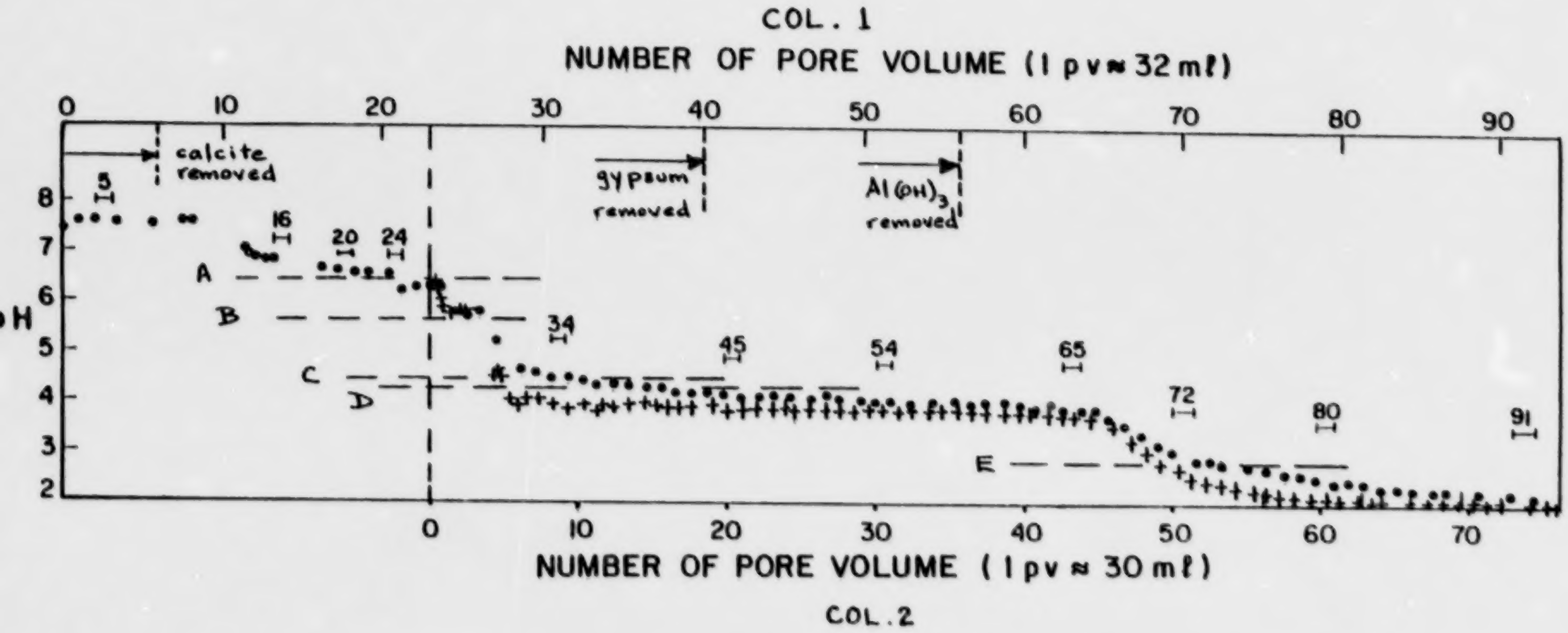

REFERENCES

Arkesteyn, G.J.M.W., 1980. Pyrite oxidation in acid sulphate soils: The role of microorganisms, *Plant and Soil*, *54*: 119-134.

Bloomfield, C. and Zahari, A.B., 1982. Acid sulphate soils. *Outlook Agricul.*, *11*(2):48-54.

Breemen, N. van, 1972. Soil forming processes in acid sulfate soils. In H. Dost (ed.) *Acid Sulfate Soils*. Internat. Inst. for Land Recl. and Improv., the Netherlands, Wageningen. Publ. 18 (1): 66 - 130.

Cathles, L.M., 1982. Acid mine drainage. *Earth Min. Sci.*, *51*(4):37-41.

Erickson, P.M.; Kleinmann, R.P.L. and Campion, P.S.A., 1982. Reducing oxidation of pyrite through selective reclamation processes. *Symp. Surf. Mining Hydrol., Sedimentology and Reclam.*, Univ. Kentucky, Lexington, Kentucky, Dec., pp.97-102.

Goldhaber, M.B., 1982. Experimental study of metastable sulfur oxyanion formation during pyrite oxidation at pH 6-9 and 30°C. *Am. Jour. Sci.* (in Press)

Holdren, G.R. and Berner, R.A., 1979. Mechanism of feldspar weathering-I. Experimental studies. *Geochim. Cosmochim. Acta*, *43*:1161-1171.

Le Roux, N.W., Dacey, P.W. and Temple, K.L., 1980. The microbial role in pyrite oxidation at alkaline pH in coal mine spoil. In P.A. Trudinger, M.R. Walter and B.J. Ralph (eds.) *Biogeochemistry of Ancient and Modern Environments*, Springer-Verlag, Berlin, 515-520.

Lowson, R.T., 1982. Aqueous oxidation of pyrite by molecular oxygen. *Chem. Rev.*, *82* (5):461-497.

Lundgren, D.G. and Silver, M., 1980. Ore leaching by bacteria. *Ann. Rev. Microbiol.*, *34*: 263-283.

Nordstrom, D.K., 1982. Aqueous pyrite oxidation and the consequent formation of secondary iron minerals. In *Acid Sulphate Weathering*, Soil Sci. Soc. Amer., Spec. Publ. No.10, pp. 37-56.

Shumate, K.S.; Smith, E.E.; Dugan, P.R.; Brant, R.A. and Randles, C.I., 1971. Acid mine drainage, formation and abatement. *E.P.A. Rept. 14010 FPR 04/71*.

Smith, E.E., Svanks, K. and Shumate, K., 1968. Sulfide to sulfate reaction studies. Second Symp. Coal Mine Res., Mellon Inst., Pittsburg, Pennsylvania, pp. 1-11.

Snodgrass, W.J., Lush, D.L. and Capobianco, J., 1982. Implications of alternative geochemical controls on the temporal behavior of Elliot Lake Tailings. Inter. Symp. Management of Wastes from Uranium Mining and Milling, Paper No. IAEA-SM-262/54.

Ball, J.W., Jenne, E.A. and Nordstrom, D.K., 1979. WATEQ2 - A computerized chemical model for trace and major element speciation and mineral equilibria of Natural Waters. In E.A. Jenne ed., Chemical Modeling in Aqueous Systems, American Chemical Society Symp. Series 93, pp 815-835.

Barker, J.F. and Chatten, S., 1982. A technique for determining low concentrations of total carbonate in geologic materials. Chemical Geology, 36: 317-323.

Blair, R.D., 1981. Hydrogeochemistry of an Inactive Pyritic Uranium Tailings Basin, Nordic Mine, Elliot Lake, Ontario. University of Waterloo, unpublished Master of Science thesis, 79 p.

Blair, R.D., Cherry, J.A., Lim, T.P. and Vivyurka, A.J., 1980. Groundwater monitoring and contaminant occurence at an abandoned tailings area, Elliot Lake, Ontario. In Brawner, C. (ed.), Proc. First Intern. Conf. on Uranium Mine Waste Disposal, Soc. Mining Engineers of AIME.

Breemen, N. van 1976. The genesis and solution chemistry of acid sulphate soils in Thailand. Ph.D. Thesis, Centre for Agric. Pub. and Doc., Wageningen, The Netherlands. 263 p.

Breemen, N. van 1973. Dissolved Aluminum in Acid Sulfate Soils and in Acid Mine Waters. Soil Sci. Soc. Amer. Proc. 37: 694-697.

Cherry, J.A., Blackport, R.J., Dubrovsky, N., Gillham, R.W., Lim, T.P., Murray, D., Reardon, E.J., and Smyth, D.J.A., 1980. Subsurface hydrology and geochemicall evolution of inactive pyritic tailings in the Elliot Lake Uranium District, Canada. Uranium Mill Tailings Management, Proceedings of the Third Symposium, November 24-25, 1980, Geotechnical Engineering Program, Civil Engineering Department, Colorado State University.

Conlin, B.H., 1980. Design considerations for earthquake-resistant mine tailings impoundment structures in northern Ontario. Unpublished M.Sc. Thesis, Department of Civil Engineering, University of Toronto.

Derry, Duncan R., 1960. Evidence of the origin of the Blind River Uranium Deposits. Economic Geology, 55: 906-927.

Feenstra, S., Blair, R.D., Cherry, J.A., Chakravatti, J.L., LaRocque, E., 1981. Hydrogeochemical Investigations of two inactive tailings areas in the Elliot Lake Uranium District, Ontario, Canada. Uranium Mill Tailings Managment, Proceedings of the Fourth Symposium, November, 1981, Geotechnical Engineering Program, Civil Engineering Department, Colorado State University.

Helgeson,H.C.,1979.Kinetics of mass transfer among silicates and aqueous solution. Geochim. Cosmochim. Acta., 35: 421-469.

Jongejan, A., 1973. An experimental study of the weathering of mill tailings in connection with water pollution Part 3: Mineralogical analyses of tailings samples from various mining companies in Canada, EMR, Mines Br. Invest. Rept. IR 73-14, 74 p.

Kaiman, S., 1978. Mineralogical examination of current Elliot Lake uranium tailings. CANMET, Energy, Mines and Resources, Canada. Report MRP/MSL 78-85 (IR).

Langmuir, D. and Whittemore, D.O., 1971. Variations in the stability of precipitated ferric oxyhydroxides. in. J.D. Hem ed, Nonequilibrium systems in Natural Water Chemistry, Adv. Chem. Ser. 106.

Lee, G.F. and Stumm, W., 1960. Determination of ferrous iron in the presence of ferric iron with bathophenanthroline. American Water Works Assoc., 52: 1567-1574.

Lin, Feng-Chih, and Clemency, C.V., 1981. The kinetics of dissolution of muscovites at $25^{0}C$ and 1 atm CO_2 partial pressure. Geochim. Cosmochim. Acta, 45: 571-576.

Miller, Stuart D., 1980. Sulfur and hydrogen ion buffering in pyritic strip-mine spoil. In P.A. Trudinger and M.R. Walter ed., Biogeochemistry of Ancient and Modern Environments Springer-Verlag, pp. 537-543.

Nordstrom, D.K., 1982. The effect of sulfate on aluminum concentrations in natural waters: some stability relations in the system Al_2O_3 - SO_3 - H_2O at 298K. Geochim. Cosmochim. Acta, 46: pp. 681-692.

Nordstrom, D.K., Jenne, E.A. and Ball, J.W., 1979. Redox equilibria of iron in acid mine waters. In Jenne, E.A. (ed.) Chemical Modelling in Aqueous Systems: Speciation, Sorption, Solubility and Kinetics. Symp. Series 93, American Chemical Society, p. 51-80.

Paces, T., 1973. Steady-state kinetics and equilibrium between ground water and granitic rock. Geochim. Cosmochim. Acta, 37: 2541-2563.

Peterson, S.R. And Krupka, K.M., 1981. Contact of clay liner materials with acidic tailings solutions II: Geochemical modeling. Symp. of Uranium Mill Tails. Mgr., Colorado State University, Oct. 1981.

Pienaar, P.J., 1963. Stratigraphy, petrology, and genesis of the Elliot Lake group, Blind River, Ontario. including the uraniferous conglomerate. Geological Survey of Canada, Bull. 83.

Roscoe, S.M., 1969. Huronian Rocks and Uraniferous Conglomerates in the Canadian Shield. Geological Survey of Canada Paper, pp. 68-40.

Smyth, D.J.A., 1981. Hydrogeological and Geochemical Studies Above the Water Table in an Inactive Uranium Tailings Impoundment Near Elliot Lake, Ontario. Unpublished M.Sc. Project, University of Waterloo.

Appendix A

LISTING OF THE PYROX1 DATA AND RESULTS

PYROX1 SERIES OXIDATION EXPERIMENT
POROUS PLATE FUNNELS WITH 5 MMOL NAHCO3 SOLUTION
-120+170 MESH PYRITE

		PYROX1-1				PYROX1-2			
DATE	DAYS	SO4	WT	ACC	RATE	SO4	WT	ACC	RATE
820824	7.	31.3	70.1	15.7	2.19	5.4	144.7	7.5	0.78
820825	8.	24.4	64.2	17.3	1.57	6.6	47.2	7.8	0.31
820826	9.	14.7	65.1	18.2	0.96	16.8	101.7	9.5	1.71
820827	10.	6.0	58.9	18.6	0.35	6.3	58.1	9.8	0.37
820830	13.	14.5	200.6	21.5	0.97	16.3	195.8	13.4	1.19
820831	14.	10.5	52.1	22.0	0.55	30.2	58.2	15.2	1.76
820901	15.	9.0	98.1	22.9	0.88	22.5	70.4	16.8	1.58
820902	16.	3.1	124.2	23.3	0.39	13.7	151.8	18.8	2.08
820903	17.	10.3	95.3	24.3	0.98	13.1	101.0	20.2	1.32
820907	21.	18.2	200.9	27.9	0.91	12.5	208.6	22.8	0.65
820908	22.	10.7	63.3	28.6	0.68	11.1	65.5	23.5	0.73
820910	24.	6.6	80.5	29.1	0.27	11.2	104.7	24.7	0.59
820913	27.	9.4	214.6	31.2	0.67	14.3	219.5	27.8	1.05
820914	28.	7.8	49.3	31.5	0.38	12.8	101.0	29.1	1.29
820915	29.	5.7	176.4	32.5	1.01	11.7	152.4	30.9	1.78
820916	30.	6.6	107.7	33.3	0.71	11.8	52.2	31.5	0.62
820917	31.	9.8	43.7	33.7	0.43	23.7	51.9	32.7	1.23
820920	34.	41.0	46.4	35.6	0.63	34.2	90.7	35.8	1.03
820921	35.	14.1	59.4	36.4	0.84	24.6	69.0	37.5	1.70
820922	36.	14.0	16.4	36.7	0.23	27.6	31.8	38.4	0.88
820923	37.	19.3	29.2	37.2	0.56	25.6	143.0	42.1	3.66
820924	38.	26.9	23.6	37.9	0.63	10.1	162.7	43.7	1.64
820927	41.	39.9	105.6	42.1	1.40	50.6	75.8	47.5	1.28
820928	42.	28.7	38.6	43.2	1.11	49.4	75.0	51.3	3.70
820929	43.	28.4	46.5	44.5	1.32	34.8	113.5	55.2	3.95
820930	44.	26.1	84.4	46.7	2.20	24.2	30.8	55.9	0.75
821001	45.	12.8	20.5	47.0	0.26	64.6	79.1	61.1	5.11
821004	48.	36.5	14.8	47.5	0.18	37.1	90.6	64.4	1.12
821005	49.	82.3	77.2	53.9	6.35	83.1	86.0	71.6	7.15
821006	50.	21.6	100.4	56.0	2.17	40.4	80.4	74.8	3.25
821007	51.	12.6	158.4	58.0	2.00	35.9	103.9	78.5	3.73
821008	52.	13.7	63.5	58.9	0.87	38.0	59.4	80.8	2.26
821012	56.	19.7	271.0	64.2	1.33	61.5	137.3	89.2	2.11
821013	57.	23.5	23.7	64.8	0.56	105.0	11.9	90.5	1.25
821014	58.	30.5	13.9	65.2	0.42	85.6	10.4	91.4	0.99
821015	59.	10.3	292.0	68.2	3.01	148.0	97.6	105.8	14.44
821018	62.	11.0	291.9	71.4	1.07	67.6	43.0	108.7	0.97
821019	63.	17.5	36.6	72.1	0.64	115.0	58.2	115.4	6.69
821020	64.	14.7	105.8	73.6	1.56	51.5	90.4	120.1	4.66
821021	65.	13.7	84.9	74.8	1.16	37.6	30.4	121.2	1.14
821022	66.	17.3	37.1	75.4	0.64	73.2	58.2	125.5	4.26
821025	69.	23.6	201.0	80.2	1.58	31.9	200.5	131.9	2.13
821026	70.	94.1	90.4	88.7	8.51	15.4	20.1	132.2	0.31
821027	71.	15.1	85.3	90.0	1.29	134.0	24.4	135.5	3.27
821028	72.	17.5	71.7	91.2	1.25	119.0	54.7	142.0	6.51
821029	73.	21.1	52.3	92.3	1.10	92.2	45.0	146.1	4.15
821101	76.	29.2	174.9	97.4	1.70	98.7	110.9	157.1	3.65
821102	77.	29.2	57.1	99.1	1.67	39.6	86.8	160.4	3.35

821103	78.	31.2	49.0	100.6	1.53	46.1	37.6	162.2	1.73
821104	79.	34.4	50.1	102.4	1.72	77.9	29.9	164.5	2.33
821105	80.	37.0	30.8	103.5	1.14	103.0	12.8	165.8	1.32
821108	83.	47.4	100.3	108.2	1.58	109.0	23.7	168.4	0.86
821109	84.	58.4	22.9	109.6	1.34	166.0	67.3	179.6	11.17
821110	85.	64.6	17.5	110.7	1.13	126.0	8.8	180.7	1.11
821111	86.	76.2	18.7	112.1	1.42	60.6	81.5	185.6	4.96
821112	87.	87.9	13.9	113.4	1.22	17.9	64.9	186.8	1.16
821115	90.	89.4	32.2	116.2	0.96	53.6	50.6	189.5	0.90
821116	91.	129.0	19.8	118.8	2.55	98.6	18.8	191.3	1.85
821117	92.	126.0	33.2	123.0	4.18	105.0	23.1	193.8	2.43
821118	93.	98.3	25.4	125.5	2.50	116.0	25.2	196.7	2.92
821119	94.	85.7	31.0	128.1	2.66	112.0	27.8	199.8	3.11
821122	97.	95.5	36.8	131.6	1.17	129.0	37.2	204.6	1.60
821123	98.	132.0	36.7	136.5	4.84	118.0	18.8	206.6	2.22
821124	99.	107.0	74.9	144.5	8.01	136.0	58.8	214.8	8.00
821125	100.	55.7	44.5	147.0	2.48	90.4	62.8	220.5	5.68
821126	101.	59.3	17.2	148.0	1.02	76.2	55.8	224.8	4.25
821129	104.	83.9	131.9	159.1	3.69	79.9	59.6	229.5	1.59
821130	105.	78.2	33.5	161.7	2.62	91.8	17.3	231.1	1.59
821201	106.	76.5	48.6	165.4	3.72	68.8	147.6	241.3	10.15
821202	107.	74.2	40.4	168.4	3.00	34.6	84.2	244.2	2.91
821203	108.	74.9	39.7	171.4	2.97	38.6	106.7	248.3	4.12
821206	111.	93.9	74.1	178.3	2.32	46.7	156.3	255.6	2.43
821207	112.	121.0	20.4	180.8	2.47	74.1	74.5	261.1	5.52
821208	113.	96.9	77.8	188.3	7.54	55.7	41.3	263.4	2.30
821209	114.	51.5	53.1	191.1	2.73	67.5	35.2	265.8	2.38
821210	115.	52.6	36.2	193.0	1.30	79.6	16.9	267.1	1.35
821213	118.	60.4	147.0	201.9	2.96	93.6	126.6	279.0	3.95
821214	119.	50.0	57.8	204.7	2.89	87.6	27.3	281.4	2.39
821215	120.	41.6	83.1	208.2	3.46	91.6	20.2	283.2	1.85
821216	121.	35.6	88.0	211.3	3.13	103.0	19.7	285.3	2.03
821217	122.	35.5	68.2	213.8	2.42	112.0	24.8	288.0	2.78
821220	125.	42.4	175.3	221.2	2.48	115.0	98.3	299.3	3.77
821221	126.	46.1	52.1	223.6	2.40	52.4	20.0	300.4	1.05
821222	127.	49.1	45.2	225.8	2.22	0.0	4.1	300.4	0.00
821223	128.	57.1	33.9	228.0	2.22	62.6	21.6	301.7	1.35
821224	129.	70.1	37.3	230.5	2.61	121.0	26.4	304.9	3.19
821227	132.	64.5	100.7	237.1	2.17	95.1	149.2	319.1	4.73
821229	134.	44.7	256.2	248.6	5.73	86.4	36.8	322.3	1.59
830102	138.	35.6	73.3	251.2	0.65	108.0	61.1	328.9	1.65

PYROX1 SERIES OXIDATION EXPERIMENT
POROUS PLATE FUNNELS WITH 5 MMOL NAHCO3 SOLUTION
-120+170 MESH PYRITE

		PYROX1-3				PYROX1-4			
DATE	DAYS	SO4	WT	ACC	RATE	SO4	WT	ACC	RATE
820824	7.	3.2	95.4	12.6	0.31	2.0	72.7	9.8	0.15
820825	8.	10.4	98.5	13.6	1.02	7.1	48.3	10.2	0.34
820826	9.	9.1	108.9	14.6	0.99	3.9	42.1	10.4	0.16
820827	10.	4.4	55.3	14.9	0.24	3.0	95.0	10.6	0.29
820830	13.	9.1	201.4	16.7	0.61	3.0	191.0	11.2	0.19
820831	14.	4.3	26.5	16.8	0.11	5.7	98.1	11.8	0.56
820901	15.	11.9	81.4	17.8	0.97	9.8	69.2	12.4	0.68
820902	16.	12.1	120.1	19.2	1.45	4.3	171.3	13.2	0.74
820903	17.	11.5	108.3	20.5	1.25	7.9	80.3	13.8	0.63
820907	21.	6.7	187.9	21.7	0.31	21.8	121.8	16.5	0.66
820908	22.	7.3	76.0	22.3	0.55	8.0	73.5	17.1	0.59
820910	24.	8.8	117.0	23.3	0.51	6.6	113.2	17.8	0.37
820913	27.	7.7	225.2	25.1	0.58	11.2	238.0	20.5	0.89
820914	28.	6.2	123.5	25.8	0.77	8.2	101.3	21.3	0.83
820915	29.	5.1	166.7	26.7	0.85	8.6	119.4	22.3	1.03
820916	30.	8.3	143.8	27.9	1.19	16.2	52.6	23.2	0.85
820917	31.	9.0	134.5	29.1	1.21	22.4	81.9	25.0	1.83
820920	34.	7.8	155.8	30.3	0.41	14.5	35.0	25.5	0.17
820921	35.	26.3	73.8	32.2	1.94	19.2	45.6	26.4	0.88
820922	36.	35.9	30.4	33.3	1.09	26.2	39.8	27.4	1.04
820923	37.	25.3	53.3	34.7	1.35	19.6	26.6	28.0	0.52
820924	38.	24.4	58.4	36.1	1.42	16.3	71.6	29.1	1.17
820927	41.	38.2	94.9	39.7	1.21	13.5	96.5	30.4	0.43
820928	42.	57.3	29.1	41.4	1.67	25.8	26.1	31.1	0.67
820929	43.	15.4	33.6	41.9	0.52	14.8	36.9	31.7	0.55
820930	44.	33.7	30.7	42.9	1.03	33.4	31.5	32.7	1.05
821001	45.	69.7	28.1	44.9	1.96	12.2	40.6	33.2	0.50
821004	48.	98.9	44.3	49.3	1.46	23.0	107.7	35.7	0.83
821005	49.	34.6	14.4	49.8	0.50	34.2	86.6	38.6	2.96
821006	50.	96.5	66.0	56.1	6.37	19.6	105.1	40.7	2.06
821007	51.	35.5	134.1	60.9	4.76	10.4	165.9	42.4	1.73
821008	52.	9.4	23.2	61.1	0.22	23.1	47.0	43.5	1.09
821012	56.	59.8	36.9	63.3	0.55	24.4	138.0	46.9	0.84
821013	57.	0.0	5.5	63.3	0.00	39.3	7.6	47.2	0.30
821014	58.	106.0	2.7	63.6	0.29	54.4	3.8	47.4	0.21
821015	59.	48.3	224.3	74.5	10.83	28.2	303.7	55.9	8.56
821018	62.	78.7	96.3	82.0	2.53	31.3	153.8	60.8	1.60
821019	63.	45.3	7.8	82.4	0.35	16.2	35.7	61.3	0.58
821020	64.	49.6	114.0	88.0	5.65	15.1	90.9	62.7	1.37
821021	65.	45.3	30.9	89.4	1.40	17.1	67.6	63.9	1.16
821022	66.	25.2	7.8	89.6	0.20	18.5	35.7	64.5	0.66
821025	69.	22.0	200.8	94.1	1.47	21.7	215.8	69.2	1.56
821026	70.	20.5	151.7	97.2	3.11	17.5	83.9	70.7	1.47
821027	71.	77.9	154.8	109.2	12.06	20.9	69.6	72.1	1.45
821028	72.	25.0	168.2	113.4	4.20	24.4	43.3	73.2	1.06
821029	73.	28.6	127.4	117.1	3.64	33.8	27.5	74.1	0.93
821101	76.	49.4	79.8	121.0	1.31	49.1	110.5	79.5	1.81
821102	77.	92.2	146.0	134.5	13.46	57.5	62.4	83.1	3.59

```
821103     78.     22.1   50.8 135.6  1.12    41.6   52.9   85.3  2.20
821104     79.     46.8   74.7 139.1  3.50    39.9   35.3   86.7  1.41
821105     80.     65.6   47.1 142.2  3.09    53.9   27.1   88.2  1.46
821108     83.     89.4  118.4 152.8  3.53    79.2   45.9   91.8  1.21
821109     84.     96.0   32.5 155.9  3.12    79.5    6.3   92.3  0.50
821110     85.     92.7   13.5 157.1  1.25   118.0   36.3   96.6  4.28
821111     86.     88.4  123.0 168.010.87   112.0   34.9  100.5  3.91
821112     87.      9.0  189.2 169.7  1.70    99.3   21.0  102.6  2.09
821115     90.      8.6    8.2 169.8  0.02    98.0   57.3  108.2  1.87
821116     91.     66.9   95.3 176.2  6.38    44.4  199.6  117.1  8.86
821117     92.     62.9   32.7 178.2  2.06     5.7  114.0  117.7  0.65
821118     93.     91.2   31.4 181.1  2.86    21.3   56.5  119.0  1.20
821119     94.     95.2   25.1 183.5  2.39    32.3  344.8  130.111.14
821122     97.    134.0   37.9 188.5  1.69    29.5  237.1  137.1  2.33
821123     98.     82.7  199.1 205.016.47    30.9   29.6  138.0  0.91
821124     99.     33.1  117.5 208.9  3.89    38.8   78.9  141.1  3.06
821125    100.     45.1  108.2 213.8  4.88    34.3   54.9  142.9  1.88
821126    101.     36.2  130.6 218.5  4.73    40.9   22.7  143.9  0.93
821129    104.     46.1  270.5 231.0  4.16    60.8   19.1  145.0  0.39
821130    105.     44.3   65.4 233.9  2.90    65.0    6.2  145.4  0.40
821201    106.     59.4   64.0 237.7  3.80    35.0   68.4  147.8  2.39
821202    107.     63.9   76.9 242.6  4.91   101.0   21.0  149.9  2.12
821203    108.     61.3   54.4 245.9  3.33    89.1   26.9  152.3  2.40
821206    111.     93.4  145.6 259.5  4.53    93.2   61.2  158.0  1.90
821207    112.     78.9   38.8 262.6  3.06     0.0    2.8  158.0  0.00
821208    113.     92.8   10.9 263.6  1.01    73.2  147.4  168.810.79
821209    114.    103.0    3.8 264.0  0.39    20.1  152.9  171.9  3.07
821210    115.      0.0   37.5 264.0  0.00     0.0  156.5  171.9  0.00
821213    118.     52.5  287.5 279.1  5.03    24.9  301.8  179.4  2.50
821214    119.     55.4   24.7 280.5  1.37    18.9  116.5  181.6  2.20
821215    120.     89.1   37.4 283.8  3.33    21.8  106.4  183.9  2.32
821216    121.     68.3  124.5 292.3  8.50    28.7   76.3  186.1  2.19
821217    122.     43.3  112.3 297.2  4.86    34.7   69.6  188.6  2.42
821220    125.     40.6  283.9 308.7  3.84    57.1  103.7  194.5  1.97
821221    126.     91.9   65.4 314.7  6.01    69.1   23.1  196.1  1.60
821222    127.     59.1   78.0 319.3  4.61    66.1   13.9  197.0  0.92
821223    128.     44.6   77.8 322.8  3.47     0.0    6.3  197.0  0.00
821224    129.     36.4  108.4 326.7  3.95    64.2   14.6  197.9  0.94
821227    132.     36.6  233.1 335.2  2.84     0.0  318.4  197.9  0.00
821229    134.     49.4  168.5 343.6  4.16    16.7  370.8  204.1  3.10
830102    138.     60.3  150.6 352.6  2.27    35.5  174.6  210.3  1.55
```

Appendix B

LISTING OF THE PYROX2 DATA AND RESULTS

PYROX2 SERIES OXIDATION EXPERIMENT
FIVE GRAIN SIZE FRACTIONS USED
FROM -60 TO +325 MESH COLORADO PYRITE

DATE	DAYS	P2-1		P2-2		P2-3		P2-4		P2-5	
		ACC	RATE	ACC	RATE	ACC	RATE	ACC	RATE	ACC	RATE
821201	0.	1.4	1.35	1.4	1.37	1.1	1.08	0.5	0.49	0.7	0.72
821202	1.	5.1	3.71	5.8	4.42	3.6	2.55	3.5	3.04	4.8	4.08
821203	2.	7.5	2.44	10.1	4.37	7.1	3.50	7.1	3.58	7.4	2.61
821206	5.	7.9	0.12	25.9	5.24	17.0	3.28	26.1	6.33	15.7	2.77
821207	6.	21.9	14.02	30.0	4.07	22.0	5.01	29.5	3.44	19.4	3.66
821208	7.	30.8	8.86	39.3	9.96	29.9	7.96	34.6	5.06	24.5	5.14
821209	8.	38.6	7.82	44.0	4.04	36.8	6.86	39.9	5.27	28.7	4.15
821210	9.	44.6	6.03	56.0	12.09	43.6	6.85	44.8	4.89	32.4	3.73
821213	10.	57.5	12.90	60.6	4.51	58.0	14.41	54.2	9.42	51.6	19.18
821214	11.	65.8	8.26	73.5	12.94	65.4	7.40	64.3	10.10	56.1	4.55
821215	12.	81.9	16.15	87.4	13.95	74.2	8.75	71.4	7.16	63.3	7.22
821216	13.	99.3	17.35	100.6	13.14	83.4	9.24	78.6	7.17	68.9	5.55
821217	14.	112.5	13.29	115.9	15.37	93.4	9.93	86.5	7.88	75.5	6.59
821220	17.	141.2	9.55	142.5	8.86	109.8	5.49	101.9	5.14	88.9	4.48
821221	18.	150.5	9.28	151.0	8.52	115.0	5.20	108.4	6.45	95.7	6.75
821222	19.	162.8	12.33	162.5	11.45	123.6	8.60	112.8	4.41	100.3	4.66
821223	20.	170.0	7.15	172.8	10.32	131.6	8.02	118.0	5.25	104.8	4.50
821224	21.	174.9	4.91	182.3	9.48	139.4	7.79	118.0	0.00	109.3	4.48
821227	24.	182.5	2.53	204.7	7.47	163.4	7.99	118.0	0.00	121.9	4.20
821229	26.	195.9	6.67	222.3	8.80	176.7	6.64	141.1	11.54	129.0	3.53
830102	30.	197.4	0.40	250.5	7.05	196.4	4.92	144.9	0.95	140.2	2.80
830106	34.	237.8	10.09	281.6	7.76	214.4	4.50	166.0	5.28	152.3	3.02
830111	39.	287.6	9.97	329.0	9.49	245.9	6.31	187.7	4.33	168.1	3.17
830114	42.	318.1	10.17	362.5	11.15	264.6	6.24	196.7	3.00	176.1	2.68
830119	46.	351.7	8.39	385.5	5.76	282.5	4.46	207.9	2.82	183.4	1.82
830121	49.	379.1	9.14	402.6	5.70	297.6	5.04	216.4	2.83	189.9	2.17
830125	53.	396.2	4.27	421.5	4.72	315.7	4.53	225.6	2.30	195.1	1.31
830128	56.	416.3	6.69	430.3	2.94	329.2	4.48	232.3	2.23	199.7	1.51
830201	60.	455.5	9.61	446.7	4.10	339.2	2.52	240.9	2.14	207.7	2.00
830204	63.	475.4	6.63	455.1	2.79	353.2	4.65	246.4	1.84	212.5	1.61
830208	67.	502.2	6.71	473.8	4.68	369.0	3.95	254.1	1.93	218.9	1.61

Appendix C

LISTING OF THE PYROX3 DATA AND RESULTS

```
 PYROX3 SERIES OXIDATION EXPERIMENT
UNSATURATED COLUMNS WITH 5 MMOL NAHCO3 SOLUTION
FIVE OXYGEN CONCENTRATIONS: 0.01%,0.10%,1.0%,5.0%,20.0%
FOR P3-1 TO P3-5
```

LISTING OF DATA FOR PYROX3-1

DATE	DAY	SO4	WT	ACC	RATE
830127	1.	22.8	536.5	12.2	12.23
830128	2.	2.7	196.3	12.8	0.53
830130	4.	3.1	106.7	13.1	0.17
830131	5.	6.7	175.9	14.3	1.18
830201	6.	4.2	133.9	14.8	0.56
830202	7.	3.1	78.0	15.5	0.63
830203	8.	7.9	48.2	15.8	0.38
830206	11.	5.3	370.9	17.8	0.86
830207	12.	6.2	148.5	18.7	0.92
830209	14.	6.8	172.7	19.9	0.59
830210	15.	3.9	168.8	20.6	0.66
830211	16.	4.7	140.5	21.2	0.66
830212	17.	5.2	144.5	22.0	0.75
830214	19.	5.1	226.6	23.1	0.58
830215	20.	6.1	151.3	24.1	0.92
830216	21.	4.4	180.9	24.9	0.80
830217	22.	4.7	196.4	25.8	0.92
830218	23.	5.3	147.3	26.6	0.78
830221	26.	7.7	278.2	28.7	0.71
830222	27.	7.5	163.2	29.9	1.22
830223	28.	4.9	170.7	30.8	0.84
830225	30.	5.5	328.7	32.6	0.90
830228	33.	9.2	229.0	34.7	0.70
830301	34.	8.1	170.1	36.1	1.38
830302	35.	5.6	165.7	37.0	0.93
830303	36.	5.3	180.2	37.9	0.96
830304	37.	5.4	197.4	39.0	1.07
830305	38.	5.5	158.5	39.9	0.87
830306	39.	5.8	160.0	40.8	0.93
830307	40.	5.6	173.4	41.8	0.97
830308	41.	4.8	164.3	42.6	0.79
830309	42.	5.9	169.3	43.6	1.00
830310	43.	5.5	168.8	44.5	0.93
830311	44.	5.5	171.3	45.4	0.94
830313	46.	6.6	220.1	46.9	0.73
830314	47.	7.3	165.0	48.1	1.20
830315	48.	5.4	168.1	49.0	0.91
830316	49.	4.6	152.1	49.7	0.70
830317	50.	4.3	158.2	50.4	0.68
830318	51.	5.6	168.3	51.3	0.94
830319	52.	3.4	198.9	52.0	0.68
830321	54.	5.0	259.1	53.3	0.65
830322	55.	3.8	170.6	53.9	0.65
830323	56.	5.0	166.2	54.8	0.83
830324	57.	10.1	63.7	55.4	0.64
830325	58.	5.7	162.6	56.3	0.93
830326	59.	4.7	168.5	57.1	0.79
830327	60.	4.3	185.6	57.9	0.80
830328	61.	4.0	172.3	58.6	0.69
830329	62.	5.5	132.4	59.3	0.73
830331	63.	5.8	252.1	60.8	1.46
830401	64.	5.7	137.3	61.6	0.79
830402	65.	5.3	137.4	62.3	0.73
830404	67.	5.0	179.9	63.2	0.45
830405	68.	9.8	123.4	64.4	1.21
830406	69.	5.3	144.8	65.2	0.77

```
LISTING OF DATA FOR      PYROK3-2

DATE      DAY        SO4        WT        ACC      RATE

830126     2.       17.6      331.4       5.8      5.83
830127     3.       11.9       56.5       6.5      0.67
830128     4.        0.7       28.2       6.5      0.02
830203    10.       24.2      228.5      12.1      0.92
830204    11.        9.4       75.1      12.8      0.71
830206    13.       10.6      127.6      14.1      0.68
830207    14.       10.1      114.0      15.3      1.15
830209    16.       11.7      174.1      17.3      1.02
830210    17.        5.2      187.1      18.3      0.97
830211    18.        6.6      126.8      19.1      0.84
830212    19.        8.5      103.7      20.0      0.88
830214    21.       10.2      194.6      22.0      0.99
830215    22.        9.3       93.1      22.8      0.87
830216    23.       15.1      167.0      25.4      2.52
830217    24.        9.1      132.5      26.6      1.21
830218    25.       10.4      116.8      27.8      1.21
830221    28.       10.8      192.3      29.9      0.69
830222    29.       21.4      109.7      32.2      2.35
830223    30.       10.6      124.3      33.5      1.32
830225    32.       12.9      200.4      36.1      1.29
830228    35.       13.5      145.3      38.1      0.65
830301    36.       28.5      107.4      41.1      3.06
830302    37.       13.4      111.0      42.6      1.49
830303    38.       14.2      120.4      44.3      1.71
830304    39.       10.1      137.8      45.7      1.39
830305    40.        8.4      119.0      46.7      1.00
830306    41.        8.4      111.8      47.7      0.94
830307    42.        6.3      127.4      48.5      0.80
830308    43.        6.4      127.0      49.3      0.81
830309    44.        7.9      116.4      50.2      0.92
830310    45.        8.3      120.8      51.2      1.00
830311    46.        8.6      125.4      52.3      1.08
830313    48.        9.0      168.4      53.8      0.76
830314    49.       12.4      114.1      55.2      1.41
830315    50.        8.2      123.2      56.2      1.01
830316    51.        7.4       82.7      56.8      0.61
830317    52.        8.7      113.7      57.8      0.99
830318    53.        6.0      116.9      58.5      0.70
830319    54.        5.3      145.3      59.3      0.77
830321    56.        6.3      170.7      60.4      0.54
830322    57.        6.8      121.6      61.2      0.83
830323    58.        7.2      121.3      62.1      0.87
830324    59.       10.9       69.9      62.8      0.76
830325    60.        8.2      117.5      63.8      0.96
830326    61.        7.5      117.6      64.7      0.88
830327    62.        9.8      129.5      65.9      1.27
830328    63.       10.2      157.9      67.6      1.61
830329    64.       12.5      105.4      68.9      1.32
830331    66.       16.9      183.1      72.0      1.55
830401    67.       15.6      114.6      73.8      1.79
830402    68.       15.3      106.8      75.4      1.63
830404    70.       14.6      129.8      77.3      0.95
830405    71.       30.7      102.0      80.4      3.13
830406    72.       16.2      116.9      82.3      1.89
```

```
LISTING OF DATA FOR      PYROX3-3

DATE      DAY         SO4         WT         ACC       RATE

830131     1.        57.2       324.7        15.6      13.57
830201     2.        19.4        73.6        20.0       1.43
830203     4.        21.1       333.0        27.0       3.51
830204     5.        14.9       163.3        29.5       2.43
830206     7.        16.9       184.7        32.6       1.56
830209    10.        21.8       300.7        39.1       2.19
830210    11.        13.8       161.5        41.4       2.23
830211    12.        11.7       165.0        43.3       1.93
830212    13.        16.3       128.0        45.4       2.09
820214    15.         5.1       251.1        46.7       0.64
830215    16.        15.4       132.4        48.7       2.04
830216    17.         9.6       132.6        50.0       1.27
830217    18.        14.9       181.1        52.7       2.70
830218    19.        16.0       148.4        55.0       2.37
830221    22.        19.2       254.6        59.9       1.63
830222    23.        32.0       159.3        65.0       5.10
830223    24.        17.3       175.1        68.1       3.03
830225    26.        13.7       341.0        74.4       3.19
830228    29.        24.4       271.6        81.1       2.21
830301    30.        30.4       159.9        85.9       4.86
830302    31.        21.8       168.7        89.6       3.68
830303    32.        22.9       167.1        93.4       3.83
830304    33.        23.6       166.3        97.4       3.92
830305    34.        23.1       145.8       100.7       3.37
830306    35.        24.8       151.5       104.5       3.76
830307    36.        19.5       164.3       107.7       3.20
830308    37.        20.5       155.3       110.9       3.18
830309    38.        21.9       113.3       113.4       2.48
830310    39.        22.8       153.9       116.9       3.51
830311    40.        21.5       158.5       120.3       3.41
830313    42.        26.0       137.8       123.8       1.79
830314    43.        25.9       152.1       127.8       3.94
830315    44.        23.8       157.9       131.5       3.76
830316    45.        22.7       138.4       134.7       3.14
830317    46.        26.1       138.0       138.3       3.60
830318    47.        21.6       140.5       141.3       3.03
830319    48.        19.3       189.4       145.0       3.66
830321    50.        29.6       227.2       151.7       3.36
830322    51.        19.2       183.4       155.2       3.52
830323    52.        22.3       162.0       158.8       3.61
830324    53.        32.6        90.7       161.8       2.96
830325    54.        27.1       151.6       165.9       4.11
830326    55.        22.5       153.7       169.4       3.46
830327    56.        22.4       173.4       173.2       3.88
830328    57.        17.8       167.7       176.2       2.99
830329    58.        24.3       119.0       179.2       2.95
830331    60.        35.3       196.8       186.1       3.47
830401    61.        27.5       133.4       189.8       3.67
830402    62.        27.4       122.8       193.2       3.36
830404    64.        26.4       170.1       197.7       2.25
830405    65.        56.2        93.1       202.9       5.23
830406    66.        34.3       109.1       206.6       3.74
```

```
 LISTING OF DATA FOR      PYROX3-4

DATE      DAY          SO4          WT          ACC        RATE

830304     1.         39.1       449.7         17.6       17.58
830305     2.         23.5       123.6         20.5        2.90
830306     3.         30.0       114.6         23.9        3.44
830307     4.         19.4       118.9         26.2        2.31
830308     5.         21.7       114.7         28.7        2.49
830309     6.         18.5       110.7         30.8        2.05
830310     7.         18.9       104.2         32.7        1.97
830311     8.         19.2        95.3         34.6        1.83
830313    10.         26.4       131.3         38.0        1.73
830314    11.         33.5        75.4         40.6        2.53
830315    12.         26.1        82.2         42.7        2.15
830316    13.         23.8        71.2         44.4        1.69
830317    14.         26.3        73.3         46.3        1.93
830318    15.         23.2        74.9         48.1        1.74
830319    16.         24.1        90.3         50.2        2.18
830321    18.         25.8       114.0         53.2        1.47
830322    19.          0.0        76.2         53.2        0.00
830323    20.         19.6        79.2         54.7        1.55
830324    21.         29.7        47.9         56.2        1.42
830325    22.         19.6        67.9         57.5        1.33
830326    23.         18.1        65.0         58.7        1.18
830327    24.         22.7        83.7         60.6        1.90
830328    25.         15.3        80.2         61.8        1.23
830329    26.         15.6        70.3         62.9        1.10
830331    28.         24.5       107.9         65.5        1.32
830401    29.         20.4        64.7         66.9        1.32
830402    30.         17.9        60.6         67.9        1.08
830404    32.         26.7        92.6         70.4        1.24
830405    33.         23.8        59.5         71.8        1.42
830406    34.         27.3        69.5         73.7        1.90
```

```
LISTING OF DATA FOR      PYROXS-5

DATE      DAY        SO4         WT          ACC        RATE

830304     1.       46.8       239.0        11.2       11.19
830305     2.       63.1       174.6        25.7       14.51
830306     3.       23.1       168.8        30.4        4.74
830307     4.       23.4       173.4        34.5        4.06
830308     5.       20.2       124.4        37.0        2.51
830309     6.       24.4       163.2        41.0        3.98
830310     7.       17.8       133.7        43.4        2.38
830313    10.       25.5       223.7        49.1        1.90
830314    11.       22.4       123.3        51.8        2.76
830315    12.       15.4       119.6        53.7        1.84
830317    14.       21.8       144.6        56.8        1.58
830318    15.       15.1       117.5        58.6        1.77
830319    16.       19.1       129.9        61.1        2.48
830321    18.       18.8       133.9        63.6        1.26
830322    19.        0.0       126.0        63.6        0.00
830323    20.       13.9       121.3        65.3        1.69
830325    22.       23.6       131.2        68.4        1.55
830326    23.       12.9       113.6        69.9        1.47
830327    24.       15.5       104.1        71.5        1.61
830328    25.       13.8       103.3        72.9        1.43
830329    26.       15.1        87.0        74.2        1.31
830331    28.       20.5       127.4        76.8        1.31
830401    29.       16.8        87.0        78.3        1.46
830402    30.       17.2        80.2        79.7        1.38
830404    32.        8.6        41.5        80.0        0.18
830405    33.       44.8        79.7        83.6        3.57
830406    34.       23.8        83.0        85.6        1.98
```

Appendix D

LISTING OF THE PYROX4 DATA AND RESULTS

PYROX4 SERIES OXIDATION EXPERIMENT
TWO TEMPERATURES USED --- P4-1 AT 3 DEG. C
P4-2 AT 15 DEG. C.   10 GRAMS OF PERU PYRITE
-120+170 MESH. WITH 90 GRAMS SILICA SAND
MOISTURE SUCTION CUPS, 5 MMOL/L NAHCO3, 20% O2, 0.5% CO2

		PYROX4-1				PYROX4-2			
DATE	DAY	SO4	WT	ACC	RATE	SO4	WT	ACC	RATE
830308	1.	8.7	129.4	1.1	1.13	14.7	127.2	1.9	1.87
830309	2.	1.4	169.0	1.4	0.24	8.7	107.7	2.8	0.94
830310	3.	1.3	148.0	1.6	0.19	8.3	79.8	3.5	0.66
830311	4.	1.3	141.1	1.7	0.18	6.9	198.6	4.8	1.37
830313	6.	3.2	103.8	2.1	0.17	11.4	92.1	5.9	0.52
830314	7.	4.0	44.9	2.2	0.18	15.6	38.7	6.5	0.60
830315	8.	4.1	43.4	2.4	0.18	17.2	34.2	7.1	0.59
830316	9.	2.5	73.9	2.6	0.18	16.9	46.8	7.9	0.79
830317	10.	2.0	80.1	2.8	0.16	15.3	42.3	8.5	0.65
830318	11.	2.4	69.4	2.9	0.17	16.8	38.8	9.2	0.65
830319	12.	2.4	66.8	3.1	0.16	20.9	34.2	9.9	0.71
830321	14.	2.6	116.9	3.4	0.15	21.4	59.7	11.2	0.64
830322	15.	4.3	37.2	3.6	0.16	23.8	24.8	11.8	0.59
830323	16.	5.9	38.4	3.8	0.23	30.9	24.4	12.5	0.75
830324	17.	8.5	30.1	4.0	0.26	30.8	23.9	13.2	0.74
830325	18.	5.8	38.5	4.3	0.22	30.9	21.9	13.9	0.68
830326	19.	9.9	34.1	4.6	0.34	35.5	22.0	14.7	0.78
830327	20.	10.0	35.4	5.0	0.35	24.5	47.4	15.9	1.16
830328	21.	8.4	33.8	5.2	0.28	17.7	33.6	16.5	0.59
830329	22.	7.3	45.2	5.6	0.33	20.4	33.8	17.1	0.69
830331	24.	4.4	167.9	6.3	0.37	24.3	63.9	18.7	0.78
830401	25.	3.1	66.9	6.5	0.21	25.9	21.0	19.2	0.54
830404	28.	11.1	90.7	7.5	0.34	28.8	48.5	20.6	0.47

Appendix E

LISTING OF THE PYROX5 DATA AND RESULTS

```
               PYROX5 SERIES OXIDATION EXPERIMENT
               PYRITE TYPES--- 1-ELLIOT LAKE CONC, 2-PERU (A)
               , 3-PERU (B), 4-ARIZONA,5-COLCRADO, 6-SIBERIA


  DATE   DAYS
                   P5-1A P5-1B P5-2A P5-2B P5-3A P5-3B

 830313     1.
             SO4   47.2 111.0  26.1  32.8  54.2  48.8
              WT  102.0  28.6  33.5  65.8  54.1  37.1
             ACC    4.8   3.2   0.9   2.2   2.9   1.8
            RATE    4.8   3.2   0.9   2.2   2.9   1.8

 830314     2.
             SO4   18.9   7.5  17.7   4.0  15.4  20.5
              WT  141.0 452.2  42.9 556.6 114.1  78.9
             ACC    7.5   6.6   1.6   4.4   4.7   3.4
            RATE    2.7   3.4   0.8   2.2   1.8   1.6

 830315     3.
             SO4    9.7  23.5  43.6  11.9  29.7  93.7
              WT  259.3 132.9  56.5 260.7 101.0  27.6
             ACC   10.0   9.7   4.1   7.5   7.7   6.0
            RATE    2.5   3.1   2.5   3.1   3.0   2.6

 830316     4.
             SO4   23.1  23.4  31.8  13.0  32.4  38.1
              WT  249.4 137.4 110.2 266.6 111.0  73.4
             ACC   15.8  12.9   7.6  11.0  11.3   8.9
            RATE    5.8   3.2   3.5   3.5   3.6   2.9

 830317     5.
             SO4   43.4  24.1  68.8  77.9  38.3  56.3
              WT   85.0 125.3  57.8  48.5  59.1  59.1
             ACC   19.4  15.9  11.6  14.7  13.5  12.2
            RATE    3.7   3.0   4.0   3.8   2.3   3.3

 830318     6.
             SO4   24.5  18.2  76.9  26.2  74.4   4.4
              WT  140.7 160.0  40.8 152.4  39.1 456.0
             ACC   22.9  18.8  14.7  18.7  16.5  14.2
            RATE    3.4   2.9   3.1   4.0   2.9   2.0

 830319     7.
             SO4   34.5  24.1  64.4  12.4  52.1  58.2
              WT  116.8 128.6  58.8 259.5  77.4  45.3
             ACC   26.9  21.9  18.5  21.9  20.5  16.9
            RATE    4.0   3.1   3.8   3.2   4.0   2.6

 830320     8.
             SO4   39.9  46.6  37.2  21.5 135.0  83.3
              WT   87.5  73.5 115.3 205.8  21.9  34.2
             ACC   30.4  25.4  22.8  26.4  23.4  19.7
            RATE    3.5   3.4   4.3   4.4   3.0   2.8

 830321     9.
             SO4   60.5  15.4  79.2  10.8  27.7  63.2
              WT   56.1 189.8  40.2 208.4 133.0  34.7
```

```
                ACC   33.8   28.3   26.0   28.6   27.1   21.9
               RATE    3.4    2.9    3.2    2.3    3.7    2.2

830322     10.
                SO4   37.4   31.2   58.9   89.0   88.3   44.0
                 WT   88.7   96.6   61.8   27.1   30.7   76.4
                ACC   37.1   31.3   29.6   31.0   29.8   25.3
               RATE    3.3    3.0    3.6    2.4    2.7    3.4

830323     11.
                SO4   28.9   31.2   56.3   23.3   52.6  123.0
                 WT   85.8   61.0   67.5  143.8   89.3   23.6
                ACC   39.6   34.4   33.4   34.4   34.5   28.3
               RATE    2.5    3.1    3.8    3.4    4.7    3.0

830324     12.
                SO4   16.7   63.8   20.0   27.4   94.5   96.1
                 WT   64.6   41.8   23.6   87.6   28.1   17.4
                ACC   40.7   37.1   33.9   36.8   37.2   30.0
               RATE    1.1    2.7    0.5    2.4    2.7    1.7

830325     13.
                SO4   16.2   15.2   55.1   56.5   17.2   28.3
                 WT  158.3  161.5   60.2   55.3  174.1  119.9
                ACC   43.2   39.5   37.2   39.9   40.2   33.3
               RATE    2.6    2.5    3.3    3.1    3.0    3.4
```

```
                         PIROX5 SERIES OXIDATION EXPERIMENT
                         PYRITE TYPES--- 1-ELLIOT LAKE CONC, 2-PERU (A)
                         , 3-PERU (B), 4-ARIZONA,5-COLORADO, 6-SIBERIA

  DATE    DAYS
                    P5-4A P5-4B P5-5A P5-5B P5-6A P5-B

 830313     1.
             SO4   43.8  72.6  36.1  37.8  49.5  54.5
              WT   46.9  34.2  38.8  36.9  42.2  41.5
             ACC    2.1   2.5   1.4   1.4   2.1   2.3
            RATE    2.1   2.5   1.4   1.4   2.1   2.3

 830314     2.
             SO4   40.0  14.6  29.1  16.3  18.1  13.0
              WT   64.2 302.6  84.6 202.4 152.5 288.7
             ACC    4.6   6.9   3.9   4.7   4.8   6.0
            RATE    2.6   4.4   2.5   3.3   2.8   3.8

 830315     3.
             SO4   23.2  28.3  39.1   2.6  23.3 108.0
              WT  193.7 117.0  83.6  22.9 141.3  27.4
             ACC    9.1  10.2   7.1   4.8   8.1   9.0
            RATE    4.5   3.3   3.3   0.1   3.3   3.0

 830316     4.
             SO4   37.1  29.6  33.5  33.1  67.3  20.4
              WT  111.0 132.1  99.8  60.7  61.8 181.7
             ACC   13.2  14.1  10.5   6.8  12.3  12.7
            RATE    4.1   3.9   3.3   2.0   4.2   3.7

 830317     5.
             SO4   38.3  46.9  29.6  21.9  91.2  64.6
              WT   59.2  86.4 113.0 125.6  32.2  69.1
             ACC   15.5  18.2  13.8   9.5  15.2  17.1
            RATE    2.3   4.1   3.3   2.8   2.9   4.5

 830318     6.
             SO4   25.8  53.1  41.5  52.1  39.4  64.4
              WT  167.9  76.3  89.4  59.7  90.0  54.7
             ACC   19.8  22.2  17.5  12.6  18.8  20.7
            RATE    4.3   4.1   3.7   3.1   3.5   3.5

 830319     7.
             SO4   61.8  31.7  26.7  16.2  42.5  47.6
              WT  167.2 137.4 165.6 182.6 113.8  74.9
             ACC   24.0  26.6  22.0  15.6  23.6  24.2
            RATE    4.2   4.4   4.4   3.0   4.8   3.6

 830320     8.
             SO4   72.2  80.9  22.2  11.6 107.0  94.7
              WT   57.7  46.5 177.6 267.5  36.9  25.7
             ACC   28.2  30.3  25.9  18.7  27.6  26.7
            RATE    4.2   3.8   3.9   3.1   3.9   2.4

 830321     9.
             SO4   61.1  11.6  19.0  34.7  13.4  29.9
              WT   53.0 260.3 161.8  91.5 238.5 123.7
              ACC   31.4   33.4   29.0   21.9   30.8   30.4
             RATE    3.2    3.0    3.1    3.2    3.2    3.7

830322      10.
              SO4   52.1   29.9   40.4   34.1    0.0   42.2
               WT   80.9  133.2   87.0   82.2  115.9   87.9
              ACC   35.6   37.3   32.5   24.7   30.8   34.1
             RATE    4.2    4.0    3.5    2.8    0.0    3.7

830323      11.
              SO4   97.7   34.8   56.2   49.8   50.4   80.5
               WT   42.4  118.5   62.7   64.9   89.2   52.8
              ACC   39.7   41.5   36.0   27.9   35.3   38.3
             RATE    4.1    4.1    3.5    3.2    4.5    4.3

830324      12.
              SO4  130.0   45.1  105.0   70.6   66.8   97.3
               WT   23.8   84.5   23.0   38.9   53.1   21.0
              ACC   42.8   45.3   38.4   30.6   38.8   40.4
             RATE    3.1    3.8    2.4    2.7    3.5    2.0

830325      13.
              SO4   44.0   57.7   32.9   91.2    0.0   18.1
               WT   91.0   66.9   90.9   26.5   37.8  211.8
              ACC   46.8   49.1   41.4   33.1   38.8   44.2
             RATE    4.0    3.9    3.0    2.4    0.0    3.8
```

Appendix F

XRD TRACES OF TAILINGS MINERALS

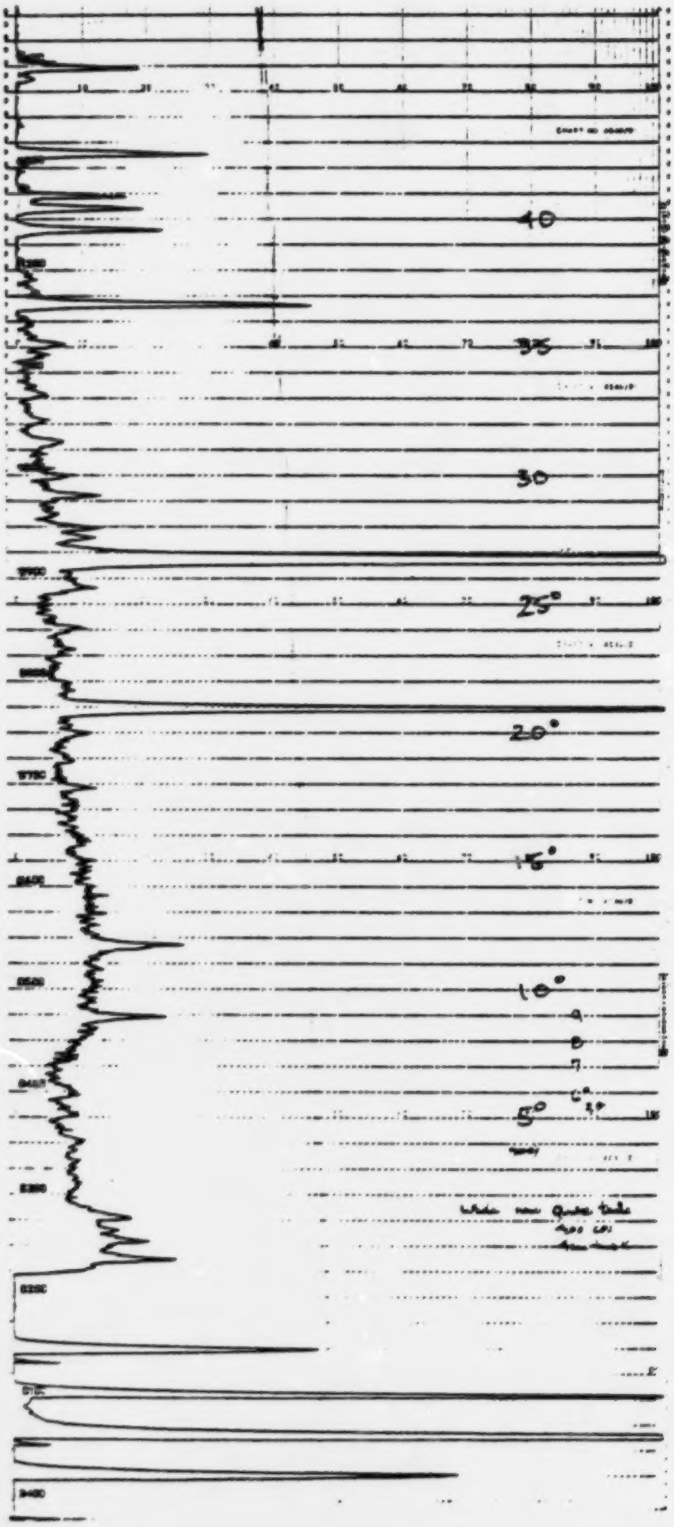

40
35
30
25°
20°
15°
10°
9
8
7
6°
5°

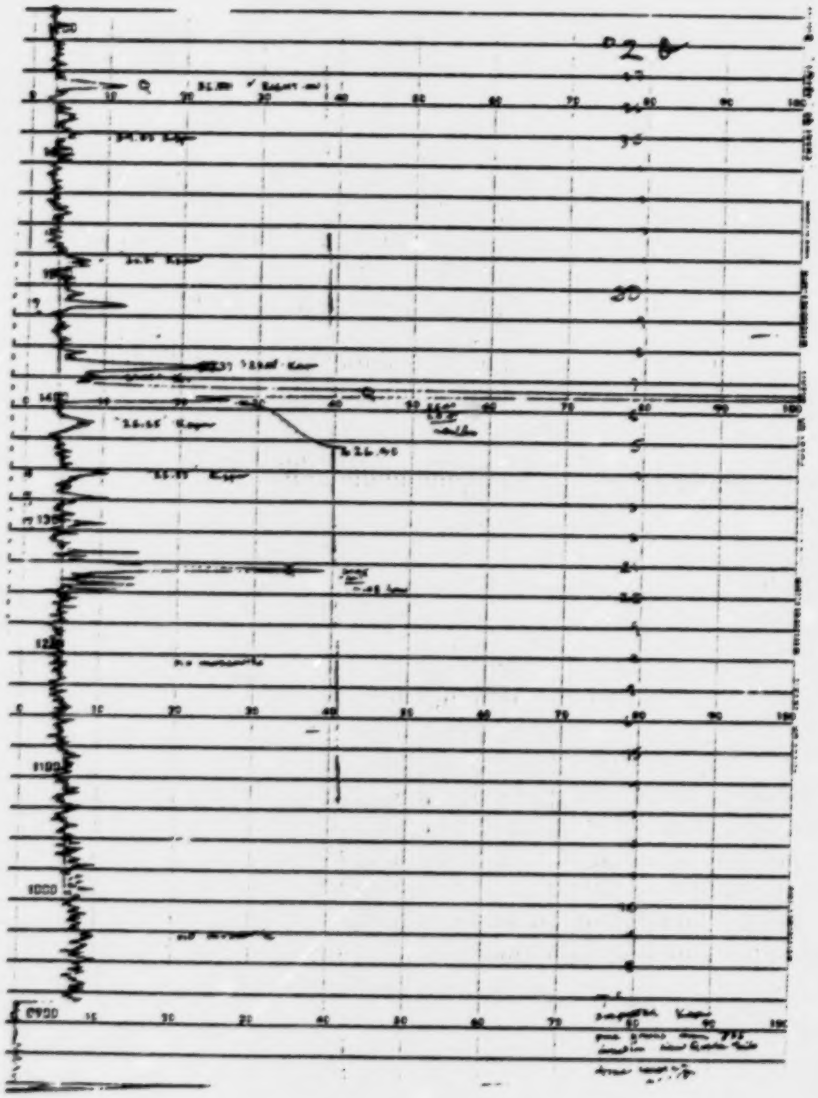
0
10
20
30
40
50
60
70
80
90
100
0900
1000
1100
1400
26.40

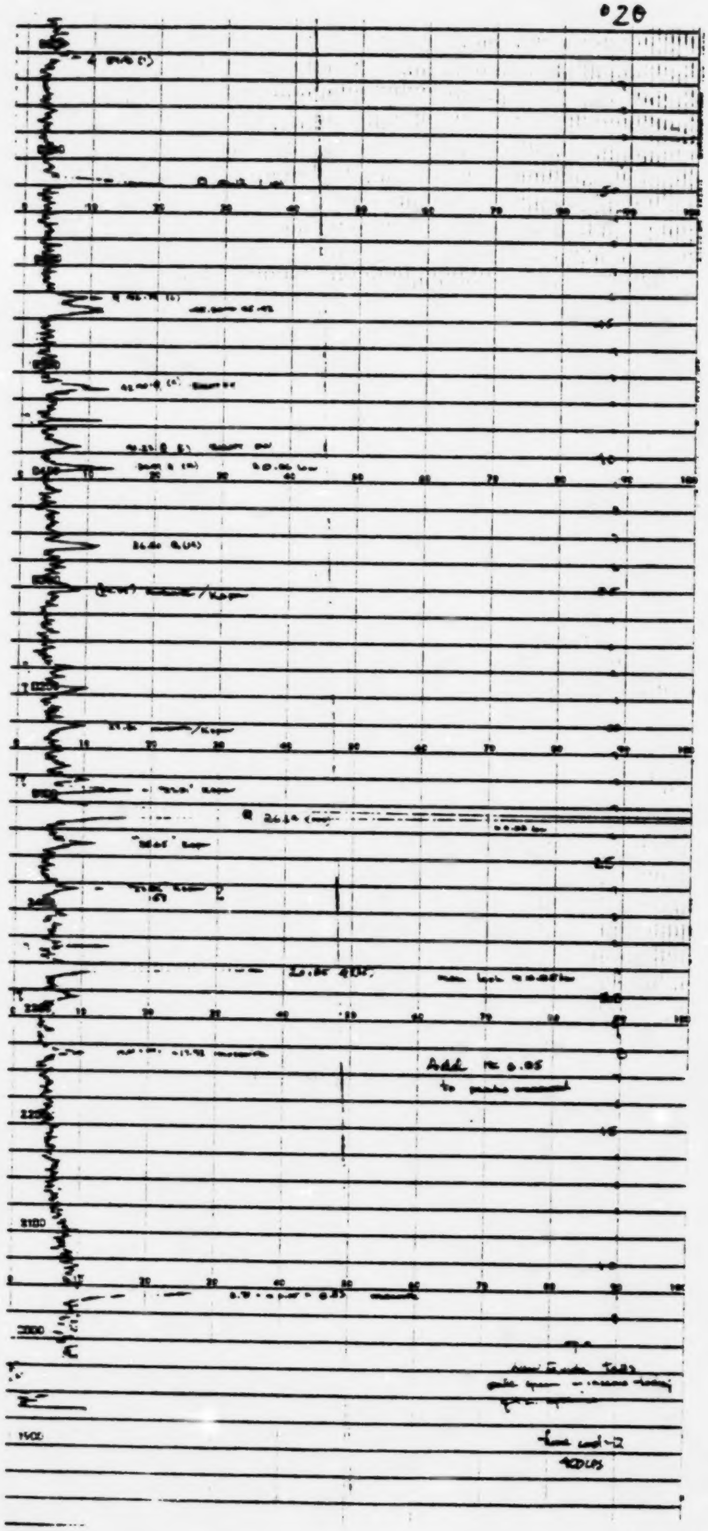

°2θ
10
20
30
40
50
60
70
80
90
100
2000
2100
2200
Add ≈ 0.05
to [illegible]

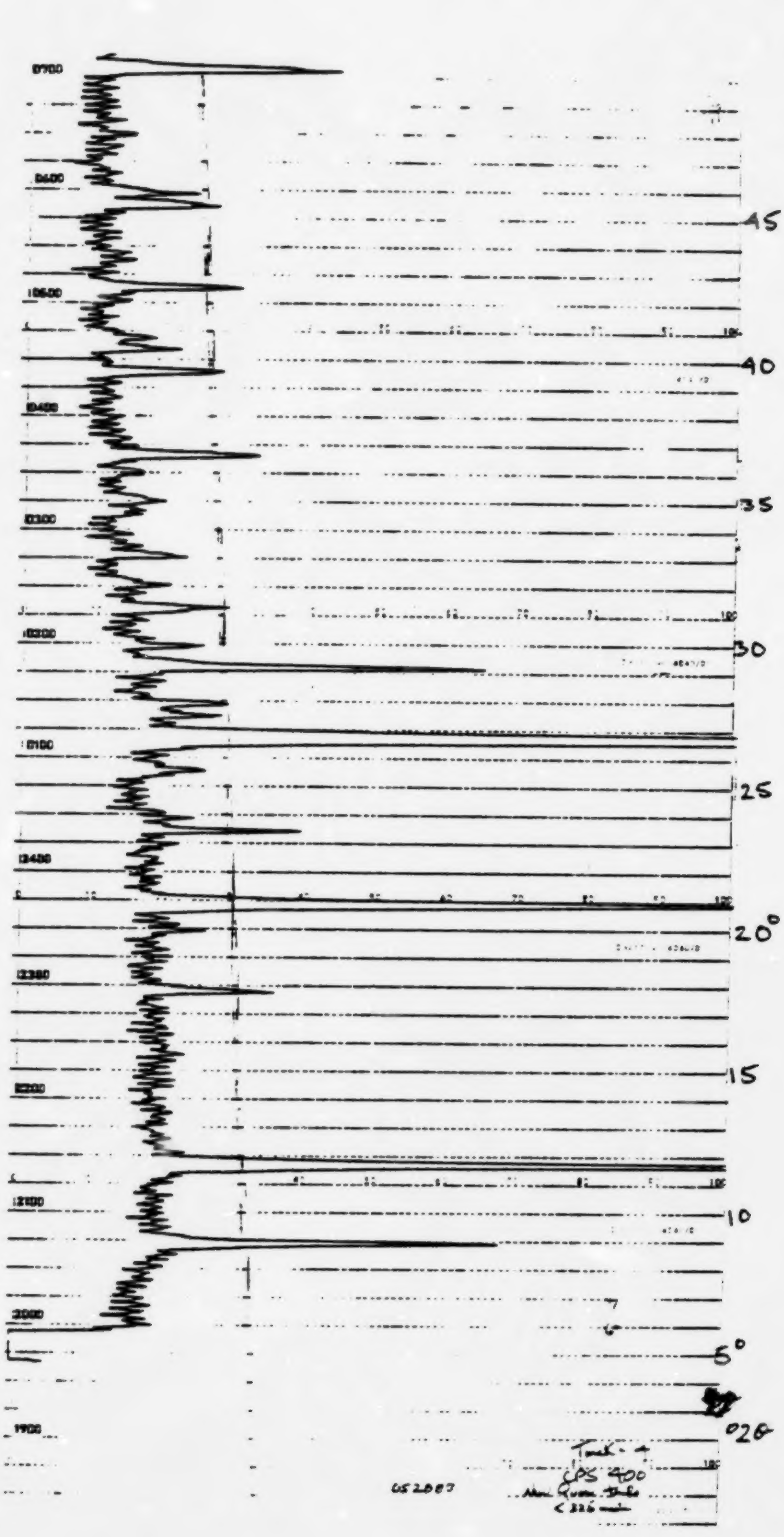
0700
0600
10600
10400
10300
10200
10100
12400
12300
12200
12100
12000
1900
45
40
35
30
25
20°
15
10
5°
02θ
052083
Track - 4
CPS 400
< 326

Appendix G

ADDITIONAL EFFLUENT ANALYSES FOR THE COLUMN TESTS

Table G.1 Chemical analysis of column 1 effluent.

The input chloride concentration of 440 mg/L was assumed. All analyses are mg/L.

Sample	1-1	1-3	1-4	5	9	10	80	91
pH	7.63	*7.63	*7.63	7.59	7.53	7.58	2.50	2.15
Eh(mV)	**0.200	**0.200	**0.200	**0.200	**0.200	0.181	**0.593	0.597
Na	3.40	0.49	0.43	0.56	0.54	0.53	0.10	0.09
K	48.5	5.4	4.75	4.85	5.00	4.90	1.62	1.44
Ca	548	613	683	810	815	790	2.65	2.65
Mg	67.0	8.85	7.50	20.8	33.6	32.2	1.13	0.40
Fe TOTAL	<1	<1	<1	<1	<1	0.12	70.5	46.0
Al	<5	<5	<5	<5	<5	<0.5	55.5	15.0
SO_4^{2-}	1521	1469	1563	1329	1354	1202	36.4	22.3
SiO_2	16.3	10.7	12.2	14.4	16.7	16.1	72.5	42.4
Alkalinity (HCO_3^-)	279	106	113	135	103	134	—	—
Calcite SI	0.922	0.567	0.629	0.748	0.572	0.736	—	—

* pH values estimated from preceding and subsequent measurements.

** Eh values estimated.

Number/
Numéro

2

University of
Waterloo Research Institute

AN ADDENDUM TO THE REPORT ON THE CONTINUATION STUDY ON HYDROGEOCHEMICAL PROCESSES IN ABANDONED URANIUM TAILINGS FROM THE ELLIOT LAKE DISTRICT

PROJECT NO. 204-02

SEPTEMBER 1983

REQ.NO. 2-9030

CONTRACT REPORT NO. OSU82-00144

UNIVERSITY OF WATERLOO
WATERLOO RESEARCH INSTITUTE

Project No. 204-02

AN ADDENDUM TO THE REPORT ON THE CONTINUATION STUDY ON HYDROGEOCHEMICAL PROCESSES IN ABANDONED URANIUM TAILINGS FROM THE ELLIOT LAKE DISTRICT

September 30, 1983

Principal Investigators:
J.A. Cherry, R.W. Gillham and E.J. Reardon

Research Assistants:
N.M. Dubrovsky and R.V. Nicholson

Department of Earth Sciences
University of Waterloo
Waterloo, Ontario
N2L 3G1

Submitted to:
Departmemt of Energy, Mines and Resourses
CANMET Mineral Sciences Laboratories
555 Booth St.
Ottawa, Ontario
K1A 0G1

23pp

APR [illegible]
MICROMEDIA

CONTENTS

page

ADDENDUM TO THE FINAL REPORT ON THE CONTINUATION STUDY ON THE HYDROGEOCHEMICAL PROCESSES IN ABANDONED URANIUM TAILINGS FROM THE ELLIOT LAKE DISTRICT 1

Results of the Repeated Oxygen Concentration Experiment 1
Experimental 1
Materials 1
Oxygen Concentration Experiment (PYROX 6) 2
Discussion 4

ADDITIONAL REFERENCES 7
LIST OF TABLES 8
LIST OF FIGURES 9
TABLES 10
FIGURES 13

ADDENDUM TO THE FINAL REPORT ON THE CONTINUATION STUDY ON THE HYDROGEOCHEMICAL PROCESSES IN ABANDONED URANIUM TAILINGS FROM THE ELLIOT LAKE DISTRICT

Results of the Repeated Oxygen Concentration Experiment

A laboratory investigation on the kinetic behavior of pyrite oxidation in dilute-alkaline solution was conducted under contract for Energy, Mines and Resources during the 1982-83 fiscal year. In that study, factors such as 1) the surface area of pyrite, 2) oxygen concentration, 3) temperature and 4) the geographic location of pyrite types were investigated to determine the effects on the oxidation rate. During those studies, it was found that results of the oxygen concentration experiments were in error due to contamination of low concentration units by atmospheric oxygen. The following represents the results of a repeat experiment to examine the effects of oxygen concentration and supercedes the results and discussion dealing with this topic in the final report submitted earlier this year (WRI Report 204-02, May 1982 to March 1983).

Experimental

Materials.

The moisture suction-cup device was further modified for use in experiments in which different oxygen concentrations were used. This device consisted of the same cup and base plate as that described in the main report but in addition, the gas outlet was modified to prevent contamination of the cup interior by atmospheric gas. This was performed by assuring that the rubber stopper was sealed around the edges of the cup as well as by providing an outlet tube for the gas phase through the stopper. This version of the moisture suction device is shown in Fig. 3.

Oxygen Concentration Experiment (PYROX 6).

Four 20 g samples of pyrite (-120+170 Colorado) were weighed to the nearest mg. Each sample of pyrite was added to 80 g of silica sand with the same grain size and the material was gently rolled in a glass beaker until the mixture appeared homogeneous. Each of the four moisture suction devices was then packed in a manner similar to that described for the surface-area experiment. Before wetting the pyritic sand, however, the rubber stopper, solution influent tubing and the gas outlet fittings were emplaced. After setting the gas effluent opening below water, gas flow with the appropriate gas phases was initiated and maintained at a rate of about 30 ml per minute through the dry sand. Concentrations of 0.01, 0.10, 1.0 and 5.0% oxygen were used in this experiment. The same gas phases were also continuously bubbled through each of the corresponding solution reservoirs. The gas in each reservoir escaped through an 18 gauge needle that was inserted through the rubber stopper. After the gas phases had been flowing for 24 hours, the pyritic sand was wetted, the effluent outlets were placed about 90 cm below the bases of the cups with collection flasks for each unit and solution inflow was initiated. The flow rates of the solutions dripping onto the surface of the pyritic sand was adjusted to about 100 ml per day and solution effluent was collected, weighed and subsamples were retained for later determinations of sulphate concentrations. A schematic diagram of the experimental system can be seen in Fig. 12.

During previous experimental runs, it was found that contamination by atmospheric oxygen of the solution reservoirs occurred over the operating period. To monitor potential contamination during this experiment, gas samples from different locations in the system were collected and analysed twice during the course of the experiment. The gas spaces in the bubbling flasks used to humidify gas entering the pyritic sand, the gas spaces above the sand in the oxidation cups and the gas spaces above the influent solution in the reservoirs were sampled and analysed for oxgen content.

The results of total accumulated sulphate released from each unit for the first 10 to 13 days of the experiment can be seen in Fig. 13. This plot reveals a linear response for each unit as well as a consistent trend of decreasing slope (rate) with lower oxygen concentration. Inspection of the response of daily oxidation rates over time shows that variations are quite small, especially in the units with lower oxygen concentrations (Fig. 14, a to d). The high apparent rates observed for the first two days of operation for all units can be attributed to the leaching of residual sulphate that is produced during processing and cleaning of the granular pyrite. The rates of oxidation were estimated by taking the average of the daily rates after the second day's data. A summary of these rates and oxygen concentrations as well as data from the PYROX 2-3 unit representing the 20% O_2 concentration are given in Table 6.

A plot of the daily rates versus oxygen concentrations on logarithmic axes is used to determine the order of the reaction with respect to oxygen (Fig. 15). This plot is linear with a slope corresponding to the order of the equation, the results of which suggest that the rate is a function of the oxygen concentration to the power of about 0.59. The linear correlation coefficient (r^2) for this log-log plot is equal to 0.999. The relationship is represented by;

$$\log(\text{Rate}) = \log(k) + 0.59 \log(O_2) \qquad (9)$$

in which (O_2) represents the concentration of oxygen and (k) is a composite rate constant.

The oxygen concentrations used for this plot are based on the results of the oxygen analyses that were conducted during the second week of the experimental run (Table 7). Analyses on samples taken during the first week of the experiment are slightly higher for the units whose gas supplies were specified as 0.01 and 0.10% O_2, but the differences between the first and second sampling do not appear to be significant (Table 8). The consistency of the resulting concentrations, whose data are derived from replicate samples, suggests that the analyses are precise. The results of similar analyses conducted during other experiments suggest that the high values observed for the 0.01 and 0.10% O_2 units are actual and are not an artifact of the sampling procedure.

Discussion.

The results of the oxygen-concentration experiment suggest that the rate of pyrite oxidation is proportional to the concentration of oxygen to the power of 0.59 ± 0.05 (95% confidence interval). This fractional order suggests that the rate is controlled by adsorption-type mechanisms in contrast to molecular- or atom-transfer processes that would be observed if first-order results were obtained.

A number of relationships between oxidation rate and concentration of oxygen have been reported in the literature (van Breemen, 1972; Nordstrom, 1982). Many studies conclude that the rate is proportional to the partial pressure of oxygen. Fractional orders of reaction have also been suggested with values of 0.8, 2/3 and 1/2 (Lowson, 1982). In addition, complex adsorption-desorption models have been used to describe the rate mechanism (Shumate et al, 1971).

The results observed in this study most closely agree with those of Clark (1966), in which the order of reaction in that study was found to be 2/3. The results reported by Clark are based on actual dissolved oxygen measurements in the solution phase and sulphate was used as a measure of the oxidation rate. The 95% confidence interval for the rate order in this investigation occurs in the range of 0.54 and 0.64. The value of the upper limit is close to 0.67 that was suggested by Clark. Unfortunately, there was very little control on surface area in Clark's study and hence comparison of rate constants cannot be made.

The fractional order found in this investigation suggests that the rate mechanism involves complex adsorption-desorption processes during the oxidation reaction. Although reports of findings in other studies (Smith et al., 1968) suggest that a Langmuir-type isotherm applies to their data, no such fit is found for the present data. Even though no mechanism involving oxygen has been proposed here for the oxidation of pyrite, the relationship or order of the reaction can, nonethless, be used to predict the rate of oxidation and subsequent acid generation under specified conditions of oxygen concentration at values of pH in the range of 7 to 8.

ADDITIONAL REFERENCES

Clark, C.S., 1966. Oxidation of coal mine pyrite. Proc. Amer. Soc. Civil Eng., J. San. Eng. Div., 92:127.

LIST OF TABLES

Table 6: Summary of the oxygen concentrations and oxidation rates observed in the oxygen concentration experiment (PYROX6).

Table 7: Summary of oxygen-gas analyses performed on samples taken from various locations in the experimental system for the PYROX6 experiment (taken July 14, 1983).

Table 8: Summary of oxygen-gas analyses performed on samples taken from various locations in the experimental system for the PYROX6 experiment (taken July 7, 1983).

LIST OF FIGURES

Fig. 3: A schematic diagram showing the modifications made to the moisture-suction device. (1)- gas inlet leading to perforated coil, (2)- gas outlet, (3)- Solution inlet, (4)- Rubber stopper.

Fig. 12: A schematic diagram showing the experimental system used for the oxygen concentration experiment (PYROX6).

Fig. 13: The total sulphate accumulated is plotted against time for each unit in the oxygen-concentration experiment (PYROX6).

Fig. 14: The rate of sulphate leached (per day) is plotted against time for each unit in the oxygen-concentration experiment (PYROX6). (a) 0.01% O_2; (b) 0.10% O_2; (c) 1.0% O_2; (d) 5.0% O_2

Fig. 15: The oxidation rate (rate of sulphate leached) is plotted against the percent oxygen concentration on log-log axes.

TABLES

Table 6: Summary of the oxygen concentrations and oxidation rates observed in the oxygen concentration experiment (PYROX6).

Unit	Oxygen* Content %	Oxidation** Rate ($mg\text{-}SO_4 d^{-1} g^{-1}$)
PYROX6-1	0.06	0.0089
PYROX6-2	5.0	0.13
PYROX6-3	0.15	0.014
PYROX6-4	1.0	0.045
PYROX2-3	20.0	0.25

* measured oxygen concentration

** average of six to eight days' data

Table 7: Summary of oxygen-gas analyses performed on samples taken from various locations in the experimental system for the PYROX6 experiment (taken July 14, 1983)

	Oxygen Concentrations (% O_2)			
Unit	Designated*	Humidifier	Cups	Reservoir
P6-1	0.01	0.06	0.06	0.08
P6-2	5.0	5.0	4.9	4.9
P6-3	0.10	0.14	0.14	0.15
P6-4	1.0	0.98	0.99	1.0

*-Designated refers to the concentration specified in each gas mixture.

-Humidifer represents the gas that is bubbled through a flask containing water before passing through the pyritic sand.

-Cups refers to the gas above the pyritic sand in the moisture suction device.

-Reservoir represents the gas above the influent solution during continuous bubbling.

Table 8: Summary of oxygen-gas analyses performed on samples taken from various locations in the experimental system for the PYROX6 experiment (taken July 7, 1983)

Oxygen Concentrations (% O_2)

Unit	Designated*	Humidifier	Cups	Reservoir
P6-1	0.01	0.07	0.08	0.08
P6-2	5.0	5.0	5.0	5.0
P6-3	0.10	0.16	0.18	0.21
P6-4	1.0	1.01	1.03	2.01

*-Designated refers to the concentration specified in each gas mixture.

-Humidifer represents the gas that is bubbled through a flask containing water before passing through the pyritic sand.

-Cups refers to the gas above the pyritic sand in the moisture suction device.

-Reservoir represents the gas above the influent solution during continuous bubbling.

FIGURES

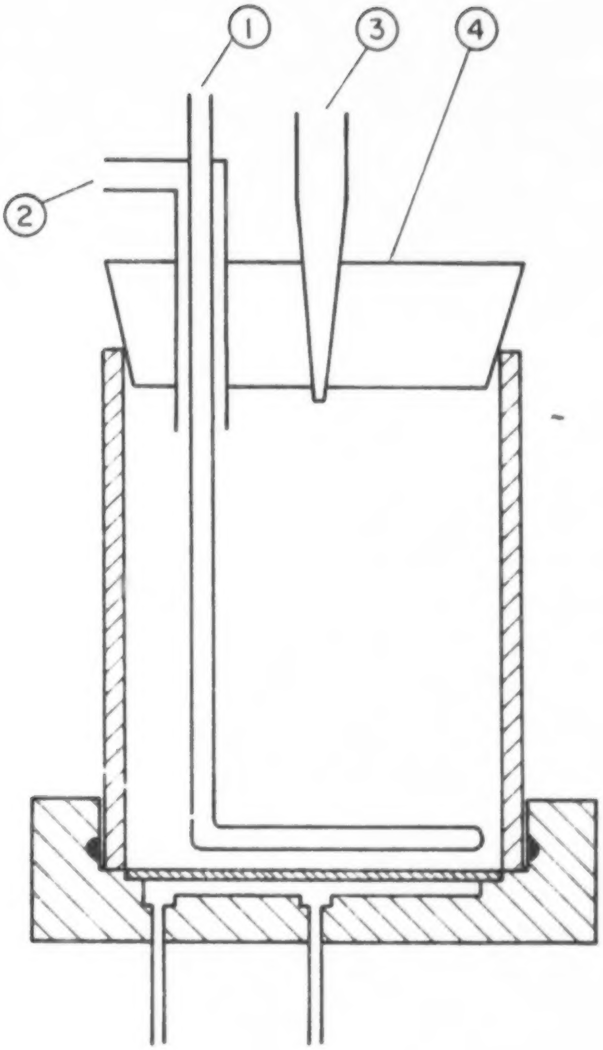

Fig. 3: A schematic diagram showing the modifications made to the moisture-suction device. (1)- gas inlet leading to perforated coil, (2)- gas outlet, (3)- Solution inlet, (4)- Rubber stopper.

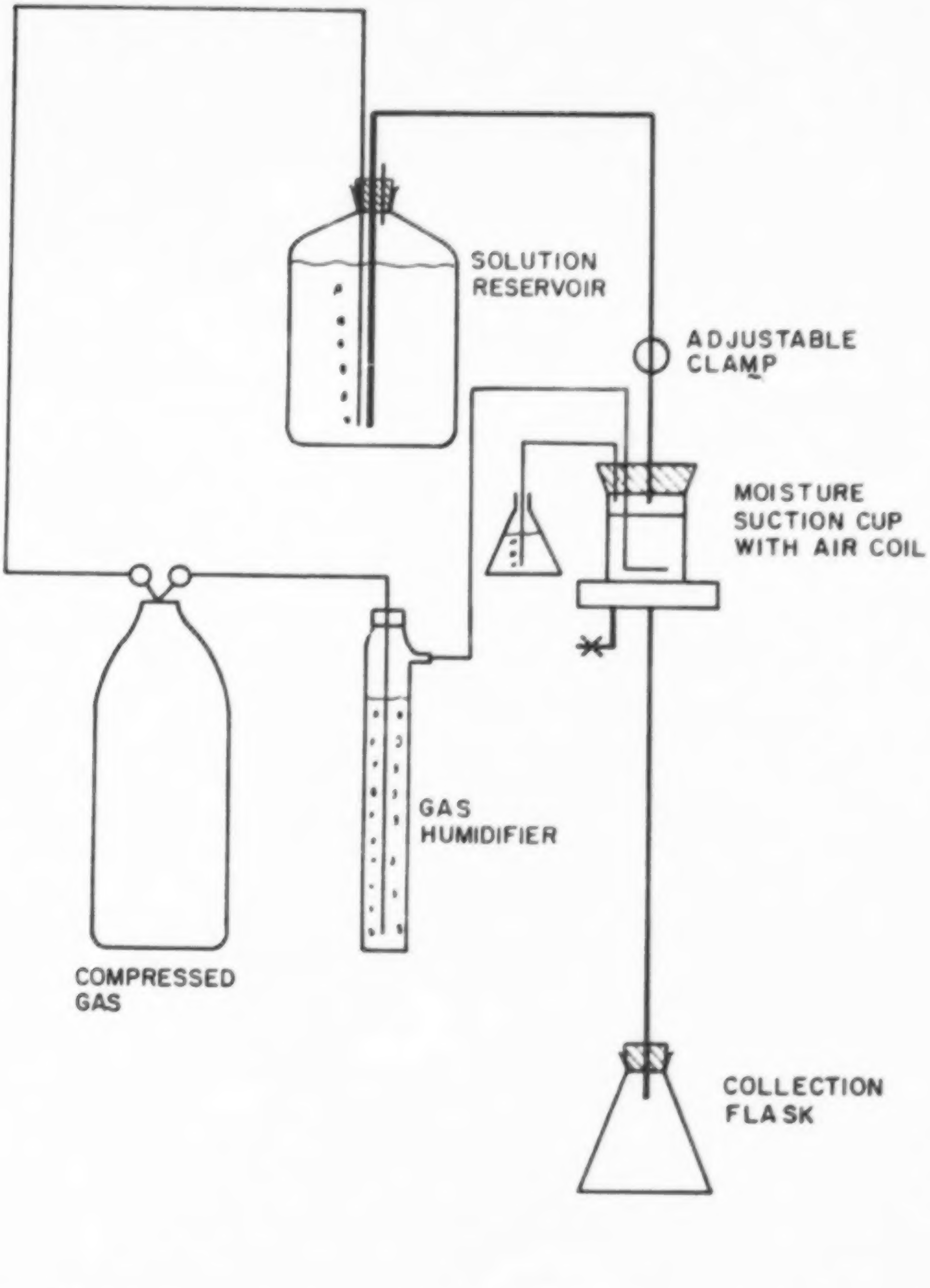
SOLUTION RESERVOIR
ADJUSTABLE CLAMP
MOISTURE SUCTION CUP WITH AIR COIL
GAS HUMIDIFIER
COMPRESSED GAS
COLLECTION FLASK

Fig. 12: A schematic diagram showing the experimental system used for the oxygen concentration experiment (PYROX6).

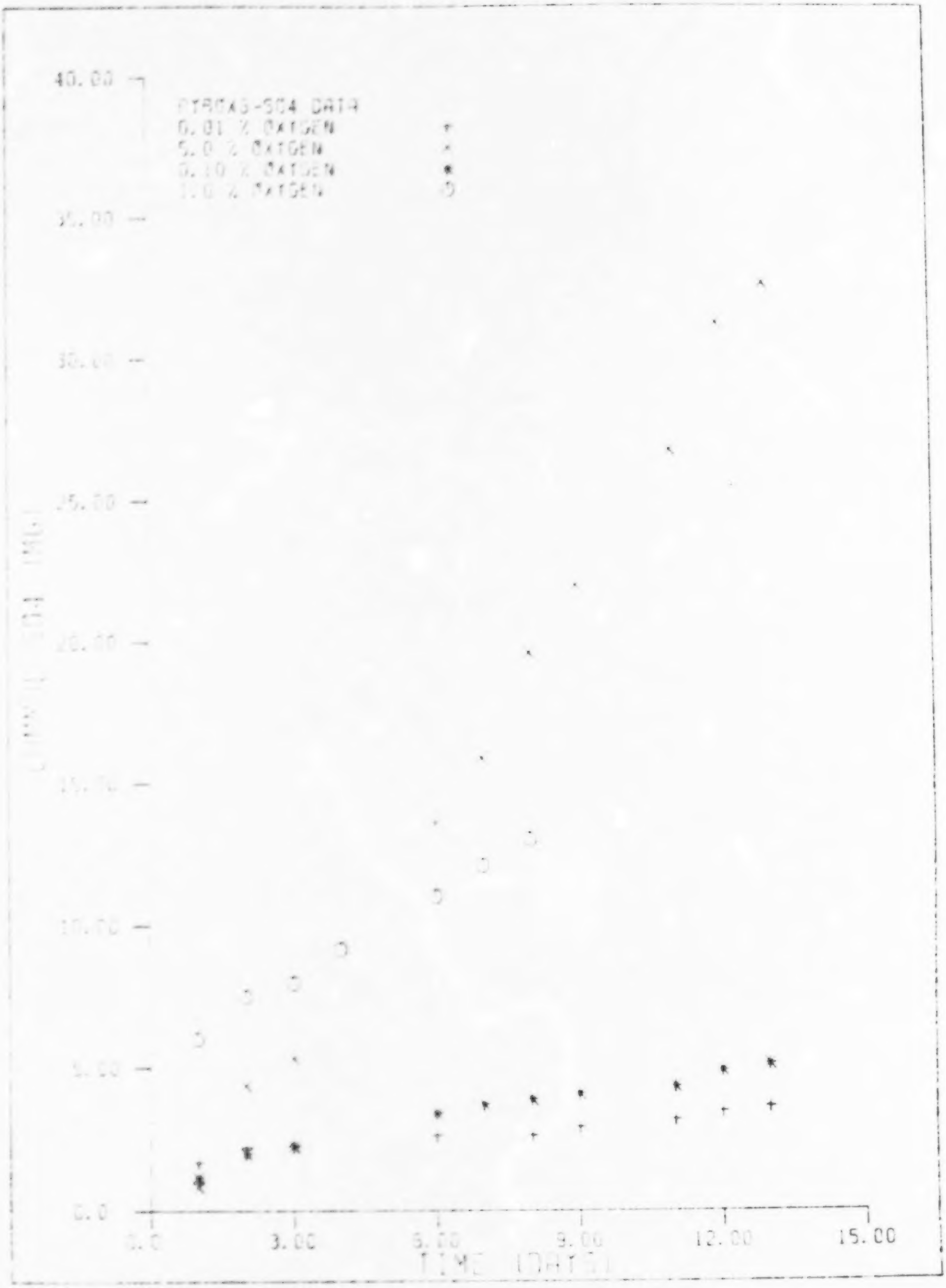

Fig. 13: The total sulphate accumulated is plotted against time for each unit in the oxygen-concentration experiment (PYROX6).

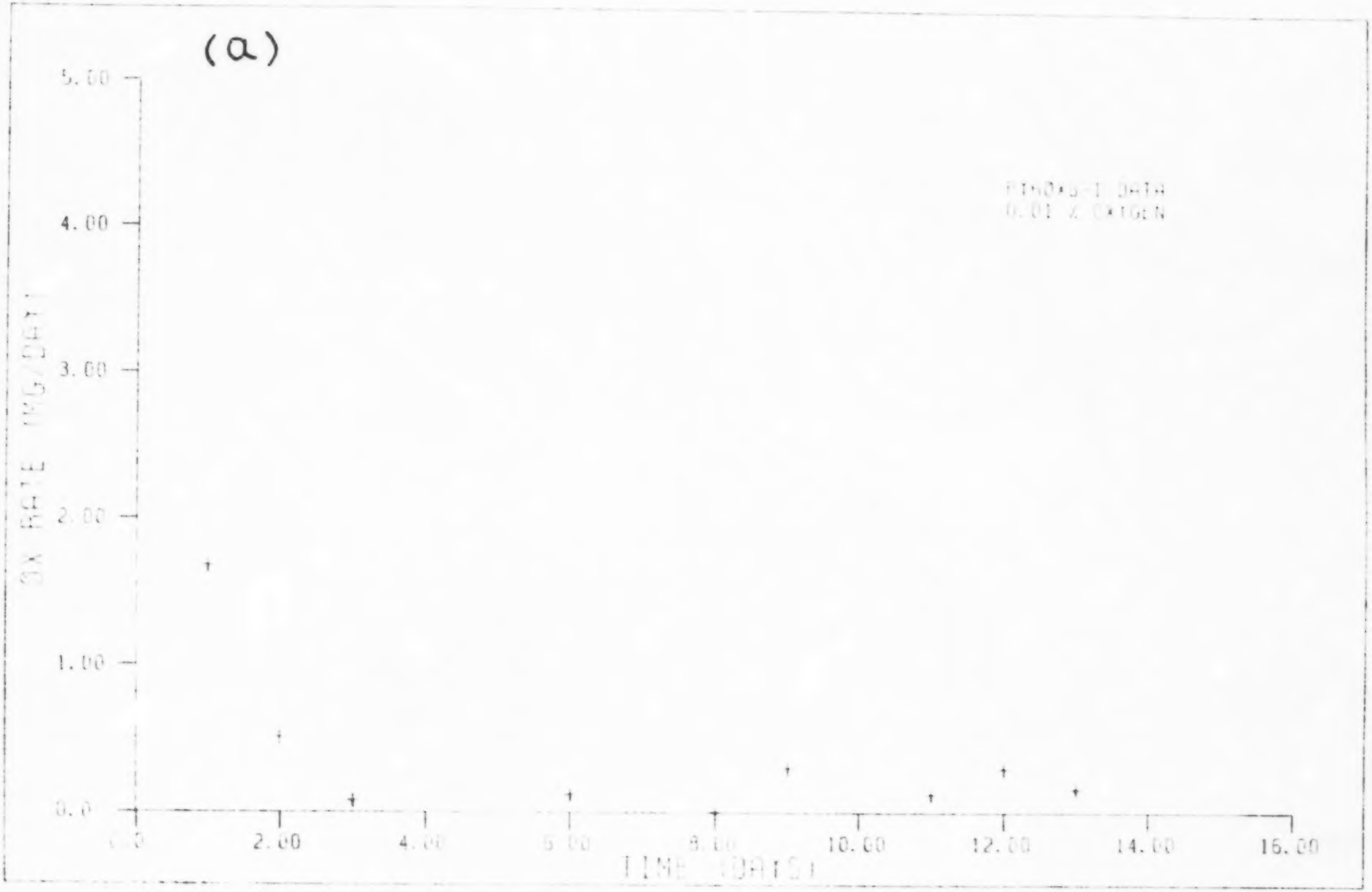

Fig. 14: The rate of sulphate leached (per day) is plotted against time for each unit in the oxygen-concentration experiment (PYROX6).

(a) 0.01% O_2; (b) 0.10% O_2; (c) 1.0% O_2; (d) 5.0% O_2

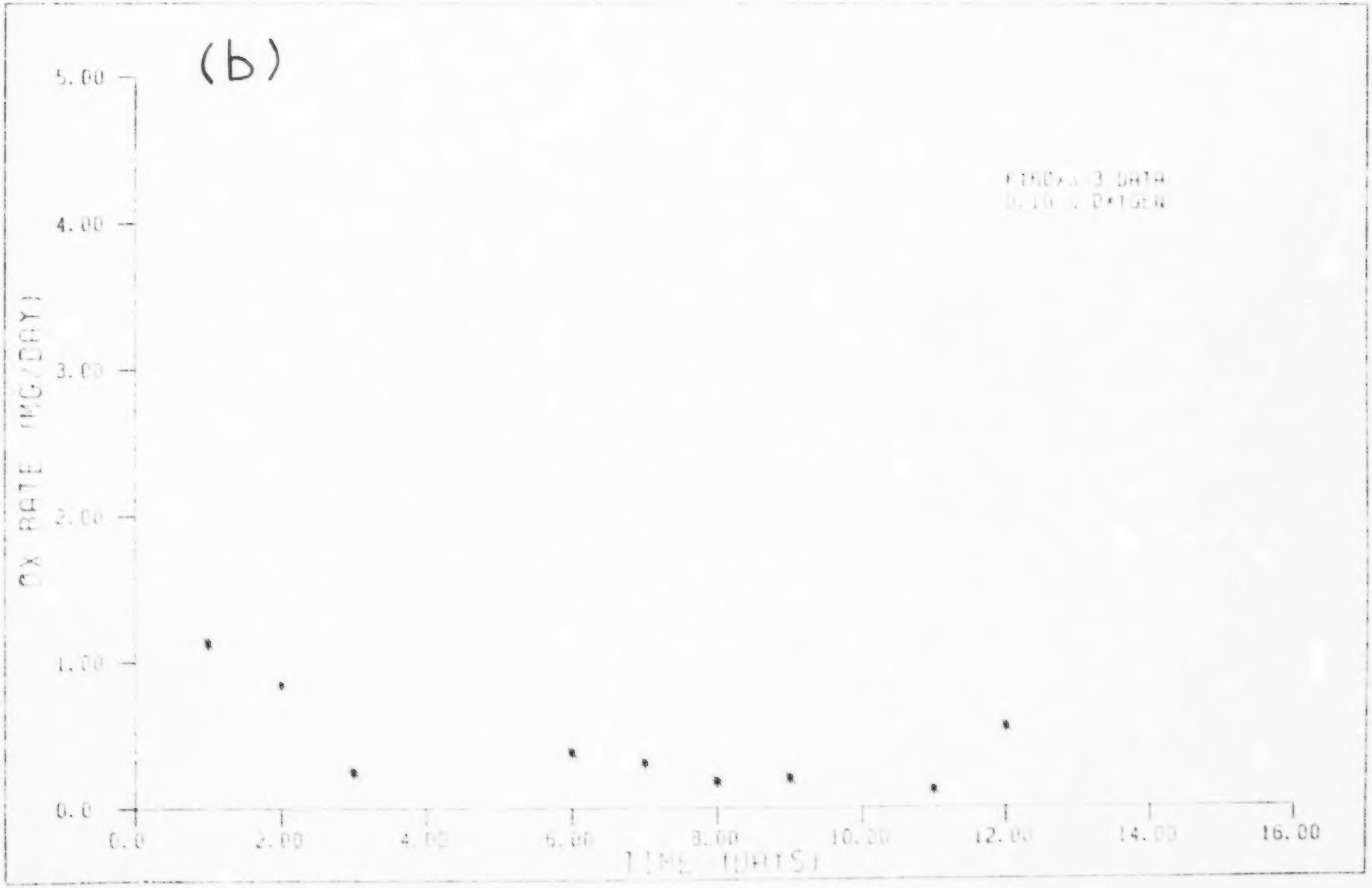(b)
F160x3 3 DATA
0.10 % OXYGEN
OX RATE (MG/DAY)
0.0
1.00
2.00
3.00
4.00
5.00
TIME (DAYS)
0.0
2.00
4.00
6.00
8.00
10.00
12.00
14.00
16.00

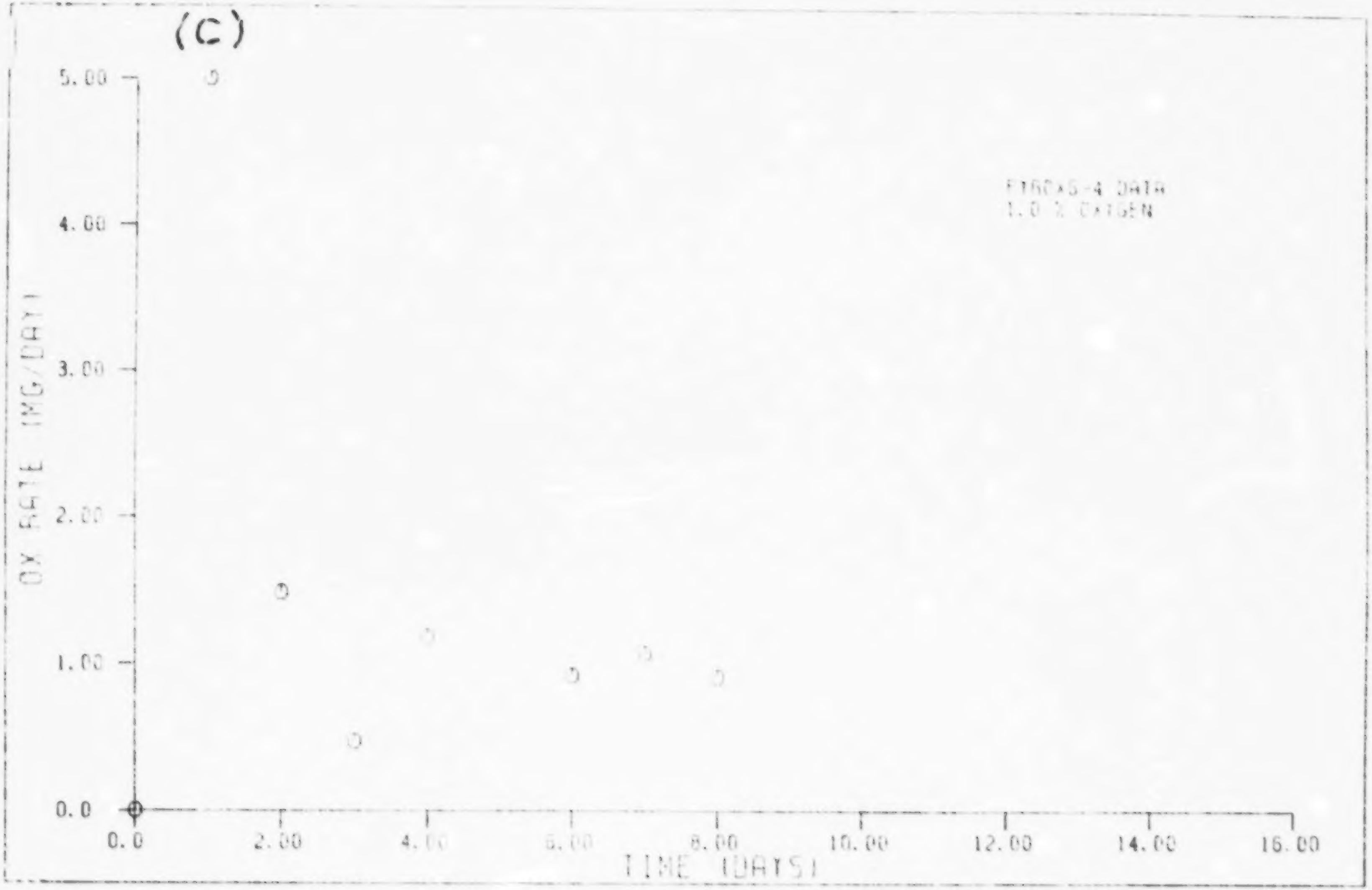
(C)
F16CX5-4 DATA
1.0 % OXYGEN
OX RATE (MG/DAY)
5.00
4.00
3.00
2.00
1.00
0.0
0.0
2.00
4.00
6.00
8.00
10.00
12.00
14.00
16.00
TIME (DAYS)

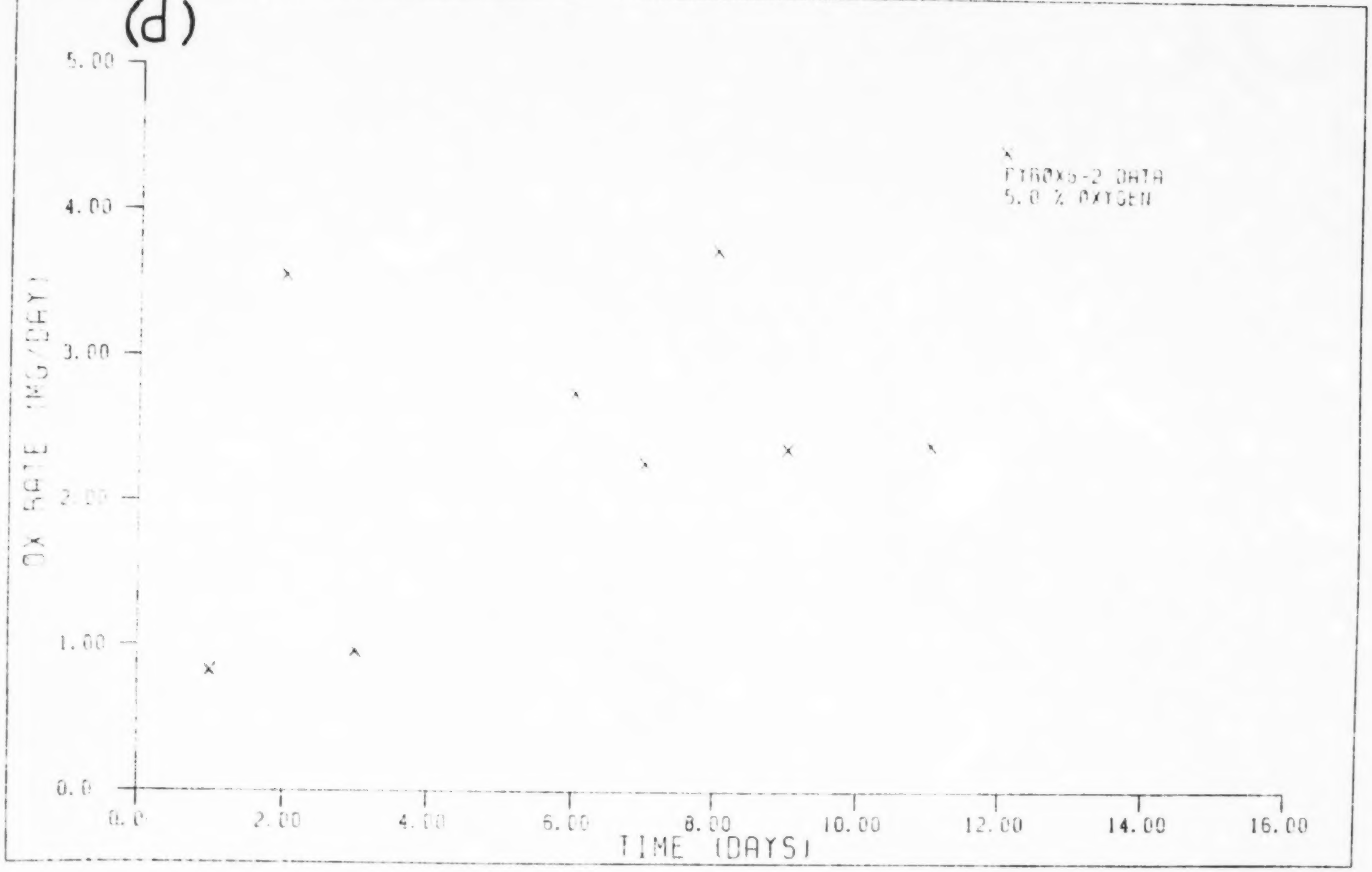
(d)
PYROX5-2 DATA
5.0 % OXYGEN
OX RATE (MG/DAY)
5.00
4.00
3.00
2.00
1.00
0.0
0.0
2.00
4.00
6.00
8.00
10.00
12.00
14.00
16.00
TIME (DAYS)

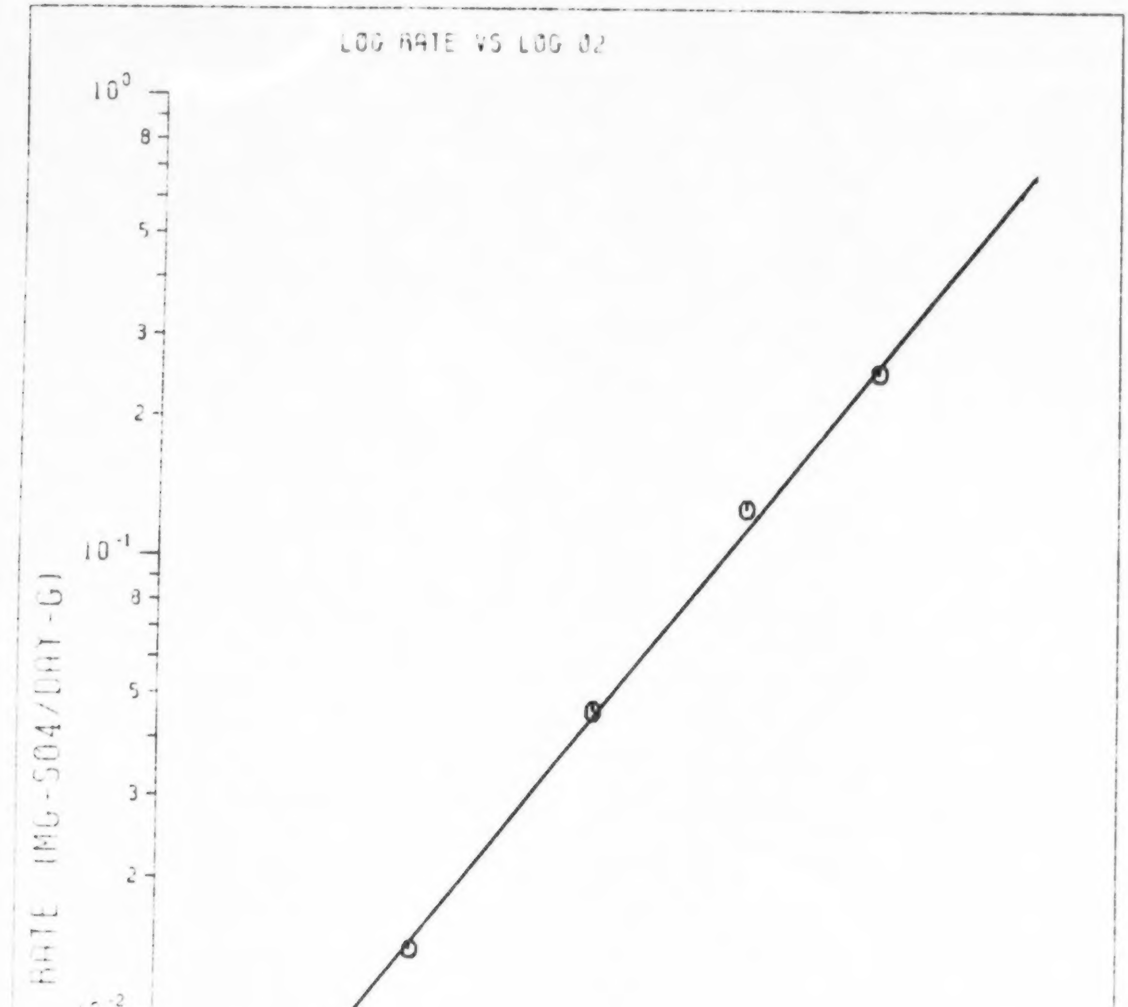

Fig. 15: The oxidation rate (rate of sulphate leached) is plotted against the percent oxygen concentration on log-log axes.

POOR

QUALITY

ORIGINAL